Instrumental and method development for multi-dimensional electrophoretic separations – coupling of capillary isoelectric focusing to mass spectrometry

Dissertation

der Mathematisch-Naturwissenschaftlichen Fakultät

der Eberhard Karls Universität Tübingen

zur Erlangung des Grades eines

Doktors der Naturwissenschaften

(Dr. rer. nat.)

vorgelegt von

Daniel Sydes

aus Kassel

Tübingen

2016

Gedruckt mit Genehmigung der Mathematisch-Naturwissenschaftlichen Fakultät der Eberhard Karls Universität Tübingen.

"Was immer du tun kannst

oder träumst es zu können,

fang damit an."

Johann Wolfgang von Goethe

Dedicated to my family

and especially my grandmother!

Acknowledgments

Declaration according to § 6 Abs. 2 of the PromO of the Faculty of Science

-Supervision and project partners in detail for each chapter-

2   Introduction

The text of the introduction was taken from the review by Kler et al. (Pablo A. Kler, Daniel Sydes, Carolin Huhn, Column–coupling strategies for multidimensional electrophoretic separation techniques, Anal. Bioanal. Chem., 2015, 407, 119-138 [Kler, 2015]) without figures and main tables and some adaptations.

Regarding the review, the contribution of Daniel Sydes was 20 % writing and 50 % literature research. The contribution of Pablo A Kler was 80 % writing and 50 % literature research.

3   Instrumental development including 3.1 Interface design and 3.2 Comparison of the 2nd and 3rd generation chip interfaces

Chip design and evolution:

The basic layout of the interface designs regarding channel layout (1st, 2nd and 3rd) is from Prof. Carolin Huhn and Dr. Pablo A. Kler (CIMEC, Santa Fe, Argentina). From the laboratory experiences with the 1st generation design, Daniel Sydes defined the shortcomings and limitations. This led to the improvements and testings for the 2nd generation design, which he implemented in his work after having organized its production in contact/discussion with the producer. Further shortcomings were observed in the experimental work. The 3rd generation chip design was fabricated at a purchase-based contract after joint discussions from Dipl. Ing. Martin Hermans – LightFab GmbH (Aachen, Germany) evaluated as 10 %. Dr. Pablo A. Kler provided the CAD files for the 3rd generation chip design as well as expertise evaluated as 30 %. Daniel Sydes contributed to the fabrication by managing the project as a central coordinator summarizing to a participation of about 60 %.

Experimental laboratory work:

All measurements regarding evaluation on the different chip interfaces, presented in this chapter were done by Daniel Sydes (100%).

Evaluation and interpretation of experimental results:

If not stated otherwise in the figure legend, the figures and the data evaluation was done by Daniel Sydes in discussion with Prof. Carolin Huhn and Dr. Pablo A. Kler. The contribution of Daniel Sydes is evaluated as 90 %. Figures were partly adapted from original CAD files from the respective manufacturers and Dr. Pablo A. Kler as stated in the thesis summarized as 10 %.

Writing:

All writing regarding evaluation and discussion of the results regarding the different chip interfaces, presented in this chapter was done by Daniel Sydes (100%).

3.3 On-chip intermediate potential detection

General idea:

General idea of on-chip interface potential detection was from Prof. Carolin Huhn, Prof. Peter Zipfl and Dr. Pablo A. Kler.

Instrumental development:

Hans Bouwes (iX-factory GmbH (Dortmund, Germany) provided the chips with integrated electrode at a purchase-based contract evaluated as 10 %. Prof. Peter Zipfl - Optoelectronics and Laser Technology Department at the University of Applied Sciences Aalen (Aalen, Germany) designed and constructed the prototype for the potential measurement setup and the potential electrode implemented in the chip interface evaluated as 80 %. Dipl.-Ing. Daniel Lutz - CalvaSens GmbH (Aalen, Germany) contributed to the design of the electrode for the on-chip potential detection evaluated as 10 %. Daniel Sydes was involved throughout the process of implementation with regard to the relation of chip design and later testing strategies.

Experimental laboratory work:

All measurements regarding evaluation of the integrated potential electrode inside the chip interface in combination with the prototype of the potential measurement setup were done by Daniel Sydes (100 %).

Computer simulations:

70% of all computer simulations were performed by Dr. Pablo A. Kler and 30% under his supervision by Daniel Sydes at the CIMEC in Argentina, financed via a DAAD scholarship.

Evaluation and interpretation of experimental results:

If not stated otherwise in the figure legend, the figures and the data evaluation was done by Daniel Sydes in discussion with Prof. Carolin Huhn and Dr. Pablo A. Kler. The contribution of Daniel Sydes is evaluated as 90 %. Figures were partly adapted from original CAD files from the respective manufacturers evaluated as 10 %.

Writing:

All writing regarding evaluation and discussion of the results regarding the on-chip intermediate potential detection, presented in this chapter was done by Daniel Sydes (100%).

3.4 Spatially-resolved on-chip intermediate light emitting diode induced fluorescence detection

General idea:

General idea of spatially-resolved on-chip intermediate light emitting diode induced fluorescence detection is from Prof. Carolin Huhn (70 %) and Daniel Sydes (30 %).

Instrumental development:

Daniel Sydes coordinated all aspects of instrumental design including discussion, implementation strategies, identification of shortcomings, redesign, optimization strategies. Hans Bouwes (iX-factory GmbH (Dortmund, Germany) provided the chips. Hans Meyer - J&M Analytik AG (Essingen, Germany) provided ideas during the discussions, CAD files and expertise for the construction of the LED-IF setup as well as the push broom imager in the framework of purchase- and project-based collaboration evaluated as 50 %. The light emitting diode (LED) was purchased from future LED (Berlin, Germany) evaluated as 5 % due to project-specific aspects of the purchase and related discussions. Alexander Schnapper and Christof Binder - Metal workshop of the University of Tübingen (Tübingen, Germany) manufactured the optical LED-IF setup according to the CAD files provided (5 %). All project communication and coordination, but also further development and optimization with redesign specifications was done by Daniel Sydes (expressed as 40 %).

Experimental laboratory work:

All measurements regarding evaluation of the spatially-resolved on-chip intermediate light emitting diode induced fluorescence detection were done by Daniel Sydes (100 %).

Evaluation and interpretation of experimental results:

If not stated otherwise in the figure legend, the figures and the data evaluation were established by Daniel Sydes in discussion with Prof. Carolin Huhn and Dr. Pablo A. Kler. The contribution of Daniel Sydes is evaluated as 95 %. Figures were partly adapted from original CAD files from the respective manufacturers evaluated as 5 %.

Writing:

All writing regarding evaluation and discussion of the results regarding the spatially-resolved on-chip intermediate light emitting diode induced fluorescence detection, presented in this chapter was done by Daniel Sydes (100 %).

4   Method development for 1st and 2nd separation dimension

General idea:

Starting with the basic idea as defined for the PhD project, its implementation strategies were developed by Daniel Sydes.

Experimental laboratory work, evaluation and data interpretation:

All experimental work was conducted and data evaluation/interpretation conducted by Daniel Sydes (100 %).

Writing:

All writing regarding evaluation and discussion of the results regarding the spatially-resolved on-chip intermediate light emitting diode induced fluorescence detection, presented in this chapter was done by Daniel Sydes (100 %).

5   Coupling of CIEF-LED-IF/CE-MS

General idea:

The necessity of on-chip intermediate fluorescence detection was visible from the first experimental results by Daniel Sydes. The coupling of CIEF and CE-MS was the goal set at the beginning of the PhD project.

Instrumental setup:

The assembly and optimization of the experiential setup using the different components listed in section 3.4 was done by Daniel Sydes (estimated as 100 %).

Experimental laboratory work:

All measurements regarding evaluation of the spatially-resolved on-chip intermediate light emitting diode induced fluorescence detection were done by Daniel Sydes (100 %).

Evaluation and interpretation of experimental results:

If not stated otherwise in the figure legend, the figures and the data evaluation was done by Daniel Sydes in discussion with Prof. Carolin Huhn and Dr. Pablo A. Kler. The contribution of Daniel Sydes is evaluated as 95 %. Figures were partly adapted from original CAD files from the respective manufacturers evaluated as 5 %.

Abbreviations

2DGE	two-dimensional gel electrophoresis
BGE	background electrolyte
BSA	bovine serum albumin
C^4D	capacitively coupled contactless conductivity detection
CE	capillary electrophoresis
CEC	capillary electrochromatography
CGE	capillary gel electrophoresis
CIEF	capillary isoelectric focusing
CSE	capillary size exclusion
EE-ITP	electroextraction−isotachophoresis
EOF	electroosmotic flow
EPC	electrochemical preconcentration
ESI	electrospray ionization
FEP	fluorinated ethylene propylene
FITC	fluorescein isothiocyanate
FQ	3-(2-furoyl)-quinoline-2-carboxaldehyde
ID	inner diameter
ITP	isotachophoresis
LC	liquid chromatography
LED	light emitting diode
LED-IF	light emitting diode induced fluorescence
LIF	laser induced fluorescence
MEKC	micellar electrokinetic chromatography
MS	mass spectrometry
OD	outer diameter
PABA	p-aminobenzoic acid
PAGE	polyacrylamide gel electrophoresis
PEEK	polyether etherketone
PMMA	polymethylmethacrylate
PTFE	polytetrafluoroethylene
RPLC	reversed phase liquid chromatography
SEC	size exclusion chromatography
SPE	solid phase extraction
tITP	transient isotachophoresis
UV-Vis	ultraviolet- visible

Table of content

Abstract

Multidimensional electromigrative separation techniques represent powerful tools meeting the complexity of analytical and bioanalytical challenges, especially regarding sample and matrix complexity as well as trace analysis. In this work a glass chip interface in a 2D capillary-chip system was further developed and optimized regarding stability and on-interface (intermediate) analyte detection sensitivity. To overcome limiting performance of previous approaches such as dead volume and capillary-chip connection, a new chip interface was addressed and compared to the previous designs. Selective Laser Etching (SLE) proved to be a promising alternative to established production processes giving rise to a nearly dead volume free capillary connection, enabling the use of screw-tight fittings at lower prototype costs.

To ensure zero potential difference at channel cross-sections or ground potential (GND) at one channel of a 2D assays if mass spectrometry (MS) is used as the detection method, on-chip potential measurements were conducted via a passivated electrode inside the chip interface. Using a low current measuring prototype in combination with a SiN passivated Ti/Pt electrode inside the interface, disturbances of the electric field lines as well as electrolysis during potential measurements conducted along electrophoretic separations were successfully avoided; resulting in an excellent setup stability. On-chip fluorescence detection was implemented to properly monitor the analyte inside the interface and thus, to perform a proper sample transfer. Therefore, spectrally and spatially resolved fluorescence detection was implemented via a linear optical fiber array and a push broom imager. In this regard, desired sensitivity as well as spectral and spatial resolution was achieved for fluorescein isothiocyanate and labeled model proteins using flushing and capillary isoelectric focusing (CIEF) experiments.

The optimized two-dimensional setup was used for the hyphenation of capillary isoelectric focusing to mass spectrometry using a 2D CIEF/CE-MS setup. For an optimized CIEF separation-based analyte positioning in the first dimension as well as separation efficiency of the protein and the ampholyte fraction within the second CE dimension, the combination of computer simulations and experimental data were used. Applying the on-chip fluorescence detection setup for intermediate analyte monitoring in the 2D setup, analyte carryover as well as peak broadening and peak splitting could be eliminated.

Abstract (German)

Multidimensionale elektromigrative Trenntechniken stellen leistungsstarke Werkzeuge dar, um sich bioanalytischen Herausforderungen zu stellen, vor allem in Bezug auf die zunehmende Komplexität von Analyten und Matrixbestandteilen. Im Rahmen dieser Arbeit wurde ein bestehender modularer zweidimensionaler Kapillar-Chip Aufbau mit einem Glas-Chip als Kopplungs-Interface hinsichtlich Stabilität und Kapillarkopplung weiterentwickelt. Im Zuge der Interface-Optimierung konnte mit Hilfe eines neuen Produktionsprozesses, dem „Selective Laser Etching", ein optimierter Chip-Prototyp mit einer nahezu totvolumenfreien Schraubverbindung für die Kapillarkopplung hergestellt und für Trennungen hoher Trenneffizienz eingesetzt werden. Zur präzisen Kontrolle des Analyttransfers wurde erstmals die spektral- und ortsaufgelöste intemediäre on-chip Fluoreszenzdetektion für die Kopplung der Kapillarisoelektrischen Fokussierung (CIEF) mit der Kapillarelektrophorese-Massenspektrometrie (CE-MS) realisiert.

Um Massepotential an einen Kanal des zweidimensionalen Aufbaus, z.B. wenn Massenspektrometrie (MS) zur Analytdetektion verwendet wird, an Kanalquerschnitten des Interfaces zur Kontrolle der Elektromigration in Seitenkanälen einstellen zu können, wurde zusätzlich eine neue on-chip Potentialmessung integriert. Mit Hilfe einer SiN-passivierten Ti/Pt-Elektrode innerhalb des Chips in Kombination mit einem Niedrigstrom-Messprototyp (nA-Bereich) konnte die störungsfreie on-chip Potentialmessungen entlang der elektrophoretischen Trennstrecke erfolgreich durchgeführt werden.

Die intermediäre on-chip Fluoresezendetektion mit hoher Auflösung wurde über ein lineares Faserarray in Kombination mit der hyperspektralen Bildgebung mittels Pushbroom Imager implementiert. Hierbei wurden eine sehr hohe Empfindlichkeit sowie spektrale, örtliche und zeitliche Auflösung des detektierten Fluoreszenzsignals innerhalb des Chipkanals für Fluorescein-isothiocyanat als Modellanalyt erreicht. Abschließend wurde der Aufbau erfolgreich für einen 2D CIEF/CE-MS Assay mit Myoglobin als Modellprotein angewand. Hierbei wurden die beiden Trenndimensionen (CIEF und CE) zunächst separat mittels experimenteller und simulierter Trennungen optimiert. Durch die Integration des optischen Detektionsaufbaus konnte Analytverschleppung sowie Peakverbreiterung und resultierendes Peak-splitting eliminiert werden, was einen hoch kontrollierten Analytransfer zwischen beiden Trenndimensionen erlaubt.

1 Motivation

Multidimensional electromigrative separation techniques well meet the challenges of bioanalytical research, especially regarding sample and matrix complexity as they provide various separation modes. With respect to the rising complexity of bioanalytical samples regarding analyte and matrix constituents, one dimensional electrophoretic separation assays have a limited resolving power. Thus, comparable to gas and liquid chromatography, two-dimensional electrophoretic assays in the capillary format are intensively investigated with a special regard to on-line sample pre-treatment and enhancement of peak capacity.

In this work, a glass microchip was used as the interface for coupling both capillary separation dimensions. In the framework of this thesis a modular capillary-chip system is applied and further optimized regarding usability and method applications. One aspect will be the optimization of the glass chip interface regarding stability and on-interface (intermediate) analyte detection. To overcome limiting performance parameters like dead volume and capillary-chip connection, new chip interfaces will be introduced produced by Selective Laser Etching as a new and promising production process for microfluidic devices. The interfaces will be evaluated and compared to those made by the classical bonding process. The aim is to provide a nearly dead-volume free capillary connection using screw-tight fittings to fixate the capillary to the chip (**Section 3.1**).

Regarding multidimensional electrophoretic separations a general challenge is the control of the leakage of sample constituents and band broadening at the channel intersections in microchips or capillary-chip interfaces, which can be achieved using fixed bias or pullback potentials. However, this is not possible for electrophoretic separations performed in a non-uniform background electrolyte like isotachophoresis and isoelectric focusing. To be able to measure the cross section potential, a novel approach was tested using a passivated electrode at the channel cross section of the interface in combination with a low current measurement device. To monitor and thus control potential variations at the cross section of the interface during electrophoretic separations, on-chip potential measurements will be conducted via a passivated electrode inside the chip interface (**Section 3.3**).

A defined transfer of the analyte from the first to the second separation dimension is one of the most crucial aspects by means of minimizing band broadening, transfer timing and ensuring compatibility of both separation dimensions. In this regard intermediate analyte detection is of crucial interest for an optimized sample transfer step, especially for

heart-cutting as the preferred sample transfer method for electromigrative separation techniques. Following a previous study [Kler, 2014], where contactless capacitively coupled conductivity detection was implemented on the chip interface, instrumental development will focus on implementing optical detection on the interface using a light emitting diode (LED) as excitation light source. With respect to the low volumes dealt with in capillary electrophoresis, fluorescence detection will be realized to reach desired sensitivity for analyte detection directly inside the chip interface. In order to monitor analyte movement in the chip, I aim at an imaging technique using spatially and wavelength-resolved signal detection (**Section 3.4**).

The 2D setup will be applied to couple capillary isoelectric focusing (CIEF) to mass spectrometry (MS), as the direct CIEF-MS coupling is still challenging due to the high number of MS-incompatible carrier ampholytes (CAs). New coupling strategies are of interest for the characterization of proteins and peptides especially for R&D and quality control of monoclonal antibodies. In this thesis, a second CE separation dimension will be implemented to separate proteins from the CAs prior to the MS detection. For a very precise heart-cutting and ideal CIEF analyte positioning in the chip as well as the separation of the protein from the ampholyte fraction within the second CE dimension, computer simulations and experimental data will be used complementarily and discussed (**Section 4**).

First proof of principle experiments will be conducted using a CIEF/CE-MS setup to separate analytes from carrier ampholytes in the second CE dimension before MS detection. Sequential and single heart-cutting experiments using myoglobin as a model analyte will be implemented to cut portions of the CIEF pH gradient and detect the model protein after second dimension CE separation with the MS. The optimization of the sample transfer regarding carryover and peak broadening will be achieved by monitoring and therefore controlling the IEF focused protein plug via intermediate on-chip LED induced fluorescence (LED-IF) detection within the common intersection of the interface (**Section 5**).

The main contribution of the work will be in the field of instrumental development for 2D electromigratve separation techniques with a special focus on novel interface design and on-interface analyte detection strategies as well as the application of the setup for CIEF/CE-MS assays.

2 Introduction

Multidimensional electrophoretic separations represent one of the most powerful tools for dealing with the complexity of the analytical and bioanalytical problems the scientific community is currently facing. This complexity arises from the combination of the number of compounds to be analyzed with different physicochemical properties (sometimes thousands), the diverse composition of the biological matrices where the analytes are present, and the broad range of possible concentrations that can span six to ten orders of magnitude [Zhang, 2013]. Under these analytical conditions, that are typical in proteomic and metabolomic studies, sample pretreatment is mandatory to eliminate unwanted matrix components (interfering solutes and inorganic salts, among others), to normalize concentrations and enhance separation performance, to improve both selectivity and sensitivity [Valcárcel, 2001]. Historically, two-dimensional electrophoretic separations have been one of the favorite tools for dealing with complex biological samples due to their separation capabilities [Smithies, 1956]. An example of this, is 2DGE [O'Farrell, 1975] used extensively in studies on protein expression, peptide mapping, and also in different metabolomic studies [Cooper, 2004]. Despite its popularity, its high selectivity and sensitivity, 2DGE as it is performed today involves manually intensive steps: casting of gels, application of samples, running, and staining of gels; all of them are time-consuming tasks that conspire against the reproducibility and quantitative reliability of the method, as well as the possibility of automation. Moreover, the combination of 2DGE with MS, the most effective and promising identification technique, is extremely problematic and inefficient [Kăsička, 2014]. All these problems are also common to most off-line sample pre-treatment techniques. In contrast, column-based electrophoretic separations offer impressive separation efficiency, the possibility to easily change separation conditions to account for different physicochemical properties of the molecules, a high compatibility with several detection methods based on electrical, optical (visible and UV range), and electrochemical properties of the analytes, and excellent coupling performance with MS detection [Geiger, 2011]. Then, electrophoretic separation techniques offer a unique chance for obtaining high throughput, automatic analysis of biomolecules, using a complete set of very powerful separation techniques (CE, IEF, ITP, MEKC, CEC, among others) that can be combined in multidimensional methods as well as with MS detection, in order to obtain a new generation of analytical tools that are able to satisfy the current analytical needs of the growing

proteomics and metabolomics sciences. The most obvious problem that arises when trying to combine column-based electrophoretic methods is the fact that columns (usually fused silica capillaries) are inherently one-dimensional. The most important question is how to implement efficient interfaces to combine the separation performance of individual 1D electrophoretic techniques in a 2D format, keeping the separation performance also in the column-coupled system compared to a naturally two-dimensional method, such as 2DGE, for the on-line analysis of proteins and peptides [Gebauer, 2011; Malá, 2013]. From a practical point of view, 35 years ago, Everaerts et al. [Everaerts, 1979] proposed a system for the analysis of small anions via the combination of two isotachophoretic separations performed in narrow-bore tubes in order to surmount the shortcomings of 2DGE and take advantage of the capabilities of column-coupling electrophoretic methods. This pioneer work revealed the advantages but also the challenges of implementing 2D separations in column-based methods. Since then, several attempts were made in order to develop coupling systems that enable efficient combination of 1D electrophoretic methods and suitable detection systems.

2.1 Sampling strategies for multidimensional electrophoretic separations

In multidimensional electrophoretic separations, four different strategies regarding sampling are frequently encountered: comprehensive one-step sampling, comprehensive multi-step sampling, heart-cut multi-step sampling, and heart-cut single sampling. Comprehensive refers to the transfer to the second dimension of the total sample that was injected at the beginning of the separation while heart-cut means that only a selected fraction of the separated sample is transferred from the first dimension to the second. Table 2-1 lists some common examples of practical applications of these sampling strategies. The influence of the sampling strategy on the degree of orthogonality is beneficial in the case of heart-cut-single sampling allowing the successful coupling of two methods with low degree of orthogonality, for example CE-CE [Michels, 2002] at different pH values. Of course, this situation is not easy to achieve: very precise detection and transfer systems are needed. Another, favorable situation is the comprehensive multi-step sampling, but in this case the restriction is that the velocity of the second dimension has to be higher than the velocity of the first one. This is the typical situation in LC-CE coupling, with their very high compatibility of time scales [Gilar, 2005].

During the transfer of components from one to another separation dimension, additional band broadening will appear, particularly if this includes the transfer to a different column [Giddings, 1987]. Commonly, these transfer effects involve simple diffusion (which can be

minimized by decreasing the transfer time), advective dispersion due to heterogeneous velocity profiles, electrochemical dispersion due to differences in buffer conductivities or surface properties between columns [Posner, 2006], or more complex interactions between solvents with different levels of polarity (Marangoni effect) [Anderson, 1984]. All these effects are directly related to the relative dimensions of the peaks, the inner diameter of the separation columns, and the geometry of the interfaces, particularly the volume/surface ratios [Bings, 1999]. Then, band broadening effects are clearly more significant for smaller columns such as fused silica capillaries or microchannels and methods with a high peak capacity such as CE (compared to LC). Due to this, the optimization of interfaces in CE is by far much more critical than in LC, generating challenging technological problems that are discussed in the following sections.

Table 2-1: Practical examples of different sampling strategies used for multidimensional electrophorecic separations.

	one-step	multi-step
comprehensive	ITP-ITP, ITP-CE	LC-LC
heart-cut	CE-CE, IEF-CE	LC-CE, IEF-CE

2.2 Column-coupling strategies

The coupling strategy between columns has a strong influence on the overall performance of the analytical methods. One of the main factors is the sampling strategy, related to the decoupling of flows due to mechanical or electrical actuation. The benefits and drawbacks of the different strategies are discussed. Several column-coupling multidimensional electrophoretic separations are presented, but also some important approaches including one non-electrophoretic separation technique. These implementations were specially selected due to their technological importance in the development of more recent, or even future multidimensional electrophoretic separations [Issaq, 2005]. The section starts first with a historical note about the most popular implementation of column-coupling electrophoretic separations developed by Kaniansky et al. [Kaniansky, 1990], based on the original idea published by Everaerts at al. [Everaerts, 1979]. It evolved into commercial devices and enabled the production of a plethora of scientific work in coupled ITP-ITP and ITP-CE separations. The section then continues with a discussion on interfaces based on fused silica capillaries and microcolumns. These types of interfaces are clearly more abundant in the

literature due to the extended use of fused silica capillaries and their high capability to adapt to different detection methods. These interfaces include some commercial devices associated to LC, such as multiport sampling valves, or PEEK microTee couplers, but also customized interfaces based on the flow gating principle, dialysis junctions or etched porous interfaces, among others. Then a particular type of implementation that is growing especially for methods using MS detection will be discussed: hybrid systems, which include fused silica capillaries or microcolumns combined with microchips or microfabricated elements. They combine the advantages of standard capillaries, such as low cost and perfect integration with injection and detection systems, and the precision and efficiency of microchips for sample transfer. Finally, some very important microchip separations are discussed due to their influence on defining current and future trends in multidimensional electrophoretic separations and their integration to modern detection systems.

2.3   Commercial column-coupling ITP devices

As mentioned before, the first work on column-coupling electrophoretic separation was presented by Everaerts et al. in 1979 [Everaerts, 1979]. In this pioneer work, small anions were separated and detected using two conductivity detectors (one at each column end) and one UV detector (256 nm) located before the second conductivity detector. The total analysis time was 15 minutes for the ITP-ITP analysis of small acids in orange juice and human urine. Following a similar concept, in the mid 80's Kanianski et al. [Zelenský, 1984] developed a column-coupling commercial device known at the beginning as CS Isotachophoretic Analyzer [Chrambach, 1985]. This device is produced in Slovakia by the company Villa Labeco since 1992. The first research paper in the literature using this commercial device appeared in 1987, but only used a single column mode [Kaniansky, 1987]. In 1990, Kanianski et al. for the first time reported an ITP-CE analysis of nitrophenols and 2,4-dinitrophenyl-labelled amino acids [Kaniansky, 1990]. An identical device, the ItaChrom Isotachophoretic System, was produced by the companies Merck (Darmstadt, Germany) from 1997 to 1999, J&M (Aalen, Germany) from 1999 to 2006, and JH-Analytik (Aalen, Germany) since 2006, and mentioned for the first time in literature by Kaniansky et al. in 1997 [Kaniansky, 1997]. In these devices, columns are made from FEP or quartz, with the pre-separation (first) column of 0.8 mm ID, and variable ID and lengths for the analytical (second) column. The coupling is made by a T-shaped plexiglass element [Foret, 1992] including also two standard conductivity detectors (these are contact amperometric detectors,

optionally the devices are provided with C^{4}D detectors) and a UV (200, 220, 254, 280 nm) or UV-Vis photometric detector (190 - 600 nm) at the end of the analytical column. These isotachophoretic analyzers include dialysis membranes between the electrode compartments and the columns, to suppress the EOF and allow efficient dissipation of joule heat. The devices also incorporate a connection for an autosampler for automatic analysis. Since 1985 the CS Isotachophoretic Analyzer and the ItaChrom Isotachophoretic System were used in more than 300 reported scientific papers according to the google scholar website. The exhaustive list of all these publications (near 300) using these two commercial devices exceed the scope of this review, it can be found on the cited scholar searches or in [Valcárcel, 2001; Mikuš 2011].

2.4 Capillary and microcolumn based implementations

The implementation of column-coupling electrophoretic separations started in the early 90's but still grows today. During the 90's Jorgenson's group conducted extensive work on LC-CE separations [Bushey, 1990; Lemmo, 1993; Moore, 1995; Lewis 1997; Hooker, 1997]. They started with a computer controlled 6-port valve [Bushey, 1990], but quickly switched to the more efficient flow-gating interface [Lemmo, 1993] demonstrating the importance of having precise control of the coupling and sampling procedure beside the excellent analytical performance of the separation methods employed (LC-CE, RPLC-CE, SEC-CE). According to the authors, the flow-gating interface is advantageous compared to the loop-valve system since it eliminates sample collection, storing, and "out-flushing" between each analysis. The interface consisted of two stainless steel plates separated by a Teflon gasket, where the outlet of the chromatographic column (SEC microcolumn in [Lemmo, 1993]) was positioned directly near the inlet of the electrophoresis capillary. Normally, a transverse flow of buffer enters through the top port of the interface for flushing, sweeps through the channel, and exits through the bottom port. This flow of CE buffer carries SEC effluent away to waste, preventing transfer of sample to the CE capillary. When an injection is desired, the flush-flow is stopped, allowing the SEC effluent flow to inject sample into the narrow gap separating the SEC microcolumn and CE capillary. When desired injection time is completed, the transverse flow is resumed, terminating the injection process. The flow-gating interface minimizes dead volume compared to the sample loop valve, but also offers the possibility of a flexible and precise control of the injection of the sample to the second dimension. Jorgenson's group and other scientists have used this interface for the successful analysis of various proteins, protein

digests and small anions [Lada, 1995]. Following the idea of using transverse flows, Dovichi's group has developed several multidimensional electrophoretic separations using different implementations of this concept. The first interface was constructed by gluing four corners of a microscope slide for alignment of the separation capillaries (left and right) and the buffer refilling tubes (top and bottom), assembled between two intact microscope slides and fastened with epoxy glue [Michels, 2004]. This very simple construction was used for the analysis of a complex sample (protein homogenate from *D. radiodurans*) using LIF detection, and achieving excellent sensitivity in the range of zeptomoles. Although the setup of the interfaces refers to a similar concept (transverse buffer flow) there are some differences between the general strategies from Jorgenson and Dovichi. First of all, Dovichi used electrophoretic separations on both columns, which enabled them to transfer the whole sample plug (in one or several steps) from the first column to the second, which is impossible when performing LC-CE due to the differences on eluent flow and separation velocity of the methods. In the case of CE-CE, the transverse flow is used exclusively for refilling the second dimension with BGE and not for eluting sample excess [Michels, 2002; Evans, 2004]. The evolution of the Dovichi's interface continued, and they produced a set of very interesting interfaces that included enzymatic reactors with immobilized pepsin [Schoenherr, 2007], alkaline phosphatase [Wojcik, 2010], and trypsin [Li, 2011]: Proteins are separated in the first dimension by CE, digested in the reactor, and the cleaved peptides are transferred to the second capillary, where they are also separated by CE. While peptides generated from one digestion are being separated in the second capillary, the next protein fraction undergoes digestion in the microreactor [Schoenherr, 2007]. Following a similar construction, a diagonal CE-CE method is used for monitoring the phosphorylation status of a mixture of peptides. Diagonal CE-CE consists in the alignment of the two electropherograms (with and without reaction) on an x-y plot in order to detect spots out of the diagonal which include the modified (in this case phosphorylated) peptides. This implementation seems to be able to detect any post-translational modification as long as an immobilized enzyme (e.g. phosphorylase) is available to react with the modification under electrophoretic conditions [Wojcik, 2010]. This setup was used again for studies of post-translational modifications using MS detection [Mou, 2013]. The third enzymatic reactor incorporates a replaceable and more generic enzymatic microreactor for on-line protein digestion. In this system, trypsin is immobilized on magnetic beads. At the start of each experiment, old beads are flushed to waste and replaced with a fresh plug of beads, which is captured by a pair of magnets at the distal tip of the first capillary. Proteins are separated in the first capillary.

A fraction is then parked in the reactor to create peptides. Digested peptides are periodically transferred to the second capillary for separation and MS detection while fresh protein fraction is simultaneously moved to the reactor for digestion [Li, 2011].

More recently, a high precision alignment interface was developed. Here, a nicked sleeve capillary interface was built, using a sleeve capillary which was cut approximately halfway through its inner diameter, resulting in a nick that exposed the inner diameter of the sleeve capillary, while maintaining an adequate length of supporting capillary under the nick. The sleeve capillary was nicked using a micro-dicing saw and diamond blades. Only transfer efficiency was evaluated for this interface showing impressive results compared to the previous devices [Flaherty, 2013]. Additionally a 5-capillary interface was developed for multiplexed LIF sheath-flow cuvette detection. CSE-MEKC expression fingerprints were obtained from homogenates prepared from a lung cancer (A549) cell line. The interface was a micromachined polycarbonate block with guide tubes for capillary alignment, with a gap of 40 μm between columns of the first and second dimension [Zhu, 2007]. The group of van der Greef developed several implementations of two-dimensional electrophoretic separations, particularly ITP-CE. Using commercial equipment at the beginning (Isotachophor; LKB, Bromma, Sweden), they tested different combinations of column diameters and materials (PTFE and fused silica) [Stegehuis, 1991]. With this set of experiments they confirmed the postulate that a self-stacking technique such as ITP considerably reduces the band broadening due to the sample transfer to the second dimension. Additionally, in order to improve the performance of their method (by reducing the ID of the CE capillary) they developed a T-shaped polyethylene interface for connecting three capillaries [Mazereeuw, 1994]. Using this setup, this group has also demonstrated successful developments for EE-ITP-CE [van der Vlis, 1995] and ITP-CEC [Mazereeuw, 2000] showing excellent performance for the analysis of important biogenic amines. Another very elegant implementation of ITP-CE was conducted by Bowerbank et al. [Bowerbank, 2001; Peterson, 2003], who produced a quartz coupling element. The interface was custom-made by Innova-Quartz (Phoenix, AZ, USA), with the capillaries fixed with epoxy glue. When the capillaries broke, the interface was submerged in acetone in order to reuse it. The surface similarity between the fused silica capillaries and the quartz interface enabled the use of commercial coatings for suppressing EOF and reduce adsorption of biomolecules. This interface was used to perform ITP-CE using UV [Bowerbank, 2001] and MS [Peterson, 2003] as final detection methods for the analysis of angiotensins.

A particular case of multidimensional separations are those that include IEF. This technique is acquiring more and more popularity in the scientific community due to its excellent properties on separation and preconcentration of proteins and peptides. Mostly, IEF is the first dimension due to the fact that the ampholytes used for generating the pH gradient interfere severely with many detection systems, particularly with ESI-MS. For this reason several groups have implemented combinations of IEF and LC. Due to the high orthogonality between these methods, the combination of the equipment necessary for the coupling is extremely complex including up to three 10-ports valves and several sample loops, requiring highly complex flow control systems [Chen, 2003; Zhou, 2004; Stroink, 2005; Zhang, 2006B; Kulka, 2006; Kang, 2006; Wei, 2011]. More interesting are those 2DCE separations that include IEF. For example, in 2002 Mohan et al. presented a coaxial arrangement of two capillaries coupled via a dialysis tube for a comprehensive multi-step IEF-tITP-CE analysis of different enzymes [Mohan, 2002]. The two separation capillaries were butted together inside a 7 mm length polysulfone dialysis tubing (nominal molecular weight cutoff of 10 000 Da) and secured with epoxy glue. The dialysis tube enables the intermediate electric connection and the dilution of the ampholytes in acetic acid prior to the CE separation in order to enhance the detection via UV [Mohan, 2002] or MS [Mohan, 2003].

Similar implementations of this idea, but using a rigid PMMA reservoir and a hollow fiber was developed by Yang et al. performing IEF-CE of ribonuclease [Yang, 2003A] and IEF-CGE of different types of hemoglobin [Yang, 2003B]. Especially, the study shows the advantages of the two-dimensional method over the independent 1D methods for the separation and detection of the studied proteins demonstrating a clear enhancement of the separation efficiency. In a subsequent work, Liu et al. performed IEF-CGE of protein mixtures excreting from lung cancer cells of rat using the same interface [Liu, 2005].

Another interesting work from this research group is the development of a porous etched interface. This is not strictly a column-coupling method, because only one capillary is used, but it is included here due to its simplicity and effectiveness. The interface is fabricated by etching a short segment in the center of a fused silica capillary tube with HF to produce a porous area to enable electric contact between inner and outer regions, and selective diffusion of small molecules. This zero dead volume interface was tested and characterized performing IEF-CE experiments with myoglobin and hemoglobin as model samples using UV detection [Liu, 2004]. This porous etched interface was extensively characterized for its use in multidimensional electrophoretic separations in a more recent work [Wu, 2012]. An

application example was presented by Wang et al. who developed an IEF-CE analysis of proteins extracted from milk [Wang, 2011]. The particular feature of this implementation was the monolithic immobilized pH gradient that avoids the use of mobile carrier ampholytes for performing IEF. Although possible, to our knowledge this strategy was not yet used for coupling to MS detection. Similar to the porous etched interface, Zhang et al. developed a microhole interface for performing CE-MEKC separations of cardiovascular drugs [Zhang, 2009]. Prior to the CE separation they performed on-line preconcentration procedures such as pH junction and sweeping to reduce the sample zone broadening at the interface. The microhole (30-40 μm) was drilled in the middle part of a PTFE tube of 300 μm ID. Then, the capillaries for the separation were inserted while hot air was blown in order to shrink PTFE tubing ID to the capillaries OD (360 μm). The gap between the capillaries was adjusted to the microhole diameter. An eppendorf tube and a platinum wire were used as reservoir and electrode respectively. The combination of CE and MEKC in the 2D separation showed clear advantages on separation efficiency compared with the individual methods.

Another simple, but very effective interface was developed by Sahlin et al. using tangentially connected capillaries: two bi-layer PTFE-FEP tubes were melted jointly at the cross intersection with the help of two tungsten wires, four capillaries (75 μm ID) were coupled to the melted PTFE-FEP tubes to configure a four branches fluidic circuit [Sahlin, 2007]. A tryptic digest of BSA was analyzed by CE-CE with a comprehensive multi-step procedure, no intermediate detection was used. Although the assay was successful, it is clear that the 3D nature of the fluid and sample flow, and the heterogeneous surface properties generated significant distortions of the peak shape of the analytes detected with UV (225 nm).

An alternative for the enhancement of sensitivity and separation efficiency of electrophoretic separations is the coupling to preconcentration techniques. Although they cannot fully count as multidimensional electrophoretic separations, due to their current importance in the analysis of samples present in complex matrices and trace analysis, in what follows some important studies of column-coupling preconcentration for electrophoretic separations are described. Electrochemical preconcentration was coupled successfully with CE using a very complex interface consisting of an electrochemical flow cell with the CE capillary precisely aligned to the working electrode [Lopes, 2010; Lopes, 2011]. Despite the laborious and the critical alignment process, the method was successfully tested for the analysis of metals. Due to its performance, the authors claimed that this EPC-CE assay is a potential alternative to atomic absorption spectrometry or inductively-coupled plasma techniques for trace analysis of toxic heavy metals. For finishing this section, another strategy that is explosively growing

is on-line SPE. This (non-electrophoretic) technique enables relatively large sample loadability. The analytes are retained by the solid phase and accompanying compounds, e.g. salts, can be removed. Upon desorption of the analytes from the column with an eluting solvent, the analytes can be concentrated in a small volume plug, leading to low detection limits [Tempels, 2006; Puig, 2007; Jooß, 2013; Lee, 2009; Lee, 2011].

2.5 Hybrid systems

Despite the outstanding analytical performance of some of the interfaces that have been discussed in the previous section they still show clear drawbacks due to: (i) their dead volume, maximized when the multiport LC valves were used, (ii) the heterogeneous surface properties of the systems where PTFE or other polymer tubing were used in combination with fused silica capillaries, (iii) and the intricate velocity profiles produced when complex 3D structures are employed as interfaces. The presence of any of these characteristics decreases the efficiency of the separation methods by increasing the broadening of the analyte bands that are transferred from the first dimension to the second. Although these characteristics are present for several interfaces, they are not critical in the overall performance of some previously shown separation methods: particularly, when LC is performed as first dimension, only a fraction of the LC sample peaks are transferred (normally a portion near the center of a Gaussian distribution), and the broadening of these fractions is still acceptable due to the statistical properties of the sampled peak. Additionally, this situation clearly illustrates the difference in the characteristic scales of chromatographic and electrophoretic methods. While for LC it is possible to use valves and loops with dead volumes in the order of nanoliters, in electrophoretic methods this is not acceptable. Nevertheless, this difference in sample volumes has its correlation in terms of analysis time, being those much longer for LC. It is thus mandatory to consider the microfluidic nature of CE, and, consequently, develop interfaces with much more precision lowering the dead volumes to the range of picoliters. At this point microfabrication configures itself as an alternative for improving the performance of column-coupling multidimensional electrophoretic separations. In the next two sections, we discuss multidimensional separations that were developed using microfabricated elements. In this section we focus on hybrid systems, i.e. implementations using standard capillaries or microcolumns combined with microfabricated structures.

The need of developing hybrid systems grounds on the tradeoff of improving the interface to the level of the microscale fabrication to minimize the broadening effects during the sample

transfer process, and the fact that capillary-based systems can work with standard equipment in terms of pressure and voltage regimes, as well as the integration with commercial equipment such as autosamplers and detection systems. In this sense, the first hybrid developments were created for coupling CE separations performed on chips with MS detection whose capillary-based CE-ESI interface is well established and validated. For example the works of Figeys et al. [Figeys, 1998] and Zang et al. [Zhang, 1999; Zhang, 2000] focus on this kind of coupling using glass microchips for the separation and ESI-MS for the detection of peptides. In these cases the uniform surface properties of capillaries and glass microchips enabled the coating of the systems to avoid peptide adsorption. In the end of the 90's, Harrison's group presented several studies for optimization of chip-capillary connections, recognizing the problems of dead volume of the connections, the importance of the surface properties, and the difficulties of direct connection of chips with MS [Bings, 1999; Li, 1999]. The developed interfaces were tested and compared by performing tITP-CE-ESI-MS analysis of amino acids and CE-ESI-MS/MS of tryptic peptides from *P. sativum* lectin digests. It is well known that microfabrication in glass is laborious and the sealing of the wafers is problematic [Madou, 2002]. As an alternative, fabrication methods in soft polymers such as PDMS have attracted much attention from the scientific community. Although, PDMS chips present several drawbacks for performing electrophoretic separations such as its highly hydrophobic surface, its low capacity for heat dissipation, and poor optical properties, many examples of electrophoretic separations have been implemented using this polymer. The main benefits of PDMS are its simple manufacturing process and its excellent capability for sealing interfaces, which configures this material as being favorable for hybrid implementations [Chiou, 2002]. For example, Samskog et al. [Samskog, 2003] presented a very simple protocol for the microfabrication of a PDMS interface, using two cross capillaries and a Petri dish for casting the PDMS. Despite its simplicity, the interface presented several problems related to the hydrophobic adsorption, and the electrolysis on the surface of the intermediate electrode. The coupling to the MS through a capillary was successful for the detection of methionine-enkephalin, neurotensin and substance P. The same research group used this interface for performing LC-CE-ESI-MS for the analysis of BSA tryptic digests [Bergström, 2006] and leucine-enkephaline [Bergström, 2003]. An implementation that became extensively used was presented for the first time by Yang et al. in 2003 [Yang, 2003; Zhang, 2004]. The idea was to perform LC in the classical way, and couple the LC column to a microfluidic chip for performing the sampling using a microfabricated interface (cross microchannels in this case), then perform the CE separation

as second dimension, and finally the detection using optical [Yang, 2003] or MS [Zhang, 2004] techniques. In these cases, the LC column was fastened to the CE chip simply using PTFE tape. Following a similar concept, Ramsey's group presented a setup for performing mapping of post-translational modifications of complex biotherapeutics [Mellors, 2013]. In this case they characterized the N-linked glycosylation of a monoclonal antibody by glycopeptide mapping using an LC-microchip(CE-ESI)-MS implementation. In contrast to other works, the coupling of the CE and ESI-MS was directly performed on-chip, including a sheath liquid channel in the glass microchip. Analogously, C. Skinner implemented a gel filtration chromatography interfaced with sub-micellar SDS-CE for on-line multidimensional separations [Skinner, 2010]. An alternative interface, where two capillary inlets were moved in continuously filled with sample or BGE streams, was developed demonstrating the potential (and complexity) for multiple array LIF detection. The system was tested by analyzing FQ-fluorescently labeled serum components. An outstanding hybrid implementation was proposed by Lu et al. for performing IEF-CGE with a close emulation of 2DGE, in capillary format [Lu, 2012]. Their implementation consists of an arrangement of three microfluidic chips: one for coupling the IEF capillaries, one for coupling the multiple CGE capillaries and one for switching the columns between the two separation modes. The main drawback of this implementation is the critical alignment of the chip used for switching separation dimensions in order to maximize the transfer efficiency. This was achieved with a micropositioner, but without any automatic closed-loop control, which means that the user has to decide on every measurement which is the right relative position of the chips. This interface was tested with a protein mixture containing ß-lactoglobulin, trypsinogen, ovalbumin and BSA, detected via LIF.

Another promising hybrid implementation was presented recently by Kler et al. [Kler, 2014] using glass microchips for coupling commercial fused silica capillaries for implementing ITP-C^4D-CE-ESI-MS. The advantages of this implementations ground on the use of similar surface properties for the capillary network and the interface, as well as the possibility of using commercial equipment for detection, control of injection, pressure, and voltage regimes. Another interesting fact is the complete exibility for selecting different lengths and inner diameters (IDs) for each capillary in the system enabling, for example, the use of higher ID for ITP to enhance loadability, and smaller ID for CE to increase resolution. Detection was performed using standard C^4D capillary heads and commercial CE-ESI-MS interfaces. The coupling of the capillaries with the microchip was achieved through powder-blasted holes in the glass chip with a precise diameter to minimize the space between capillaries and

glass wall [Tiggelaar, 2007]. Capillaries are fixed with epoxy glue to cover this gap and reduce the dead volume to a few picoliters. This interface was successfully tested for the separation and detection of four types of human angiotensins, using a comprehensive one-step (back-cutting) sampling strategy. The method employed C^4D intermediate detection for the ITP, and MS detection for the final CE separation [Kler, 2013A].

2.6 Some important microfluidic chip implementations

Since the use of microfabricated structures for analytical applications was proposed by Manz et al. in the early 90's [Manz, 1990], almost any kind of analytical separation technique has its counterpart on a microfluidic platform. We here consider some of the microfluidic platforms that have been important for the development of two-dimensional electrophoretic separations in general. Their study enables us to understand future trends of these separations and the key technologies involved such as detection systems, coupling techniques, etc. A more exhaustive analysis on the implementation of multidimensional electrophoretic separations on chips can be found in several excellent reviews [Kăsička, 2014; Tia, 2009; Kaniansky, 2003; Gao, 2013; Guihen, 2014].

As shown in the previous sections, one of the main goals of scientists working on multidimensional electrophoretic separations has always been to transfer classical 2D IEF-PAGE into a column format, ideally with multiplexing. In contrast to the fact that a direct implementation of this method with spatial sampling is impossible using capillaries or microcolumns due to the high number of necessary elements, in a microchip, the simultaneous manufacturing of hundreds of columns in a reduced area is possible. In this sense, Becker et al. [Becker, 1998] packed 500 columns for performing the second dimension of an IEF-GCE assay. The first separation dimension consists of a single channel, 16 mm long, 80 μm wide and 37 μm deep; the second separation dimension of an array of 500 channels, 5 mm long, 900 nm wide and 36 μm deep. The channels were fabricated using reactive ion etching under maximum anisotropic etching conditions, yielding an aspect ratio of up to 5 for the narrow channels. The use of PDMS and soft lithography techniques was also extensively employed for multidimensional electrophoretic techniques, e.g. by Chen et al. [Chen, 2002]. They presented a complex 3D network of microchannels including vertical structures for performing 2DGE. Here, it was clearly shown, that despite its convenient fabrication costs, PDMS is neither a suitable material for working with proteins (suffering selective adsorption) nor with high electric field strengths due to its low heat

dissipation capacity. The wish of implementing 2DGE on chips continuously grew, and Emrich et al. [Emrich, 2007] presented another version of multichannel on-chip 2DGE. They manufactured a two-layer borosilicate glass microdevice consisting of a single 3.75 cm long channel for IEF, which was sampled in parallel by 20 channels effecting a second-dimension separation by CE. They tested this design performing separations of complex cellular protein mixtures produced by *E. coli*. Detection was performed with a Berkeley rotary confocal scanner with laser excitation at 488 nm. Despite its apparent success, the importance of MS detection for proteomics and metabolomics studies was admitted as well as the difficulties of combining this detection system to 20 output channels. Another implementation of IEF-CE was developed by Herr et al. but using a simpler setup, using LIF detection for heart cut sampling into a single second column [Herr, 2003]. In contrast to the three strategies described so far, this implementation inspired several microchip and capillary implementations of IEF-CE and IEF-CE-MS that can be found in the literature of the last 10 years [Tia, 2009]. In terms of ITP-CE, of course the Kanianski group continues their excellent work implementing such techniques on chips [Kaniansky, 2000]. Here, C^{4}D and MS detection systems were more efficiently coupled, compared to the commercial column-coupling device, and such developments are still part of the research activities of the group and collaborators including novel CE-CE separations [Smejkal, 2013]. Other techniques that have been implemented for the first time on chip and continue being developed particularly on hybrid systems were proposed by the Ramsey's group for MEKC-CE [Rocklin, 2000] and open channel electrochromatography-CE [Kutter, 1998]. In this case authors manufactured the chips on glass and employed LIF at two detection points. A clear advantage of microchips is their ability to integrate efficient microelectromechanical structures such as microvalves, as was presented for the first time for multidimensional separations by Wang et al. [Wang, 2004]. In their work IEF-CE and IEF-GCE were successfully implemented. In contrast to their ability to integrate different components, these complex systems required special devices for controlling microvalves and pressure regimes as well as highly skilled operators, and other particular laboratory characteristics restricting its extensive or routine use.

2.7 Intermediate detection methods

Regarding multidimensional electrophoretic separations the implementation of intermediate detection methods in the respective interface offers the possibility to both construct the first

axis of a 2D analysis for a comprehensive sampling method and to greatly facilitate sample transfer especially for heart-cut sampling experiments. By observing the analyte of interest during the sampling procedure from the first into the second dimension the transfer procedure can easily be controlled and optimized regarding co-migration of analytes, matrix removal and even leakage phenomena occurring at the interface and therefore increase the selectivity and sensitivity of the second separation step and final detection method, respectively. Contact and contactless (C^4D) conductivity [Kaniansky, 2000; Kubáň, 2004], optical UV-Vis [Végvári, 2002] and LIF [Mao 2003; Mao, 2006], electrochemical [Zhang, 2009] detection methods are already successfully integrated into multidimensional electrophoretic separation setups. Applications are for example contact conductivity and C^4D detection in the case of ITP/ITP and ITP/CE assays. UV-VIS and laser or LED induced LIF detection are extensively used in CE/CE and LC-CE setups but also for ITP/CE or FIA/CE applications, depending on the analytical detection strategy. Regarding CIEF and CIEF/CE applications electric current detection is already used for determining the time point where the ampholytes and proteins are focused after the detected current exponentially decreased to a steady state minimum normally in the µA range. Regarding single column CIEF also whole column detection is already mentioned in the literature and also successfully implemented e.g. in the iCE analysers of ProteinSimple.

3   Instrumental development

3.1   Interface design

Previously [Kler, 2013A; Kler, 2014], the working group introduced a modular two dimensional ITP/CE-MS setup for the analysis of human angiotensins and amino acids with intermediate on column conductivity detection. Here, a glass microchip was used as the interface for coupling both separation dimensions. The benefit of the glass chip interface for coupling glass capillaries is the very low dead volume, as well as the same surface properties of the interface compared to the silica surface of the glass capillaries traditionally used in capillary electrophoresis separations as mentioned in the introduction. In this PhD thesis the goal was to further develop the chip interface [Kler, 2013A; Kler, 2014] with regard to the optimization and implementation of different intermediate detection techniques e.g. optical (LED-IF), conductivity (C^4D) and potential detection for a better control of the sample transfer from the first to the second separation dimension. Furthermore, the interface was improved for an optimal sensitivity regarding these aforementioned intermediate detection techniques, while ensuring mechanical long-term stability and ease of connecting the separation capillaries in the 2D separation setup. The improvements for accomplishing these requirements as well as general sample transfer strategies are discussed in detail in the following sections.

Additionally, intermediate optical detection was implemented on the chip interface using a high power LED at 455 nm. First proof of principle applications of a 3D spatial and wavelength-resolved on-chip intermediate fluorescence (LED-IF) detection setup for the hybrid 2D capillary-microchip setup was achieved. Potential future applications are ITP/ITP, ITP/CE, CE/CE and IEF/CE assays in combination with MS as final identification method.

3.1.1   General introduction: chip interfaces

Regarding multidimensional electrophoretic separations one of the most crucial aspect is the interface for coupling the different separation capillaries to perform the respective consecutive separation dimensions (see introduction). The volumes of the columns, and consequently of the injected sample, are in the µl or even nl range and therefore significantly smaller compared to other separation techniques such as Liquid Chromatography (LC). Thus, the coupling interface between two separations channels must be very efficient in terms of

providing geometrical precision with low dead volume. Likewise, very sensitive detection methods are required for intermediate as well as final analyte detection. Additionally, in electromigrative separation techniques the surface properties of the columns play a fundamental role for electroosmosis as well as the undesired adsorption of proteins or other biomolecules. In this sense, the requirements for a suitable interface for an efficient coupling of electromigrative separation techniques has to take microfluidic effects and physicochemical interactions of the electrolyte solutions and analytes with the capillary walls into account [Kler, 2015], especially when the surface properties of separation columns and interface are different due to the choice of materials. Meeting these requirements, Kler et al. [Kler, 2013A] introduced a glass microchip for interfacing multidimensional electrophoretic separation in 2013 (see Figure 3-1). The glass chip interface has similar surface properties as the fused silica capillaries coupled to it, as well as a very low dead volume resulting in excellent peak performance comparable to that of an intact capillary. Due to the similarity of surface properties, the native electroosmotic behavior across the interface is similar to the one in capillaries due to nearly undisturbed electric field lines during separations. The same is valid in case of capillary and interface surface modifications via coatings. The capillary to chip sealing is achieved via an optimized gluing step, resulting in the desired very low dead volume. In the following, the basic design of the chip interface and its further optimization is presented and discussed in more detail.
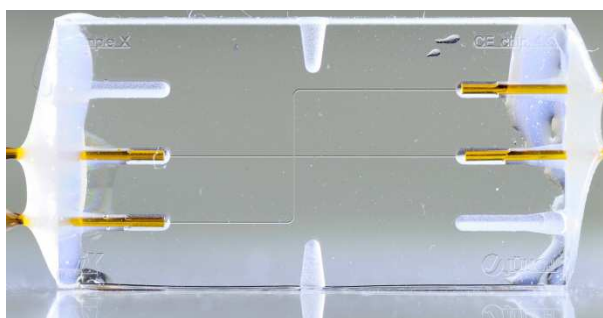
Figure 3-1: Example of the bonded glass microchip made by iX-factory (Dortmund, Germany) with a cross channel arrangement used as capillary interface for multidimensional electrophoretic separations. The chip dimensions are $20 \times 10 \ mm^2$.

3.1.2 Specifications of the 1st generation chip design

The microfluidic glass chip interface produced by ix-factory was constructed following a work by Tiggelaar et al. [Tiggelaar, 2007]. Briefly, as a first step a photomask with the desired microfluidic channel geometries is created. Then, the photomask is placed on a

coated wafer of BOROFLOAT 33 glass from SCHOTT Technical Glass Solutions (Jena, Germany) and is exposed to light; the desired channel structures are then etched with hydrofluoric acid (HF) into the bottom plate of the glass wafer. Finally, the cover plate glass wafer is bonded to the bottom plate wafer forming the respective channel structures of the glass chip. The lid plate glass wafer can have different thicknesses as discussed in Section 3.1.4. Afterwards, the chips are isolated from the bonded wafer by dicing with the dimensions of 20 × 10 mm. The resulting semi-cycle shaped chip channels are 25 µm deep and 60 µm wide with a volume of approximately 20 nl per cm as shown in Figure 3-2. The chip channels can be connected to all conventional fused silica capillary formats with an outer diameter of 360 µm via powder-blasted side-accesses for the capillaries called capillary cups or chip ports.
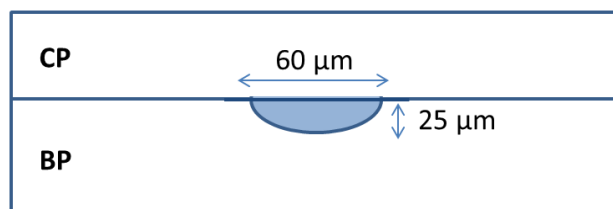
Figure 3-2: Schematic drawing of the general semi-cycle shaped chip channels with 25 µm deep and 60 µm wide channels in the glass chip interface, cover plate (CP) and bottom plate (BP).

To seal the interface region between the chip port and the respective capillary a previously developed gluing process was applied [Tiggelaar, 2007] resulting in a very low dead volume as mentioned before. The low dead volume in the low pl range (~ 20 pl), depends on the depth of the glue front introduced into the chip port as shown in Figure 3-3. The resulting dead volume (V_{DV}) can be further reduced by introducing the glue front (GF) deeper into the capillary cup (c) without blocking the capillary (a) or the channel (b) present in the chip cup. For the chip interface different channel layouts inside the chip were designed to create a modular interface with channel geometries adaptable to the analytical coupling or transfer question. Figure 3-4 shows the different chip configurations used in this thesis. The parts colored in green on the left/right side are the powder-blasted chip cups housing the capillaries as well as an adapter for the potential measurement electrodes (see Section 3.3). The purple structures represent the HF-etched chip channel geometries. Regarding the inner HF-etched fluidic chip channel structure different configurations were designed to meet the desired highly modular approach for the junction for different separation or flushing protocols in the 2D assays. Depending on the complexity of the analytical separation strategy and therefore

the desired coupling of the separation channels, different channel geometries within the chip interface were designed.
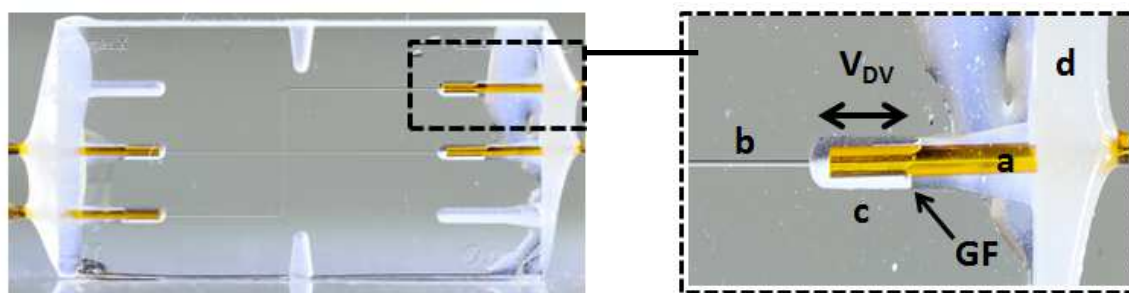
Figure 3-3: Detailed image of the capillary (a) to chip channel (b) connection via the chip cup (c). The resulting dead volume (V_{DV}) of ~ 20 pl of the interface is determined by the penetration depth of the glue front (GF) of the used epoxy glue (d).

The structures include T- and cross- configurations of the chip channels as well as their combinations with and without a common intersection segment (V_c) connecting all channel layouts to one channel section. This common intersection channel segment can be used as the heart-cut injection volume from the first to the second separation dimension see Section 5. To keep the chip production as cost-efficient as possible the general chip appearance was constructed in a way that it is independent from the number of implemented ports and the applied channel geometries and therefore the used production mask was as simple as possible. Thus, the production costs were reduced, while having the highest possible variablility of the interface regarding the 2D applications, for potential future applications. Following this approach, every chip was constructed to house up to 6 capillaries, as visable from the 6 capillary ports (P1 – P6), although only some of them are connected to chip channels (P1 up to P4), depending on the respective chip layout. To reduce band broadening of analytes during the transfer step from the first to the second separation dimension, the general migration path of a respective analyte plug or zone was chosen to be always straight through the channel [Paegel, 2000; Molho, 2001] of the interface as illustrated in Figure 3-5. In the 1D mode the sample zone (S) migrates straight forward (blue arrow) from the 1D separation capillary into the interface following the direction of the applied separation potential (black arrow). When the analyte reaches the channel cross section the potential is switched to the 2D mode and the analyte follows the applied potential difference of the second dimension always migrating straight forward throughout both separation steps, as indicated by the blue arrow. This migration strategy was applied for all 2D assays.

For first 2D experiments using the described single-T glass chip interface (see Figure 3-4A), Kler et al. [Kler, 2013A] coupled isotachophoresis (ITP) with on capillary C^4D detection to capillary electrophoresis (CE) with mass spectrometry (MS) as the final detection method. In the following this coupling is referred to as ITP-C^4D/CE-MS.
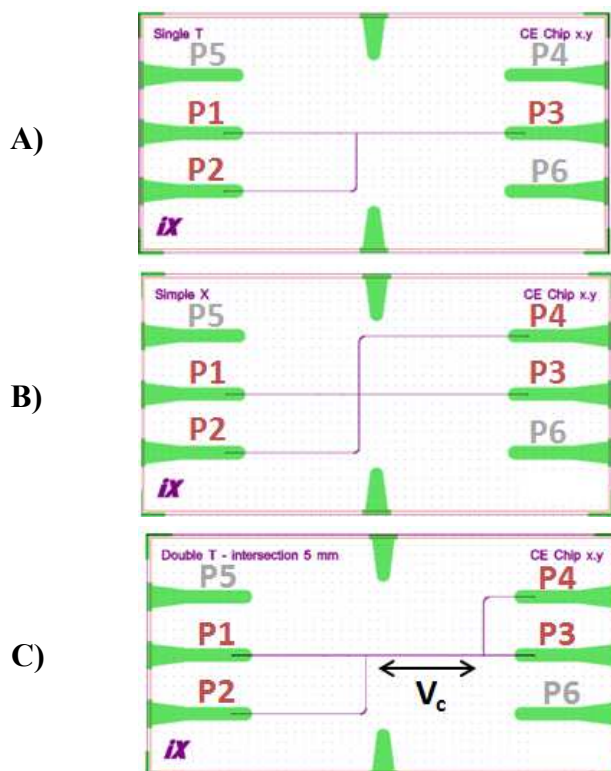
Figure 3-4: The different chip configurations used in this thesis, P = (chip) port for capillary connection - grey ports not connected to chip channels, V_c = volume of common intersection. A) 3-port single-T, B) 4-port chip with single X-interface and C) 4-port chip with double T-interface with 5 mm common intersection segment length (V_c = ~ 7 nl). Green colored parts = powder blasted chip cups housing the separation capillaries as well as placeholder on the top/bottom for the integration of potential measurement electrode; purple structures = HF-etched chip channel geometries and red lines = chip dimension after dicing. Modified CAD drawings from iX-factory (Dortmund, Germany).

In this first work the chip interface was evaluated in comparison to a commercially available PEEK micro-T interface from IDEX Health & Science (Wertheim, Germany). Three cationic compounds were separated: norharmane and histidine as a fast and closely migrating analyte pair and phenylalanine as a slowly migrating analyte in a 10 mM ammonium acetate running buffer at pH 4.5. The work revealed the impressive performance of the chip interface regarding peak performance being comparable even to an intact capillary, due to the previously discussed very low dead volume and similar surface properties of the interface and the capillary surface.
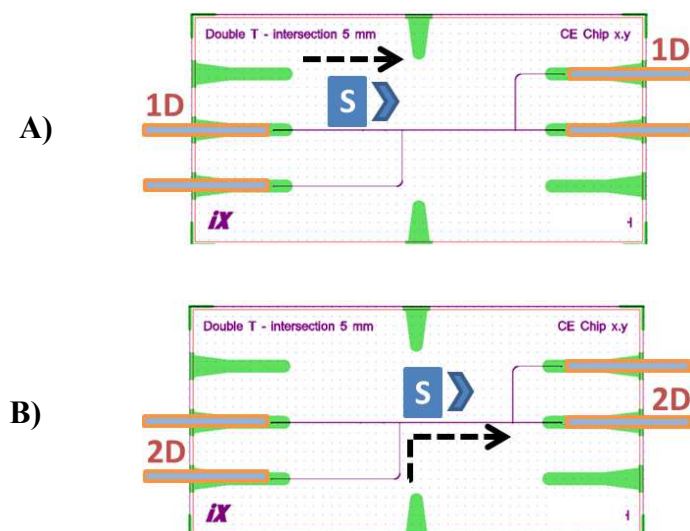
Figure 3-5: Schematic description of the sample plug transfer from A) the first (1D) to B) the second (2D) separation dimension, using only straight migration paths inside the glass chip interface for the sample zone (S). Black arrows = direction of the applied electric field, blue arrows = migration direction of the analyte plug zone. Modified CAD drawings from iX-factory (Dortmund, Germany).

Finally, the glass chip interface was used to perform ITP-C^{4}D/CE-MS analysis of 4 human angiotensins, using ITP in the preconcentration mode for on-line concentration of different concentrations of the angiotensins with excellent peak and enrichment performance of the setup. For these experiments a first generation 3-port chip was used with a large cover plate thickness of 1000 µm with on-capillary C^{4}D detection shortly before the chip interface for monitoring the time point when the analyte is in the desired region of the interface to enforce the plug transfer from the first to the second separation dimension. To further optimize the interface, intermediate on-chip detection methods were implemented for a better controllable sample transfer.

3.1.3 Implementation of intermediate on-chip detection methods

First 2D experiments [Kler, 2013A] were conducted using on-column C^{4}D detection for the determination of the time point for switching for the transfer of the sample band from the first to the second separation dimension. Here, the detector was placed as close as possible to the chip interface and the time interval from the analyte detection in the C^{4}D detector until its arrival inside the chip interface was calculated. This time interval depends on several highly variable experimental parameters such as the EOF, the applied separation voltage, capillary lengths, etc. Therefore, the switching process has to be optimized for every 2D separation assay, if one of the afore-mentioned parameters changes. Despite changes in buffer

composition or surface properties of the capillary surface during repetitive measurements, migration time differences of analytes can occur and therefore the proper time point for switching slightly changes and, as a result, the proper transfer time point can be missed. To optimize the transition process of the sample band from the first to the second separation dimension, C^4D as the first intermediate detection technique was implemented on the chip interface [Kler, 2014] to monitor the respective channel cross-section. Using this approach the laborious calculation of time point for switching is not necessary anymore and the analyte can be detected directly at the channel cross-section, indicated by the red circles in Figure 3-6. The transfer can now directly be monitored and thus controlled, depending on the chip model used by means of a simple "transfer" for a single T- interface (3-port chip) or heart-cut for a double T- interface (4-port chip) including the common intersection arrangement of the chip channels. The volume of the common intersection (V_c) (Figure 3-4) can then be used as a well-defined "heart-cut" sample volume for the injection into the second separation dimension. A first on-chip C^4D detection prototype system developed in cooperation with CalvaSens (Aalen, Germany) was successfully used in a ITP-C^4D/CE-MS setup by Kler et al. for the separation of 20 proteinogenic amino acids in a non-aqueous buffer system [Kler, 2014]. For ITP, C^4D detection is ideal.
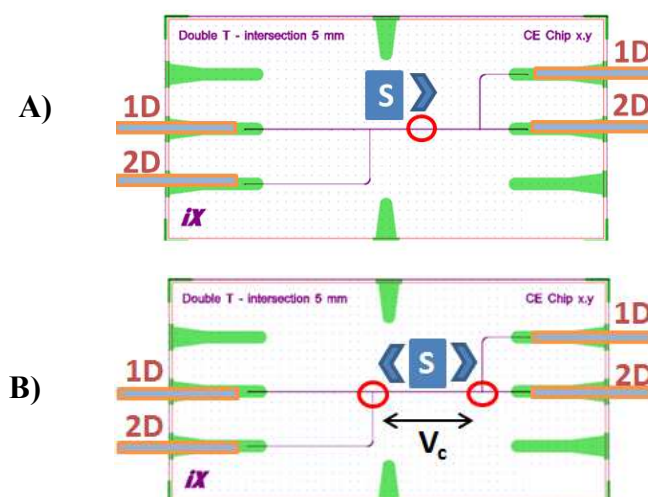
Figure 3-6: Different transfer strategies for sample constituents from first (1D) to second (2D) dimension, depending on the chip model used: A) 1D to 2D transfer via 4-port double T-interface and B) 1D to 2D heart-cut via 4-port double T-interface including the common intersection arrangement (V_c) of the chip channels with a length of 5 mm. V_c is used as a fixed 2D injection volume of ~7 nl. Red circle = chip channel cross section detection points, S = sample zone, blue arrows = migration direction of the analyte plug zone. Modified CAD drawings from iX-factory (Dortmund, Germany).

However, in this thesis coupling capillary isoelectric focusing (CIEF) as the first separation dimension to the 2D setup is envisaged, an on-chip optical detection system has to be

implemented. For this instrumentation for LED-induced fluorescence (LED-IF) detection for the coupling of capillary isoelectric focusing (CIEF) with CE-MS detection for the analysis of intact proteins using a 2D CIEF-LED-IF/CE-MS setup was developed as discussed in detail in Section 3.4. While conducting 2D separation assays, the channels not used in the respective separation dimension are blocked to prevent directional current (floating current) and hydrodynamic flow while respective pressure and/or potential regimes are applied to the separation channels. In order to block specific channels during a 2D assay, conventional CE vials from Agilent Technologies (Waldbronn, Gemany) were filled with silicone b1 from Chemphar Handels & Export GmbH (Hamburg, Germany) (see Section 5) to immerse the inactive separation capillary into the cured silicone [Zhang, 2006A]. If, instead, the inactive separation channel was left in solution e.g. background electrolyte solution, leakage currents - very low directional current flow to the floating channel appeared, which can lead to the so called leakage effect induced by electroosmosis and diffusion, which evokes band broadening and in extreme cases splitting of the sample band, indicated by multiple peaks of a certain analyte, and sample loss, reducing the quality of the cutting or transfer process and therefore analytical separation and quantification performance. The most common way to completely avoid the leakage effect is to apply a bias or pullback voltage to the respective channels not used for separation (former floating channels) during separation to ensure zero potential difference at channel cross-sections; or ground potential (GND) if mass spectrometry is used as the final detection method. To be able to determine these required pull back potentials, we implemented a silicon nitride (SiN) passivated Ti/Pt electrode at the channel cross section inside the glass microchip interface in combination with a low current potential measuring prototype, discussed in detail in Section 3.3. A chip with the implemented electrode is shown in Figure 3-7. The Ti/Pt channel electrode was 15/235 nm in its dimensions covered by a 500 nm layer of non-conductive SiN. In order to increase detection sensitivity and therefore to allow better sensitivity for on-chip C^{4}D and LED-IF detection the cover plate thickness of the chip interface was reduced from 1000 to 200 μm. In Section 3.4 and Section 5 the adjusted chip design with respect to the intermediate on-chip detection is discussed in more detail.
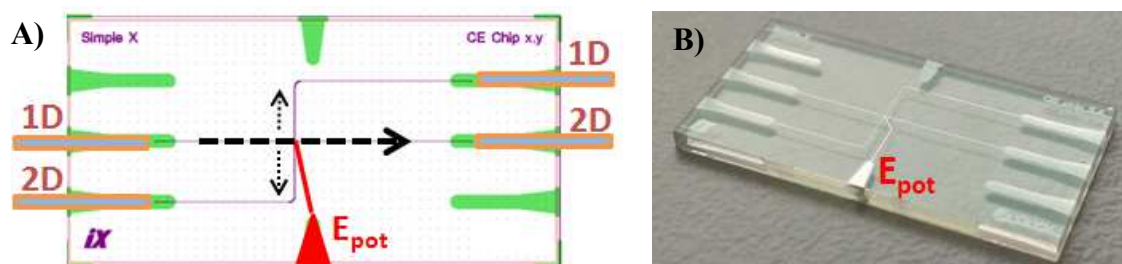
Figure 3-7: Customized 4 port microfluidic glass chip with a cross-arrangement of the channel network and an integrated Ti/Pt intra-channel electrode (thickness 15/235 nm) for electrically contacting the intersection of the chip channels (iX-factory, Dortmund, Germany). A 500 nm passivation layer of silicon nitride was deposited onto the electrode material to passivate the separation channel from the electrode. Chip dimensions were $20 \times 10~mm^2$. The cover plate thickness of the chip was 180 µm. Left = modified CAD drawing from iX-factory (Dortmund, Germany).

3.1.4 Interface stability vs. on-chip detection sensitivity

As mentioned before, to increase the general on-chip detection sensitivity, a 200 µm thick cover plate was used for the chip which included the potential measurement electrode. By reducing the cover plate thickness, chip breakage occurred frequently at the epoxy glue front in the chip port housing the capillary. The onset of the material fatigue was visible by the appearance of Newton's rings (R_N), a typical interference pattern created by reflected light at a spherical surface and an adjacent flat surface [Airy, 1833] at the glued chip-capillary interface region as shown in Figure 3-8, indicating the detachment of the bonded cover plate from the bottom plate. Shortly after, complete breakage occurred together with liquid leakage upon flushing by external pressure, leaving the chips unusable. Possible reasons for the mechanical stress are:

- Temperature driven extension and chemical swelling of the dried epoxy resin due to the applied separation voltage (due to Joule heating) or buffer solutions and the resulting mechanical stress on the capillary-chip interface region in the chip cup.
- Mechanical stress due to the bending of the capillaries and the resulting stress on the glued interface region.
- Deformation of the epoxy glue front inside the chip cup due to the used pressure regimes up to 3 bar.

Due to the observed circular breakage pattern around the glue front, deformation of the glue front can be assumed to be the main cause. The mechanical stress on the capillary-chip interface region can be ruled out, because the breakage should occur near the region of the

entrance of the separation capillaries into the chip cup and not at the glue front. In order to increase the stability, both the chip and the capillaries were fixated to a microscopic glass slide with epoxy glue as indicated in Figure 3-8B, however, this did not reduced the frequency of the chip breakage.
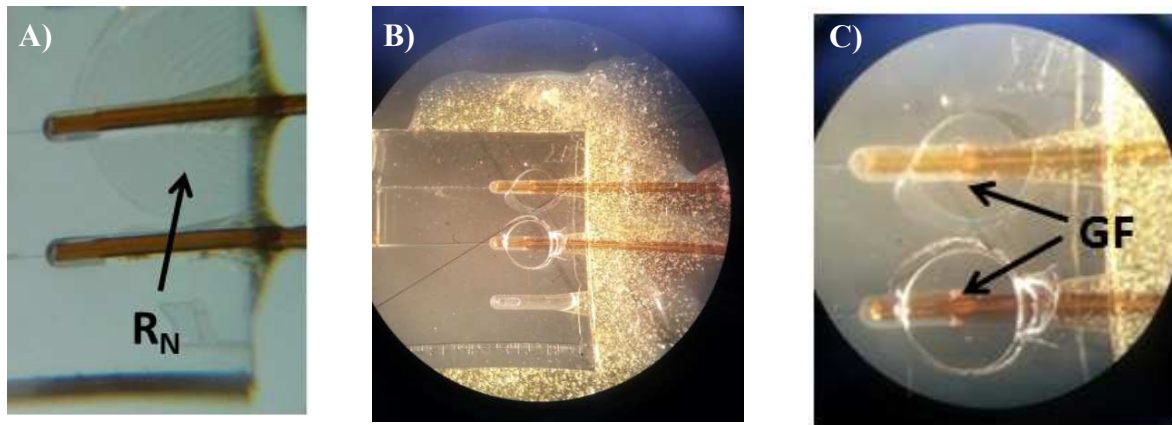
Figure 3-8: Evolution of 200 μm cover plate breakage at the chip cups. A) Material fatigue of the cover plate visible via Newton's rings (R_N), followed by B) the breakage of the cover plate at the chip cup with C) a circular breakage pattern around the glue front (GF).

Pressure can be ruled out from the possible reasons, because the chip also suffered breakage after usage, leaving the chip-capillary setup filled with air during long-term storage. Therefore, the most likely reason is a swelling of the epoxy glue front (GF) at the interface, see Figure 3-8C. The thermal expansion coefficients of the epoxy glues in the temperature between 15 to 40°C of epoxy glues are in the range of 60 - 120 x 10^{-6} ($1/K^{-1}$) [www.weicon.de, 2015; www.wiko-klebetechnik.de, 2015]. Thus, the temperature-induced swelling is relatively small, when taking into account the glue volume used, but in combination with the brittle nature of the resin, expansion of the glue front inside the chip cup can be the reason for the breakage. The temperature range was estimated with regard to the air conditioning in the laboratory and the possible temperature increase due to Joule heating. Due to the fact that the chip suffered breakage also when stored filled with air e.g. overnight, the most possible reason is a rest-swelling or contraction of the cured epoxy resin in the μm range, despite the chemical resistivity of epoxy glue to almost all typically used chemical solutions, except solutions with extreme acidic or basic pH values or methanol for example [www.weicon.de, 2015; www.wiko-klebetechnik.de, 2015]. If the swelling of the glue is more affected by different chemicals, temperature or pressure was not further studied in the framework of this thesis. Epoxy glue suppliers have only limited experimental data regarding the behavior of the cured glue, especially in the μm-range, to the exposure to

different stress parameters, like pressure and temperature changes or different chemical solutions (organic and inorganic solutions). Most stability tests are done in a macroscopic scale and are therefore not completely transferable to the μm-range with respect to microfluidic structures. Problems from both chemical as well as temperature-induced swelling of the glue was only observed when the cover plate thickness was reduced from 1000 to 200 μm pointing to a diminished stability.

In order to find a compromise between cover plate stability and detection sensitivity, the design of the cover plate of the chip was optimized to meet two major requirements: A thick cover plate in the area of the chip cups to increase long-term mechanical stability and a small cover plate thickness at channel cross sections on the chip for an optimal signal to noise ratio in terms of intermediate optical and conductivity detection. Figure 3-9 and Figure 3-10 show the optimized 2nd generation chip design, where a 200 μm chip cover plate was used in combination with a 500 μm cover plate bonded to each other. Starting from a full 3 plate setup, the third bonded 500 μm cover plate was partly removed in the middle of the chip interface by micro sandblasting, resulting in a 7.6 mm gap with a 200 μm glass thickness in the area of the channel cross section. The triangular shaped offset (~0.2 mm) from the outer to the inner part of the gap is due to the applied micro sandblasting procedure. The lifetime of the 3 plate chip interface is comparable to that of a chip with 1000 μm cover plate thickness. It proved to be stable up to several months of constant usage. The resulting gap in the middle of the chip is also considered in further designs of the afore-mentioned on-chip C^{4}D detection system.
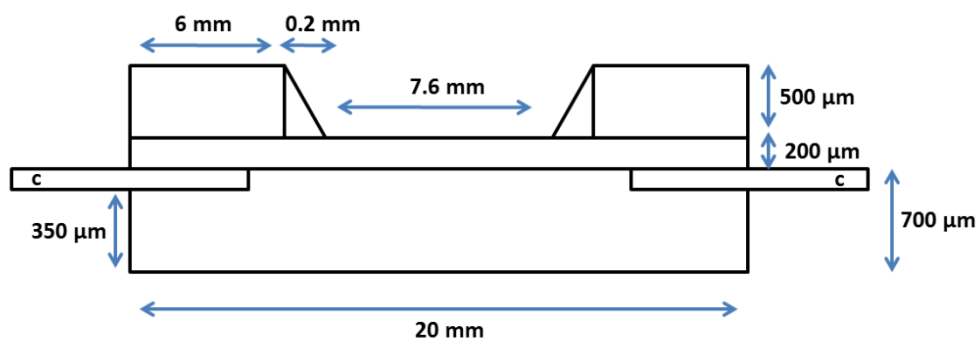
Figure 3-9: Optimized 2nd generation chip design with dimensions: a 200 μm chip cover plate was used in combination with a 500 μm glass blocks bonded on top of the cover plate near the chip cups to increase long term stability. c = separation capillaries

The detection head for C^{4}D was redesigned and tested in cooperation with the project partner CalvaSens (Aalen, Germany) using the gap as a guidance for the future C^{4}D detection head

designs which is discussed in the master thesis of Jonas Staschik at the University of Duisburg-Essen [Staschik, 2015].
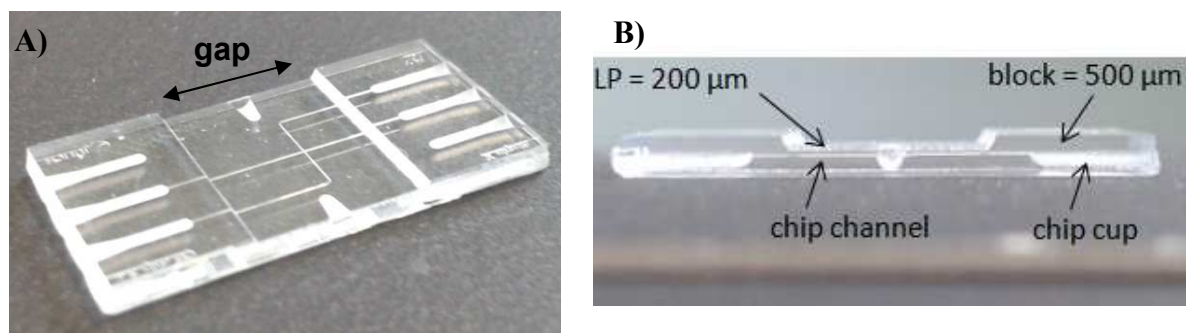
Figure 3-10: A) Optimized 2nd generation chip design with resulting gap for positioning are on-chip C4D detection head, B) dimensions are as in Figure 3-9.

3.1.5 SLE based chip production: 3rd generation chip design

Despite stability issues, the usage of glue to fixate and seal the capillary/chip connection has two main further disadvantages:

- The application of different coatings in the first and second separation dimension is not possible, due to capillary effects present in the cross section interfaces of the chip channels and resulting ill-defined liquid flow in this region during the flushing protocols of the coating process. Coating solution thus enters all channels despite the use of the silicone blocker vials at the end of a separation capillary, where no coating is wanted.

- If a glued capillary is clogged e.g. due to particles entering the system or a capillary breaks, the chip cannot be used anymore as a capillary exchange is not possible. Once the capillary/chip interface is glued, it is very laborious to remove the cured epoxy resin from the chip interface without clogging the chip channels. Due to the chemical resistivity of epoxy glue, only a few very toxic solutions can be used. Here, heated dimethylformamide (DMF) is known to dissolve the cured epoxy glue. Under these conditions applied coatings are also removed, leaving the surface properties of the chip channels with unknown characteristics and thus undefined EOF.

In general, valves for LC, GC or microfluidic applications are based on a modular screw-tight fitting system [Evans, 2004; François, 2009; Adahchour, 2006], using a nut-based assembly

of different separation columns or capillaries to create a certain multidimensional setup. Following this approach the chip interface was further developed together with the company LightFAB (Aachen, Germany) to create a new chip generation (3rd generation) using the Selective Laser-induced Etching (SLE) technique in combination with a screw-tight system for connecting capillaries to the chip interface. SLE is a very young and promising technique for the production of microfluidic components, like glass chips [Hörstmann-Jungemann, 2009]. A laser, e.g. a fs-NIR laser with a wavelength of 1199 nm is used to selectively write microfluidic structures into a certain substrate. For a successful writing process the substrate has to be transparent for the chosen wavelength. To create microfluidic structures inside a substrate the laser beam is focused and the respective volume is chemically modified at the focal point. Due to the radiation, the substrate is heated to over 1000°C in a very short period of time (fs) at the focal point of the laser and cools down again very fast. During this process the molecular characteristics of the substrate changes. For example, the crystalline structure of sapphire is transformed into an amorphous vitreous structure, with the result of having a lower resistivity against acidic solutions (e.g. HF or KOH) than the untreated material. During this harsh treatment the restructured parts of the substrate are etched much faster upon ultrasonication than the untreated material usually with process factors up to 10000, leaving the treated areas of the glass block as hollow space or channel system as illustrated in Figure 3-11. For fused silica materials process factors of ca. 500 are reached.
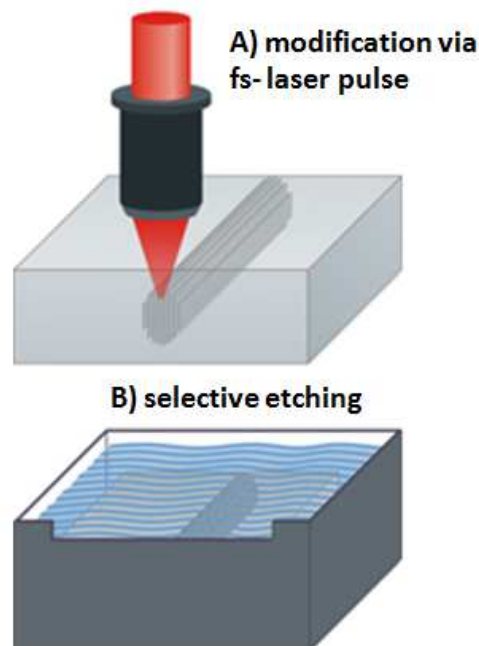
Figure 3-11: Schematic illustration of the production of microfluidic channel structures into a substrate with the selective laser etching process: A) Modification of defined substrate volumes via focused fs- laser beam and B) selective etching of the modified substrate material using aqueous KOH. Modified figure from LightFAB with permission [http://www.lightfab.de].

Details regarding the theoretical background of the SLE process [Hörstmann-Jungemann, 2009] as well as first applications [Hermans, 2014; Gottmann, 2013] are discussed elsewhere. The exact mechanism of the restructuring process is not fully understood, underlining the novelty of the method. Regarding the production of microfluidic components, the SLE process has some crucial advantages compared to the traditional photolithographic etching and bonding procedures for creating channel systems in glass chips used for capillary electrophoretic separations. These are:

1) With the SLE process, the whole chip can be made out of a solid block of the fused silica glass substrate, increasing the mechanical stability of the microfluidic structures and especially the interface region between the chip and the separation capillaries compared to the conventional bonding process.

2) Regarding on-chip intermediate detection techniques the minimum cover plate thickness is 100 μm for the conventional mask-based process due to the commercial availability of glass wafers. With the laser supported etching the microfluidic channel very close to the substrate surface (below 100 μm), enhancing the on-chip detection sensitivity, especially for C^4D, due to a reduced distance of the chip channel to the electrodes of the detector. Another argument for using SLE is, that the 3D characteristics of the manufacturing method enables the implementation of circular electrodes around the chip channels, e.g. for C^4D or potential measurement, or even valves directly into the micro fluidic interface, enhancing its usability, whereas the implementation of electrodes consisting of multiple layers of different materials, e.g. electrodes as for on-chip potential measurements (as discussed in Section 3.3) is still challenging.

3) The SLE technology has the ability to create microfluidic channels with a truly circular cross section with submicron tolerances (down to a minimum of the 2 μm laser spot size), instead of the half-circular channel cross-sections of the 1st and 2nd generation glass chips. With the software-guided laser the channels can be created in completely free 3D arrangements, and thus with a higher flexibility than the traditional process.

4) It enables the perfect matching between capillaries and the micro channels of the chip interface, with a minimal change in the cross section and thus nearly no dead volume is present enabling the efficient analyte transfer through the capillary/chip interface and avoiding any distortions of pre-separated analyte zones with band broadening or mixing effects. It is possible to create a chip cup with a flat connecting surface, perfectly adapted to the dimensions of the inserted capillary in a nearly 90° angle arrangement, in comparison to the rounded chip cup cross section for the 1st generation chips.

5) Due to the combination of the features discussed in 1), 3) and 4) it is possible to implement screw-tight fitting systems for the connection of capillaries to the 3rd generation chip interface, which is discussed in detail at the end of this section. With this very revolutionary system, the application of different coatings in the first and second separation dimension is possible. In addition, the overall practicability, usability and cost efficiency of the whole 2D modular interface strategy is enhanced due to the removable capillary-chip couplings, see Section 3.2.

6) Finally, the costs for the chip production itself, especially for prototype development are much lower, due to savings regarding mask production which is the main cost factor for the conventional methods, as well as the fact that the costs are not linearly related to the complexity of the microfluidic structures. The main cost factor for the SLE technology is the running time of laser and not the complexity of the microfluidic object. However, with regard to mass production the conventional method is still the most cost efficient technology due to the possibility of parallelization of the mask-based concept.

Despite the vast number of advantages, the SLE process has some disadvantages as well. The main disadvantage lies in the limitation of the physical length to values below 10 cm of the microfluidic chip structures. This limit is due to the etching process of the channel structures: During ultrasonication the etching liquid gradually moves forward into the chip while the channel structure already etched at the beginning gradually widens. By the time the liquid reaches the chip center the channels are not cylindrical but conical narrowing from the chip entrance to the middle. Despite the high process factors of up to 500 for fused silica, for structures longer than 5 cm this effect is of relevance. In addition, the limit for the minimum

distance of a channel structure to the chip surface is 100 µm, which is comparable to the classical mask manufacturing process. For the SLE process, the surface roughness is defined by the resulting grooves produced by the laser carving of the substrate material and is in the range of 2 - 5 µm, whereas the classical process produces smoother surfaces.

For a first prototype of the 3rd generation glass chip interface a 3D CAD-drawing of a 4-port chip with double T-interface with a 3 mm common intersection segment length was created. The 3D CAD-drawing as well as the first prototype of the 3rd generation chip interface fabricated in synthetic fused silica glass SK-1300 from OHARA CORPORATION (Branchburg, NJ, USA) are shown in Figure 3-12.
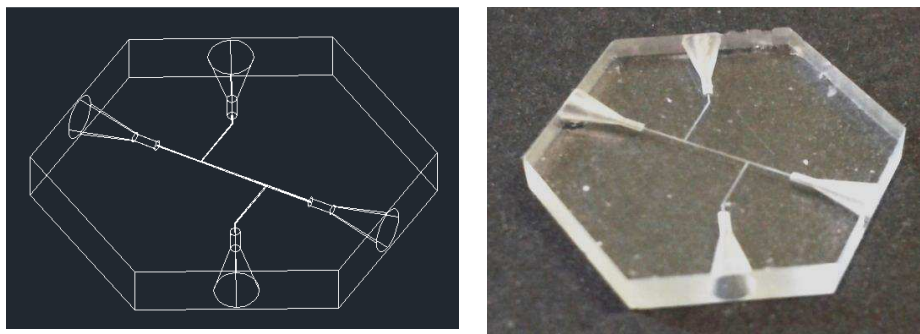
Figure 3-12: 3D CAD-drawing as well as the first prototype of the 3rd generation chip interface fabricated in silica glass with the SLE process. The length and volume of common intersection are 3 mm or ~ 6 nl, respectively.

In Figure 3-13, the 2nd and the 3rd generation interface dimensions are directly compared to the dimensions of a one euro cent coin.

Figure 3-13: Dimensions of 4 port double T-interface with a common intersection of the 2nd generation interface (iX-factory) and 3rd generation (LightFAB) chip interface directly compared to the dimensions of a one euro cent coin.

The common intersection length was reduced from 5 mm (half-circular channels) to 3 mm (circular channels) to match the common intersection volume of the used 5 mm V_c length of the 2nd generation chip with a double T-interface channel configuration. The general

dimensions as well as an overview of the advantages and disadvantages of both interfaces discussed before are listed in Table 3-1. As mentioned in 5) one crucial step of the interface development was to implement a screw-tight fitting for the capillary/chip cross section to allow an easy exchange of capillaries of various inner diameters and lengths for the new interface.

Table 3-1: Overview and characteristics of the 2nd generation (iX-factory) and 3rd generation (LightFAB) chip interfaces regarding both production processes.

parameters	2nd generation interface (iX-factory)	3rd generation interface (LightFAB)
dimensions [mm]	$20 \times 10 \times 1.5$	$14 \times 16 \times 2$
dead volume [pl]	~20	< 20
costs	+ for mass production	+ for prototype production
capillary connection via	(epoxy) glue	nut connection
interface sealing via	(epoxy) glue	silicone plug
channel geometry	half-circle	full-circle
chip stability	bonded glass plates	solid glass block
channel flexibility in z direction	limited	almost limitless
flexibility in chip dimensions (length and cross section)	- in flexibility + in length	+ in flexibility - in length
flexibility in capillary length and inner diameter	yes	yes
exchange of capillaries	no	yes
minimal distance channel/surface [μm]	100	100
channel roughness [μm]	< 1	2 to 10
channel cross section diameter [μm]	~ 25 x 60	~ 50
volume / length of common intersection	~ 7 nl / 5 mm	~ 6 nl / 3 mm

- = disadvantage and + = advantage

To be able to use up to 6 capillaries attached via relatively large screw-tight fittings, the chip was fabricated as a hexagon together with the highest possible distance of all of the

implemented nuts. The most crucial part was the design of the chip cup, it consists of two segments: A conical cup entry is followed by a cylindrical section which leads directly to the chip channel. The conical part was built to house the tip of a standard Nut 6-32 Coned 360 µm made from biocompatible PEEK polymer, available from IDEX Health & Science (Wertheim, Germany) as shown in Figure 3-14. The inner diameter of the second cylindrical part was adapted to a diameter of approximately 360 µm, as 356 ± 10 µm is the usual outer diameter for commercially available fused silica capillaries e.g. from Polymicro Technologies (Phoenix, AZ) used for electrohoretic separations. To be able to hold and tighten the capillaries, a chip holder made from Teflon (Figure 3-14) was built in cooperation with the workshop of the University of Tübingen, with suitable threats to house the PEEK nuts to seal the interface region between the chip and the capillary. This holds the chip in a fixed position, connects the capillary to the chip and hydrodynamically seals the interface via the nut tip inside the conical part of the chip cup.
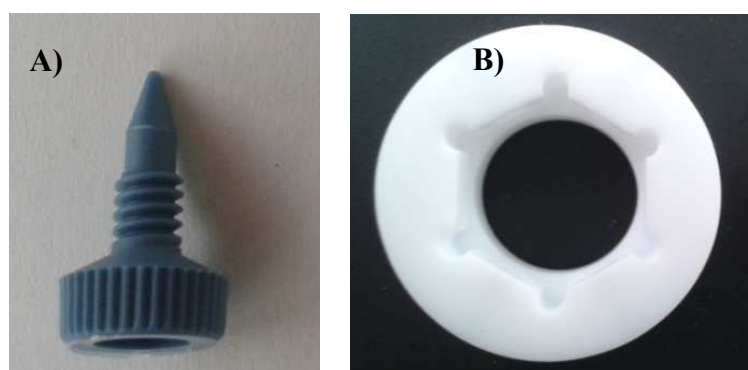
Figure 3-14: Screw-tight fitting assembly used for the capillary to chip connection for the 3rd generation interface prototype: A) Standard Nut 6-32 Coned 360 µm made from biocompatible PEEK polymer, available from IDEX Health & Science (Wertheim, Germany). B) First chip holder made of Teflon with threats to house the PEEK nut.

For first flushing experiments, one of the capillaries was fixed to the inlet of a 7200 Agilent CE system and water was flushed through the system. Using this setup liquid leakage was observed at the capillary/chip interface directly at the capillary fixed to the inlet of the Agilent CE system using 1 bar pressure and no liquid was passed through the chip channels. Obviously, the interface between the tip of the PEEK nut and the conical part of the chip cup was not properly sealed. Having a closer look at the surface of the chip cup, some grooves were observed as shown in Figure 3-15A, which are due to the laser spot writing in the material. The dimensions of the grooves are in the range of the diameter of the optical focus of the laser spot used for the writing process. The roughness produced due to theses grooves was about 5 µm and not completely avoidable, but can be minimized by minimizing the laser

spot focus width (minimum 2 μm) or optimizing the etching time to produce smoother transitions between grooves. The brittle PEET material of the nut could not adapt to the roughness of the conical chip cup part, producing a proper sealing. As a more flexible material for the nuts was not commercially available, a silicone seal was implemented: The nut tip was cut by about 1 mm to give space for a silicone plug of about 1.5 × 2 mm dimensions, cut with a scalpel from a cured silicone block as shown in Figure 3-16A. The silicone plug is very flexible and in combination with the pressure applied via the screw-tight fitting by the PEEK nut, the silicone plug easily adapts to the surface roughness (Figure 3-16B) of the conical chip cup part and therefore seals the interface. Using this approach the whole setup shown in Figure 3-16C was properly sealed even for pressure applications of up to 6 bar (higher values were not tested). To evaluate the performance of the interface regarding band broadening of analytes and the overall peak performance, first CE separation assays were performed as described in detail in the following section.
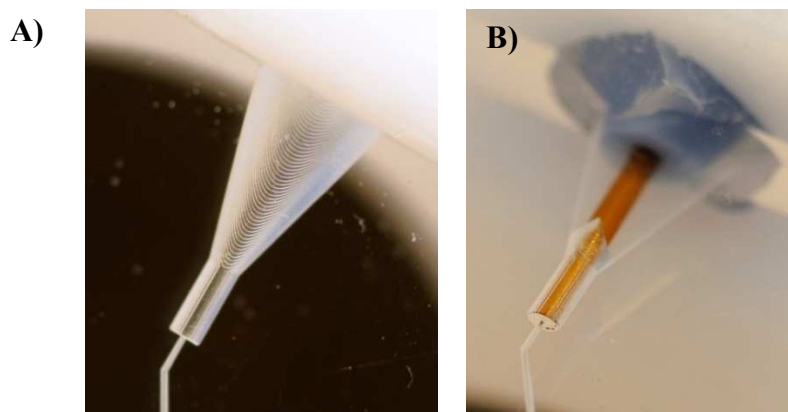
Figure 3-15: The surface roughness produced due to the grooves from the laser writing process in the substrate material, here at the chip cup.
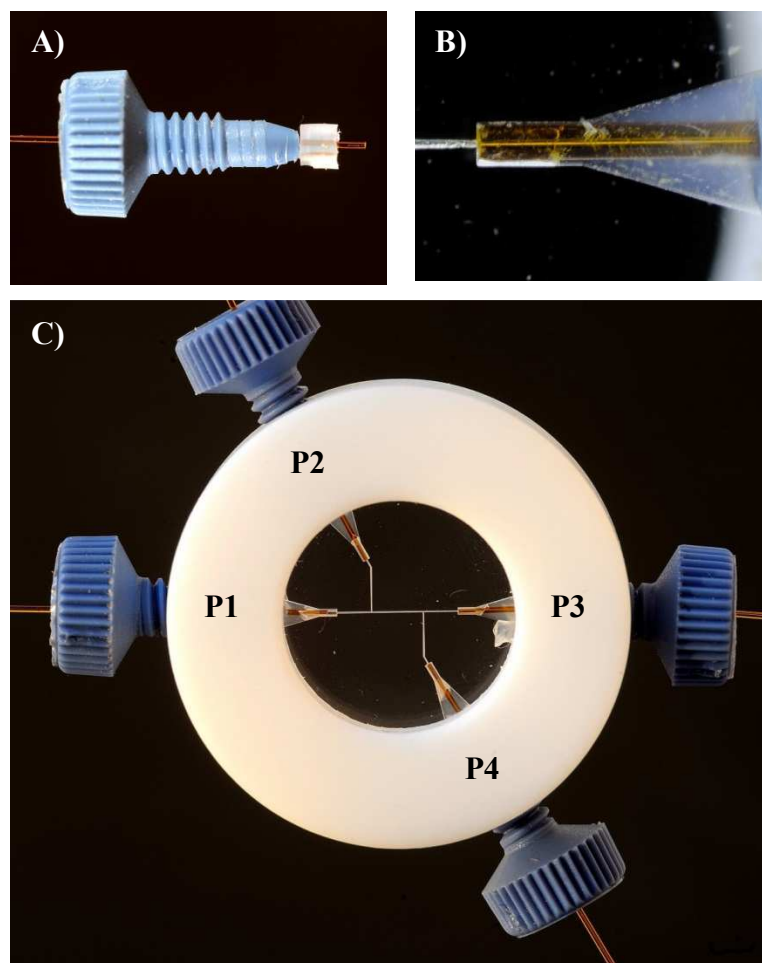
Figure 3-16: Sealing by silicone plug: A) PEET nut from the nano port assembly. B) Same nut with shortened tip and a silicone plug of about 1.5 × 2 × 2 mm³ dimensions to seal the capillary/chip interface. C) Assembled 2D setup with the 3rd generation chip interface, Teflon chip holder, PEEK nuts, silicone plugs and capillaries. P1 to P4 = capillary to chip ports.

3.2 Comparison of the 2nd and 3rd generation chip interfaces

In this chapter the optimized 2nd generation chip is compared to the 3rd generation chip (SLE process) interface regarding sample transfer characteristics using an intact capillary as a reference. For more details regarding both interfaces see Table 3-1. The comparison was made via CE separations of two amino acids (arginine and lysine) under different bulk flow conditions with and without EOF using acidic and basic back ground electrolyte conditions. Additionally, bias potentials were applied to the secondary channels of both interfaces during the separations for sample band stabilization during the sample transfer to evaluate the influence on peak performance. Both amino acids were chosen with respect to their similar migration behavior and close effective electrophoretic mobilites under both background electrolyte conditions. To evaluate the transfer characteristics in more detail, analyte

migration times and resolution as well as respective peak shape, height and width are compared and discussed.

3.2.1 Experimental section

3.2.1.A Chemicals

Formic acid (98 - 100 %), L-arginine monohydrochloride (Arg, for biochemistry) were purchased from Merck (Darmstadt, Germany). L-lysine (Lys, $\geq$ 98%), isopropanol (LC-MS grade) and ammonium hydroxide (25%) were purchased from Sigma Aldrich (Steinheim, Germany). All solutions were prepared with doubly-deionized water (Milli-Q purification system from Millipore, Bedford, MA).

3.2.1.B Material and Instrumentation

The fused silica capillaries were purchased from Polymicro Technologies (Phoenix, AZ). All electrophoretic separations were performed using an Agilent 7100 CE system (Agilent Technologies, Waldbronn, Germany) providing pressure and voltage regimes, injection control, and vial handling. MS detection was achieved using an Agilent 6100 Series Single Quadrupole system (Agilent Technologies, Palo Alto, USA). The CE was coupled to the MS via a coaxial sheath liquid interface from Agilent using an Agilent isocratic pump 1260 (Agilent Technologies, Waldbronn, Germany) for delivering sheath liquid (50:50 (v/v) mixture of water and isopropanol, containing 0.1% formic acid at a constant volume rate of 4 µl/min). Nebulizer pressure was set to 0.28 bar and the drying gas was delivered at rate of 4 l/min at a temperature of 300 °C. The single quadrupole was used in single ion mode (SIM) and scanning mode (scan). The respective modes and related m/z values are given for each experiment in the figure legends.

3.2.1.C Chip interfaces

2nd generation chip interface: Following a previous study [Tiggelaar, 2007; Kler, 2014] the microfluidic borofloat glass chip interface (iX-factory, Dortmund, Germany), a double T- or a cross channel design (if not stated otherwise) with etched channels of 60 µm in width and 25 µm in depth (2nd generation chip design, Section 3.1.5) was used. Bottom plate thickness was 700 µm and cover plate thickness was 200 µm including two bonded 500 µm glass

blocks. The fused silica capillaries (50 µm ID) were purchased from Polymicro Technologies (Phoenix, AZ), cut to the desired length using a capillary cutter (SHORTIX - Capillary Column Cutter, SGT, The Netherlands and Singapore) and cleaned with isopropanol. The glass chip was cleaned in isopropanol upon ultrasonication for 10 min. The coupling was performed by gluing the capillaries to the chip using epoxy glue (Araldite, Huntsman Advanced Materials, Ratingen, Germany) as previously reported [Tiggelaar, 2007]. A double T- arrangement of the separation channel with a common intersection length of 5 mm was used (see Figure 3-17).
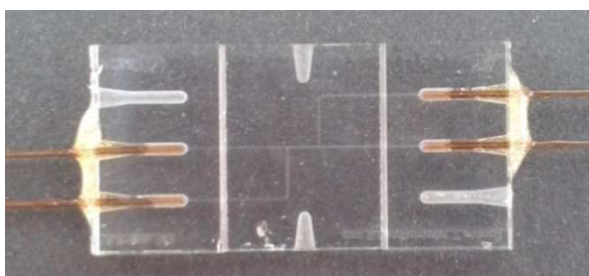
Figure 3-17: 2nd generation chip interface with a double-T arrangement of the separation channel with a common intersection length of 3 mm and glued separation capillaries.

3rd generation chip interface: It was produced via the Selective Laser Etching process (SLE) and was a 4-port chip, with 50 µm ID channels and a double T-interface with a 5 mm common intersection segment length. In order to be able to fit 4 screw-tight fittings in combination with the SLE interface, the chip was manufactured in a hexagonal shape. Chip design includes a conical cup entry that is followed by a cylindrical section which leads directly into the respective chip channel. The conical part was built to house the tip of standard PEEK polymer nuts, available from IDEX Health & Science (Wertheim, Germany). The inner section of the fitting region was adapted to a diameter of approximately 360 µm, as the usual outer diameter for commercially available fused silica capillaries for electrohoretic separations. To be able to hold and tighten the capillaries, an ad-hoc chip holder was built, with suitable threats to house the PEEK nuts. This holds the chip in a fixed position, connects the capillary to the chip and hydrodynamically seals the interface via the nut tip and a silicone seal inside the conical part of the chip cup. For conditioning the respective 2D setup was flushed with 1 mol/l NaOH, 1 mol/l HCl and water for a minimum of 30 min for each solution at 1 bar using the Agilent 7100 CE system. To verify the quality of the capillary before the first separation, the capillary was flushed with the respective separation buffer (1 mol/l acetic acid). Afterwards +25 kV were applied to monitor if the current reaches a stable value over the respective separation time. Both systems were left in doubly-deionized

water when not in use. For a long-term storage the capillary-chip setups were flushed with air and left at room temperature.

3.2.1.D CE separations throughout the 2nd and 3rd generation chip interface

Formic acid at a concentration of 1 mol/l (pH 1.87) was used as the background electrolyte for the CE experiments without electroosmotic flow. Ammonium formate at a concentration of 300 mmol/l (pH 9.3) was used as the background electrolyte for the CE experiments with electroosmotic flow. L-lysine and L-arginine 1 mmol/l were prepared in water as injection solutions for both CE experiments with 10 % of the respective BGE solution [Huhn, 2010]. Sample transfer performance was evaluated in terms of peak shape distortion and migration time shifting. Experiments were performed first using a single capillary of 70 cm length and 50 µm ID The 2nd and 3rd generation chip interfaces were tested using four capillaries of 35 cm length and 50 µm ID. The main channels (those which define a straight path, ports P1 to P3, see Figure 3-18) were used for the separation, secondary channels were connected to vials containing BGE and carefully leveled in order to avoid hydrostatic pressure driven flows. Hydrodynamic and electrical parameters for the separations were: 2 sec at 100 mbar for injection in both cases, 12 min at +20 kV for separation at acidic pH, and 8 min at +20 kV for separation at basic pH. Each experiment was repeated four times (n = 4) in order to determine the precision of the experimental results. All solutions were introduced into the chip interfaces via port P1.
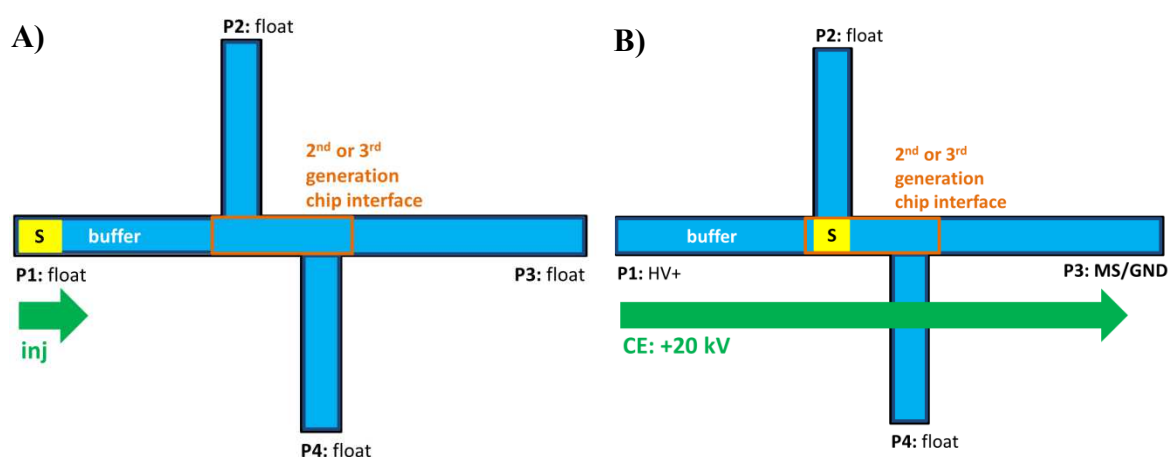
*Figure 3-18: Operational scheme for the two steps involved in 1D CE-MS separation performed with the 2D hybrid capillary-microchip setup for multidimensional separations: **A)** Prior to the sample injection the 2D setup was flushed with background electrolyte. After the sample injection step, **B)** the separation voltage was applied from port P1 to port P3 with MS detection, while ports P2 and P4 were left floating.*

3.2.2 Chip interface comparison - results

Figure 3-19 and Figure 3-20 show the electropherograms of the separation of the two amino acids lysine and arginine for the two interfaces vs the intact capillary as a reference, with and without EOF. The separation traces or electropherograms of both amino acids in the intact capillary is shown in green, for the 2nd generation (photolithography wet etching anodic bonding - PWEAB) in blue, for 3rd generation (SLE) in red. The RSD values for migration time, peak area and peak width at half height (w$_{1/2}$) of the respective experiments (n = 4) are summarized in Table 3-2 and Table 3-3. Figure 3-19 shows the electropherograms of the separation of the two amino acids lysine and arginine in an acidic background electrolyte using 1 mol/l formic acid (pH 1.87). Under these conditions no EOF is present. Both analytes were baseline separated within 10.3 min using the intact capillary with highly symmetrical peak shapes. Performing the separation with the 3nd generation chip design as the interface between the two separation capillaries the migration times are shifted by about 0.25 min to higher detection times. Both analyte peaks appeared broader with peak widths at half height (w$_{1/2}$) increased by 52 % and 44 % and ca. 50 % decreased peak height compared to the intact capillary, but still baseline separation was achieved. A slight peak tailing especially for the later migrating arginine was recorded. Regarding the 2nd generation chip interface the detection times are shifted by about 0.5 min to higher detection times compared to the intact capillary and an increased peak widths (in terms of w$_{1/2}$) are observed for lysine and arginine (121 % and 166 %) resulting in a decreased resolution and diminished peak height. Especially for the slower migrating arginine the peak tailing about 3 times higher compared to the separation in the intact capillary. RSD values for the migration time of 1.0 % or the intact capillary and comparable values both interface setups (2nd generation chip design: 1.2 %) for both analytes. For the peak area RSD values of 4.6 % and 1.4 % were reached for the intact capillary, compared to 15.8 % and 5.8 % of for 2nd generation and 8.9 % and 1.2 % for the 3rd generation chip design. Performing the separation at basic separation conditions (pH 9.3) nearly all silanol groups are deprotonated and EOF to the cathode is present. As a result, overall migration times for each setup are shifted to lower detection times in average from 10.5 min to 6.5 min of separation time, due to the increased analyte transport by EOF. The analyte migration pattern (intact capillary, 3nd and 2nd chip design) is the same as for separation conditions without EOF, but overall sharper peak shapes (lower peak widths) were obtained but also a lower resolution between both analytes (Δμ smaller). Especially for the 2nd generation chip interface, baseline resolution is not reached anymore. The increase in

55

peak widths for the 2nd generation chip was 88 % (Lys) to 104 % (Arg) and for the 3rd generation chip design 26 % for both lysine and arginine. RSD values for the migration times of 0.3 % for the intact capillary and comparable values for the 3rd generation chip design of 0.4 % were reached, being slightly higher for the 2nd generation chip design with about 1.0 % RSD for both anaytes. For the peak area RSD values of 3.0 % and 4.9 % were reached for the intact capillary. These values were comparable to both interface setups (e.g. arginine being below 2.0 % for both interfaces).
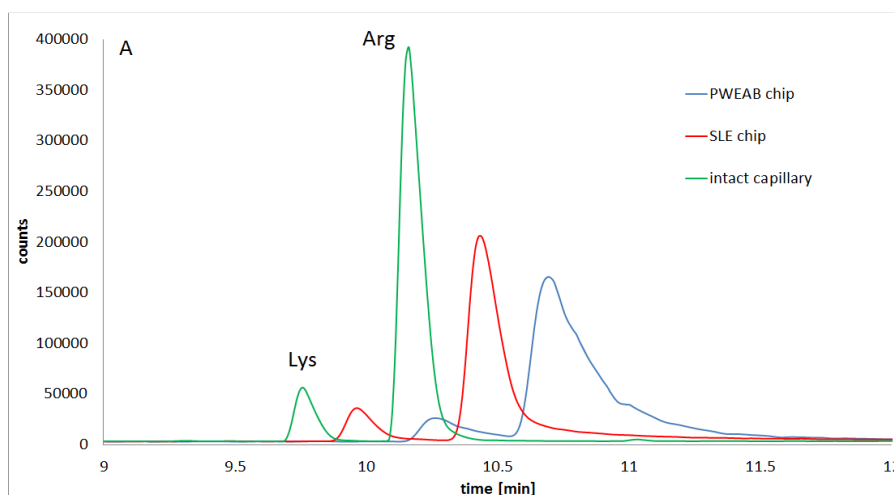
Figure 3-19: Comparison between electropherograms obtained using the different interfaces and the intact capillary as reference for the separation of lysine and arginine without EOF in 1 mol/l formic acid (pH 1.87) as the BGE. The detection traces of Lysine (Lys) and arginine (Arg) (combined EIE of $[M+H]^+ = 147.2$ m/z (Lys) and $[M+H]^+ = 175.0$ (Arg)).
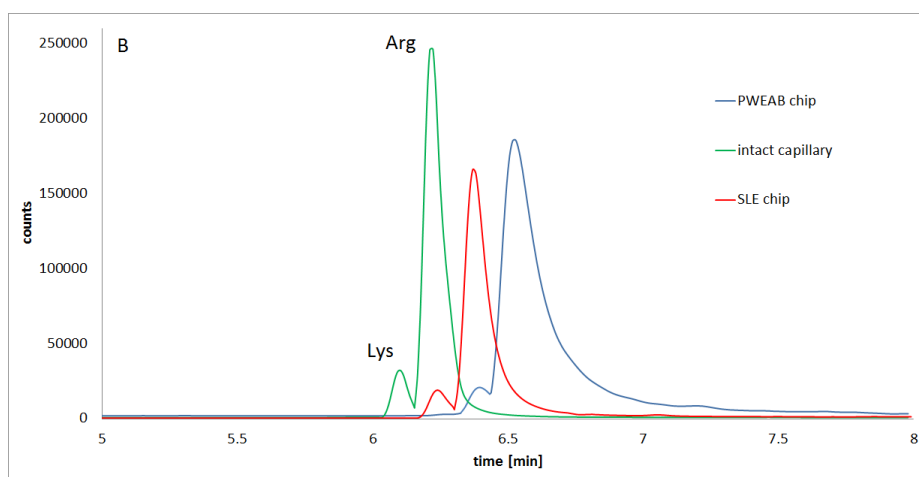
Figure 3-20: Comparison between electropherograms obtained by using the different interfaces and the intact capillary as reference for the separation of lysine and arginine with EOF in 300 mmol/l ammonium formate (pH 9.3) as the BGE. The detection traces of Lysine (Lys) and arginine (Arg) (combined EIE of $[M+H]^+ = 147.2$ m/z (Lys) and $[M+H]^+ = 175.0$ (Arg)).

Table 3-2: Repeatability (n = 4) of measurements for intact capillary (reference) compared to the 2ⁿᵈ and 3ʳᵈ generation chip interface without EOF (acidic BGE) for the separation of lysine and arginine.

	intact capillary		2ⁿᵈ generation chip		3ʳᵈ generation chip	
	lysine	arginine	lysine	arginine	lysine	arginine
time [min]						
Mean	9.85	10.26	10.25	10.68	9.95	10.41
SD	0.10	0.10	0.12	0.13	0.09	0.10
RSD%	1.01	1.01	1.19	1.24	0.95	0.96
peak area						
Mean	313448	2349826	253860	2366826	259367	1770944
SD	14359	31679	40074	136109	23182	21941
RSD%	4.58	1.35	15.79	5.75	8.94	1.24
peak width						
Mean	0.09	0.10	0.19	0.26	0.13	0.14
SD	0.01	0.01	0.01	0.01	0.01	0.01
RSD%	6.12	5.51	4.22	4.19	1.00	2.11
increase of peak width [%]	*-*	*-*	*121*	*166*	*52*	*44*

Increase peak width in % ($w_{1/2}$) for the respective chip interface using the intact capillary as the reference

Table 3-3: Repeatability (n = 4) of measurements for intact capillary (reference) compared to the 2ⁿᵈ and 3ʳᵈ generation chip interface with EOF (basic BGE) for the separation of lysine and arginine.

	intact capillary		2ⁿᵈ generation chip		3ʳᵈ generation chip	
	lysine	arginine	lysine	arginine	lysine	arginine
time [min]						
Mean	6.11	6.23	6.43	6.56	6.21	6.34
SD	0.02	0.02	0.06	0.07	0.02	0.03
RSD%	0.33	0.34	0.90	1.01	0.36	0.41
peak area						
Mean	138631	1288184	160742	1916527	101055	1062404
SD	4209	62539	5433	34395	3350	15849
RSD%	3.04	4.85	3.38	1.79	3.32	1.49
peak width						
Mean	0.07	0.08	0.12	0.16	0.08	0.10
SD	0.003	0.01	0.01	0.01	0.003	0.001
RSD%	4.99	1.14	5.14	6.31	3.29	1.49
increase of peak width [%]	*-*	*-*	*88*	*104*	*26*	*26*

Increase peak width in % ($w_{1/2}$) for the respective chip interface using the intact capillary as the reference

3.2.3 Discussion and outlook for chip design

Symmetric peak shapes and baseline separation as well as RSD values of 1.0 % or lower for migration times and below 5 % for peak areas for the separation of lysine and arginine with and without EOF inside an intact capillary shows stability and repeatability of the chosen separation systems. The RSD values for the migration times and the peak areas of both analytes for the separation done through the respective glass chip interface are comparable to those recorded for the intact capillary (with and without EOF). Only for the smaller lysine peak for separations without EOF, the RSD value for the peak area is doubled (8.9 %) for the 3rd generation and with 15.8 % three times higher for the 2nd generation chip design. This indicates that for low analyte concentrations (small peaks) at low separation velocities (no EOF) the interfaces have a slightly higher variance in peak area compared to the reference capillary, most probably due to the remaining dead volume of the respective capillary to chip intersection. For both separation systems, the 3rd generation chip design shows better separation and peak performance compared to the 2nd generation interface. The resolution as well as the peak symmetry is comparable to separations carried out in the intact capillary. Using the 3rd generation chip design without EOF the peak width is increased by 50 % and with EOF by about 26 % compared to the reference. The lower peak width differences for the separation with EOF are due to the fact that the dwell time of the analytes within the separation setup is decreased and therefore peak broadening caused by dispersion is minimized. The sample band broadening can be minimized by using the EOF as an additional flow (higher analyte velocities). The 2nd generation chip design shows 3 to 4 times higher peak widths compared to the intact capillary, increased peak tailing and therefore decreased analyte resolution and detection sensitivity. For separations with EOF both amino acids are only partially resolved. The slight shift in the detection time of the analytes for both interface designs is due to different back pressures induced by the doubled total capillary length as well as the respective dead volume and the different counter-influence to the sucking effect induced by the electrospray of the ESI source. The characteristics of the 3rd generation chip design are closer to the intact capillary due to the nearly dead volume-free (< 20 pl) capillary connection. The application of counter potentials to the secondary channels during analyte separation using each of the tested interfaces showed no influence on peak height or symmetry nor on the resolution of both amino acids (data not shown). Therefore, the decreased separation and peak performance of both amino acids is due to the resulting dead volume of the respective capillary chip cup geometry. Consequently, the 3rd generation chip

design shows a better transfer performance compared to the 2nd generation due to the nearly dead volume-free screw-thigh fitting capillary connection in combination with cylindrically shaped capillary chip cups (SLE process). The SLE fabricated chip interface shows nearly the same separation and peak performance as the intact capillary, proving the extraordinary suitability of this technique for chip interface production for coupling separation capillaries for multi-dimensional electrophoretic assays.

3.3 On-chip intermediate potential detection

3.3.1 Abstract

One of the greatest challenges for multidimensional channel networks for electromigrative separation techniques is the control of the leakage of sample constituents and band broadening at the channel intersections in microchips or capillary-chip interfaces, which can be met using fixed bias or pullback potentials. This is especially true when using isotachophoresis as the first separation dimension in a 2D setup, where the electric potential at the interface to the second dimension changes with time. Here, a dynamic control via on-line potential measurement in combination with a feedback system is needed to control electromigration into the side channels. In this chapter for the first time a prototype for in-channel potential measurements is presented using a low measuring current in combination with a SiN passivated Ti/Pt electrode at the intersection of the channels in a microfluidic interface: Parallel on-chip intersection potential measurements were successfully conducted without disturbing capillary zone electrophoretic and isotachophoretic analysis regarding separation and peak performance of amino acids chosen as model analytes. This was possible due to a SiN passivation layer, but also due to an ad-hoc developed high impedance instrumentation, resulting in a very low measuring electric current. Simulations of the detected isotachophoretic cross-section potential allowed a deeper understanding of the potential development during the separation. In addition, the migration of the fronts of leading buffer, terminating buffer, and sample, can be monitored in order to estimate the time point for voltage-switching between first and second dimension separation.

3.3.2 Introduction

Multidimensional electrophoretic separation techniques in the capillary format enable analyte pre-concentration, matrix removal and the enhancement of separation peak capacity in case of orthogonal separation mechanisms [Kler, 2015; Kohl, 2015; Mikuš, 2011]. The coupling of different separations can be accomplished with valves, custom-made interfaces [Mohan, 2003; Dickerson, 2010], microfluidic chips [Cong, 2008; Shadpour, 2006; Herr, 2003; Wang, 2004; Bruin, 2000; Bodor, 2002], as well as capillary-chip hybrid systems and may also include the hyphenation to mass spectrometry (MS) [Kler, 2013A; Kler, 2014; Tomáš, 2008; Lu, 2012]. In case of valve-free couplings the greatest challenge is the efficient transfer of sample constituents between channels by using electric fields (via electrophoresis

and electroosmosis). The fluid velocity field behavior in the region of microchannel intersections has extensively been studied regarding injection strategies and applications for chip platforms [Bruin, 2000; Shultz-Lockyear, 1999; Alarie, 2000; Seiler, 1994; Harrison, 1993; Fan, 1994; Belder, 2003; Wenclawiak, 2006]. The most frequent channel designs used are T- [Seiler, 1994], cross- [Alarie, 2000; Fan, 1994] or double T-shaped [Shultz-Lockyear, 1999] designs. The transfer control is straight-forward if a potential difference is applied only at one channel or capillary, leaving other channels at floating electric potential [Berli, 2008; Cong, 2008]. However, some sample leakage in the order of about 1-3 vol% [Seiler, 1994] will occur at the intersection due to hydrodynamic and diffusion effects leading to band broadening and increased detector backgrounds [Shultz-Lockyear, 1999]. This leakage can be circumvented using bias or pullback voltages to ensure zero potential difference in the side channels and can easily be achieved calculating the intersection potential V_i using Ohm's and Kirchhoff's law in case of buffers of uniform electrical conductivity (such as in CE) [Seiler, 1994; Jacobson, 1999; Fu, 2007; Crabtree, 2001].

Further parameters have been shown to account for possible sample leakage: intersection geometry and induced counter pressures [Shultz-Lockyear, 1999], length of each connected microchannel, induced junction potentials and field fringing effects at sample buffer interfaces due to concentration gradients [Shultz-Lockyear, 1999], dispersion effects resulting from differences in the ionic strengths of the solutions used, as well as pressure differences due to zeta potential variations and differing EOF velocities which can lead to pressure-induced volume flows [Shultz-Lockyear, 1999; Crabtree, 2001; Dose, 1992]. Numerical modeling was performed to study the effects responsible for the leakage in detail and therefore develop preventive strategies [Bianchi, 2000; Tsai, 2005; Fu, 2003]. Data from experimental as well as simulation results show that counter, bias or pullback voltages in combination with a double T- or double L-geometry of the cross-section are most suitable to minimize leakage effects [Wenclawiak, 2006; Fu, 2007; Bianchi, 2000; Tsai, 2005; Fu, 2003; Lin, 2004; Tsai, 2006].

These solutions will fail if separation modes like isotachophoresis (ITP) or isoelectric focusing (IEF) using buffer systems with a dynamic variation of the conductivity during the separation process are applied [Mikuš, 2011; Kler, 2013A; Hühner, 2015]. The same holds true if one end of the channel network is at a fixed potential like for the coupling with mass spectrometric detection. In both cases, a control of electromigration and electroosmosis is

only achieved if the intersection potential V_i is known and used to continuously adjust the bias potentials at all other channel ends [Tomáš, 2008].

In this study we introduce - to our knowledge for the first time - a low current in-channel potential measurement, which is applied for ITP and CE applications: A passivated electrode embedded in a microfluidic glass chip [Kler, 2013A; Kler, 2014] for interfacing capillary-based multi-dimensional electrophoretic separations was used for on-chip potential measurements for CE and ITP separations of amino acids as model analytes. Numerical simulations are performed for a deeper understanding of the resulting ITP intersection potential measurements.

3.3.3 Experimental section

3.3.3.A Materials and methods

Acetic acid (glacial, 100 %), ammonium acetate ($\geq$ 98%), L-arginine monohydrochloride (Arg, for biochemistry) and L-glycine (Gly, $\geq$ 99.7) were purchased from Merck (Darmstadt, Germany). L-histidine (His, USP grade) was bought from AMRESCO (Solon, Ohio USA). L-lysine (Lys, $\geq$ 98%) and isopropanol (LC-MS grade) were from Sigma Aldrich (Steinheim, Germany). All solutions were prepared with doubly-deionized water (Milli-Q purification system from Millipore, Bedford, MA). As leading and terminating electrolyte for ITP experiments, 10 mmol/l ammonium acetate, pH 4.5 (acetic acid) and 28 mmol/l acetic acid, pH 3.2 were used, respectively. The background electrolyte (BGE) for CE was 2.3 mmol/l acetic acid, pH 2.2. L-histidine and L-arginine 1 mmol/l and L-glycine and L-lysine 0.1 mmol/l solutions were prepared in water as injection solutions for ITP and CE experiments. The high-impedance voltage sensor was connected to the chip electrode by a wire with the conductive carbon glue WireGlue (Anders Products, Melrose, USA).

3.3.3.B Instrumentation

A custom-made multiport HV source (CalvaSens GmbH, Aalen, Germany) enabled the independent operation of 12 high voltage channels, 6 positive (from 0 to 15 kV) and 6 negative (from -15 to 0 kV) [Kler, 2014]. Together with a home-made multi-vial unit [Kler, 2014] this enabled the simultaneous and independent control of pressure and high voltage regimes for up to four vials. Pressure application in the range of 30 mbar to 2 bar for injection and flushing was achieved via the pneumatic unit of an Agilent 7100 CE system

(Agilent Technologies, Waldbronn, Germany) by-passing the pneumatic connection of the inlet port via the pneumatic valves Festo MFH-3-M5 (FESTO AG, Neuss, Germany) [Kler, 2014] controlled manually with an ad-hoc switch module. Following a previous study [Tiggelaar, 2007] the microfluidic borofloat glass chip interface (iX-factory GmbH, Dortmund, Germany) had a cross-channel design with etched channels of 60 µm in width and 25 µm in depth (Figure 3-21).
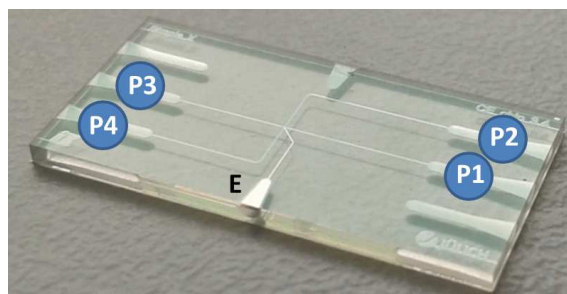
Figure 3-21: Customized 4 port microfluidic glass chip with a cross-arrangement of the channel network and an integrated Ti/Pt intra-channel electrode (E) for electrically contacting the intersection of the chip channels (iX-factory GmbH, Dortmund, Germany). A 500 nm passivation layer of SiN was deposited to electrically passivate the electrode. Chip dimensions were 20 × 10 mm^2. P1-P4 = capillary ports of the chip interface.

The thickness of bottom and cover plate were 700 µm and 200 µm. The chip contained an integrated channel electrode made of Ti/Pt for electrically contacting the intersection of the chip channels. The electrode thickness was 15 nm for the titanium and 235 nm for the platinum layer with an additional 500 nm passivation layer of silicon nitride (SiN). Capacitively coupled contactless conductivity detection (C^{4}D) was performed using an eDAQ ER125 with PowerChrome software Version 2.7.6 (eDAQ, Denistone East, Australia) using the following parameters: 100 Hz sampling rate, 1200 kHz excitation frequency, 50 % amplitude. The electrical potential was measured using a home-made high-impedance voltage sensor connected to the chip electrode.

3.3.3.C Numerical simulations

Numerical simulations were performed using a finite element method code using the program PETSc-FEM as platform through a Python interface [Kler, 2013B; Kler, 2011]. The simulations were performed on a beowulf cluster at CIMEC using five compute nodes with two quad-core Intel Xeon E5420 2.5 GHz processors, 8 GB DDR3–1333 MHz memory, interconnected via a switched Gigabit Ethernet network [Dalcin, 2011]. Data postprocessing

was performed with Paraview [Ayachit, 2015], NumPy, SciPy and Matplotlib [van der Walt, 2011].

3.3.3.D Preparation of the hybrid capillary-chip setup

The fused silica capillaries (50 µm ID, length 40 cm) were purchased from Polymicro Technologies (Phoenix, AZ), cut to the desired length using a capillary cutter (SHORTIX - Capillary Column Cutter, SGT, The Netherlands and Singapore) and cleaned with isopropanol. The glass chip was cleaned in isopropanol upon ultrasonication for 10 min. Afterwards, the capillaries were glued into the chip capillary ports of the glass chip with epoxy glue. For conditioning the setup was flushed with water and leading electrolyte (for ITP) or background electrolyte (for CE) by pressure application at 2 bar for 10 min. The system was left in doubly-deionized water when not in use. All solutions were introduced via port P1 (see Figure 3-22).

3.3.3.E ITP and CE conditions

The ITP and CE experiments were conducted in the 1D working mode using two active capillaries with the chip interface in the middle to follow the instantaneous electrical potential during the separation (Figure 3-22). Port P1 was used for injection and ports P1 and P3 for voltage application, while ports P2 and P4 were blocked with silicone stoppers and left floating during sample injection and separations (see Figure 3-22A). Model analytes were injected into capillaries filled with BGE (CE) or leading electrolyte (ITP): at a concentration of lysine and glycine of 0.1 mmol/l (CE) or histidine and arginine of 1.0 mmol/l (ITP) for 3 sec at 2 bar. For the ITP separation the inlet port P1 contained terminating electrolyte. The separations were performed in triplicate at 11 kV (ITP) or 18 kV (CE) applying 10 kV at the inlet and -1 or -8 kV at the P3 outlet. C^4D detection was accomplished 5 cm after the chip interface. For CE measurements Fast Fourier Transformation smoothing with 25 points was applied (Origin Lab software, Version 9.1) to increase the signal to noise ratio.
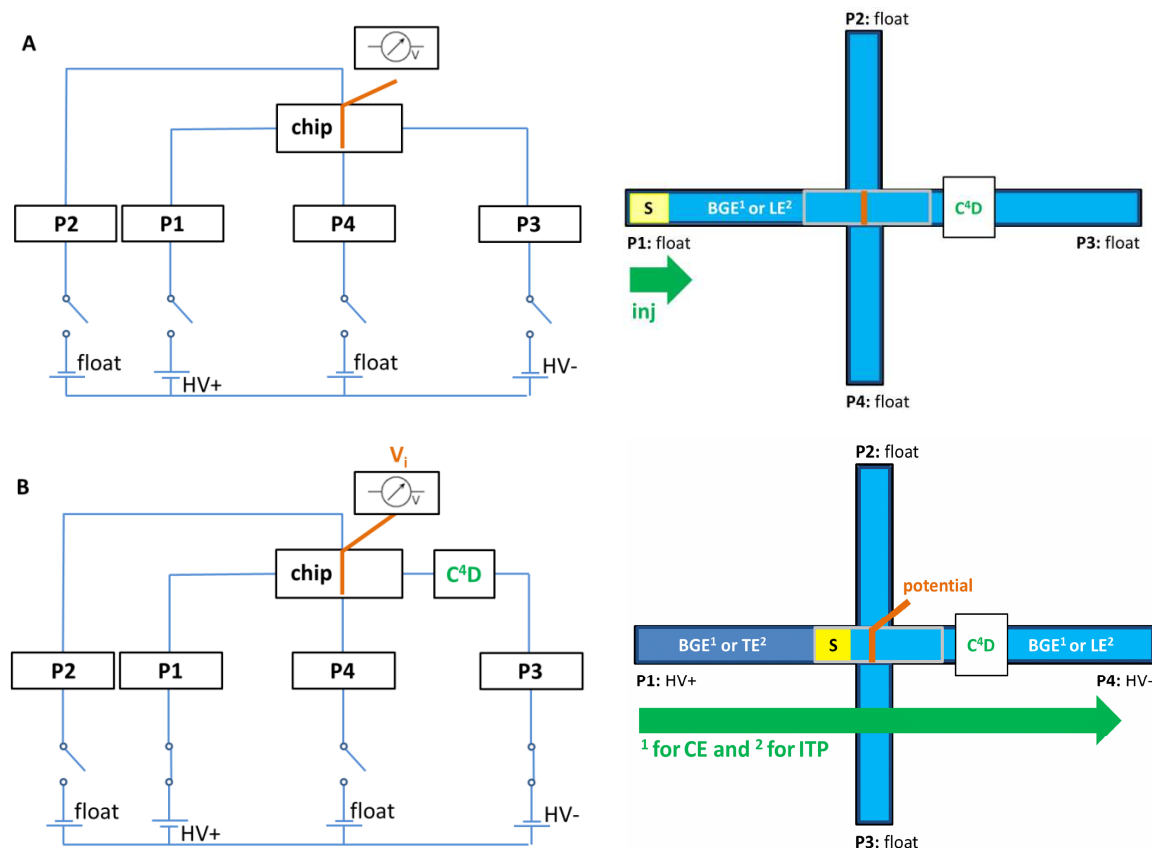
*Figure 3-22: Electrical circuit and operational scheme for the three steps involved in the on-chip potential (V_i) measurements for ITP and CE experiments: P1-4 = ports of the chip interface, S = Sample, inj = Sample injection. **A)** Prior to the sample injection the 2D setup was flushed with BGE or LE, respectively. **B)** After the sample injection step ITP and CE separations were conducted loading the TE or the BGE vial to P1 followed by voltage application to P1 and P3 as well as the on-chip potential measurement.*

3.3.4 Results and discussion

3.3.4.A Concept of on-chip intersection potential measurements

While several HV sources for multidimensional CE and microchip CE applications were reported [Felhofer, 2010; Jiang, 2007; Li, 2009], the problem of monitoring V_i and its implementation has hardly been discussed [Jiang, 2007]. In principle the following basic aspects have to be taken into consideration:

1)   Polarizable or conductive materials inside the electric field distort the field lines, which should ideally be parallel to the surface. Charged molecules accumulate on the surface of such materials, and consequently produce a heterogeneous double layer [Zhang, 2011]. Thus, a dielectric cover has to shield the intra-channel electrodes to avoid electrical

disturbances [Shin, 2012], which we achieve here using a silicon nitride (SiN) passivation layer over the electrode made of Ti/Pt, where the Ti layer accounts for enhancing adhesion to the glass and the Pt layer for enhancing surface stability [Madou, 2002]. The choice for SiN, resulted from a compromise of surface similarity to fused silica as well as sufficient chip bonding efficiency [Shin, 2012].

2)   In order to avoid electrolysis at the point of potential determination, the electric current intensity circulating through the electrode into the electrolyte should be as low as possible [Oh, 2009]. We here defined a working current of 1-10 nA which is at a level below the usual detection limits for redox-reaction-based electrochemical techniques [Keynton, 2004] to achieve a negligible reaction rate [Martin, 2006]. In this work, the intersection potential V_i was determined via a high-impedance voltage measurement in the form of a differential measurement of the potential at the intersection vs. a reference potential, determining the final voltage. With the current at the measuring input not exceeding 10 nA and a potential difference on a high common mode voltage range, a very high common mode input impedance is reached. The prototype for the potential measurements was optimized to allow measuring with a maximum measuring current of 10 nA. The technical implementation includes a high-impedance sensor input with a low input capacitance, for the front end of the voltage sensor and a high-voltage field-effect transistor (FET) with a low input capacitance was utilized. A setup in a basic source follower mode provides a common voltage range of approximately ±400 V. This range is clearly not sufficient for the intended operation; therefore, an additional controllable high-voltage supply was utilized in order to track the reference potential of the voltage sensor close to the potential of the passivated sensor electrode. The potential difference of the electrode and the reference should never exceed the common voltage range of the FET front end (i.e. ±400 V) in order to avoid excessive currents flowing through the sensor electrode.

3.3.4.B CE separation with on-chip intersection potential measurement

In order to show that the on-chip potential measurements are neither influencing the separation performance nor the analyte peak shapes, amino acid model samples were analyzed with adapted CE [Coufal, 2003] and ITP [Kubačák, 2006] methods, thus comparing separation modes of continuous vs. discontinuous buffer systems. Figure 3-23A and B show the C^4D trace of the electropherograms for the CE separations with and without on-line

potential measurements. Both electropherograms show very good agreement regarding detection time, peak area and peak shape of the two analyzed amino acids.
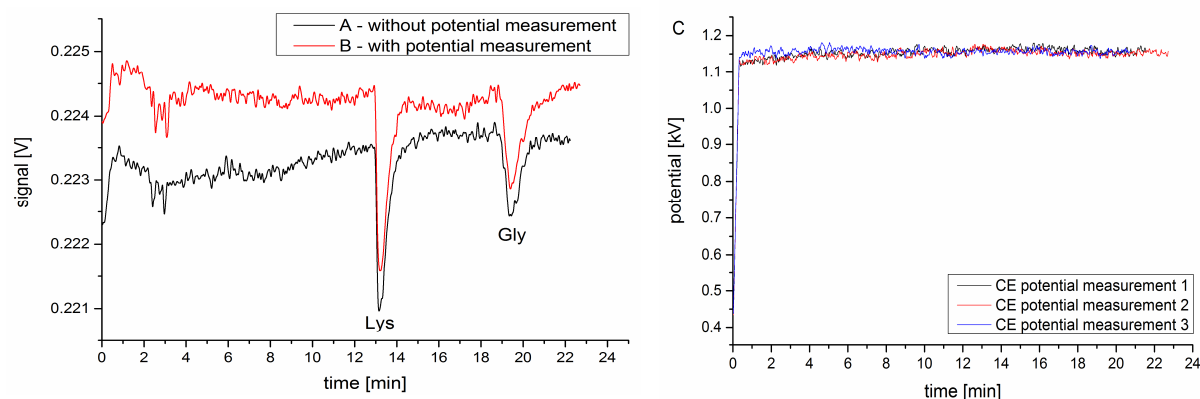
Figure 3-23: Electropherograms recorded via a C⁴D detector of CE separation of Lys and Gly in 2.3 M acetic acid as BGE in the modular hybrid 2D capillary-chip setup at 18 kV. Sample injection at 2 bar for 3 sec from port P1 (Figure 2). CE-C⁴D measurement without A) and with B) on-chip potential measurement. C) On-chip potential detection traces of B).

After the potential increase from voltage ramping during the first 30 s (Figure 3-23C) the measured potential remained stable at 1.18 kV throughout the whole separation process. The RSD value (n = 3) for the migration time was below 1.5 % and for the peak areas at 11 and 8 % (Lys and Gly), showing an acceptable precision for the analyte concentrations close to the detection limit. Figure 3C shows on-chip potential measurements with good repeatability of the potential patterns recorded during the 3 CE runs with an RSD value of 1.7 % (averaged potential values over the whole separation time, except the first 30 sec). The RSD values for the potential signal noise determined via averaging the values at 10.0 – 10.2 min and 16.6 – 16.8 min with a measuring rate of 1 Hz did not exceed 0.4 %, underlining the stability of the prototype.

3.3.4.C ITP separation with on-chip intersection potential measurement

A very good agreement regarding detection time, ITP step length and step shape for a sodium zone, the two analyzed amino acids, as well as the leading and terminating electrolyte zones can be deduced from Figure 3-24 comparing the isotachopherograms with and without on-line potential measurements. After 30 sec of voltage ramping the potential measured at the intersection reached its highest value of 3.5 kV at the start of the ITP separation (Figure 3-24C). It then decreased to a minimum of 0.7 kV between 10.0 and 12.5 min but then

increased almost linearly from 0.7 kV at 12.5 min to 3.8 kV at 30 min. Further potential application shows asymptotic convergence to a value of ca. 4.2 kV.
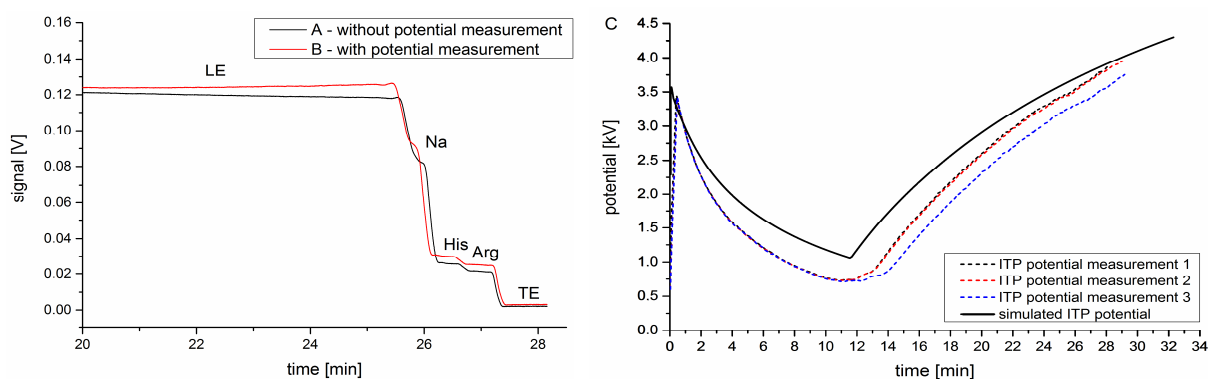
*Figure 3-24: C⁴D traces of isotachopherograms for His and Arg in the 1D working mode of the modular 2D capillary-chip setup. LE: 10 mM ammonium acetate, TE: 28 mM acetic acid. Sample injection at 2 bar for 3 sec from port P1. Separation voltage 18 kV: ITP-C⁴D measurements **A)** without and **B)** with on-chip potential measurement. **C)** Experimental on-chip potential measurements for ITP-C⁴D (n = 3) (dotted lines) and simulated ITP potential (without electroosmotic effects) under experimental separation conditions (solid line).*

Repeatabtilies (n = 3) were below 1.4 % for the detection time were and 4 % and 8 % for ITP step lengths of His and Arg. Figure 3-24C displays three on-chip potential measurements with excellent repeatability of the potential patterns of the first two measurements of the set of 3. The third measurement shows a slight offset most likely due to buffer changes not exchanging electrolyte vials. The experimental potential patterns showed a good correlation to simulations regarding the time course of the potential (see Figure 3-24C). The sharp simulation minimum was found at 1.2 kV at a time point of 11.5 min well comparable to the experiment (10.0 - 12.5 min) and the same final value of 4.2 kV as in the experiment. Especially the difference in the sharpness of the minimum of the potential values can be ascribed to the electroosmotic flow (EOF) present in the experiment but not taken into account for the simulation. A boundary TE/TE' between adapted and non-adapted TE will be transported through the capillary at the velocity of the EOF, changing the conductivity in the capillary over time in addition to the pure ITP process. A potential value of 4.77 kV is reached when the whole capillary filled with TE' by applying pressure (2 bar) at the end of the ITP run (Figure 3-25B). This is well correlated to the change in local conductivity visible in the C⁴D trace (Figure 3-25A).
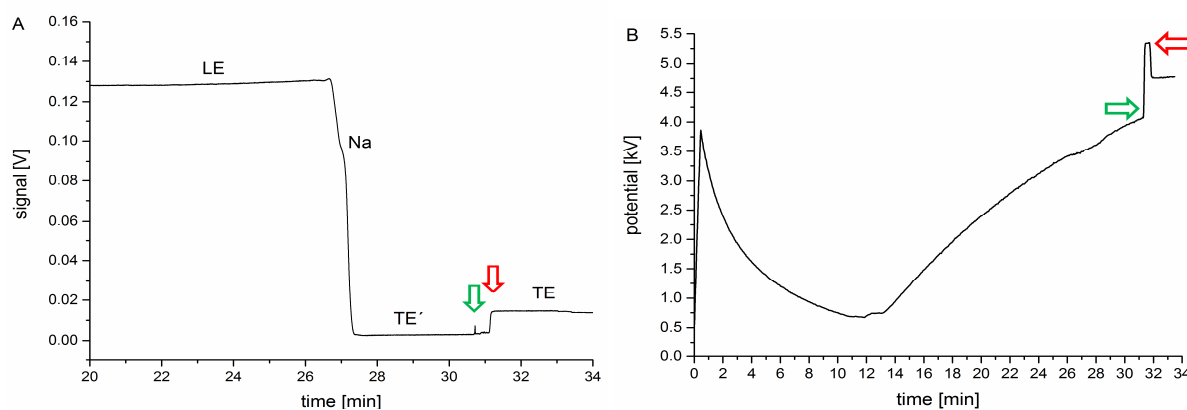
Figure 3-25: A) C⁴D detector signal for on-chip potential measurements for ITP-C⁴D (blank run; parameters for the separation were the same as in Figure 4.) B) on-chip potential trace; green/red arrows indicate start/stop of pressure application (2 bar).

3.3.5 Discussion

The results show that the on-line potential measurements do not disturb CE and ITP separations. No signs of migration time or separation efficiency changes or run failures due to gas bubble formation from electrolysis were visible. After full application of the separation voltage, the measured potential for CE runs stabilized at about +1.18 kV (1.7 % RSD, n = 3) for the whole separation time with very low noise levels. From the difference of the applied separation voltages, +10 kV and -8 kV, a value of +1 kV is expected with the potential measurement electrode placed in the middle of the separation path. The slight offset of +0.18 kV was due to a native component offset of the custom-made multiport HV source. The potential measurement conducted during the separations clearly showed that for uniform buffer systems such as in CE separations (see Figure 3-23C) the intersection potential is stable throughout the whole separation process as expected, thus demonstrating the feasibility of the presented on-chip potential measurements which could now be used for the control of the potential difference in side channel or even pinched injection modes [Alarie, 2000].

The systems also proved to be able to determine the dynamic potential changes due to conductivity changes in ITP. The high correlation of the repetitive measurements also during the first 30 sec of increasing potential of voltage ramping is worth to be noticed pointing to a highly dynamic reaction towards potential changes. Furthermore, the prototype will also be applicable when fixed potential e.g. ground potential in the hyphenation to MS is used. It is then possible to continuously adapt the bias voltages to electrokinetically close separation channels and thus reduce sample leakage at channel interfaces.

From the simulation results given in Figure 3-24C in comparison to the experimental results it is clear that the prototype adequately follows the dynamic potential changes in the system. The potential decline after application of full separation voltage for the ITP experiments is exponential due to the very fast migration of the leading electrolyte front within the capillary and is slowed down progressively with separation time because of the entrance of the adapted and non-adapted terminating electrolyte front into the separation channel. The minimum electric potential is reached when the capillary portion between port P1 and the electrode is filled with TE (half of the capillary for a symmetric setup, as in our case) that is, when the sample zone is present in the interface. The broadness of the minimum correlates with the detected ITP sample stack and therefore depends on its length. The ITP sample plug length detected via the conductivity detector is 2 min (25.5 to 27.5 min, see Figure 3-25A and B) and the width of the potential minimum ca. 2.5 min (see Figure 3-25C). Therefore, in this example the on-chip potential measurements can complement on-chip [Kler, 2014] or intermediate [Wang, 2004; Kler, 2013A] C^4D measurements for sample transfer in 2D setups [Kler, 2015; Kler, 2013A; Kler, 2014]. The further potential changes after 13.3 min are related to filling the second capillary with TE.

This filling takes longer than at the beginning of the separation as visible from the shown potential increase, due to the lower mobility of the terminating electrolyte (ITP separations were conducted at constant separation voltage). A final potential of 4.5 V is expected for a separation path homogeneously filled with concentration-adapted TE´ with separation voltages of +10 kV and -1 kV at ports P1 and P3. For the simulations as well as for the experimental data a final potential of approximately 4 kV was obtained. The difference of 0.5 kV at the minimum is due to the non-adapted TE zone entering the capillary due to EOF (not considered in the numerical simulations), resulting in a slightly non-uniform TE/TE´ zone [Beckers, 1991]. As for the CE experiments, the offset of +0.27 kV is due to the component uncertainty of the custom-made multiport HV source.

3.3.6 Conclusion and outlook

We here present intersection potential measurements for multi-dimensional electrophoretic separations using a low current measuring prototype in combination with a SiN passivated Ti/Pt electrode inside a glass microchip interface. On-chip intersection potential measurements were successfully conducted without disturbing CE and ITP analysis regarding separation and peak shape efficiency. The results obtained underline the excellent stability of

the potential measurement and the suitability of the passivation of the electrode clearly avoiding disturbances of the electric field lines as well as electrolysis during potential measurements conducted during electrophoretic separations. Successful simulation of the ITP intersection potential allowed a deeper understanding of the potential development during the separation. The gradual exit of the leading electrolyte and the entrance of the adapted terminating electrolyte were monitored by potential changes.

In order to accomplish a feedback system of potential adjustment by using bias voltages, a future development will be a software-controlled electrical feedback regulation of the applied potential via different HV power supplies to be implemented in the presented setup. With this combination it will be possible to electrokinetically close side channels and enable the hyphenation to systems at fixed potentials, e.g. mass spectrometry.

3.3.7 Acknowledgements

3.4 Spatially-resolved on-chip intermediate light emitting diode induced fluorescence detection

3.4.1 Abstract

Monitoring the analyte during the transfer step from the first to the second dimension in multidimensional electrophoretic separations is crucial to determine and control the proper time point for sample transfer and thus to avoid band broadening or unwanted splitting of the sample band and sample loss. A spatially-resolved intermediate on-chip LED-IF detection system was successfully implemented for a hybrid capillary-chip glass interface. The setup includes a high power 455 nm LED prototype as the excitation light source and a linear light fiber array consisting of 23 active 100 μm light fibers for spatially-resolved fluorescence detection in combination with a push broom imager for hyperspectral detection. Due to an increase of light scattering fluorescence signals, the channel cross section as well as the surface edge of the bonded glass block of the chip interface can be detected performing flushing experiments with an FITC solution at high pH (9.2) and therefore a very precise chip interface alignment can be performed. A calibration curve was recorded for concentrations of the basic FITC solution ranging from 0.125 to 25 μg/ml being highly linear with a correlation coefficient of 0.999 using a single light guide and 1000 ms exposure time. The LOD for FITC as a model analyte at a basic pH of 9.2 for a S/N ratio of 4 was determined to be 0.04 fmol. The presented setup was used for intermediate detection of the peak pattern of two injected FITC plugs with the on-chip optical detection prior to mass spectrometry (MS) as final detection. In addition, the surface analysis of solid samples can be performed as shown for FITC contaminated TLC plates and a tablet. With the setup presented here CIEF-focused labeled ß-lactoglobulin was detectable on-chip with a sufficient intensity to monitor the analyte band transfer in the glass chip interface. Therefore, the on-chip fluorescence imaging is applicable for on-chip intermediate optical detection in 2D CIEF-LED-IF/CE-MS assays.

3.4.2 Introduction

Regarding multidimensional electrophoretic separations with sample heart-cutting monitoring the analyte during the transfer step from the first to the second separation dimension is crucial to determine the proper time point for sample band transfer to precisely control the sampling step and thus to avoid band broadening or unwanted splitting of the sample band and sample

loss. Therefore, in general all non-destructive detection methods normally used in capillary electrophoretic separations are applicable as intermediate detection methods, e.g. absorption or fluorescence detection. With respect to the low detection volumes (nl-range) in capillary electrophoresis due to the small capillary inner diameters, laser induced fluorescence (LIF) detection is well suitable due to high light intensities and ease of focusing also into small volumes as well as its inherently high sensitivity and selectivity, especially for analyte derivatization assays. As excitation light sources commonly Nd:YAG (266/355/532 nm), He-Cd (325/442 nm), argon ion (488/514.5 nm), and He-Ne (543.5 nm) lasers are used [Wu, 1992; Chiang, 2000; Horká, 2001; Schwarz, 2001; Lin, 2003; Liu, 2003; Götz, 2007; Jung, 2007; Liu, 2006; Fu, 2006; Dada, 2010]. With LIF setups, detection limits as low as zeptomolar (10^{-21} mol) can be reached [Ramsay, 2009] which is not possible with any other detection method in combination with capillary electrophoresis. Classical fluorescence detection setups (using a laser or a LED as excitation source) usually require complex optical instrumentation, as well as labeled analytes, although some target molecules exhibit native fluorescence, e.g. at wavelengths in the UV range [Huhn, 2008]. With a special interest in the miniaturization of capillary electrophoretic assays, the use of laser diodes as well as light emitting diodes (LEDs) [Schwarz, 2001; Götz, 2007; Ryvolova, 2010] is gaining popularity due to their ability to be integrated into very small chip platforms (dimensions in the mm range), but in general this goes along with a loss in sensitivity compared to lasers, due to less efficient focusing of the excitation light. Particularly, for chip applications the use of LEDs is most promising due to their small-size, long lifetime, low-power consumption and low-costs, since the first reported usage of an LED in a CE assay [Tong, 1995; Xiao 2007; Xiao 2009]. Due to intensive research in the last 20 years, LEDs are getting more and more powerful owing to the optimization of transmission properties by means of beam width, intensity, coherence and monochromaticity of the LED light to improve selectivity and sensitivity of LED-induced fluorescence (LED-IF) assays. Nowadays, LEDs are covering much of the UV-visible and parts of near-infrared spectral regions (280-1300 nm), giving rise to a wide spectrum of potential applications. The low costs compared to lasers, as well as the LEDs small dimensions make them extremely interesting as excitation light sources especially for microfluidic analytical devices.

Beside the optical beam properties of the LED light source itself, the optical geometry of the detection setup is crucial in terms of optimizing the detection sensitivity of an LED-IF setup. For the collection and guidance of the fluorescence light to the detector, lenses, light guides and even fiber arrays can be used. There are three general geometries for fluorescence

detection setups: 1) collinear or confocal-types using microscopy optics, 2) right-angle or orthogonal setups using lenses or optical fibers, and 3) bevel angle arrangements with the excitation light focused at angles of 45° or 30° and fluorescence detection perpendicular to the chip surface [Chabinyc, 2001; Sluszny, 2005; Fu, 2006; Götz, 2007]. In general, scattered excitation light, reflections and refraction from the cover plate and channel walls, Rayleigh and Raman scattering from the sample and background fluorescence from optical lenses and the chip are responsible for increased background signals and therefore low signal to noise (S/N) ratios. Fu et al. [Fu, 2006] demonstrated via simulations and experimental data that for a perpendicular excitation setup best S/N ratios were obtained for collection angles of the fluorescence light of the 45° and 135°, respectively. Furthermore, the use of filter combinations for excitation and fluorescence light such as bandpass and long pass filters generally increase S/N rations due to decreased background fluorescence from the lenses and the chip substrate. In general, short channel-to-surface as well as excitation source-to-channel distances are most beneficial for increased detection signals [Liu, 2008]. Photodiodes and photomultipliers are commonly used for detection [Schwarz, 2001; Novak, 2007; Liu, 2008] or - if wavelength-resolved detection is of interest - charge-coupled device (CCD) cameras and diode array detectors (DAD) [Wu, 1992; Wu, 1995; Beck, 1993]. New developments implement hyperspectral imaging using a push broom imager to simultaneously obtain spectral and spatial information of a certain sample area [Panic, 2011; Schäferling, 2012]. Spectral ranges from ultraviolet, visible to the near-infrared spectral regions (300 nm - 2.600 nm) are accessible, as discussed in detail in Section 3.4.4.D. The advantage of the spatially-resolved over point detection is that a certain sample or separation channel segment can be monitored in greater detail, making the hyperspectral detection especially interesting for monitoring the interface region and thus analyte movement of e.g. channel couplings. To our knowledge, spatially-resolved fluorescence detection has not yet been implemented as intermediate detection method in multidimensional electrophoretic separations. To expand the modular two-dimensional hybrid capillary-chip separation platform (Section 1 Motivation), intermediate spatially-resolved LED-IF detection was implemented for the glass chip interface using a linear optical light guide array in combination with a push broom imager. In the following sections the general strategy and the development of each optical part is described in detail.

3.4.3 Experimental section

3.4.3.A Chemicals

Carrier ampholyte solution Pharmalyte 3–10 for isoelectric focusing was purchased from GE Healthcare Bio-Sciences AB (0.36 meq/mL pH, Uppsala, Sweden). β-Lactoglobulin (β-Lact, bovine milk > 90%, pI: 4.83–5.4, 18.4 kDa), 3-glycidoxypropyl-trimethoxysilane (GPTMS, 97%) and sodium tetraborate decahydrate ($Na_2B_4O_7$, puriss p.a.) were purchased from Sigma-Aldrich Chemie GmbH and isopropanol (LC-MS grade) from Fluka (Steinheim, Germany). Acetic acid (glacial, 100 %) and hydroxyethyl cellulose (HEC, for synthesis) were from Merck KGaA, sodium hydroxide (0.1 mol/l, for analysis) was used from AppliChem GmbH (Darmstadt, Germany) and methanol (HPLC gradient Grade) from BDH PROLABO CHEMICALS VWR (Darmstadt, Germany). Triethylamine (TEA, 99%) was purchased from Alfa Aesar GmbH + Co. KG (Karlsruhe, Germany). All solutions were prepared with doubly-deionized water (Milli-Q purification system from Millipore, Bedford, MA).

3.4.3.B General instrumentation

All electrophoretic separations and flushing experiments were performed using an Agilent 7100 CE system equipped with a UV absorbance detector (Agilent Technologies, Waldbronn, Germany) providing pressure and voltage regimes, injection control, and vial handling. MS detection was achieved using an Agilent 6100 Series Single Quadrupole system (Agilent Technologies, Palo Alto, USA). The CE was coupled to the MS via a coaxial sheath liquid interface from Agilent using an Agilent isocratic pump 1260 (Agilent Technologies, Waldbronn, Germany) for delivering sheath liquid (50:50 (v/v) mixture of water and isopropanol, containing 0.1 % acetic or formic acid (depending on the used background electrolyte)) at a constant volume rate of 4 μl/min. Nebulizer pressure was set to 0.28 bar and the drying gas was delivered at rate of 4 l/min at a temperature of 300 °C. The fragmentor was set to +150 V, the capillary voltage was +4 kV and the nozzle voltage +2 kV. The single quadrupole was used in single ion mode (SIM) and scanning mode (scan). The respective mode and related m/z are given in the respective figure legends.

3.4.3.C Instrumentation for intermediate on-chip LED-IF detection

Intermediate LED-IF on-chip detection was realized via the setup discussed in Section 3.4 and applied to on-chip as well as solid samples using Thin Layer Chromatography (TLC) plates and tablets. TLC plates and tablets were measured directly without any pretreatment.

For the TLC plate characterization the plates were immersed in aqueous solutions of different concentrations of fluorescein. The LED-IF measurements for the solid samples were done via the same setup as for the chips, but without the aluminum bottom plate housing the chip slide holder (aluminum part (2) in Figure 3-9). The LED prototype as well as its control software were developed and fabricated in cooperation with FutureLED (Berlin, Germany). For tempering the LED a Peltier element from head electronic (Prien am Chiemsee, Germany) was used. The fluorescence light was collected via a linear fiber array fabricated at art photonics (Berlin, Germany) see Section 3.4.4. The push broom imager used for hyperspectral detection of the fluorescence light and the push broom software for signal data recording version 1.0 (V.1.0) were from J&M Analytik AG (Essingen, Germany) (Section 3.4). The respective conditions and parameters for measurements using the push broom imager are listed in the figure legends.

3.4.3.D Chip interface - 2nd generation interface design

Following a previous study [Tiggelaar, 2007] the microfluidic borofloat glass chip interface (iX-factory GmbH, Dortmund, Germany) generally a double T-or a cross channel design (if not stated otherwise) with etched channels of 60 μm in width and 25 μm in depth (2nd generation chip design, Section 3.1). Bottom plate thickness was 700 μm and cover plate thickness was 200 μm including two bonded 500 μm glass blocks. The fused silica capillaries (50 μm ID) were purchased from Polymicro Technologies (Phoenix, AZ), cut to the desired length using a capillary cutter (SHORTIX - Capillary Column Cutter, SGT, The Netherlands and Singapore) and cleaned with isopropanol. The glass chip was cleaned in isopropanol upon ultrasonication for 10 min. The coupling was performed by gluing the capillaries to the chip using epoxy glue (Araldite, Huntsman Advanced Materials Ratingen, Germany) as it was previously reported [Tiggelaar, 2007]. All solutions were introduced via port P1 (see Figure 3-26).

3.4.3.E Procedure for (3-Glycidoxypropyl)trimethoxysilane (GPTMS) coating

The coating protocol was taken from X. Shao et al. [Shao, 1999; Horka, 2001]. First, the 2D setup was rinsed with a cleaning solution of 1.0 mol/l NaOH, 1.0 mol/l HCl followed by water for 30 min at 2.0 bar for each solution. Finally, the GPTMS coating solution (c = 10 % w/w, pH ≈ 5) was introduced at 2 bar for 120 min. Then, the setup was gently purged with compressed air overnight (minimum 10 hours at 1 bar). This process was repeated in order to achieve a homogeneous coating on the capillary surface. For conditioning

the respective 2D setup was flushed with water and anolyte for a minimum of 30 min for each solution at 2 bar using the Agilent 7100 CE system. To verify the quality of the coated 2D setup first separation, the capillary was first flushed with anolyte. Afterwards +25 kV were applied to monitor if a stable current was reached. Both systems were left in doubly-deionized water when not in use. For long-term storage the capillary-chip setups were flushed with air and left at room temperature.

3.4.3.F Determination of detection limits and linear range

To characterize the optical on-chip LED-IF setup for the hybrid capillary-chip system in more detail, flushing experiments were performed using a fluorescein isothiocyanate (FITC) solution in $Na_2B_4O_7$ buffer (10 mmol/l, pH 9.2). For cleaning the setup was rinsed with the borate buffer between experiments. Unused vials were blocked with silicone filled blocking vials. They were prepared using conventional CE vials from Agilent Technologies (Waldbronn, Gemany) filled with silicone b1 from Chemphar Handels & Export (Hamburg, Germany) to immerse the respective capillary in the cured silicone [Zhang, 2006A]. For the experiments first the whole setup was flushed with buffer and then the sample was injected from port P1 as indicated by Figure 3-26A. After that the respective buffer vial was loaded to P1 and 1 bar pressure was applied to flush the sample stack through the capillary-chip setup as indicated by Figure 3-26B.
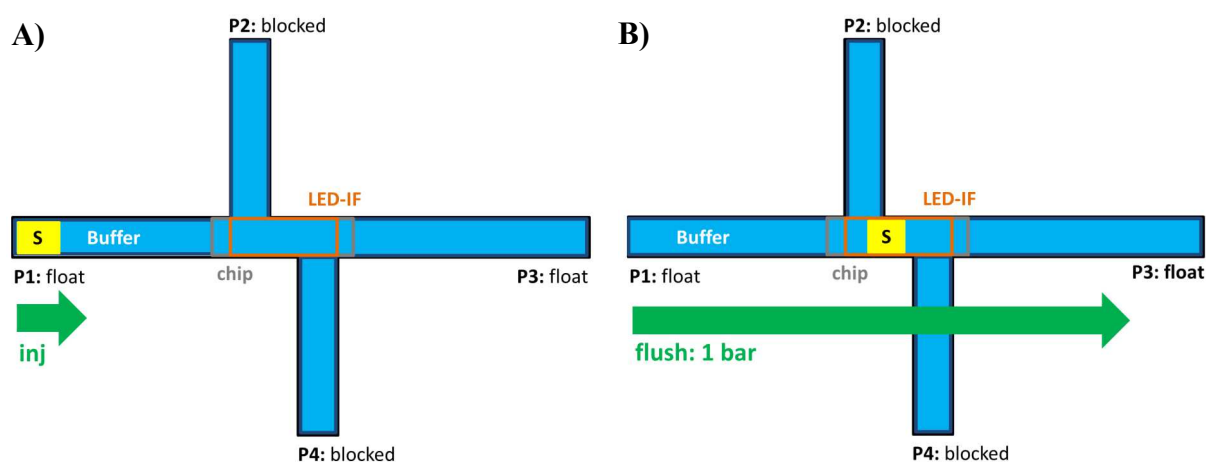
*Figure 3-26: Operational scheme for the flushing experiment with on-chip LED-IF detection: P1-4 = ports of the chip interface, S = Sample plug, inj = Sample injection. **A)** The 2D setup was flushed with buffer. **B)** After the sample injection step, the sample plug was flushed from port P1 to P3 with P2 and P4 being blocked.*

3.4.3.G Protein labeling

Model proteins were labeled with Chromeo P503 [Wetzl, 2004; Craig, 2005; Wojcik, 2008] from Active Motif (Carlsbad, CA, USA) was used. 10 µL of a protein stock solution (β-lactoglobulin, c = 5 mg/ml in water) was mixed with 15 µl of $Na_2B_4O_7$ buffer solution (10 mmol/l, pH 9.2) and 1 µL of P503 labeling solution (2.5 mmol/l in methanol). The labeling reaction took 30 min at room temperature. To quench the reaction 40 µL H_2O were added. Right before the experiment water was added to a final volume of 100 µl [Dickerson, 2010].

3.4.3.H Conditions and parameters for 1D CIEF-LED-IF in the 2D setup

The sample contained 2.0 % v/v Pharmalyte 3-10 carrier ampholytes and 0.1 % v/v HEC as a dynamic EOF modifier to minimize EOF velocity [Verzola, 2000]. A 1.0 % w/v HEC stock solution was prepared by dissolving 0.4 g HEC in 40 ml doubly-deionized water at 70°C. 1 mol/l aqueous acetic acid was used as anolyte and 250 mmol/l aqueous triethylamine (TEA) as catholyte containing 0.1 % w/v HEC, respectively. The solution with the labeled protein was mixed with the carrier ampholyte stock solution with the final concentration of the model protein of 1 mg/ml. A custom-made multiport HV source (CalvaSens, Aalen, Germany) enabled the independent operation of 12 high voltage channels, 6 positive (from 0 to 15 kV) and 6 negative (from -15 to 0 kV) [Kler, 2014]. Together with a home-made multi-vial unit this enabled the simultaneous and independent control of pressure and high voltage regimes for up to four vials. Pressure application of 1 bar for injection and flushing was achieved via the pneumatic unit of an Agilent 7100 CE system (Agilent Technologies, Waldbronn, Germany) by-passing the pneumatic connection of the inlet port via pneumatic valves Festo MFH-3-M5 (FESTO, Neuss, Germany) [Kler, 2014] controlled manually with an ad-hoc switch module. The CIEF separations were carried out with detection at the anodic end. The injection protocol for the experiment is described by Figure 3-27A. First, the whole setup was flushed with anolyte for 600 sec at 1 bar followed by the injection of the sample solution containing the carrier ampholytes (CA) and the labeled protein (S) for 15 sec at 1 bar. Finally, a catholyte plug was injected as a sacrifice zone due to cathodic drift during potential application (see Section 4.1.2.C). Finally, with the catholyte vial loaded to port P1 and the anolyte vial loaded to port P3 separation potential was applied. During the experiment a separation voltage of -19 kV (-10 kV at port P1 and +9 kV at port P3, see Figure 3-27B) was applied over the 2D setup and the focusing time was 7 min with ports P2 and P4 being

blocked with silicone filled vials. Mobilization of the pH gradient was obtained by applying a pressure of 1 bar to the inlet vial P1 while maintaining the final voltage of -19 kV.
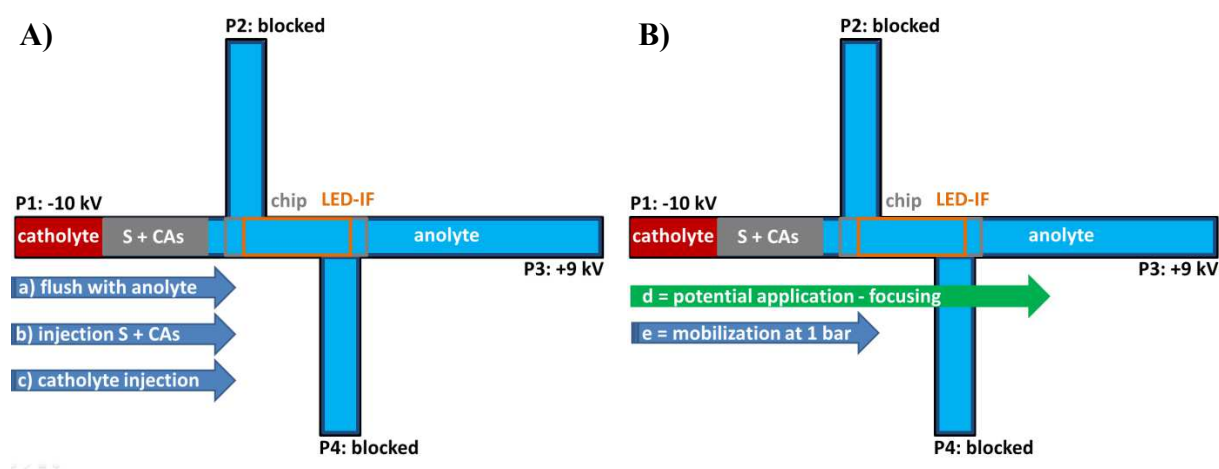
Figure 3-27: Operational scheme for the two steps involved in 1D CIEF-LED-IF separation performed within the 2D hybrid capillary-microchip setup for multidimensional separations: A) Prior to the sample injection the 2D setup was flushed with anolyte. After the sample injection step a catholyte plug was injected as a sacrifice zone due to cathodic drift during potential application. B) After application of the focusing step the CIEF pH gradient was mobilized by pressure application from port P1 to port P3 to the intermediate on-chip detection system, while ports P2 and P4 were blocked via commercial CE vials filled with cured silicone.

The current profile started at an initial value of about 12.0 µA and exponentially declined upon the progress of the focusing process to a final value of 3.0 µA. Detection of the labeled protein was achieved via the on-chip LED-IF setup described in Section 3.4.4.

3.4.4 *Intermediate on-chip LED-IF detection - strategy and realization*

One goal of the work was to implement on-chip intermediate light emitting diode (LED) induced fluorescence detection (LED-IF) to monitor and therefore properly control the heart-cutting transfer of a CIEF focused sample band from the first to the second electrophoretic separation dimension via the common intersection segment of the microfluidic interface. Ideally, this is achieved with a spatial resolution imaging the whole segment to monitor analyte movement or transport. For this, the excitation light is first focused to a line exciting to the whole channel segment of interest (volume of the common intersection, V_c and the length of the fiber array L_{FA} in Figure 3-28) using different lenses. To allow spatial resolution the fluorescence light is collected from this region via a certain number active light guides linearly oriented inside a fiber array covering the excited channel length (L_{AF}). For a spatial, time and wavelength resolved fluorescence signal detection the

fiber array is guided into a push broom imager. The common intersection length (V_c) used for the experiments in this study was 5 mm as shown in Figure 3-28.
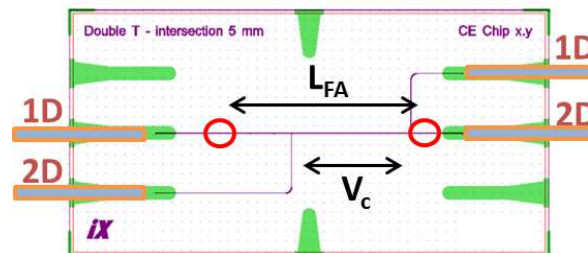
Figure 3-28: 4-port chip with double T-interface with 5 mm common intersection segment length (Vc = ~ 7 nl and 5 mm length). L_{FA} = length of the fiber array was 8750 μm (~ 9 mm).Modified CAD drawing from iX-factory (Dortmund, Germany).

The full instrumental setup of the intermediate optical LED-IF on-chip setup is shown in Figure 3-29. The design of the optical geometry and the technical drawings were developed in cooperation with J&M Analytik AG (Essingen, Germany). The setup consists of two aluminum parts (1) and (2). The aluminum part (1) keeps the optical excitation and detection elements in a fixed 45° angle to each other with an optical focal point at the middle of the channel system inside the microfluidic interface. The bottom plate part (2) of the setup houses the glass chip interface (3) which is sits in a chip holder slide (4). Both aluminum parts can be tightly fixated to each other with the fixation screws S_1-S_4. With the screws S_{c1}-S_{c3} inside the bottom plate the chip holder slide and thus different separation channel segments (e.g. the common intersection) of the chip interface can be moved in x- and y- direction into the optical excitation and detection focal point of the optical setup. The excitation light, emitted from the used LED prototype is coupled into the optical setup via an optical light guide connected to an SMA-connector (5). The optical path for excitation is arranged in a 45° angle to the glass chip interface located in the chip slide holder to achieve optimal sensitivity for the labeled analytes.
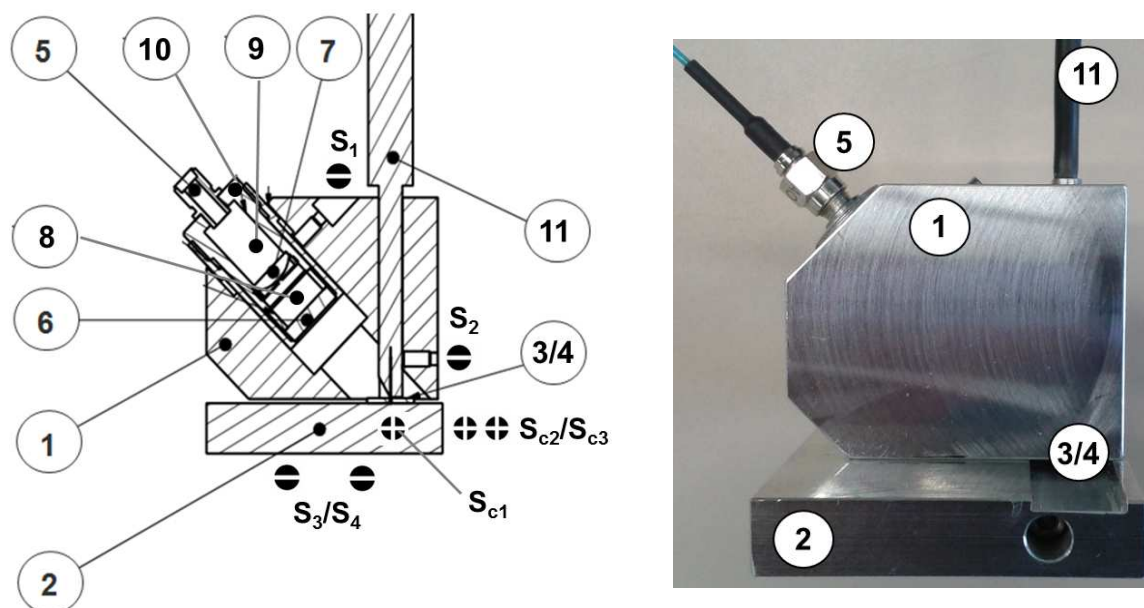
Figure 3-29: Intermediate LED-IF on-chip detection setup: (1) Aluminum housing, (2) aluminum bottom plate, (3) the hybrid capillary-microchip, (4) chip holder slide, (5) SMA-connector for light guide connection from excitation light source, here: LED with 455 nm, (6) cylindrical lens for slit focusing and (7) plano-convex lens for collection and parallelization of excitation light and (8) 452 nm bandpass filter from Edmund Optics (Karlsruhe, Germany), (9) optics Shell 1 and (10) optics Shell 2 and (11) detection light guide: linear fiber array 24 × 100 μm active fibers. S1-S4 = screws for fixation of the optical setup and Sc1- Sc3 = screws for alignment of the chip holder slide and thus the chip channel. Left = Modified CAD drawing from J&M Analytik AG (Essingen, Germany).

The emitted light from the light guide is collected and focused via a system of optical lenses (6) and (7) to a 10 mm long line, representing the maximal length of a chip channel inside the glass chip interface as discussed in Section 3.1. The bandwidth properties of the excitation light can be further optimized by placing a band pass filter (8) in the optical path if needed (optional). The optic Shells 1 (9) and 2 (10) are used for the fixation of the respective lenses and the filter as well as for maintaining the correct distances of each optical element to one another regarding their respective focus lengths. The optical Shell 2 houses the plano-convex lens (7) for collection and parallelization of excitation light and the optical Shell 1 houses the cylindrical lens for slit focusing (6) as well as the bandpass filter (8). The fluorescence light emitted from the labeled analytes inside the common intersection is collected by a linear fiber array (11). This array was placed in a 90° angle to the chip cover plate surface and 45° to excitation. The linear fiber array consists of 24 active 100 μm diameter light fibers spanning over a distance of 8.75 mm (L_{FA} in Figure 3-28) using for each active two blind fibers of the same kind, to achieve a spatially resolved image of the chip channel with the common intersection. For detection, the fluorescence light was guided via the linear fiber array to a push broom imager (not shown), consisting of a spectrograph and a CCD camera as detector (see Section 3.4.4). On the detection side the linear fiber array is enlarged using three blind

fibers to separate each active fiber to a final length of 11.63 mm to gain maximal detection sensitivity (number of pixels per active light guide) using the CCD sensor inside the push broom detector. Using the combination of a linear light fiber array and push broom imager 3D spectral, spatial and time-resolved fluorescence detection is enabled, and therefore the monitoring of the dynamics of the incoming analyte band regarding peak shape and position in the interface's common intersection is possible. Figure A3 shows a 3D CAD file with a complete overview of the setup. In the following, the different parts of the setup and their respective design are discussed in more detail.

3.4.4.A Excitation light source: 455 nm LED prototype

The wavelength of the LED was chosen to be universal to excite common low-cost fluorophore labels used for fluorescence detection as for example fluorescein [Sjöback, 1995] or aminopyrene trisulfonic acid (APTS) [Evangelista, 1995] and their derivates, as well as P503 a specific dye especially designed for CIEF [Wetzl, 2004; Craig, 2005; Wojcik, 2008; Dickerson, 2010], which was used in this work. These fluorophores have absorption maxima in the range of 440 to 500 nm. For this reason, a temperature-controlled high power LED with an emission wavelength of 455 nm was chosen as the excitation light source. The prototype as well as the software were developed and fabricated in cooperation with FutureLED (Berlin, Germany). The general parameters of the LED source are listed in Table 3-4. For tempering the LED chip the prototype included a Peltier element from head electronic (Prien am Chiemsee, Germany). A simple plug-in connection was used to couple the LED to the light guide with one end of the light guide placed directly placed in front of the LED chip as shown in Figure 3-30. The other end of the light guide was connected to the optical setup via an SMA connector (5) as shown in Figure 3-29.

Table 3-4: *General parameters of the LED in this study*

Parameter LED	
wavelength [nm]	455 ± 50
power [watt]	1
coupling efficiency into light guide [%]*	$15 - 20$
working temperature [°C]	25 ± 0.1
temperature range	$0 \ldots +60 \pm 0.1°C$
Coupling of LED to light guide	plug-in connection

* = Silica glass fiber with 600 μm diameter and 1 m in length

A) Control software for Peltier element

Figure 3-31 shows a screenshot of the control software for the Peltier element. First, the working temperature was set to 25 ± 0.1°C (Temp. set point) comparable to ambient room temperature. Second, (TEC controller data) several parameters of the cooling device were monitored, e.g. "ready", temperature and the power consumption during the cooling process.

.
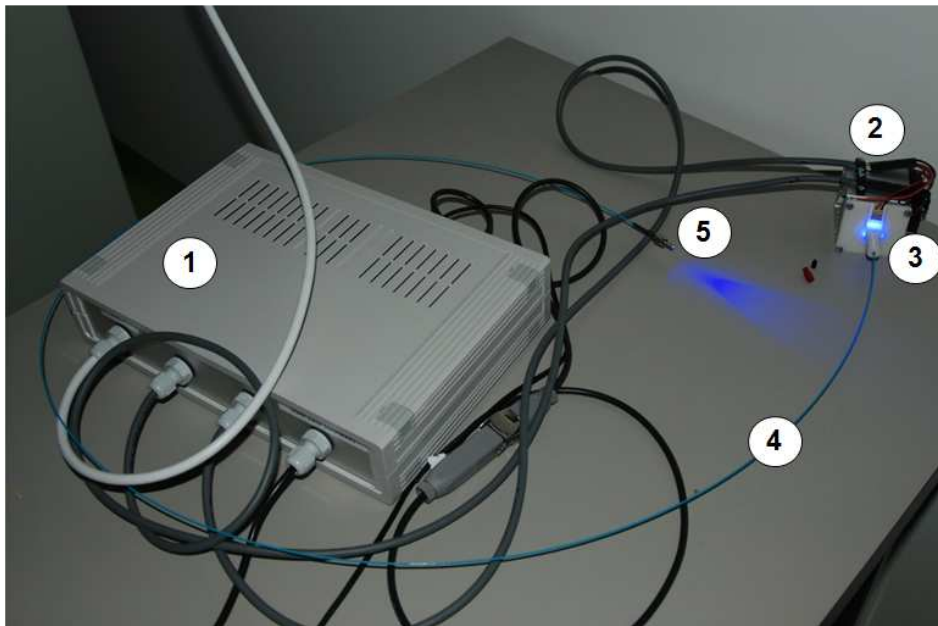
Figure 3-30: Prototype of 1 W LED 455 nm: 1) control unit, 2) Peltier element 3) plug-in connection for coupling of LED to light guide, 4) light guide and 5) SMA connector

B) Software for power control

The software to control power of the LED is shown in Figure 3-32. The power of the LED can be set in % of total power labeled as the *Helligkeit* (brightness) as well as the running time in *Sekunden* (seconds). Finally, the LED can be activated or deactivated via the Start and Stop button.
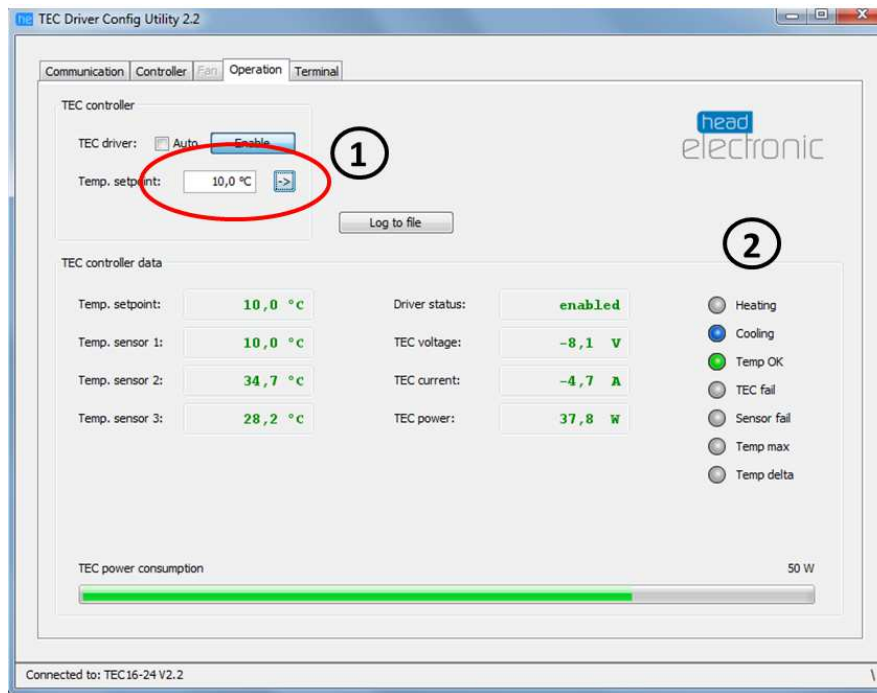
Figure 3-31: LED cooling software to control the Peltier element.
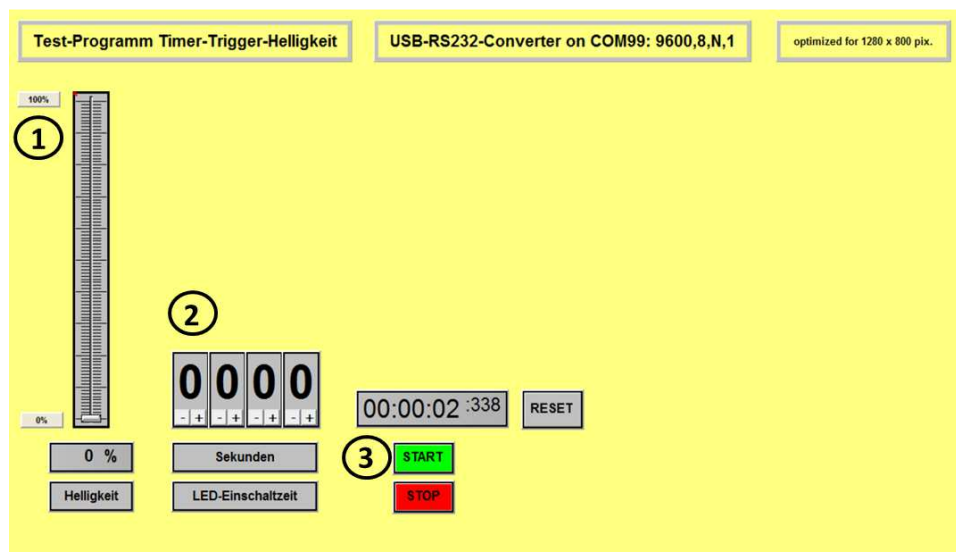
Figure 3-32: The software to control power of the LED.

3.4.4.B Optical excitation setup in detail

The SMA-connector to couple the light guide coming from the LED to the optical excitation setup as well as the a plano-convex lens used to collimate and focus the excitation light to a 10 mm long slit was purchased from J&M Analytik AG (Essingen, Germany). The uncoated PCX cylindrical lens used for collection of the emitted LED light from the light guide as well as the used band pass and cut off long pass filter were from Edmund optics (Karlsruhe, Germany). The general parameters of the used lenses and filters are summarized in Table 3-5.

Table 3-5: General parameters of the lenses and filters of the optical excitation setup.

Parameter LED	Unit
collector lens	PCX cylindrical lens, uncoated, focal length 25 mm, 12.5 mm diameter (article-No. 68-168)
slit focusing lens	plano-convex lens focal length 15 mm (J&M article-No. 51 551 83)
band width reduction of LED emission spectrum	band pass filter 452 nm, 51 nm FWHM, OD >6.0 Coating Performance, OD6 blocking, 12.5 mm diameter (article-No. 86-340)
cut off filter for excitation light	long pass filter 500 nm, OD >4, 12.5 mm diameter (article-No. 62-976)

The P503 label used in this work is a dye designed especially for labeling proteins for fluorescence detection using CIEF separation assays. The dye is covalently bound to the protein analyte at its amide groups and therefore preserves the native charge and the pI value of the labeled protein [Wetzl, 2004; Craig, 2005; Wojcik, 2008; Dickerson, 2010]. The dye changes its absorption and emission characteristics upon being covalently bound (pink lines) vs non-bound (blue lines) as indicated in Figure 3-33. The labeled protein shows an absorption maximum (2 abs in Figure 3-33) at 503 nm (red dashed line) and has an emission maximum at 603 nm (2 em) as indicated by the black dashed line, with a Stokes shift of 100 nm. For the non-bound label the absorption maximum (1 abs) is shifted to 604 nm and the emission (1 em) is nearly completely suppressed as indicated by the blue line. Therefore, the P503 label can be used without further purification steps after the labeling reaction. With the LED prototype used (emission maximum at 455 nm) in combination with the chosen band pass filter (Table 3-5) the derivative analyte was excited at about 70 % of the intensity at the absorption maximum as indicated by the blue dashed line (Figure 3-33). Prior to the detection, the fluorescence light was cut off below 500 nm using the 500 nm long pass filter to minimize the reflected high intense excitation light before detection.

Figure 3-34 shows the general on-chip optical setup discussed in Section 3.4.4 in more detail (see also photography in Figure 3-29). As mentioned the focal point (red circle) of the excitation and detection light path is located in the center of the separation channel of the glass chip interface (orange) placed in the chip slide holder (blue) as indicted by the red (excitation) and green (detection) dashed lines. The yellow arrows indicate the distances of the optical elements within the excitation light path: The distance (x_1) from the SMA connector of the excitation light guide to the plano-convex lens (L_{pc}) is 15 mm according to

the focal length of the lens, followed by the cylindrical lens (L_c) with a distance of $x_2 = 10$ mm.
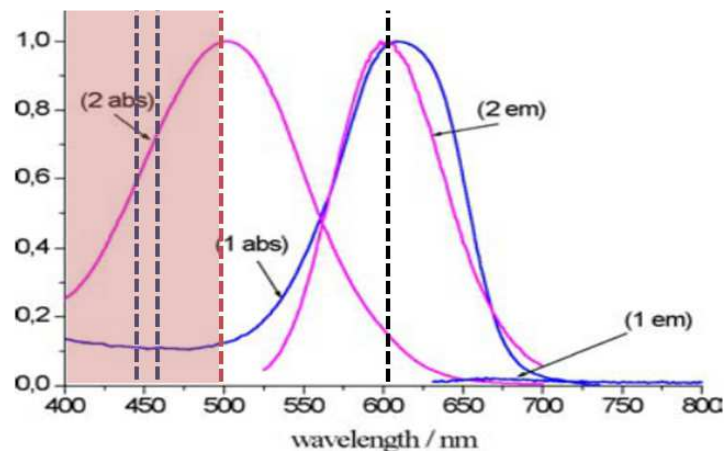
Figure 3-33: Absorption and emission spectra for the P503 label and labeled proteins: Covalently bound to a protein the absorption maximum (2 abs) is at 503 nm (red dashed line) and the emission maximum at 603 nm (2 em) black dashed line, with a Stokes shift of 100 nm. For the non-bound label the absorption maximum (1 abs) is shifted to 604 nm and the emission (1 em) is very low indicated by the blue lines. Light red area = cutting window of the used 500 nm long pass filter. Adapted figure from the technical data sheet Chromeo P503 [www.activemotiv.com]

The 10 mm between both lenses is left for inserting optical filters to better define the excitation light as for example with the band pass filter listed in Table 3-5. The focal length ($x_3 = 25$ mm) of the cylindrical lens defines the distance $x_3 = 25$ mm to the channel system of the chip interface. To vary the shape of the excited area at the chip channels a second version of the optical Shell 2 (Figure 3-35) with a variable length x_1 was developed in cooperation with J&M and the constructed in-house in the metal work shop of the University of Tübingen. A screw thread was implemented into the shell housing a cylinder (with a suitable thread) where the light guide from the LED can be fixed via the SMA-connector. With this shell the optical excitation path length can be varied at position x_1 in Figure 3-35 by moving the cylinder in the screw thread clock or counter-clockwise to increase or decrease the effective length of the optical path. To be able to monitor different separation channels segments of the chip interface during a separation assay, the chip holder slide was implemented into the bottom aluminum part of the setup as mentioned in Section 3.4.4. The chip holder slide (blue in Figure 3-36) was constructed in a way to allow moving every channel segment of the imbedded glass chip (orange) via the x- and y- direction into the fixed focal point of the optical path as shown in Figure 3-36. This is done via adjustment screws and springs located opposite on the aluminum bottom plate.
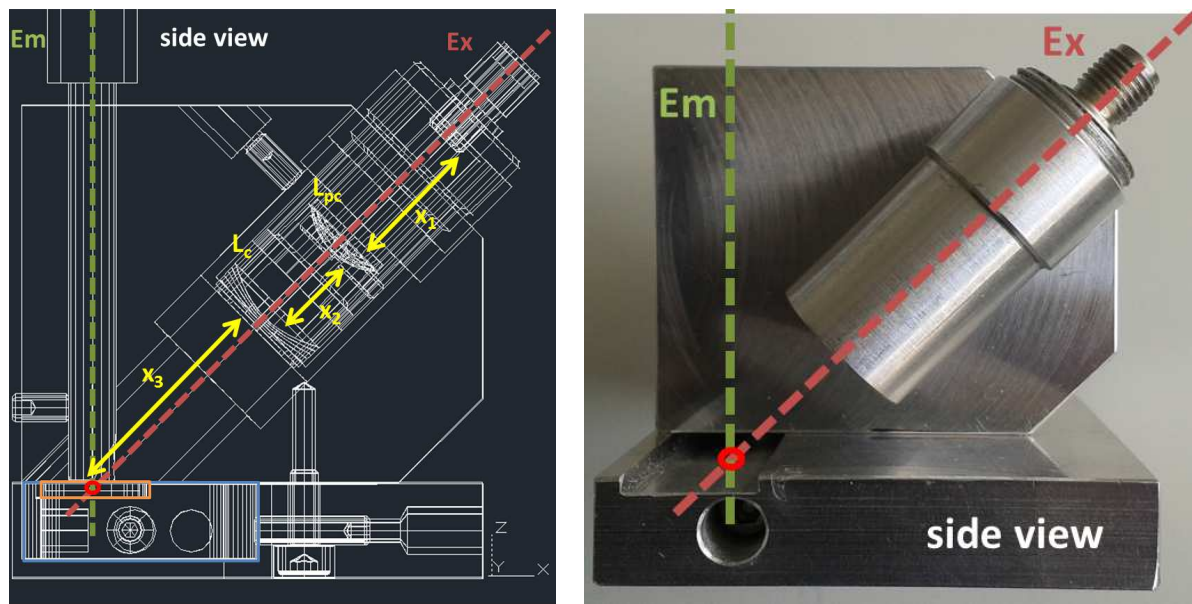
Figure 3-34: Detailed outline of the aluminum housing of the on-chip optical setup housing the optical lenses. Left picture is modified from the 3D CAD file shown in Figure A1. Right picture is a photograph of the on-chip optical setup with the assembled optical shell on top of the aluminum block for a better visualization on the setup for comparison. x_1-x_3 = distances of optical elements: x_1 = 15 mm, x_2 =10 mm , x_3 = 25 mm, L_c = cylindrical lens, focal length 25 mm, 12.5 mm diameter and L_{pc} = plano-convex lens focal length 15 mm. Ex = optical path of excitation light (LED) and Em = optical path of the light emission used for fluorescence light collection. Left = Modified CAD drawings from J&M Analytik AG (Essingen, Germany).
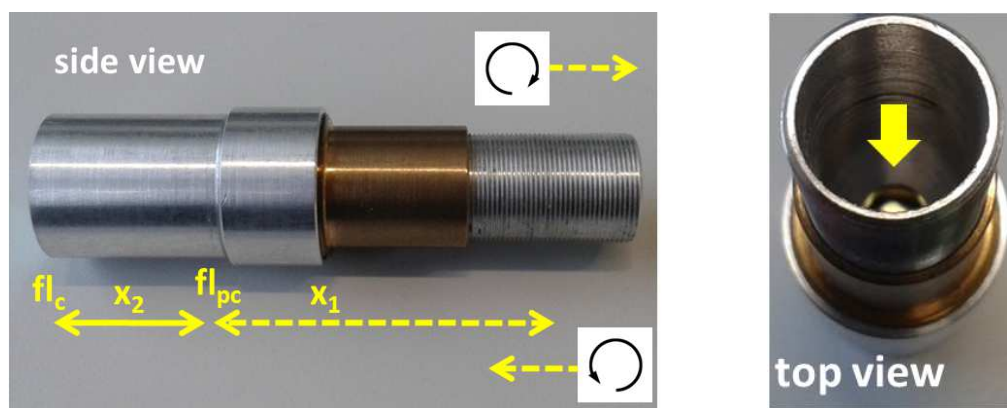
Figure 3-35: Detailed side and top view of the assembled optical Shell 1 and the variable optical Shell 2: Left picture: x_1 = 15 mm, x_2 = 10 mm, fl_c = position of the cylindrical lens and fl_{pc} = position of the plano-convex lens. Circles indicate the screwing direction to increase and decrease the length x_1 of the variable optical Shell 2. Right picture: The yellow arrow indicates the position for the SMA connector from the light guide from the excitation light source

Figure 3-37 illustrates the complete optical on-chip detection setup including the variable version of the optical Shell 2 as used for all experiments in the framework of this thesis.
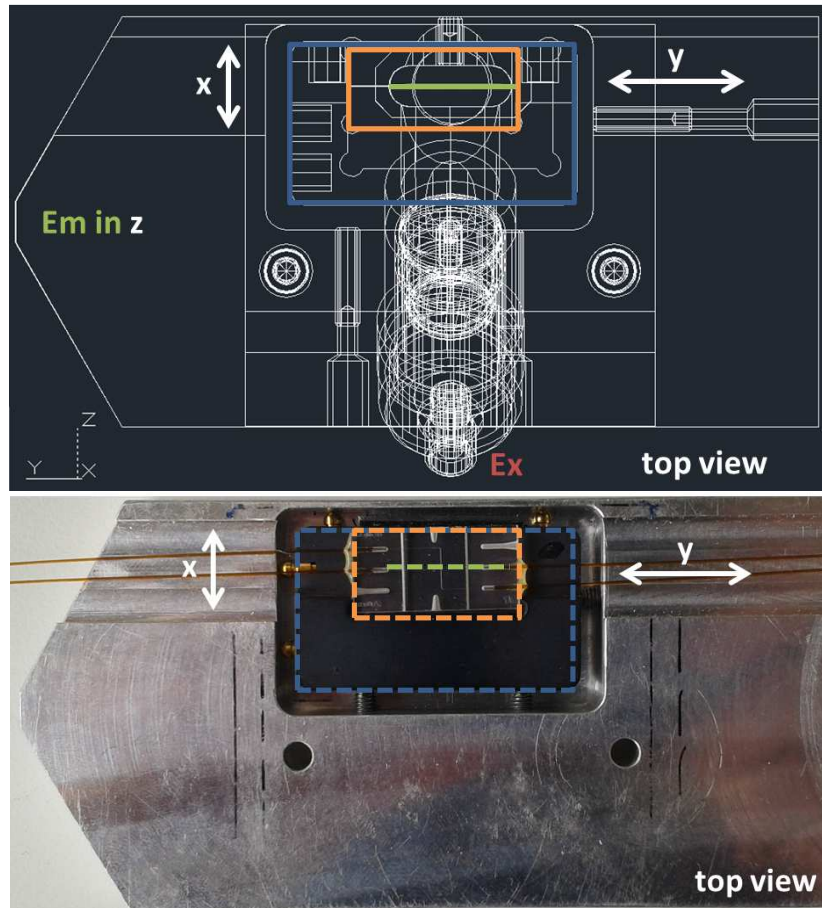
Figure 3-36: Detailed outline of the aluminum bottom plate of the on-chip optical setup housing the glass chip interfaces. Top picture is a modified picture from the 3D CAD file shown in Figure A1. Bottom picture is a modified photograph from the on-chip optical setup. Ex = optical path of excitation light (LED) and Em = optical path of the light emission used for fluorescence light collection. Solid and dashed orange line = glass chip interface for capillary coupling, Solid and dashed blue line chip holder slide, its position being variable in x- and y- direction and solid and dashed green line represents the line segment of the optical focus. Top = Modified CAD drawings from J&M Analytik AG (Essingen, Germany).
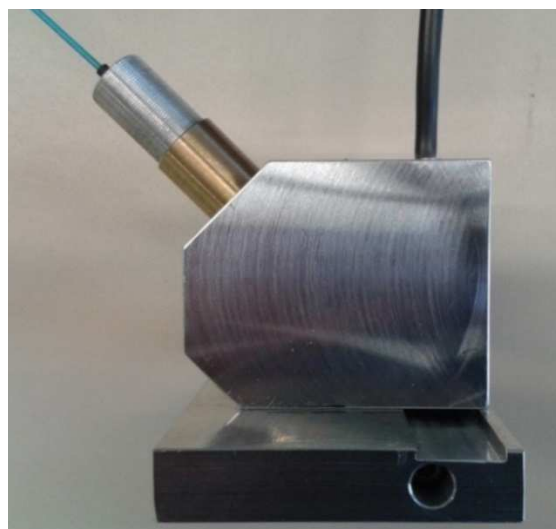
Figure 3-37: Illustration of the final on-chip optical setup including the variable optical Shell 2, compare Figure 3-29.

3.4.4.C Fiber array for collection emission light

To realize spatially-resolved on-chip intermediate detection of the emitted fluorescence light of the labeled analytes inside the common intersection (Figure 3-29 in Section 3.3.4) of the interface a linear fiber array consisting of 24 active light fibers was designed in cooperation with J&M and constructed by art photonics (Berlin, Germany). The fiber array consists of 24 × 80 cm long active UV-VIS light guides, see Figure 3-38. For a maximal spatial resolution for the active detection area, light fibers with the technically smallest realizable diameter of 100 μm (125 μm with coating) were used. A hyperspectral push broom imager was used for detection. In short, this detector consists of a spectrograph followed by a CCD camera with a defined active sensor area for the detection of electromagnetic radiation in the wavelength range of 380 nm – 980 nm. Using this combination the spectral information collected by each single light fiber of the linear fiber array is projected onto the CCD chip without overlap, giving rise to a spatially-resolved image of a channel segment of ca. 9 mm (see Figure 3-28). Here, at the chip side (LF2, Figure 3-38) 46 blind and 24 active fibers (70 in total) are connected with a total length of 70 * 125 μm = 8750 μm (9 mm). At the push broom detector side (LF1, Figure 3-38) 69 blind and 24 active fibers (93 in total) with a total length of 93 * 125 μm = 11625 μm (11.63 mm) were connected. The signal intensity detectable via each light fiber depends on the illuminated number of pixels of the active sensor area per light fiber. The active CCD sensor area of the push broom imager was 11.84 x 8.88 mm; to maximize the detection sensitivity the linear array used was widened from 8.75 mm to a maximum of 11.84 mm by adding blind fibers. In order to also monitor the analyte prior to its entry into the common intersection as well as after its heart-cut transfer to the second separation dimension the light guide array was constructed with an active length (L_{FA} in Figure 3-28) of ~9 mm (8.75 mm). The channel segments to be monitored thus include e.g. 3 mm before and 1 mm after the common intersection segment (length = 5 mm) as indicated by the red circles in Figure 3-28. To minimize cross-collection of fluorescence light from the chip channel by two neighboring fibers, each pair of active fibers was separated by two inactive blind light fibers - 46 blind fibers - thus 70 fibers in total. In order to achieve the maximum spectral and spatial resolution on the detection side (no overlapping of pixels of the active sensor area of the CCD camera) the linear light fiber array was also widened at the detection end by inactive fibers to use the maximum entrance slit length of the push broom imager of 14 mm via 69 blind fibers (93 fibers in total) - three for each pair of active light

fibers. The construction of the fiber array preserved the order of excitation and detection fibers.
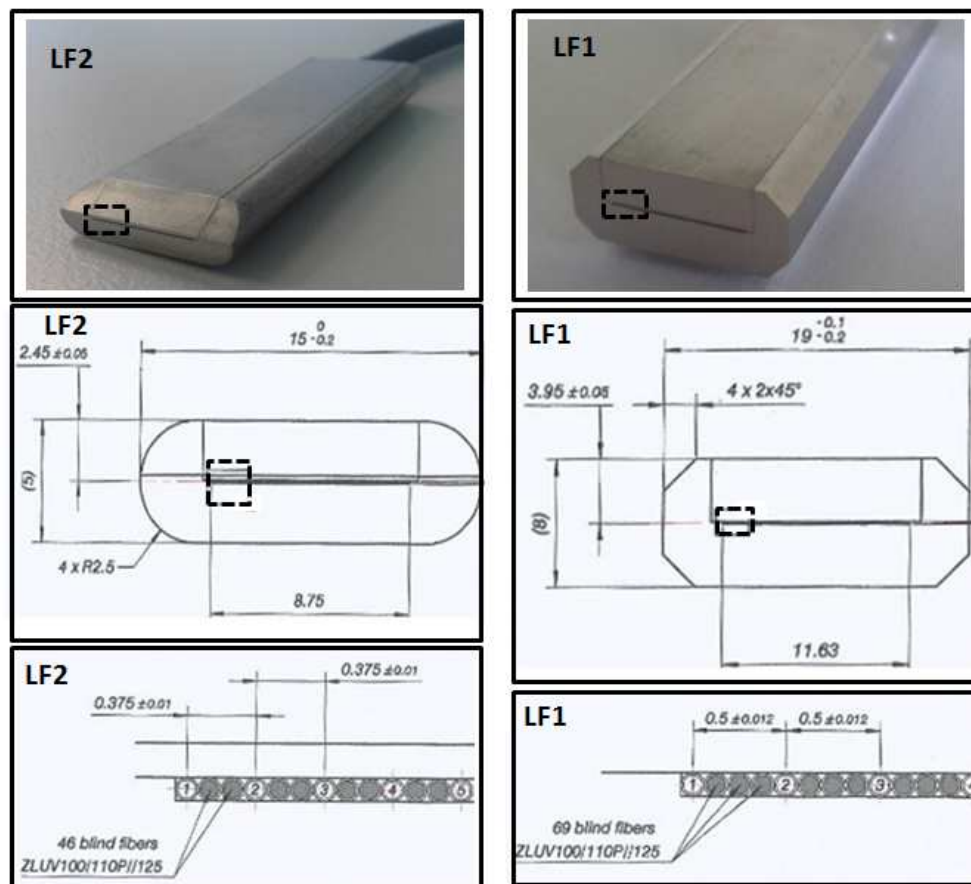
Figure 3-38: Illustrations of the on-chip detection side (LF2) as well as push broom side (LF1) of the constructed fiber array.Bottom four drawings = modified CAD file from art photonics GmbH (Berlin, Germany).

To ensure that no cross-collection of fluorescence light by two neighboring 100 µm light fibers, several parameters like distance of the light fiber array to the chip surface, the resulting air layer, and the channel-to-surface distance were taken into account. It is important to know the segment length of the chip channel which is contributing to the signal collected via one single 100 µm light fiber. For this, the light cone which would be present if the light would be emitted from the fibers instead of collected via the light guide fibers is used to estimate the illuminated segment as indicated by the light blue cone in Figure 3-39. For the calculation of the width of the light cone base D, the angle of radiation α from one active light guide to the chip channel at a distance of 1000 µm (exemplarily), the numerical aperture (NA) of the light guide and the refraction index n of the glass chip interface are needed.

Figure 3-39: Detailed illustration of the channel segment of the chip interface that is illuminated by one active light guide within the detection fiber array. F = physical width of three light guides (one active and 2 inactive blind fibers, OD = 125 µm), NA = numerical aperture (0.22), α = angle of radiation, y = distance of light fiber array to the chip channel = 1000 µm, d and x = distances contribution to the final cone diameter, D and L = length of the light cone overlap of two neighboring active light fibers of the fiber array.

The angle α (Figure 3-39) can be calculated via Equation 1 with a known numerical aperture *NA* of the used light fiber material (here, silica glass with a value of 0.22) and the refractive index n of the material into which the light is emitted (here, the glass chip interface made of fused silica with $n = 1.46$):

$$NA = \sin(\alpha) \times n \qquad\qquad Eq.\ 1$$

To calculate the angle of radiation α *Eq. 1* is converted to Equation 2:

$$\alpha = \text{Arcsin}\left(\frac{NA}{n}\right) \qquad\qquad Eq.\ 2$$

With α and the known distance y of the light guide end to the chip channel (here, 1000 µm = bottom plate thickness of the chip interface) the distance x (see Figure 3-39) can be calculated via Equation 3:

$$x = tan(\alpha) \times y \qquad\qquad Eq.\ 3$$

The width of the light cone D is then given by the light fiber inner diameter d and twice the distance x and can be calculated via:

$$D = 2x + d \hspace{4cm} Eq.\ 4$$

Following this approach, the resulting width of the light cone D was calculated for distances of 200, 700 and 1000 μm of the light fiber array to the chip channel in μm, representing the cover plate thicknesses of the chip interface as discussed in Section 3.1. The results are listed in Table 3-6. Compared to the factor F with 375 μm representing the width of 3 light fibers (3 times 125 μm OD) (that is one active fiber flanked by two inactive spacing light fibers (Figure 3-39)) the maximal estimated chip cover plate thickness without overlapping light cones ($L \leq 0$), is 900 μm with a value of $D = 374$ μm. For cover plate thicknesses below 900 μm the active light fibers have to be separated by two inactive blind fibers. With 3 spacing inactive light fibers the maximum would be 500 μm which would mean that the chip channel would not be fully covered as blind segments up to 97 μm (25 % of each light cone) 500 − 403 μm would be present. Therefore, two spacing light fibers were implemented also with respect to the aim of using lower cover plate thicknesses for better signal intensity as discussed in Section 3.1. Here, 200 μm proved best regarding intensity.

Table 3-6: Resulting width of the light cones D, calculated for 200, 700, 900 and 1000 μm distance of the light fiber array to the chip channel in μm.

distance light guide to chip channel (thickness of chip cover plate) [μm]	width of the light cone D [μm]	F for 2 spacing fibers [μm]	F for 3 spacing fibers [μm]	L for 2 spacing fibers
200	161			-
700	329	375	500	-
900	**374**			**0**
1000	403			+

bold = no overlapping of light cones for a chip cover plate thickness of 900 μm using 2 spacing fibers

The chip is not in direct contact to the light fiber array, but a discrete layer of air of about 1.0 mm is present between the chip cover plate and the linear fiber array. To evaluate the influence of different air layer thicknesses the model shown in Figure 3-39 was extended to the one given in Figure 3-40.
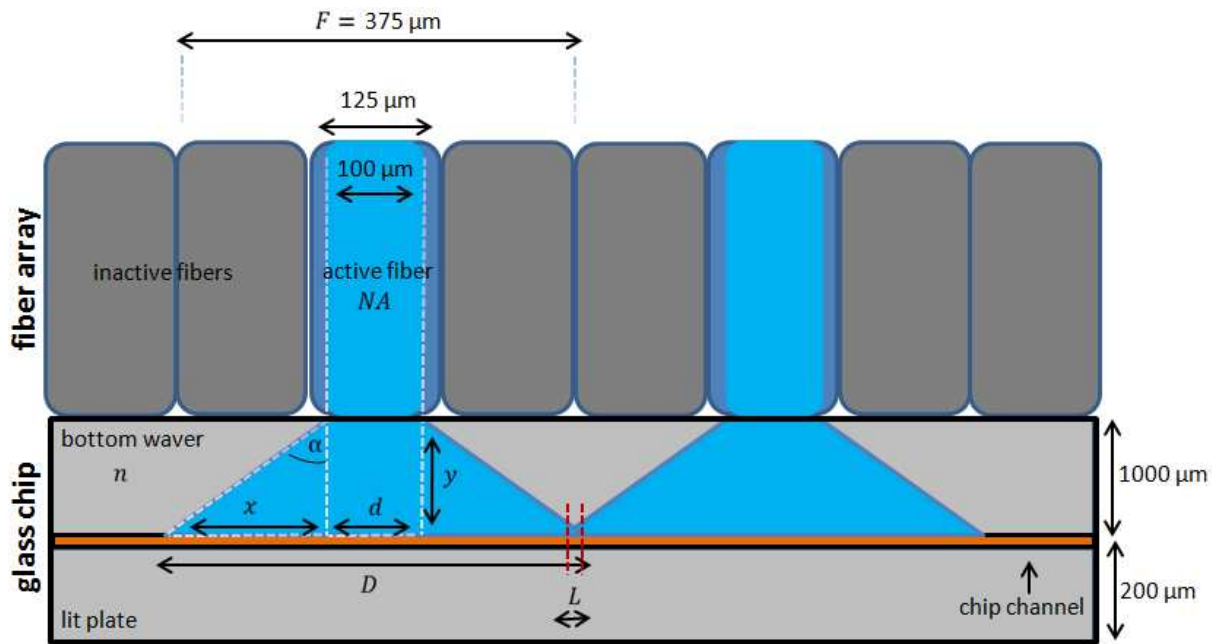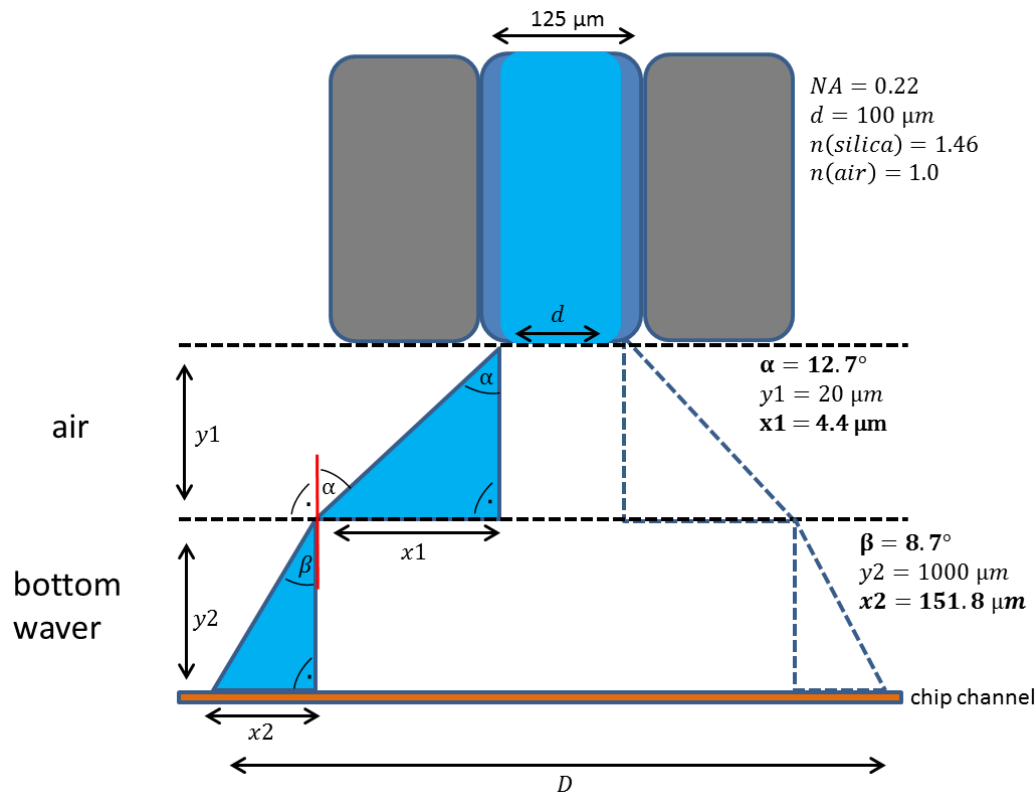
Figure 3-40: Detailed illustration of the channel segment of the chip interface that is sampled by one active light guide of the detection fiber array with respective parameters. α, β = angles of radiation, y1 (width of air layer), y2 (chip-channel to surface) = distances of surface interfaces, d, x1 and x2 = lengths contributing to the final cone diameter D of one active light fibers of the fiber array.

A similar discussion as before can be followed, exemplarily taking an air layer of 20 µm into account for the model shown in Figure 3-40 (due to visual clarity, the scaling of the respective distances is not congruent). The distance x1 from the air layer was calculated again via Equation 3 using the refractive index of air (n = 1.0). From there on using the width $(d + 2 \times x2)$ of the first resulting light cone base, the additional expansion of the cone due to the light passing from the air layer into the glass chip interface was determined via Snell's Law as indicated in Figure 3 with Equations:

$$\frac{\sin \alpha}{\sin \beta} = \frac{n_2}{n_1} \qquad\qquad Eq.\ 5$$

The angles for the calculation can be taken from Figure 3-40. The length x2 can be calculated according to Eq. 3 via Eq. 6:

$$x2 = tan(\beta) \times y2 \qquad\qquad Eq.\ 6$$

The width of the light cone D including a defined air layer is then given by the light cone diameter d and twice the distances $x1$ and $x2$ and can be calculated via Equation 7, as indicated in Figure 3-40:

$$D = ((x1 + x2) \times 2) + d \qquad\qquad Eq.\ 7$$

The influence of different air layer thicknesses was calculated for a chip cover plate thickness of 200 µm (as chosen for the optimized 2nd generation chip design (Section 3.1.4)) and given in Table 3-7 as increase of the light cone D for air layer thicknesses from 10 to 1500 µm (10, 20, 40, 60, 80, 100, 1000 and 1500 µm), representing different distances of the light fiber array to the chip surface. Plotting the straight line D vs. y1, the resulting slope of the equation of the trend line can now be used to directly calculate the increase of the light cone in dependence of the distance of the fiber array to the chip surface or the respective air layer (see Figure 3-40 or Figure 3-41).

To calculate the resulting light cones for the optimized 2nd generation chip interface (as used for most experiments in this work) performing the on-chip detection at the top of the glass chip, the width of the light cone is 161 µm multiply the 1500 µm total air layer with the slope of the trend line from Figure 3-41 (0.447) and add it to the initial light cone width of 161 µm (in case of a cover plate thickness of 200 µm).

Table 3-7: Resulting width of the light cones D, calculated for 10, 20, 40, 60, 80, 100, 183, 1000 and 1500 µm distance of the light fiber array to the chip surface in µm using the chip interface with a cover plate thickness of 200 µm.

distance light guide to chip surface (air layer thickness) [µm]	width of the light cone D [µm]	F for 2 spacing fibers [µm]	F for 3 spacing fibers [µm]	L for 2 spacing fibers
10	165			-
20	170			-
40	179			-
60	188			-
80	197	375	500	-
100	205			-
183	**375**			**0**
1000	608			+
1500	832			+

$$D = d + 0.447 \times y1 \qquad\qquad Eq.\ 8$$

The total air layer results from the 500 µm gap created by the bonded stability glass blocks on the glass chip interface and 1000 µm (fixed position of the fiber array in the optical detection setup) for the distance of the light fiber array to the chip surface. The final light cone width of one single light guide of the fiber array is 832 µm (see also Table 3-8).

Table 3-8: Calculated final light cone base diameters in µm for the two different chip orientations (bottom or top) within the chip holder slide.

chip orientation to on-chip optical detection setup	cover plate/air layer thickness [µm]	glass substrate to air layer thickness ratios	diameter of light cone [µm]	overlap (L) [µm]
bottom	700/1000	0.7	851	476
top	200/1500	0.13	832	457

Under these experimental conditions the spatial resolution is decreased by a factor of 2.2 from the minimum of 375 µm (OD of 3 optical fibers (F)) to 832 µm (L = 457 µm). Taking the active length of the light fiber array of 8750 µm dividing it by 832 µm ca. 10 (10.5) points along the chip channel can be distinguished, giving rise to 10 data points. Under the assumption of a typical peak widths of an analyte peak in capillary isoelectric focusing of 4000 - 8000 µm (see Section 3.4.5.H) about 5 to 10 data points describe the peak within the common intersection segment of the chip interface which is sufficient to evaluate its appearance and movement through the channel.
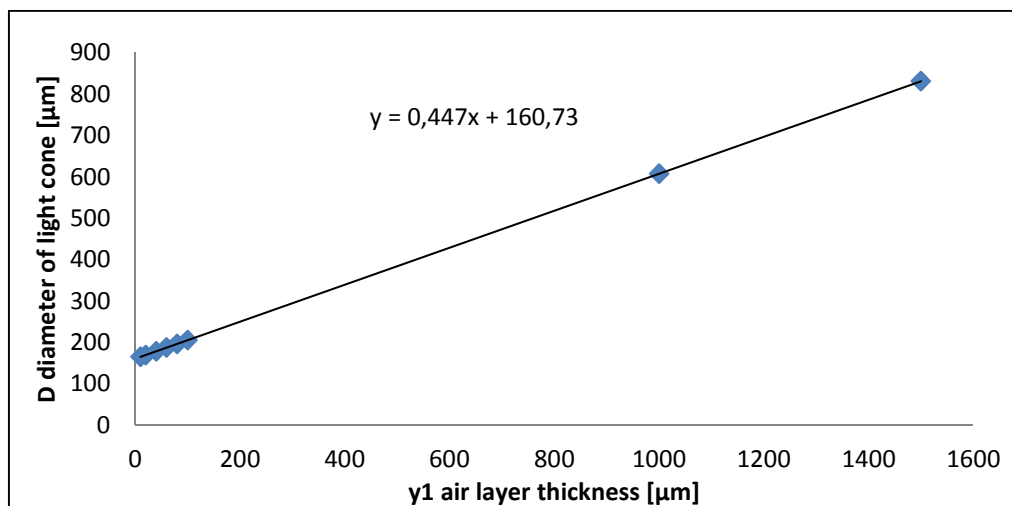
Figure 3-41: Air layer thickness between the linear fiber array and the surface of the glass chip interface in µm vs. the resulting diameter of the light cone for one active light guide of the fiber array in µm.

3.4.4.D Hyperspectral imaging - Push broom imager as detector

Hyperspectral imaging was initially developed for remote sensing of the earth's surface [Goetz, 1985]. By now, due to its great potential, it has been realized in a multitude of scientific fields like agriculture, pharmaceutical and material science as well as food quality and safety applications [Dale, 2013]. Using the push broom imager in spatial scanning mode it can record a time dependent full spectrum (e.g. 380 nm – 980 nm) over a defined array length and therefore it generates a 4 dimensional (intensity, space, wavelength and time resolved) analyte signal e.g. in a channel of a microfluidic system, as shown by Panic et al. [Panic, 2011]. The detection setup used in this work as well as the software used to record and display the detected dimensions space, time, wavelength and intensity were developed in cooperation with J&M Analytik AG (Essingen, Germany). The imager included a QSI 620i 2.0mp cooled CCD camera from Quantum Scientific Imaging, Inc. (Poplarville, USA) (see (1) in Figure 3-42). The spectrograph (2) had a slit (4) for optical filters with dimensions up to 2.0 × 12.5 mm as shown in Figure 3-42. The technical parameters of the push broom imager are summarized in Table 3-9. The detection end of the linear fiber array (see (3) in Figure 3-42) was adapted to the entrance slit width of 14 mm of the spectrograph of the push broom imager as shown in Figure 3-38. Here, the highest possible resolution was achieved by using the full length of the fiber array of 11.63 mm as discussed in the previous section.
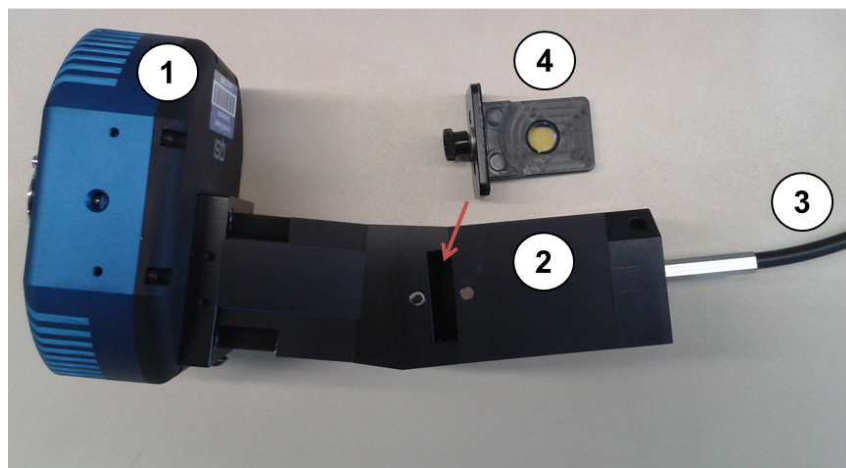
Figure 3-42: Illustration of the used push broom imager from J&M Analytik AG (Essingen, Germany): (1) QSI 620i 2.0mp cooled CCD camera from Quantum Scientific Imaging, Inc. (Poplarville, USA), (2) spectrograph, (3) the detection end of the linear fiber array and (4) slit for optical filters with dimensions up to 2.0 × 12.5 mm,

Additional software was commissioned and optimized in cooperation to control the push broom imager and to record the hyperspectral data. Using the software the exposure time of

the CCD can be varied from 500 to 5000 ms (0.2 to 2 Hz) to be able to adjust/increase the signal to noise ratio of the CCD sensor if needed. Generally, a minimum of 10 data points is necessary to properly describe the appearance of a signal peak. Therefore the user has to define the tradeoff between data point measuring intervals and the signal intensity. In capillary electrophoresis assays the peak width is in the range of 6 to 15 sec and especially for proteins separated with capillary isoelectric focusing of 20 to 40 sec. As a result the exposure time for CIEF experiments can be set nearly to the limit of 0.2 Hz with an acceptable number of data points for the description of the analyte peak. Exemplarily the 2D capillary-chip setup was flushed with a solution containing FITC at a concentration of 2.0 µg/ml.

Table 3-9: Specifications of the used push broom imager

Parameter	Specifications
QSI 620i 2.0mp cooled CCD camera	
resolution	1600 x 1200 pixels @ 7.4 x 7.4 µm
active sensor area	11.84 x 8.88 mm
framerate	6 fps
didital output	16 bit
exposure time	100 µs – 240 min
Iiterface	USB2.0
cooling:	2-stage thermoelectric cooler max. up to 45 K below ambient temperature
VIS/NIR Spektrograph	
wavelength range	380 nm – 980 nm
spectral resolution (FWHM)	< 7 nm with 80 µm entrance slit
working f#:>3 / RMS spot sizes	< 65 µm
dispersion	81 nm/mm
aberrations: Smile	< 135 µm
keystone	< 20 µm /without entrance lens
light output	CMount
adapter plates for input	
	1x fiber bundle adapter plate 19 mm x 8 mm
	1x adapter plate for CMount

The on-chip detection was performed by using the setup as discussed in Section 3.4.4. A software-controlled monitoring function allows to display the actual hyperspectral signal

recorded by the CCD camera sensor of the push broom detector in dependence of the set exposure time (e.g. 1 Hz) (Figure 3-43). In Figure 3-43A the resulting three dimensional hyperspectral plot, showing the intensity of the excitation wavelength of the 455 nm LED as well as the resulting fluorescence light of the FITC at 520 nm for each of the 23 active light guides of the linear fiber array. Using the two red cursor lines in Figure 18 the detected signal can be analyzed in more detail regarding its spectral properties (y axis = λ in nm) and the position or region (x axis = position in pixel) within the active sensor area of the CCD camera. With the horizontal cursor, the plot intensity vs. wavelength, with the vertical cursor the plot intensity vs. pixel and thus intensity for each light guide can be chosen. Examples are given in Figure 3-43B for the intensity of the LED light at 438 nm and in Figure 3-43C for the spectrum recorded for light guide #10. The latter plot was used in order to adjust the common intersection channel segment of the chip interface to the optical focus path of the on-chip detection setup as discussed in the next section.
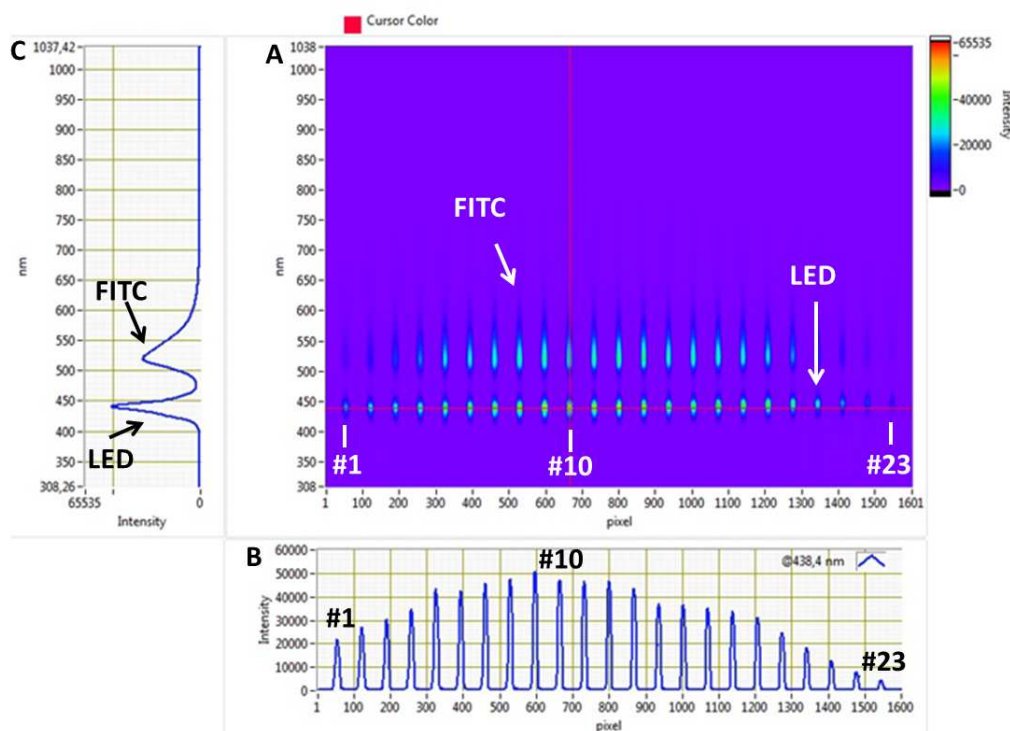
Figure 3-43: Monitoring option of the push broom imager: A) three dimensional hyperspectral plot for the 23 active light guides, B) spatially-resolved fluorescence signal for a chosen wavelength with respect to exposed pixels of the CCD camera of the push broom imager and C) the spectral plot for the wavelength range of 308 to 1037 nm for the chosen position (vertical red cursor line).

A time dependent signal recording function was implemented to display the respective electropherograms for each (or chosen) active light guides of the fiber array for a certain

wavelength as shown in Figure 3-44. Here, a plug (injection of the 2.0 µg/ml concentrated FITC solution for 5 sec at 100 mbar into the capillary filled with borate buffer) was flushed through the chip interface of the hybrid capillary-chip setup and was detected via the LED-IF on-chip setup (Figure 3-44A). The exposure time was set to 1 Hz and the total recording time was 3 min. In addition to the chosen detection wavelength of 520 nm (λ_{em} for I_{max} FITC) the software displays the recorded spectrum from 380 - 980 nm for each chosen light guide (tick box for channels Chan_01 to Chan_23) of the fiber array for each measuring time point in real time (chosen exposure time) as shown in Figure 3-44B. This feature allows the user the possibility to identify any spectral interference from eventually co-migrating analytes or matrix constituents during the measurement. For overall monitoring purposes, with special regard to the sample band transfer step inside the intersection channel segment of the chip interface a three dimensional plot (comparable to Figure 3-43A) is available as shown in Figure 3-44C.
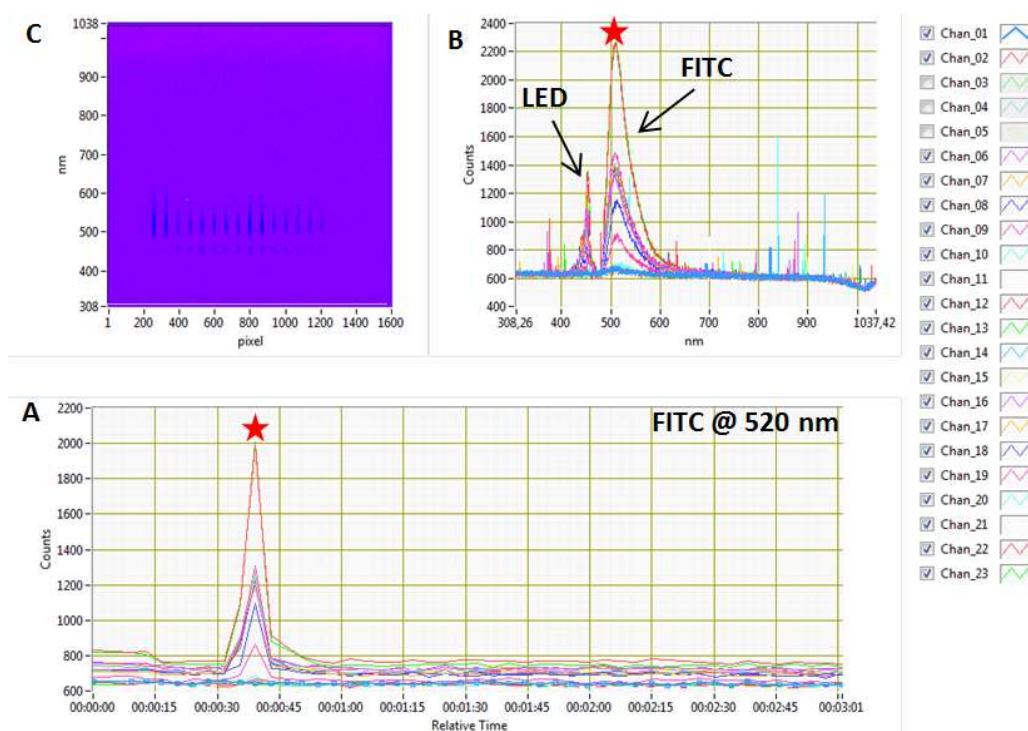
*Figure 3-44: Time-dependent signal recording function: **A)** time-dependent signal recorded for 3 min for all active light guides of the fiber array (different colors at 520 nm), B) three dimensional hyperspectral plot for the 23 active light guides, **B)** spectral plot for the wavelength range of 308 to 1037 nm for all active light guides and **C)** three dimensional hyperspectral plot for the 23 active light guides. ★ = respective detection time point.*

3.4.5 Characterization of the fluorescence detection setup

To characterize the optical on-chip LED-IF setup for the hybrid capillary-chip system, flushing experiments were performed using a solution of 2.0 µg/ml fluorescein isothiocyanate (FITC) in $Na_2B_4O_7$ buffer (10 mmol/l, pH 9.2). The hybrid capillary-chip system was used without a surface coating. If not stated otherwise, the LED was set to 98% intensity and detection was done with an exposure time of 1000 ms (data rate = 1 Hz) for the push broom imager. The FITC solution was flushed from port P1 into the setup and MS detection, if used, was located at port P3 (see Section 3.4.4.D). The ports P2 and P4 were filled with buffer solution. Between experiments, residual FITC was flushed out with $Na_2B_4O_7$ buffer solution (10 mmol/l, pH 9.2). Results are presented in Section 3.4.5.G.

It is interesting to note, that the optical setup can also be used for the surface analysis of solid samples due to the fact that the aluminum part (1) is housing the optical excitation and detection setup in a fixed arrangement. To show solid state fluorescence capabilities, 20 × 20 cm TLC cellulose plates (cut to 5 × 5 cm sections) purchased from Merck (Darmstadt, Germany) were contaminated dropwise over 10 mm spot with 10 µl of a 2.0 µg/ml FITC solution in $Na_2B_4O_7$ buffer solution (10 mmol/l, pH 9.2). In addition, a pink tablet (incubated with 0.33 % w/w erythrosine solution and 1 % w/w quinine) from Glatt Systemtechnik (press: Fette Compacting 102i, Glatt Ingenieurtechnik, Weimar, Germany was chosen as model sample. The results are given in Section 3.4.5.K.

3.4.5.A Quality and performance of light fiber array

All 23 detection light fibers of the fiber array are imaged by the push broom imager in one line (see Figure 3-45, showing in-channel measurements of the reflected excitation light at 455 nm) demonstrating the high quality of the fiber alignment and gluing process of the fiber array production. Baseline separation of the detected stray light signal for each of the 23 active light guides was achieved using the two and three blind fibers at the on-chip and push broom side. The active detection length of the fiber array is 8.75 mm represented by 1600 pixels on the active sensor of the push broom imager. Therefore, 1 pixel equals ~5.5 µm and one 100 µm (125 µm with coating) light guide illuminates 23 pixels. The different response of the light fibers regarding detected intensity visible in Figure 3-45 correlates with the visual appearance of the beam line shape of the excitation light when using the fixed optical Shell 2. Due to the implemented optics, the excitation light was focused on a line but the light intensity within the resulting beam line spot is not homogeneous - being brighter in

the center and deceasing at the outer part of the beam spot. This phenomenon is independent from the samples (channels or solids). To correct this inhomogeneity the beamline appearance can be adjusted using the variable optical Shell 2, as discussed in Section 3.4.5.C.
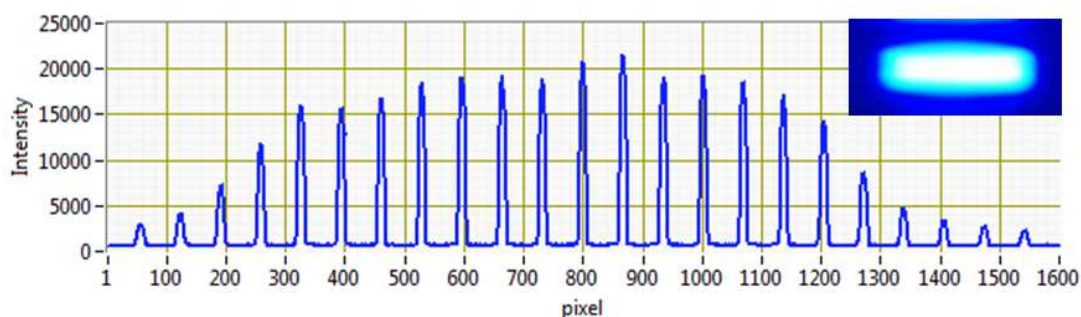
Figure 3-45: In-channel measurement (2nd generation chip design) of the reflected excitation light at 455 nm using the on-chip optical detection setup. The beam spot shown is a photograph of the visual appearance of the respective light beam spot detected via the push broom imager.

In principle, the intensity distribution may be corrected mathematically via dividing the fluorescence intensity for a signal by a known intensity distribution from a standard or the LED excitation light. Another way would be to normalize the detected fluorescence signal for each active fiber to the detected fluorescence light of e.g. Fiber #12 being in the center of the fiber array and therefore detecting the highest intensity. These corrections can also be used to identify any potential saturation or bleaching effects with respect to higher fluorescence light intensities (higher analyte concentrations or longer exposure times). In this work a signal correction was not considered as the optical detection setup was only used as an intermediate detection to monitor analyte movement but not for quantification purposes.

3.4.5.B Chip positioning and alignment procedure for in channel measurements

For a correct alignment of the chip relative to the optical on-chip detection setup, the glass chip was first fixated in the chip holder slide and the two aluminum blocks of the optical setup were assembled. Next, the whole capillary-chip setup was flushed with a fluorescing sample solution or FITC solution (see Section 3.4.4.D). For an initial alignment of the optical path to the studied chip channel segment a visual alignment was performed, adjusting the LED light beam spot to the respective channel segment by looking through the notch of the detection fiber array (see Figure 3-46). After that, for a more dignified alignment the fiber array was integrated into the setup and the monitoring option of the hyperspectral software was used in combination with the adjustment screws for positioning the chip interface inside the chip holder slide to the position where the highest fluorescence intensity can be detected.

In addition, the exposed length as well as the needed exposure width can be adjusted via the adjustable optical Shell 2 (see Figure 3-35).

An exact alignment of the chip interface and a respective channel segment to the optical setup is possible because of the chip geometry and its influence on the detected fluorescence signal:

1. The channel cross sections are detectable via higher fluorescence intensity due to the collection of fluorescence light from the side channels.

2. The increased fluorescence signal at the substrate edge of the 500 µm glass block depending on the orientation of the chip to the optics is due to the fact that the fluorescence light emitted from the channel is reflected at the additional edges of the block so that more fluorescence light reaches the detection fiber array at the respective position.
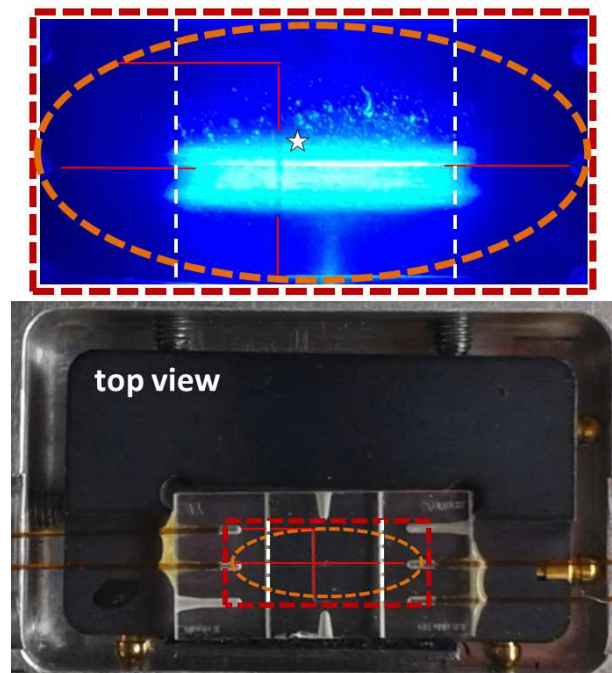
Figure 3-46: Top view on the chip holder slide, including a 2nd generation chip with a cross arrangement of the channel intersection. Enlarged red box shows the chip interface and the linear beam of the excitation light by looking through the notch of the detection fiber array. For an initial alignment of the optical path to the studied chip channel segment a visual alignment was performed, adjusting the LED light beam spot to the respective channel segment. White star =position of the chip channel cross section, red lines = separation channels of the chip interface and white dashed lines = surface edge of the bonded glass blocks for stabilizing the capillary chip cups for coupling the separation capillaries.

For all measurements the optimized 2nd generation chip design was used. Detection at top (A) or bottom (B) position of the chip interface is possible as indicated in Figure 3-47. Modes A and B differ in the glass substrate as well as air layer thicknesses with a total distance for both

of 1700 μm with glass substrate to air layer thickness ratios for (A) of 0.13 and (B) of 0.7 (see Table 3-8) as discussed in Section 3.4.4.C. A further aspect is the channel cross section with the flat channel part facing the detection setup for mode (A) and the curved side facing it for (B). To investigate if the (A) or (B) mode yields higher signal intensities, the chip interface was flushed with FITC solution and optical detection was performed for both orientations. There was no significant difference in the detected signal intensities for the respective light guides of the fiber array, as shown in Figure 3-48. Therefore, it is irrelevant whether the flat or semi-circle channel geometry part is facing the detection setup with respect to the detected fluorescence intensity under the chosen experimental conditions. In literature the distance of the separation channel to the excitation and detection optics is mentioned to be one of the most crucial parameters regarding the detected fluorescence signal intensity [Fu, 2006; Liu, 2008]. The distance is the same (1700 μm) for both detection arrangements (A) and (B) (though with different glass-air-ratios). The free choice of Mode A or B is advantageous if additional C^4D detection is envisaged.
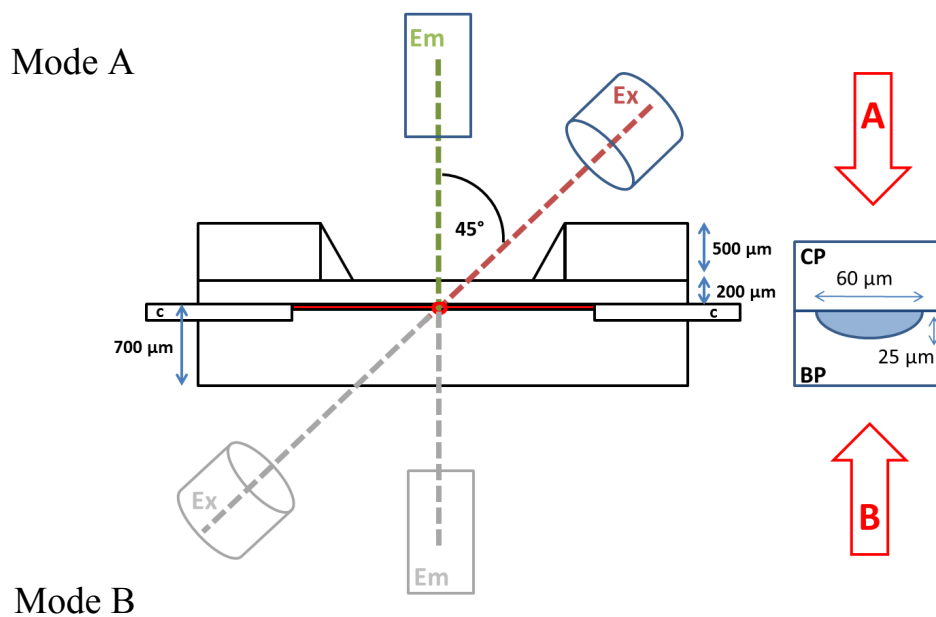
Figure 3-47: Sketch of the optical on-chip detection setup using the 2nd generation chip design. (A) and (B) are the respective detection positions at both sides of the chip interface and therefore representing for (A) detection at a planar channel surface through the cover plate (CP) and from (B) detection at a semi-circular channel surface through the bottom plate (BP). Total distance for both positions is 1700 μm from the fiber array to the separation channel inside the chip interface with glass substrate to air layer thickness ratios for (A) of 0.13 and (B) of 0.7 (see also Table 4).

As shown in Figure 3-48, the line of the focused light beam of the excitation light was positioned directly in the middle of the chip and did not reached the surface edge of the

stabilizing bonded glass blocks on top of the chip channel cups on the left and right side of the interface (Mode A). It was noticeable that two light guides (#10 and #11) were detecting a higher fluorescence intensity than the rest of the light guides of the fiber array, here, #10 (see Figure 3-48A and B). That was in contrast to the LED stray light intensity. These respective light guides detect the fluorescence light emitted from the cross section point and thus also monitor a small section of the side channels. As pointed out in Section 3.4.4.C these pixels record almost the same increased fluorescence intensity through the two neighboring light fibers because of the overlay of neighboring light cone lengths ($L = 457$ µm). According to Section 3.4.4.C, the base length (D) of a light cone is 832 µm (distance light guide to chip channel for the top part of the interface facing the optics). This length evokes the overlap of the neighboring light cones over the length L = 457 µm. Further intensity variations are due to the differences in the intensity distribution from the LED excitation. The visibility of the cross section in the detection system can advantageously be used to further optimize the chip positioning.
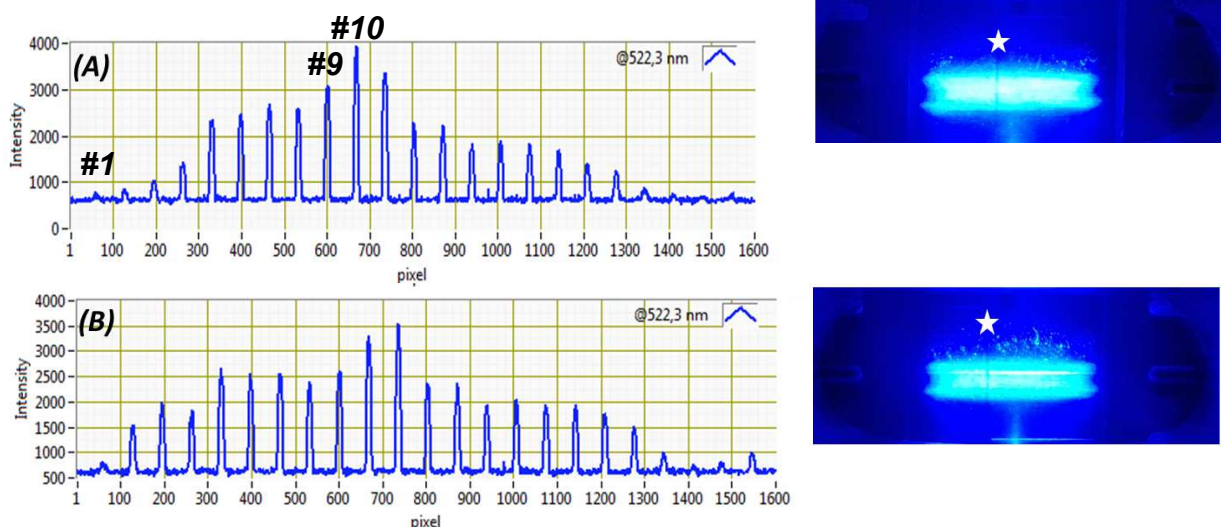
Figure 3-48: Recorded detector signals for each light guide of the fiber array as well as a photograph of the linearly focused light beam of the excitation light for detection Modes (A) and (B), see Figure 3-47. White star = position of the chip channel cross section arrangement (here, cross arrangement) and # = number of light guide in the fiber array.

This is further evidenced by the intensity changes due to reflection at the surface edges of the additionally bonded glass blocks (Figure 3-47 as visible in Figure 3-49). The chip was moved inside the chip holder slide to the left (L) and right (R) to record the fluorescence intensity distribution pattern of the light guides for both, bottom and top detection arrangement of the interface. Using the chip in Mode *(A)* the position of the channel cross section was visible via the increased intensity signal of the light guides #13, #14 and #15 for the Mode *(A)L*

(Figure 3-49*(A)L*) vs. #7 and #8 for the Mode *(A)R* which is corroborated by the photographs of the visual light beam line with the cross section marked by the white star. The interface of the surface edge of the additionally bonded 500 µm glass block is not detectable.
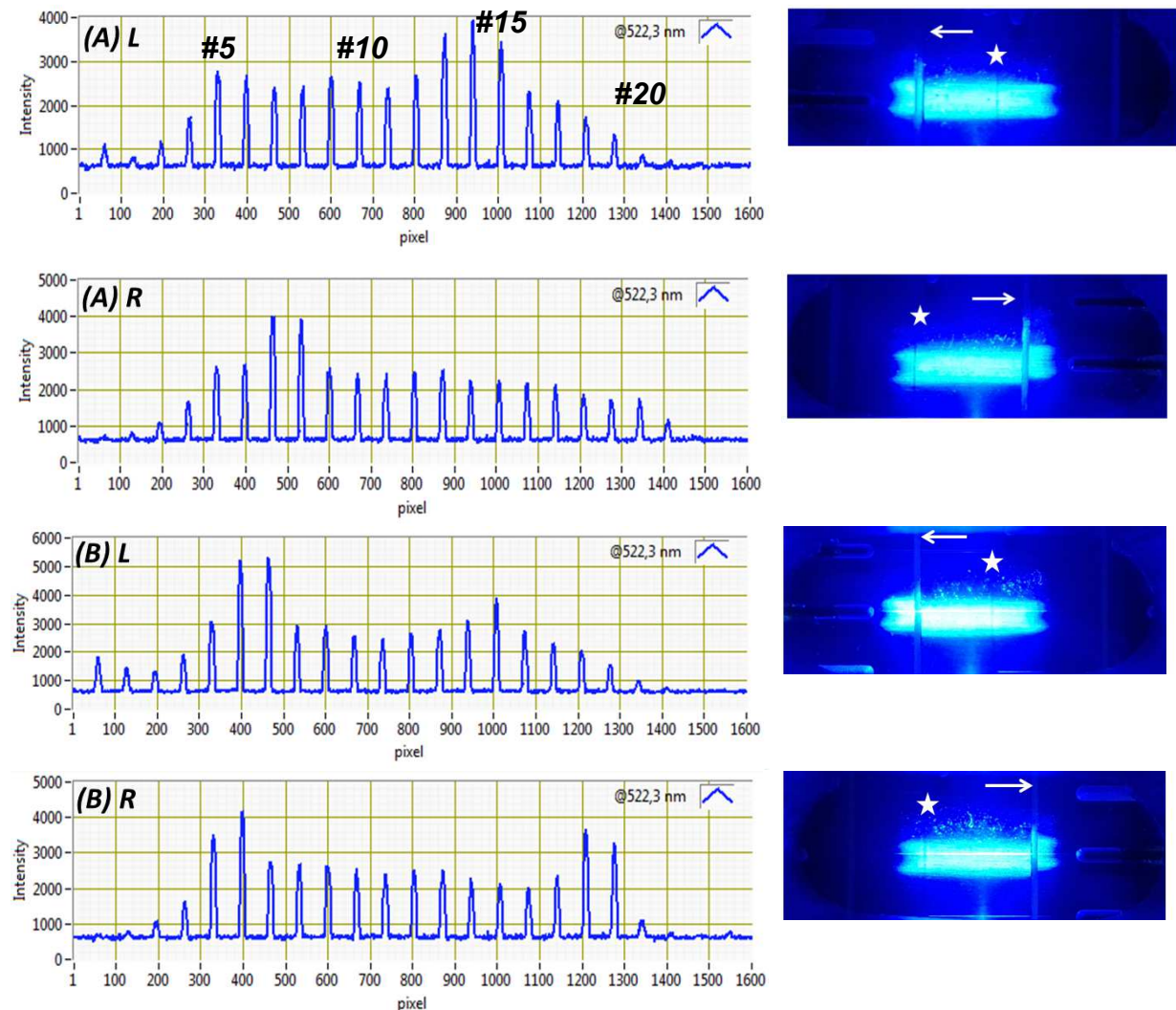
Figure 3-49: Recorded detector signals for each light guide of the fiber array as well as photographs of the light beam line of the excitation light for detection Modes (A) and (B) (Figure 3-47) with the chip moved to the left L and right R relative to the surface edge of the additionally bonded 500 µm glass block. White star = position of the chip channel cross section (here, cross arrangement) and white arrow = position of the surface edge of the additionally bonded 500 µm glass block. (A)L = Mode A of the optical detection setup and L chip interface moved to the left until the surface edge of the bonded glass block (white arrow) was in the exposed area.

Compared to an intermediate position (Figure 3-47), different light guides now detect increased intensity. In contrast, for the change in position (white arrows) for the Mode *(B)* the respective substrate edge by the 500 µm glass blocks is indicated by an additional increase of the detected fluorescence light intensity at the respective edge position for light guides #6 and #7 for Mode *(B)L* as well as #18 and #19 for Mode *(B)R*. Furthermore, the channel cross

section point is now indicated by #15 for *(B)L* and #5 and #6 for *(B)R*. This gives rise to an advantageous two-point positioning for Mode *(B)* but only a one point alignment for Mode *(A)*. Using a two-step alignment procedure, first with a visual inspection of the proper position of the excitation light beam to the chip channel of interest followed by a detailed positioning using the detection light fiber pattern, any channel segment of interest can properly be aligned to the excitation line. Due to the increased information regarding the position, the detection Mode *(B)* was chosen for all further experiments.

3.4.5.C Variation of excitation light beam spot appearance

Using the standard setup with the chip channel being in the focal plane of Lens (7) with $x_1 = 15$ mm (Figure 3-34) focusing the excitation light to a thin line the illuminating ca. 6 mm long and 1 mm wide and therefore it is suitable to expose the whole common intersection segment of the chip interface with dimensions of 5 mm × 0.06 mm as well as a defined length before and/or after each intersection point as shown in Figure 3-28. To be able to vary the imaged area with special regard to intensity homogeneity and shape of the excitation light beam the variable optical Shell 2B was implemented into the optical setup as shown in Figure 3-37. The distance of the optical excitation path length was varied from the initial distance of 0 mm (same as for the fixed Shell 2A) to ±1 mm. As shown in Figure 3-50, increasing the excitation light path by 1 mm the light beam appears more diffuse and lenticular compared to the line-shaped appearance for position 0 mm but it then covers a larger area with its length reaching nearly 9 mm as indicated in Figure 3-50B. The respective intensity plot indicates that all 23 active light guides of the fiber array are now detecting the fluorescence light, however, with decreased absolute intensity values of 2000 to 1500 counts compared to only 16 exposed light guides with intensity values of 3000 to 2000 counts for the initial distance of 0 mm. The possibility of positioning the chip via the fibers at the channel intersection is kept with light guides #9 and #10 showing increased intensity. Overall, it is important to note that the beam light intensity in the middle of the fiber array is decreased but increased for the outer light guides of the array giving a more uniformly exposed image area for the +1 mm position, but with the downside of a global decline of excitation intensity. By decreasing the excitation light path by 1 mm the linear light beam appears more intense but shorter with an overall more spherical appearance compared to the beam spot for position 0 mm. The exposed area is smaller, reaching only 4.5 mm in length as indicated in Figure 3-50C. The respective intensity plot indicates that only 14 active light guides of the fiber array are detecting the fluorescence light in this position, but with increased intensity

values of 4000 to 2500 counts compared to 16 exposed light guides with a maximum intensity value of 3000 counts for the initial distance of 0 mm. At the cross section point the light guides #9 and 10# detect the highest fluorescence intensity with 6300 counts. By using the variable version of the optical Shell 2B, the beam spot appearance can be adjusted to the needs of the respective analytical problem with a compromise regarding the covered channel segment length and the required excitation intensity and related analyte LODs. In general, the 0 mm position was chosen for the following experiments if not stated otherwise.
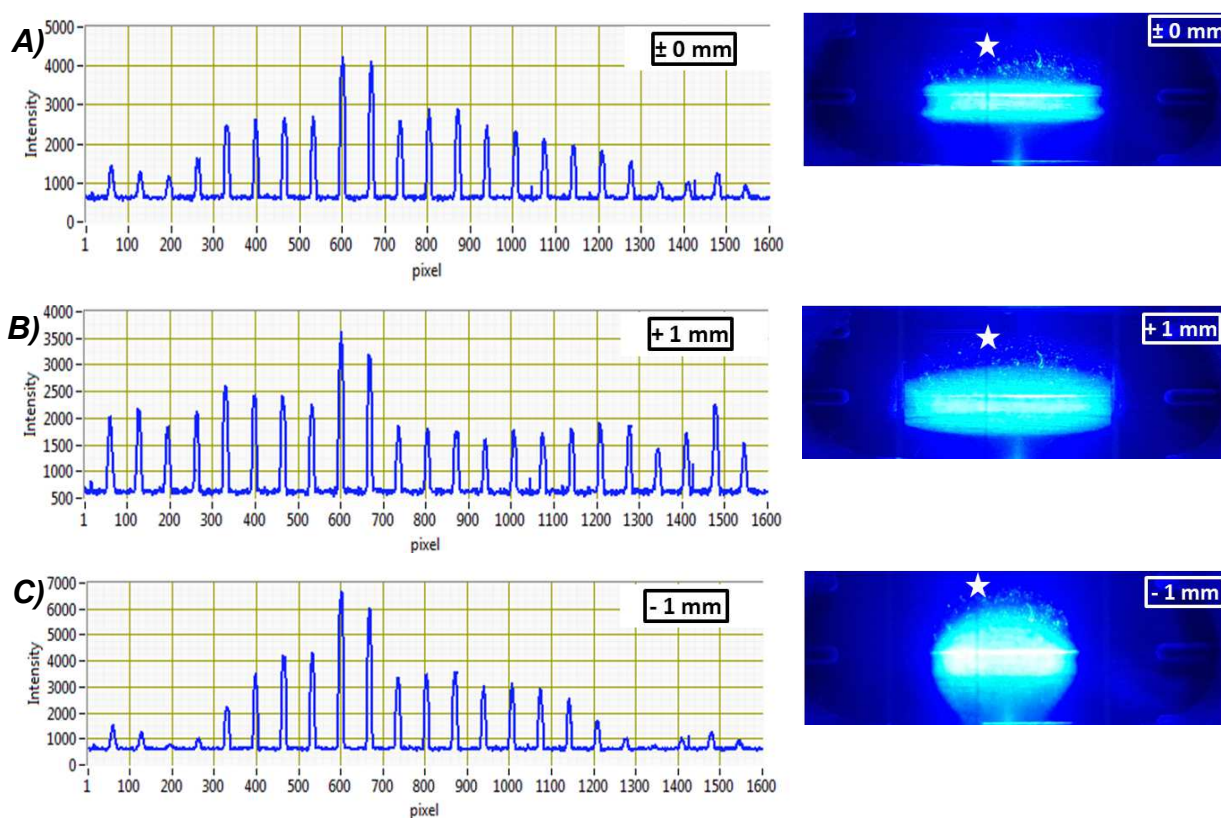
Figure 3-50: Recorded detector signals for each light guide of the fiber array as well as photographs of the resulting light beam line of the of the excitation light for different lengths of the optical excitation path length. The position ±0 mm represents the initial length of the optical path using the fixed optical Shell 2A. The position +1 mm represents an increase of the optical path of 1 mm using the variable optical Shell 2B. The position -1 mm represents a decrease of 1 mm of the optical path using the variable optical Shell 2B. White star = position of the channel intersection (here, cross design).

3.4.5.D LED vs. fluorescence intensity

To study the influence of the LED intensity on the detected fluorescence signal intensity of the 2.0 µg/ml FITC solution, the LED light intensity was varied from 30, 40, 60, 80 to 98 % and the respective stray light (455 nm) and fluorescence signals (520 nm) were recorded by the push broom imager with an exposure time of 1000 µs (data rate = 1 Hz). The detected

signals were evaluated exemplarily for the light guide #12 of the fiber array. Figure 3-51 demonstrates a linear dependency of both the detected LED stray light intensity and FITC fluorescence intensity on the LED light intensity (R^2 = 0.999). For best LODs the LED was generally used at maximal intensity of 98 % for all measurements, if not stated otherwise.
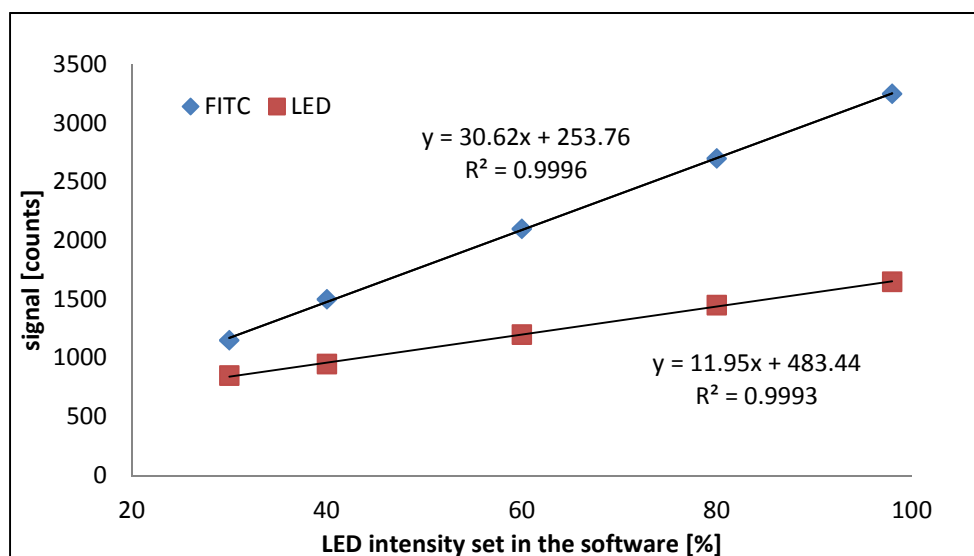
Figure 3-51: The detected signal intensity of the excitation and fluorescence light in counts plotted against the different LED intensities in % set in the software. The hybrid capillary-chip setup was flushed with a 2.0 µg/ml FITC solution, the LED light intensity was varied from 30, 40, 60, 80 and 98%. Excitation stray light (455 nm) and fluorescence (520 nm) signals were recorded by the push broom imager with an exposure time of 1000 msec. The detected signals were evaluated exemplarily for the light guide #12 of the fiber array.

3.4.5.E Push broom exposure time vs. fluorescence intensity

To evaluate the influence of the exposure time of the push broom imager on the detected fluorescence signal intensity of light guide #12 of the 2.0 µg/ml FITC solution, different exposure times of 500, 1000, 2500 and 5000 msec were used (Figure 3-52). A correlation coefficient (R^2) of 0.9999 was obtained. The experiment was repeated for FITC concentrations of 0.125, 0.25, 0.5 as well as 0.1 µg/ml all showing R^2 values higher than 0.999 (data not shown). The saturation of the push broom detector was reached at 70000 counts (data not shown). To reach high detection sensitivity a high exposure time should be chosen with the compromise of a low data rate problematic for very sharp signals in electrophoretic separations. As mentioned previously, a minimum of 8 to 10 data points should be used for peak description. An exposure time of 1000 to 2500 msec (data rate = 1.0 to 0.4 Hz) for peak widths from 10 to 25 sec are suitable and were used in this work. For on-chip experiments with low analyte concentrations exposure times up to 4500 ms were

used. The intercept of the trend line defines the offset of the detector with 644 counts which was generally subtracted from the measured signal, if not stated otherwise.
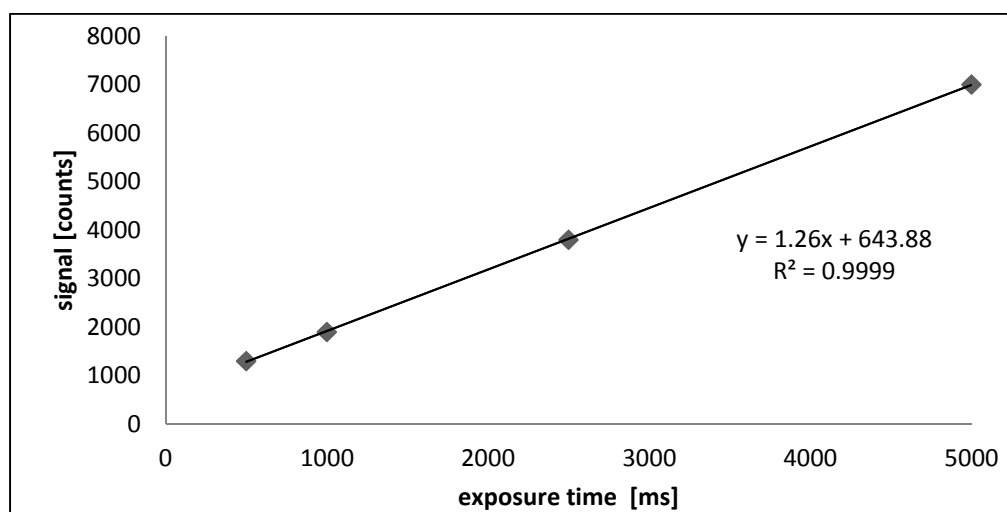
Figure 3-52: The detected signal intensity of the fluorescence light (520 nm) in counts plotted against the different exposure times of the push broom detector in ms. The hybrid capillary-chip setup was flushed with a 2.0 µg/ml FITC solution, the LED light intensity was 98%. Studied exposure times of the push broom detector were 500, 1000, 2500 and 5000 ms. The detected signals were evaluated exemplarily for the light guide #12 of the fiber array.

3.4.5.F Determination of linear range and detection limit for FITC

Using the on-chip detection setup for intermediate detection purposes the limit of detection (LOD) for the respective fluorophore is crucial. In order to characterize the optical setup in terms of the LOD and linear range, different concentrations of the FITC solution with concentrations of 0.125, 0.25, 0.5, 1.0, 2.0, 5.0, 25, 35 and 50 µg/ml (stock solution was 0.5 mg/ml) were flushed through the chip at 100 mbar and detected within the chip interface with an exposure time of 1000 msec (data rate = 1 Hz). The LED intensity was at 98 %. Here, the different concentrations were measured from lowest to highest concentration and with an intermediate 600 sec flush with borate buffer pH 9.2 to reach blank conditions the procedure was repeated. Measurements were repeated 3 times (n = 3) with overall RSD values below 1 % for the measured counts. The detected offset (see Figure 3-52) was subtracted from the detected intensities. The resulting calibration curve for fiber #12 is shown in Figure 3-53 and proves to be highly linear with an R^2 value of higher than 0.999 for FITC concentrations from 0.125 to 25 µg/ml. Therefore, the maximum linear working range is about two orders of magnitude. With higher concentrations starting from 35 µg/ml the respective detected signal intensity is declining most probably due to fluorescence saturation and quenching effects [Woltmann, 2014].
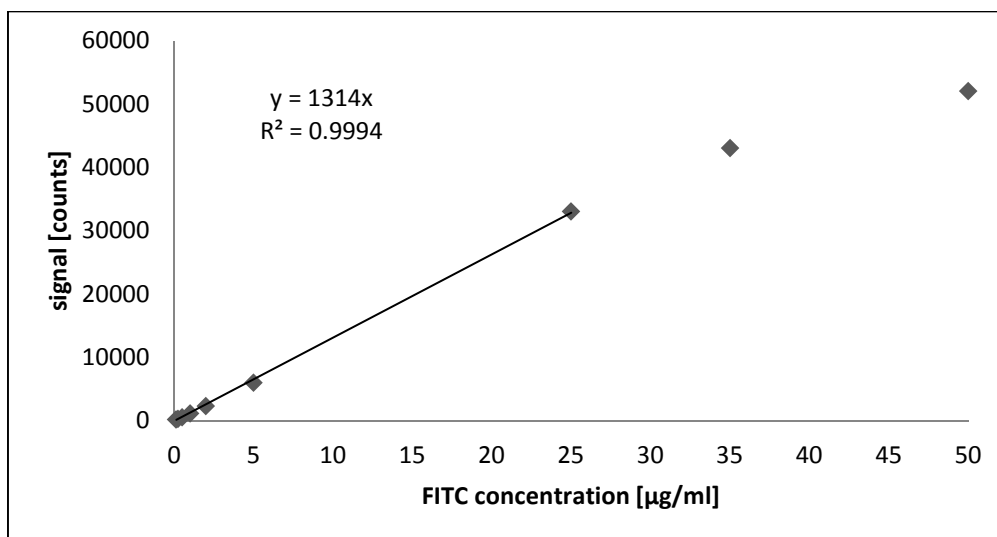
Figure 3-53: *Detected signal intensity (detector offset of 644 counts was subtracted) of the fluorescence light (520 nm) in counts plotted against the different concentrations of the FITC solution (0.125, 0.25, 0.5, 1.0, 2.0, 5.0, 25, 35 and 50 µg/ml). The hybrid capillary-chip setup was flushed with the respective solution and the LED light intensity was fixed at 98%. Fluorescence (520 nm) signals were recorded by the push broom imager with an exposure time of 1000 µs (1 Hz). The detected signals were evaluated exemplarily for the light guide #12 of the fiber array.*

Regarding LOD, a 0.125 µg/ml (0.32 µmol/l) concentration of the FITC was still detectable with 400 counts (measured value minus offset signal of 600 counts). The detected noise of the offset is very low with ±100 counts, due to the fact that a cooled CCD camera was used as the detector inside the push broom imager. The respective signal-to-noise (S/N) ratio is 4 (see Figure 3-54). As discussed in Section 3.4.4.C, one light guide of the fiber array detects the fluorescence light over a length of 0.83 mm in the chip. The volume of the common intersection with a length of 5 mm is 7 nl (Table 3-1) and therefore 0.83 mm represents a volume of ca. 1.2 nl. 0.32 µmol/l times 1.2×10^{-9} l equals 0.4×10^{-16} mol. Therefore the LOD for FITC at the basic pH of 9.2 for a data rate of 1 Hz and an S/N ratio of 4 is 0.04 fmol. By increasing the exposure time 5 fold one can reach 0.01 fmol or even lower absolute LODs but with the downside of decreased temporal resolution. The LOD reached is comparable with data from literature, where pmol LODs were reached during flushing experiments with fluorescein and CE separations of FITC labeled amino acids (AS) at pH 9.2 using a laser as excitation light source [Fu, 2006]. Thus, using the presented detection setup, compatible LODs were reached using an LED instead of a laser as excitation source in combination with a push broom detector. Despite the spatial resolution, the chosen push broom imager is a very powerful detector because it includes an air-cooled CCD sensor area, reaching very low noise levels as well as very high selectable exposure times (up to 5000 msec) for the hyperspectral analyte detection.
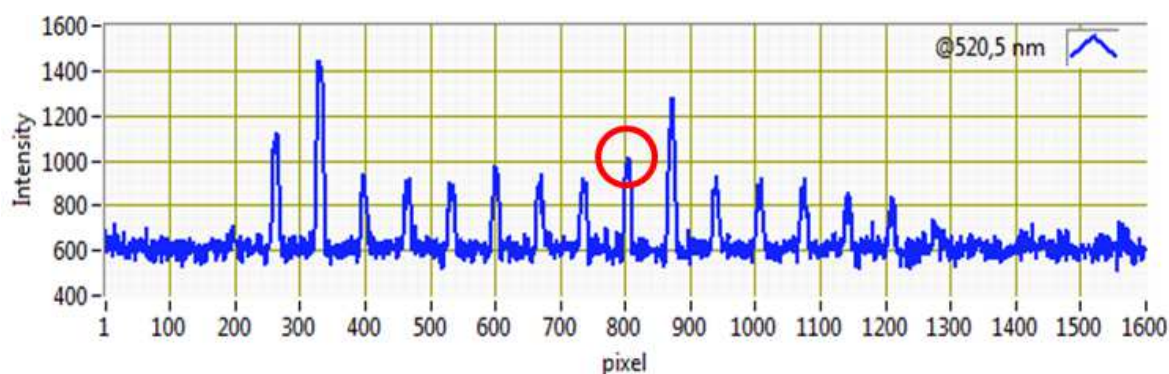
Figure 3-54: Recorded detector signals for each light guide of the fiber array for the 0.125 µg/ml FITC concentration for the determination of the LOD for FITC at basic pH of 9.2 for a data rate of 1 Hz and an S/N ratio of 4. The detected signal was evaluated exemplarily for the light guide #12 of the fiber array (red circle).

3.4.5.G Time-dependent intermediate and final analyte detection

For first proof of principle experiments for time dependent intermediate LED-IF detection, followed by MS as final detection method of two FITC plugs were performed flushing the hybrid capillary-microchip setup with a buffer of 100 mmol/l formic acid (pH 2.4), followed by injecting two plugs of a basic FITC solution (in borate buffer with pH 9.2) at a concentration of 0.5 mg/ml (1.28 mmol/l). The injected plugs (A and B for 1 sec at 1 bar) each were separated by a plug of 100 mmol/l formic acid (injected at 1 bar for 12 sec). Finally, the buffer vial was loaded to port P1 (with 100 mmol/l formic acid) and the injected plugs were flushed at 1 bar to the mass spectrometer (port P3) while intermediate LED-IF on-chip detection was performed with a detection rate of 1 Hz (1000 msec exposure time). The FITC plugs (A) and (B) were detected after 0.7 and 0.9 min at the chip interface and after 1.8 and 2.1 min in the MS using the single ion mode of the single quadrupole MS detecting the $[M+H]^+$ ion of FITC at m/z 390.2 (see Figure 3-55A and B), proving the principal applicability of the setup for time-dependent analyte monitoring for 2D LED-IF-MS detection assays. The peak patterns detected are comparable for both detectors. With the optical detection further information on the spatial and temporal peak progression is available comparing the intensities recorded via all optical fibers.
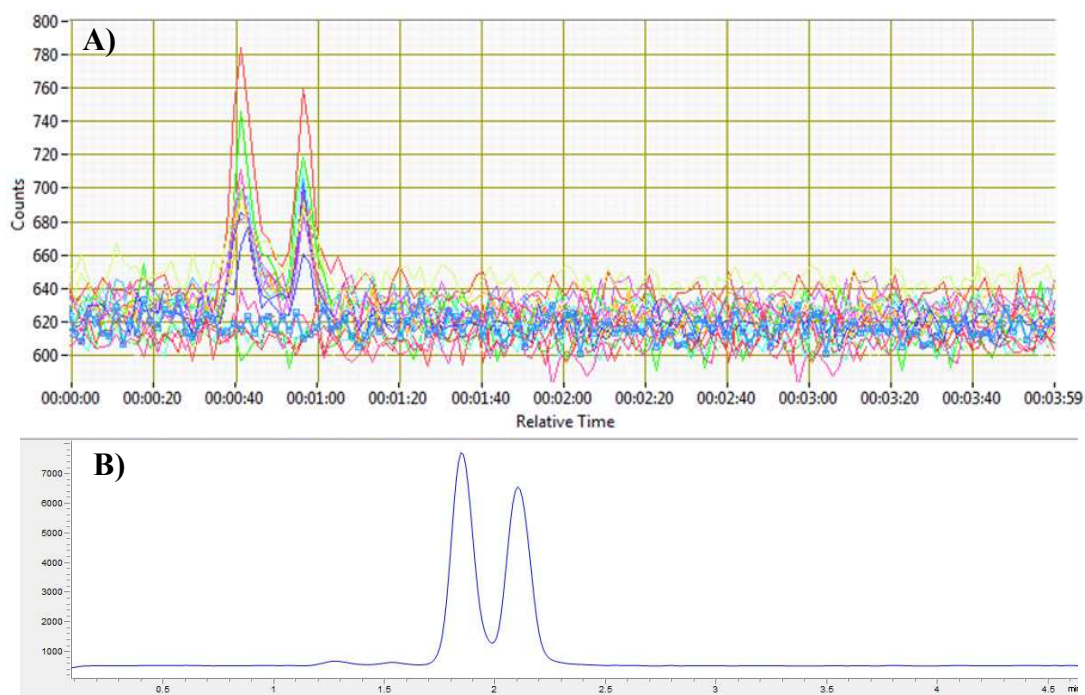
Figure 3-55: Time-dependent intermediate LED-IF detection for all active light guides of the fiber array at 520 nm (A), followed by MS (B) as final detection of two FITC plugs (SIM at [M+H]$^+$ at m/z 390.2). The hybrid capillary-microchip setup was initially flushed with 100 mmol/l formic acid (pH 2.4), followed by injecting two plugs of a basic FITC solution (borate buffer with pH 9.2) with a FITC concentration of 0.5 mg/ml (1.28 mmol/l). Plug injection was performed for FITC plugs A and B for 1 sec at 1 bar. They were separated by a plug of 100 mmol/l formic acid (12 sec at 1 bar). Finally, the formic acid buffer vial was loaded to port P1 (100 mmol/l formic acid) and the injected plugs were flushed to the mass spectrometer (port P3) at 1 bar while performing intermediate LED-IF on-chip detection at a data rate of 1 Hz (1000 msec exposure time).

The different signal heights for each light guide are due to the non-homogeneous appearance of the excitation beam of the used 0 mm position (Figure 3-45) discussed before. Due to the lower fluorescence intensity of the FITC at low pH values (here pH 2.4 for 100 mmol/l formic acid used as the background buffer), the used FITC concentration of 0.5 mg/ml (1.28 mmol/l) is close to the LOD and about four orders of magnitude higher compared to the LOD evaluated in basic buffer conditions as described in the previous section. The acidic pH for the background buffer was chosen to provide efficient ionization properties in the ion source of the mass spectrometer to detect the FITC in the positive mode as a pseudomolecular ion [M+H]$^+$.

3.4.5.H On-chip monitoring of CIEF-focused P503 labeled protein

To test the on-chip LED-IF detection system, a classical CIEF assay was performed in the first separation dimension of the 2D setup using pressure mobilization after the focusing step to flush the analyte (P503-labeled ß-lactoglobulin) past the LED-IF detection system. Protein labeling was done according to the procedure described in Section 3.4.3.G. CIEF

experimental conditions were described in Section 3.4.3.H, capillary lengths were 40 cm. After 7 min of focusing the ampholyte stack was mobilized using 100 mbar pressure applied to port P1 of the setup and the optical on-chip detection was started. The labeled protein was detected in the chip interface after 7 min with a peak width of 40 sec (see Figure 3-56). The slight tailing of the peak is due to the relatively high concentration of the protein of 2 mg/ml chosen here to demonstrate the option to monitor the movement of the analyte band inside the chip interface using the hyperspectral plot as illustrated in Figure 3-56C.
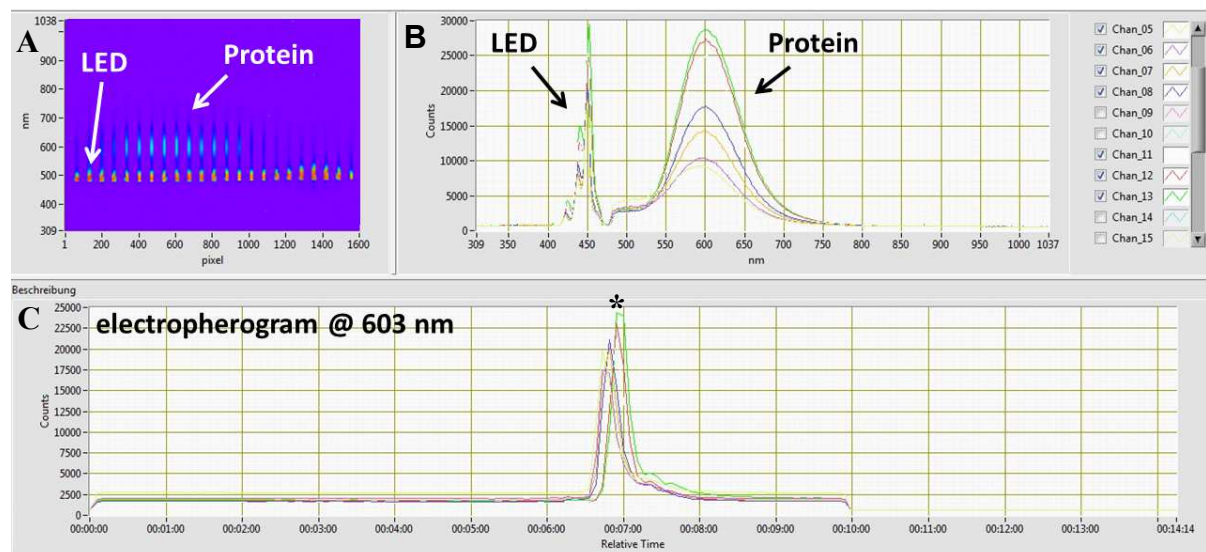
Figure 3-56: On-chip LED-IF detection of P503 labeled ß-lactoglobulin by CIEF with pressure mobilization. All three diagrams of the hyperspectral software of the push broom imager are shown. A) the hyperspectral plot, B) the spectral plot in detail and C) the time dependent signal recording (here at 603 nm) of the fluorescence signal for each active light guide of the fiber array. * = time point of C) of 7 min for display in A) and B). Light guide intensities plotted in A) and B) for fibers #2 to #8. The increase of the excitation light at ca. 500 nm is due to reflection phenomena at the surface edge of the additionally bonded 500 μm glass block.

In Figure 3-57 the time-dependent recording via the hyperspectral plot is shown for time points 8, 16, 24 and 32 sec of the protein movement through the chip interface. The ports P2 and P4 were hydrodynamically closed using the silicone filled sample vials. The peak width of the CIEF-focused peak can directly be determined via the hyperspectral plot of the push broom software to be approximately 3.5 mm spreading over about half of the channel image. The slight increase for the excitation light at ca. 500 nm is due to reflection phenomena at the surface edge of the additionally bond 500 μm glass block. Clearly, the setup is suitable for intermediate (or final) detection of CIEF focused labeled protein and can be used to monitor on-chip analyte band transfer from the first to the second separation dimension.
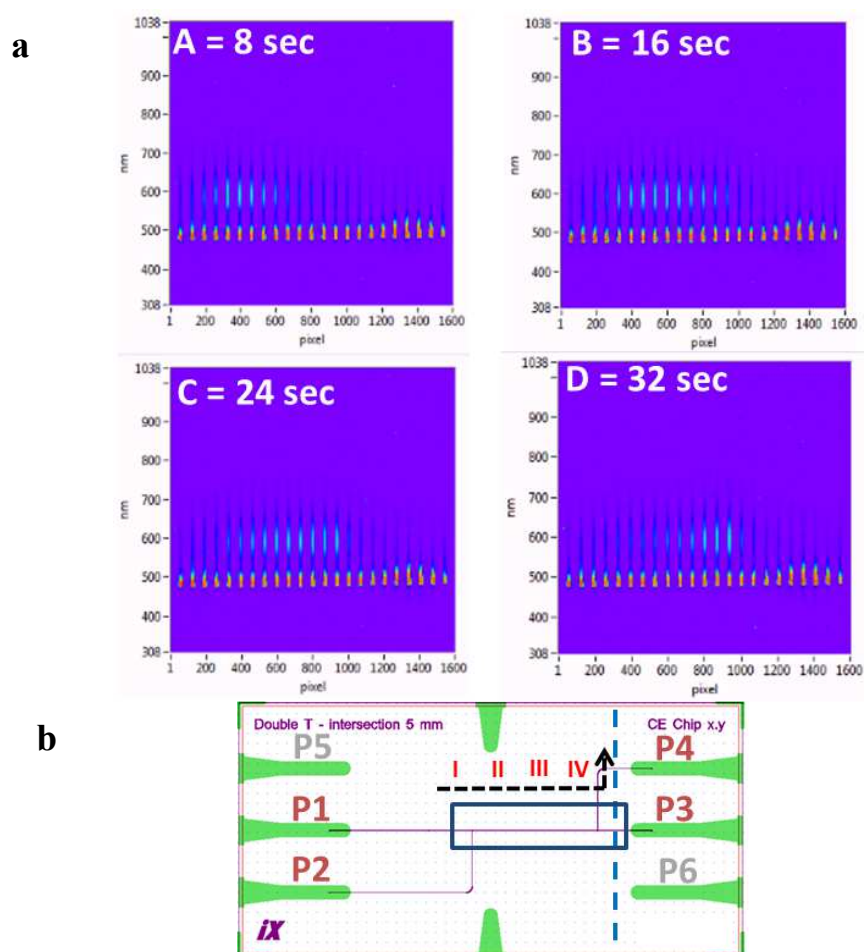
Figure 3-57: ***a)*** *Time-dependent recording via hyperspectral imaging plots shown for time points 8, 16, 24 and 32 s of the protein moving through the chip interface after CIEF focusing by applying 100 mbar from ports P1 to P4. The ports P2 and P4 were hydrodynamically closed using silicone-filled vials.* ***b)*** *Relation of time points to the position of the protein in the chip (e.g. A = I). The blue square shows the imaged part of the interface via the LED-IF detection setup. The dashed black line gives the flow direction of the protein sample band through the interface by applying 100 mbar from P1 to P4 with P2 and P3 being hydrodynamically closed using the silicone filled vials.*

3.4.5.I Using the LED-IF detection setup for solid state fluorescence

With the fixed alignment of the complete optical excitation and detection optics inside the aluminum block 1 (Figure 3-29), the setup can also be used for the characterization of solids in reflection mode. As an example, the setup was used for fluorescence imaging on TLC plates and solid dosage forms (here, a tablet). TLC plates with FITC fluorophore were prepared as described in Section 3.4.5 the appearance of the image was varied via optical Shell 2 with 0 and ± 1 mm of the initial optical path length as discussed in Section 3.4.4.B. According to the on-chip detection experiments, with increasing the distance (+1 mm) the image line becomes longer and more homogeneous regarding signal intensity, but with an overall decreased signal intensity for all light guides of the fiber array, see Figure 3-58. For smaller distances of the optical path length the spot size became smaller but showed higher

signal intensities. Here, the fluorescence signal pattern detected by the light guides of the fiber array is very homogenous.
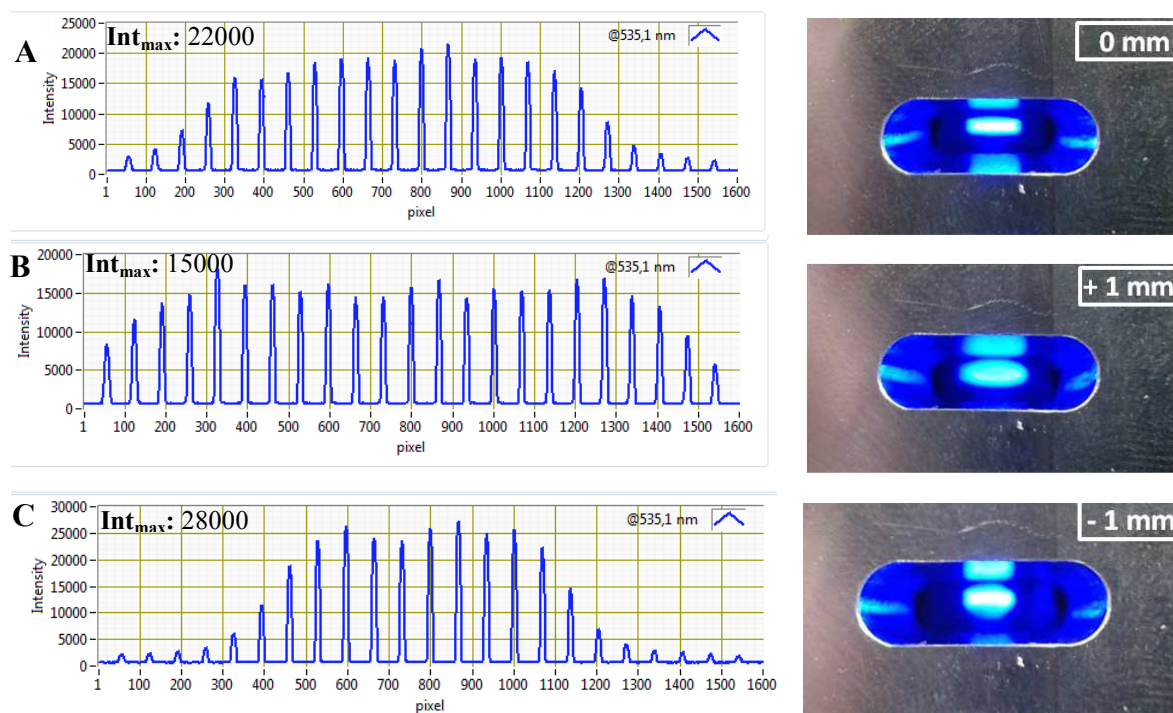
*Figure 3-58: Appearance of the excitation light beam of the 455 nm LED in the focal point of the optical geometry and the resulting intensity plot for the fluorescence of FITC at 535.1 nm for different lengths of the optical path using the variable optical Shell 2. **A** ± 0 mm comparable to the non-variable optical Shell 2, **B** increase of the excitation light path length by 1 mm and **C** decrease of the excitation light path length by 1 mm. Experiments were done for a TLC plate contaminated with an FITC solution (2 µg/ml). Int_{max} = maximum intensity*

The solid state fluorescence intensity for the contaminated TLC plate was ca. 1000 times higher than for the on-chip detection at line detection parameters (Figure 3-58) vs. (Figure 3-50) for approximately the same FITC concentrations. Therefore, lower LODs can be reached performing analyte detection on solids e.g. after TLC separations.

3.4.5.J Linear vs. point excitation

Especially for the surface analysis of solid dosage forms like tablets a single spot sample excitation over a defined small spot can be interesting to characterize the homogeneity of the distribution of the active agent at different spots on the tablet surface [Woltmann, 2014]. In Figure 3-59, the linear excitation (about 6 mm in length) B compared with nearly point excitation of a small and defined area by turning the optical shell inside the aluminum block in a 90° angle as indicated in Figure 3-59B. With excitation beam line is now positioned perpendicular to the fiber array in a right angle; the exposed area is only 1.8 × 8 mm².
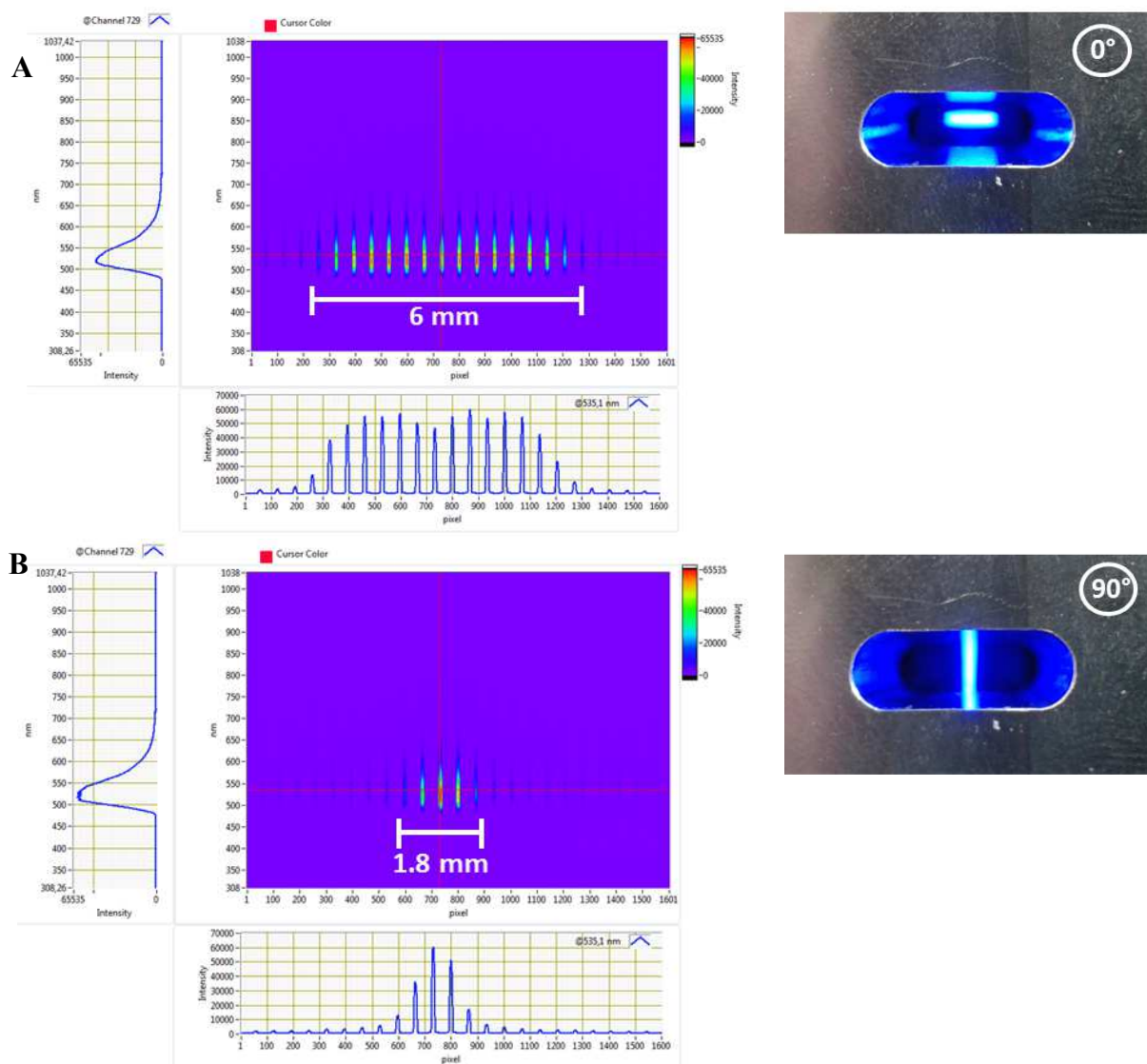
*Figure 3-59: Appearance of the excitation light beam in the focal point of the optical geometry and the resulting hyperspectral plot for **A** the linear (0° angle) and **B** the spot point (90° angle) excitation arrangement by turning the optical shell within the setup. Experiments were done for a TLC plate contaminated with an FITC solution.*

3.4.5.K Solid dosage forms (e.g. tablets)

Using a 356 nm LED (LEDMOD 365.100, λ_{ex} = 360-370 nm, $P_0 \leq$ 500 mW, Omicron Laserage, Rodgau, Germany) a pink tablet (fluorescent agents erythrosine (tablet was incubated with 0.33 % erythrosine solution) and 1% w/w quinine) was characterized with the optical setup, resulting in an intensity distribution of the measured intensity profiles (see Figure 3-60), due to the curvature of the analyzed tablet (see Figure 3-61). Respective fluorescent signals are for quinine at 400 nm and erythrosin at 580 nm, respectively. Here, mostly pairs with very similar intensities were detected from the pair of fibers having an

identical distance to the curved tablet surface and thus similar response. Using the fiber array in combination with the push broom imager also for solid dosage forms, a detailed analysis of the sample is possible regarding parameters such as compaction, particle size and composition as shown by Woltmann et al. [Woltmann, 2014]. The ease of exchange of light source and filters further demonstrates flexibility of the setup.
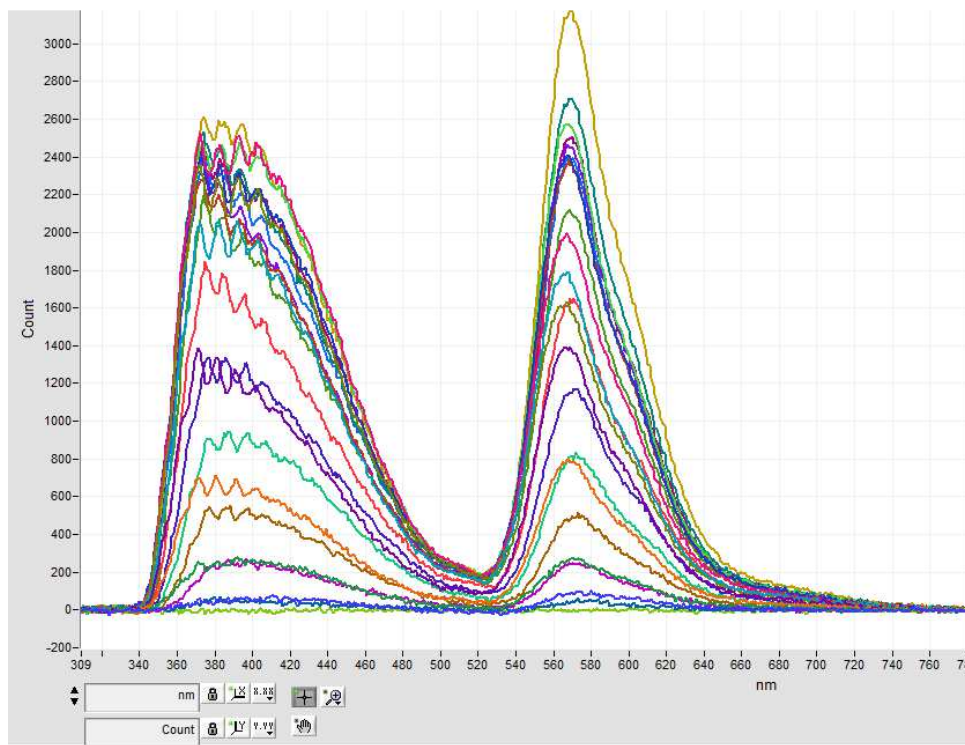
Figure 3-60: Fluorescence spectra for the 23 active light guides of the fiber array for the analysis of a pink tablet containing erythrosine and quinine. Excitation was done using a 365 nm LED.

Figure 3-61: Photographs of the pink tablet Series 5594 with a diameter of 10 mm (top and side view).

3.4.6 Spatially-resolved on-chip LED-IF detection – summary and outlook

A spatially-resolved intermediate on-chip LED-IF detection system was successfully implemented for the hybrid capillary-chip glass interface described in Section 3.1. The setup includes a high power 455 nm LED prototype as excitation light source and a linear light fiber array consisting of 23 active 100 μm light fibers for spatially-resolved fluorescence detection in combination with a push broom imager for hyperspectral imaging. The optical parts were arranged in a bevel angle setup with the excitation light focused at an angle of 45° and fluorescence detection perpendicular to the chip surface. The optical elements were fixated in an aluminum block housing lenses for focusing the excitation light. Filters were used for optimization of excitation and fluorescence light characteristics. By varying the optical excitation path length the light beam spot appearance can be adjusted with respect to exposed channel or sample length and excitation light intensity. Due to increased fluorescence signals, the channel cross section as well as the surface edge of the bonded glass block on the chip interface can be detected during flushing experiments with a basic fluorescent FITC solution and therefore a precise chip interface alignment is enabled. Using the variation of excitation light beam spot appearance as well as alignment strategies using the FITC solution, the channel segment to be studied (e.g. the common intersection) as well as a defined channel length before and/or after the cross section segments can be properly monitored. The optical on-interface detection therefore allows a precise control of sample transfer step(s) from the first to the second separation dimension as discussed in Section 3.4.5.H. A special software hereby allows temporal, spatial and spectral resolution of a sample peak migrating or being flushed through the chip channel.

The dependence of the intensity of the measured fluorescence light of the FITC as well as the reflected excitation light from the LED on the set LED intensity is highly linear with correlation coefficients (R^2) larger than 0.999. To gain maximum fluorescence intensity for the on-chip detection experiments, the LED was generally used at maximal intensity of 98 % for all measurements. Due to the fact that fluorescence saturation was not reached using maximum LED intensity indicates that even lower LODs can be reached using a more powerful excitation source (e.g. a laser). A calibration curve was exemplarily recorded for concentrations of the basic FITC solution ranging from 0.125 to 25 μg/ml of the basic FITC solution being highly linear with a R^2 value of 0.999 at 1000 ms exposure time. RSD values (n = 3) below 1 % for the measured counts were obtained. A linear working range of about two to three orders of magnitude was determined. To estimate analyte detection sensitivity

the LOD for FITC as a model analyte at basic pH of 9.2 for an S/N ratio of 4 was determined to be 0.04 fmol. By working at maximum detector exposure times (5000 ms, 0.2 Hz) even 0.01 fmol or even lower LODs may be reached with the downside of decreased detection points per time. The correlation of the detected fluorescence signal intensities in dependence of the set detector exposure time or data rate (500 to 5000 ms or 2 to 0.2 Hz data rate) is highly linear with R^2 values higher than 0.999. The high linearity allows interpolation of signal intensities using different exposure times of the push broom imager. The saturation of the detector was reached at 70000 counts. Flushing experiments were conducted by injecting plugs of FITC as well as P503-labeled protein solutions into the 2D capillary-chip setup followed by analyte detection using time dependent intermediate on-chip LED-IF detection followed by MS as final detection: Here, the peak patterns of two injected FITC plugs were comparable for the on-chip optical as well as final MS detection, proving the general applicability of the optical on-chip detection system. The setup can also be used for solid state fluorescence in reflection mode as shown for an FITC-contaminated TLC plate and a tablet sample. CIEF analysis of P503-labeled ß-lactoglobulin was monitored by the on-chip detection setup with a sufficient intensity to monitor the analyte band transfer within the glass chip interface. Therefore, the implemented on-chip LED-IF detection setup is also suitable for the intermediate detection of labeled proteins being transferred from the first to the second separation dimension.

4   Method development for 1st and 2nd separation dimension

4.1   First dimension CIEF

4.1.1   Abstract

With respect to 2D CIEF-LED-IF/CE-MS separations the method development for the CIEF and the CE separation dimension were evaluated separately and optimized using experimental and simulation data. At first, two covalently bound neutral coatings, PVA and GPTMS, were evaluated regarding CIEF peak performance for commercial pI markers and model proteins, and the resulting pH gradient linearity. GPTMS and PVA showed comparable performance for CIEF separation assays using 0.1 % HEC as an additional EOF modifier. RSD values for the detection time below 1.2 % and for the peak area below 2.5 % except the most basic marker for the PVA coating (7.3 %) in the reversed separation mode were achieved (Section 4.1.4.A). Using an EOF counter flow to the flow from the applied mobilization pressure, a better linearity ($R^2 > 0.98$) of the pH gradient was achieved due to the elimination of pH-induced EOF velocity differences. GPTMS was finally chosen as the coating due to a less laborious and better reproducible coating process. To control analyte position inside the first CIEF separation dimension, different anolyte and catholyte plug lengths were used to position the pH gradient (4.1.4.D). A linear relationship between the injected catholyte plug length and the analyte position for experimental and simulation data enabled to create a positioning tool "Focus" to estimate peak positioning within the separation capillary based on using experimental parameters. Using a 250 mmol/l concentration of aqueous TEA instead of a 20 mmol/l concentrated aqueous NaOH solution as the catholyte, nearly the same pH and ionic strength were obtained with the benefit of a better chemical atability of the GPTMS coating due to lower pH. Switching of the anolyte from non-volatile phosphoric to volatile acids such as formic acid was successful and ensured compatibility of the anolyte with MS detection, also used as the 2nd dimension background electrolyte. Simulated and experimental CE separations showed that the ampholytes migrate as a bulk zone under CE separation conditions, most probably due to similar charge to mass ratios of the respective compounds. Stable CE experimental condition (n = 3) with RSD values for the detection times of below 2 % and for the peak area of below 4 % were achieved using a GPTMS coated capillary. Simulations indicate a better separation when using acidic background electrolyte with a lower pK_a and thus pH value. Using formic acid

instead of acetic acid as the background electrolyte the ampholyte stack appeared narrower, most probably due to a more uniform charge to mass ratio of the ampholyte components, and both the stack as well as the protein are shifted to shorter detection times due to a higher charge and therefore increased mobility at increased pH value. The acidic protein ß-lactoglobulin was not separated from the ampholytes using an acidic background electrolyte. Simulations indicated that separation would be achieved using a basic electrolyte system. As a conclusion, the pH value of the background electrolyte of the second CE separation dimension should be as different as possible from the pI of the analyzed protein to create a highly charged protein compared to the respective markers and ampholytes and therefore achieve undisturbed MS detection.

4.1.2 Introduction

4.1.2.A Capillary isoelectric focusing - CIEF

Isoelectric focusing (IEF) is a powerful and high-resolution technique for separation and analysis of amphoteric biomolecules [Foret, 1995; Righetti, 1997; Rodriguez-Diaz, 1997; Sosic, 2008; Hempe, 2009; Righetti, 2011; Righetti, 2013] and particles (viruses and cells [Horka, 2007; Kostal, 2008; Salplachta, 2012]) in an established pH gradient by means of their respective isoelectric point (pI). IEF in solid platforms such as gels is routinely used in the biopharmaceutical industry for protein characterization e.g. for the determination of charge heterogeneity, purity and identity of proteins, as well as stability of protein-based therapeutics [Liu, 1996; Dou, 2008; Sosic, 2008; Cao, 2014]. IEF is also used to analyze post-translational modifications of proteins [Fonslow, 2010; Ouidir, 2014]. With regard to direct optical detection, high throughput and automation the capillary format (CIEF) is advantageous. Therefore, during the last two decades, CIEF became a widely used alternative to traditional gel and paper-based formats [Righetti, 1997; Manabe, 1998; Michels, 2002; Liu, 2006; Simpson, 2005; Xu, 2012; Righetti, 2013]. CIEF-UV and fluorescence detection are used for quantification and identification based on the pI value. Further identification is only possible, when MS detection is used. In quality control of the pharmaceutical industry the direct coupling of CIEF to MS would be desirable for a fast analyte or batch impurity identification, but, unfortunately, this is not possible due to the incompatibility of the used ampholytes with MS detection [Tang, 1996; Wei, 1998; Páger, 2011]. In general, ampholytes are zwitterionic compounds containing a variable number of basic and acidic moieties spanning a wide range of different pI value increments and thus, reaching a maximum

resolution of down to ~0.01 ΔpI [Shim, 2008; Shen, 2000A; Shen, 2000B; Páger, 2012]. The ampholytes are in the same m/z-range as many of the proteins studied and have an overall much higher concentration and therefore suppress the analyte signal in the ESI-MS ion source. In addition, so called MS source fouling due to contamination occurs [Lamoree, 1997; Storms, 2004]. In CIEF assays, generally, the whole separation capillary is filled with the sample solution containing a certain concentration of commercially available carrier ampholyte (CA) stock solution. After that the capillary ends are immersed into the anolyte (e.g. H_3PO_4 at the anode) and catholyte (e.g. NaOH at the cathode). The focusing process starts by applying a positive voltage to the inlet of the CE instrument being the anode for the so called normal separation mode for using reversed polarity in the reversed mode. Upon voltage application H^+ and OH^- enter the capillary from the anodic and cathodic end, respectively, and titrate the carrier ampholytes within the separation capillary, and thus create a pH gradient in which the amphoteric analytes (e.g. proteins) are focused according to their respective pI value. During this process the measured current declines exponentially until a certain threshold value is reached indicating the finalization of the focusing process. The result is a stationary state [Righetti, 1997; Rodriguez-Diaz, 1997]. Here, the analytes are focused in the pH gradient induced by the ampholytes according to their respective pI value as in the simulation shown in Figure 4-1.
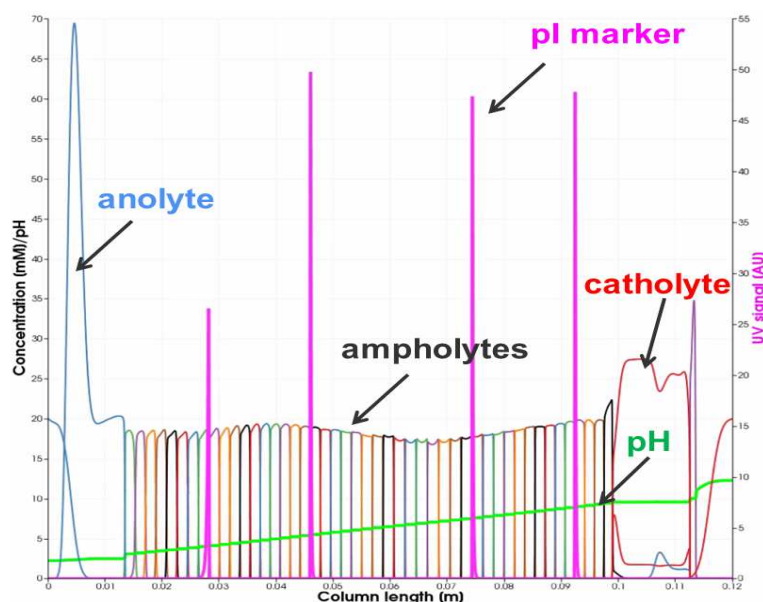
Figure 4-1: CIEF simulation of four pI markers (pink) using 50 ampholytes to create the pH gradient. Simulations were performed as described in Section 4.1.3.G. The catholyte and anolyte used were 250 mmol/l TEA and 1 mol/l acetic acid.

After the focusing time is completed the mobilization pressure is applied e.g. at the anodic end (anodic mobilization) of the CIEF pH gradient and the analytes are pushed towards the UV-detector placed at the cathodic end of the setup as shown in Figure 4-2A [Kilár, 1998]. Using this arrangement the basic analytes or pI markers are detected first, followed by the acidic ones. For an uncoated capillary the EOF is cathodic and thus for the "normal mode" in the direction of the applied mobilization pressure. Reversing the system (catholyte at the inlet), CIEF can be performed in the so called "reversed mode" with the EOF as a counter flow to the mobilization direction by applying a negative separation voltage to the inlet of the CE instrument (now serving as the cathode) using anodic detection by applying mobilization pressure to the cathode as shown in Figure 4-2B. Filling the whole separation capillary with protein (S) and carrier ampholytes (CAs) increases sensitivity for protein detection in CIEF but on the other hand can also increases the possibility of protein precipitation due to the high concentration upon focusing. The tendency of precipitation is especially high after the focusing process is completed and the proteins are concentrated at their respective pI and thus are uncharged. To quickly and easily adjust the injected protein concentration a portion of a blank solution only containing the CAs can be injected prior to the sample solution as indicated in Figure 4-2C. By varying the relative plug length of both solutions the amount of protein, injected can be adapted while keeping the same pH gradient.
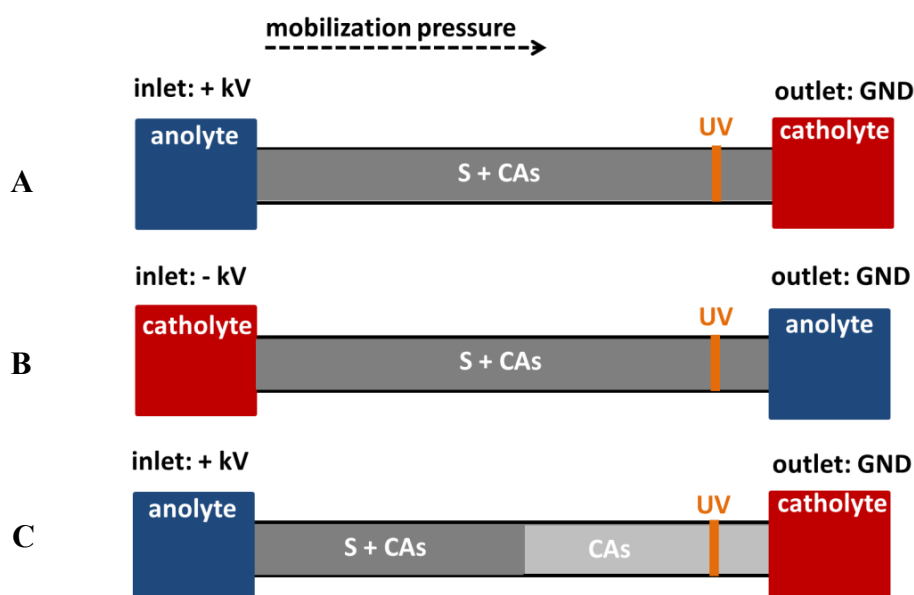
Figure 4-2: CIEF separation and injection modes: A) Normal mode with cathodic detection B) Reversed mode with anodic detection and C) Adjustable sample and blank solution plug injection for adaptation of sample amount being injected.

4.1.2.B Coatings

To achieve reproducible and stable CIEF separation conditions for the analysis of proteins, it is necessary to use separation capillaries with a coated inner surface to eliminate protein adsorption to the fused silica surface as well as to control or eliminate EOF velocity [Rodriguez, 1999; Shen, 2000B; Gao, 2004; Silvertand, 2008; Shimura, 2009].

In general, the interaction of proteins with the bare fused silica surface depends on several parameters like the size (diffusion coefficient) and pI (net charge at a certain pH) of the protein, the orientation and number of hydrophilic, hydrophobic and charged groups or regions of the 3D protein structure leading to reversible or unwanted irreversible adsorption of proteins to the surface. In general, the interaction can be of two types: First, specific interaction comparable to antibody-antigen interaction where a specific group or area of the protein binds to one or more Si-O⁻-groups present on the capillary surface at medium or basic pH of the separation buffer. Second, nonspecific interactions that include electrostatic attraction or repulsion, hydrophobic interactions, and van der Waals forces [Egodage, 1997; Ostuni, 2001]. Due to the inhomogeneous charge and characteristics of proteins, different interactions are present simultaneously. Once a protein is adsorbed to the capillary surface it may undergo conformational changes e.g. loss of helix and ß-sheet, or other secondary and tertiary structural changes enhancing the binding to the surface and increasing residence time. Once bound irreversibly, the protein layer itself can act as a coating, hence influencing or altering the capillary surface properties regarding protein adsorption and ζ-potential EOF properties [Soderquist 1980; Chan, 1981; Norde, 1986; Doherty, 2003]. To influence EOF velocity and reduce protein adsorption, a variety of coatings are reported in the literature to be applied for capillary electrophoretic separations [Hjertén, 1985; Verzola, 2000; Horvath, 2001; Doherty, 2003; Pattky, 2013]. There are three major categories: The dynamic surface modification using small or large molecule additives (dynamic coatings), physically adsorbed and covalently bound coatings. In general, the complexity of the coating process but also the stability of the resulting surface modification is increased from the category of the dynamic to the covalently bound coatings. In general, homogeneous and stable coatings improve stability and repeatability of detection times and peak areas by reducing protein wall interactions as well as EOF velocity changes by modifying the ζ-potential via the elimination of ionizable Si-OH groups on the fused-silica surface, "shielding" remaining charged groups on the surface as well as increasing the viscosity near the capillary wall by the coating layer itself.

The most prevalent coating strategy for the analysis of proteins in capillary electrophoresis is the use of covalently bound polymers e.g. polyacrylamide (PAM), polyethylene oxide (PEO) or polyvinyl alcohol (PVA) as well as covalently bound alkylsilane reagents like (3-glycidoxypropyl)trimethoxysilane (GPTMS) [Verzola, 2000; Doherty, 2003; Hutterer 2003]. Additionally, covalently bound coatings are most suitable for the coupling of capillary electrophoretic separations to mass spectrometric detection due to the fact that no coating material can enter the MS and source contamination is avoided. In this study two covalently bound coatings protocols using PVA [Kitagawa, 2006; Qu, 2007; Xu, 2009; Xu, 2010] and GPTMS [Shao, 1999; Horka, 2001] as coating material were evaluated regarding repeatability of migration times and peak areas for the CIEF analysis of pI markers and proteins, elimination of EOF velocity, complexity and time effort for the coating process as well as related costs.

4.1.2.C CIEF pH gradient positioning in the separation capillary

The positioning of the pH gradient in the capillary and the understanding of physicochemical phenomena at the surface boundary between the ampholyte gradient, the catholyte and anolyte at its outer ends is crucial to control analyte positioning and therefore the detection process. In this regard so called spacer or blocker substances with extremely basic or acidic pI values are introduced to spatially define the ampholyte pH gradient within the capillary. Their task is:

- To prevent proteins with extreme acidic or basic pI values from focusing in the distal region of the capillary [Cao, 2014; Mack, 2009] if the detection is at the anodic [Cao, 2014; Mack, 2009] or cathodic [Liu, 1996; Mohan, 2002; Vlckova, 2008] end of the capillary. During the focusing step these compounds fill the corresponding blind segment (distal region) of the capillary shifting the whole pH gradient between inlet and detection window.

- To extend the separation range in the capillary on the anodic or cathodic side to allow the separation of extremely acidic or basic proteins with pI values of $3 > pI > 10$. Usually, for CIEF separations carrier ampholytes ranging from pI 3-10 are used to separate a wide range of different proteins in a single analysis. For proteins with pI values smaller than 3 and higher than 10 spacer substances can be used to increase the pI range covered. In addition, narrow cut ampholyte mixtures can be used, e.g. pI

9-11, to enhance resolution in the basic pH regions, if needed [Yang, 2005; Poitevin, 2007].

- Sacrificial ampholytes are consumed due to bidirectional ITP phenomena, where the acidic and basic outer edges of the ampholyte gradient are migrating out of the capillary into the catholyte and anolyte vial, respectively [Chrambach, 1973; North, 2008; Lalwani, 2005; Lalwani, 2006]. The bidirectional ITP can be slowed down using anolyte and catholyte solutions with high ionic strengths, but unfortunately cannot be eliminated completely. Therefore, suitable concentrations of spacers must be injected at the beginning of the CIEF run, so that their amount in the capillary is higher than the amount consumed by bidirectional ITP during analysis [Righetti, 1983; Mosher, 1990; Liu, 1996; Mosher, 2002].

- For the positioning of the pH gradient in the capillary e.g. in whole column detection CIEF [Wang, 1992; Fang, 1998; Mao, 1999; Liu, 2008], two dimensional separation applications and preparative applications. Regarding two dimensional separation experiments in gas or liquid chromatography as well as for preparative separations, a common approach is to sample the first separation dimension by a heart cutting interface and subsequently inject an aliquot as the sample volume into the second separation dimension [Deans, 1981; Tranchida, 2012; Evans, 2004]. Following this approach for coupling CIEF to a second separation dimension, the positioning of the pH gradient and therefore of an analyte is crucial to ensure a proper sample transfer.

In literature, substances such as N,N,N',N'-tetramethylethylendiamine (TEMED) [Liu, 1996; Mohan, 2002; Vlckova, 2008] or arginine (pI = 10.7) as cathodic, and iminodiacetic acid (IDA, pI = 2.2) as anodic spacers or blockers [Cao, 2014; Mack, 2009], as well as directly the anolyte and the catholyte itself were introduced. Here, non-ampholytic compounds such as TEMED can increase the maximum CIEF current to a defined potential in comparison to an amphoteric compound, e.g. arginine, and therefore counteract temperature increase by Joule heating [Mack, 2009]. Hence, the optimization regarding suitable concentrations and types of each spacer depends on several experimental parameters such as the ratio between total and distal length to the detector of the capillary, pI value of the analytes, extent of the bidirectional ITP phenomena and applied potential. In this work, the positioning of the ampholyte pH gradient in the capillary was studied using different plug lengths of the anolyte and catholyte as a straight-forward approach. In addition, the experimental results were

compared to results from simulation experiments via the tool Focus to predict pH gradient positioning within the separation capillary based on the chosen experimental parameters.

4.1.3 Experimental section

4.1.3.A Chemicals

Carrier ampholyte solutions Pharmalyte 3-10, Pharmalyte 2.5-5, Pharmalyte 8-10.5 and Pharmalyte 5-8 for isoelectric focusing were purchased from GE Healthcare Bio-Sciences AB (0.36 meq/ml pH, Uppsala, Sweden). β-Lactoglobulin (β-lact, bovine milk > 90%, pI: 4.83–5.4, 18.4 kDa), myoglobin (myo, equine heart > 90%, pI: 6.8–7.4, 17.8 kDa), ribonuclease A (RNase A, equine heart > 90 %, pI: 9.6, 13.7 kDa), 4-aminobenzoic acid (PABA, pI: 3.9), 3-glycidoxypropyl-trimethoxysilane (GPTMS, 97 %), (3-aminopropyl)triethoxysilane stock solution (APTS, 97 %), potassium tert butoxide (C_4H_9KO, tert-BuOK, 1.0 mol/l in THF), polyvinyl alcohol (PVA, Mw 89 000 – 98 000, 99 %, hydrolyzed), n-Hexane (>97.0 % (GC) for HPLC), fluorescent IEF-Marker-Mix (200 μl stock solution, 5 markers with pI values 4.0, 5.5, 7.2, 7.6 and 9.0 each at 2 mg/ml), sodium chloride and sodium tetraborate decahydrate ($Na_2B_4O_7$, puriss p.a.) were purchased from Sigma-Aldrich (Steinheim, Germany) and isopropanol (LC-MS grade) from Fluka (Steinheim, Germany). Acetic acid (glacial, 100 %), formic acid (98 - 100 %), phosphoric acid (85 %), sodium hydroxide (30 %), glutaraldehyde (50% in water for synthesis) and hydroxyethyl cellulose (HEC, for synthesis) from Merck, sodium hydroxide (0.1 mol/l, for analysis) was used from AppliChem GmbH (Darmstadt, Germany) and methanol and acetone (HPLC gradient grade) from BDH PROLABO Chemicals VWR (Darmstadt, Germany). Hydrochloric acid 32 % was bought from Fisher Scientific (Loughborough, UK). Sodium sulfate (Na_2SO_4, ≥ 99 %) was purchased from Carl Roth (Karlsruhe, Germany). Triethylamine (TEA, 99 %) was purchased from Alfa Aesar (Karlsruhe, Germany). All solutions were prepared with doubly-deionized water (Milli-Q purification system from Millipore, Bedford, MA).

4.1.3.B Separation capillaries - preparation and conditioning

Fused silica capillaries, ID 50 μm, total length of 35 cm, effective length of 27 cm to the detection window, were purchased from Polymicro Technologies (Phoenix, AZ). Before burning the detection window the capillaries were coated with GPTMS or PVA to create a

hydrophilic surface and therefore minimize both EOF and surface interactions with proteins (Section 4.1.2.B). For quality control, each coated capillary was flushed with the respective anolyte and a voltage of +25 kV was applied to monitor if the current reaches a stable plateau over the respective separation time. The coated capillary was conditioned at the start of each working day by rinsing for 5 min with 0.9 % aqueous sodium chloride solution and 10 min at 1.0 bar with doubly-deionized water. Prior to each run the capillary was rinsed for 3 min with the NaCl solution and 3 min at 1 bar with double-deionized water. At the end of each working day the capillary was rinsed for 5 min with the sodium chloride solution and 30 min at 1 bar with doubly-deionized water. Finally, for overnight storage, both capillary ends were immersed into doubly-deionized water. For long-term storage the capillary-chip setups were flushed with air and left at room temperature.

4.1.3.C Procedure for 3–(glycidoxypropyl)trimethoxysilane coating

The coating protocol described in Section 3.4.3.E was followed but adapted for a 1D capillary setup. First, the capillary was rinsed with a cleaning solution of 1.0 mol/l NaOH, 1.0 mol/l HCl followed by water for 10 min for each solution at 1 bar. Finally, the GPTMS coating solution (c = 10 % w/w, pH ≈ 5) was introduced into the capillary with 1 bar for 40 min. Then, the capillary was gently purged with compressed air overnight (minimum 10 hours at 1 bar). This process was repeated in order to achieve a homogeneous coating on the capillary surface.

4.1.3.D Procedure for polyvinyl alcohol coating

The coating protocol for the covalently bound polyvinyl alcohol (PVA) coating was adapted from Xu et al. [Kitagawa, 2006; Qu, 2007; Xu, 2009; Xu, 2010]. First, the capillary or 2D setup was rinsed with an activating solution of 12.5 mmol/l potassium t-butoxide (tert-BuOK, 12.5 µl of a 1 mol/l stock solution was added to 987.5 µl hexane dried with sodium sulfate) for 60 min, followed by rinsing with water for 15 min. In the next step, 2 % APTS solution (20 µl of APTS stock solution added to 980 µl acetone dried over sodium sulfate) was introduced into the capillary for 15 min, and then the column was flushed at 1 bar with water and methanol for 15 min to remove the unreacted APTS. Thereafter, the capillary was rinsed with acetone and then blown dry with air (15 min at 1 bar). The third step was aldehyde-group functionalization of the amino groups. Therefore, 10 % v/v glutaraldehyde dissolved in 50 mmol/l borate buffer (pH 9.0) was used to wash the capillary for 60 min at 1

bar. The capillary was then flushed with water for 15 min at 1 bar and then prepared for the last step for PVA immobilization. In the final step, the aldehyde-modified capillary column was rinsed with an acidified PVA solution (a mixture of 900 µl of 5 % w/w aqueous PVA solution and 100 µl of 5.0 mol/l HCl) for 60 min at 1 bar. The PVA stock solution was prepared by dissolving 1 g PVA (99+%, hydrolyzed, M_w: 89 000 – 98 000 g/mol) in 20 ml H_2O at a temperature of 70°C. The solution was stirred for minimum 4 hours at 70°C. Subsequently, the capillary was washed with water for 15 min and then flushed with methanol for another 15 min at 1 bar. The coated capillary was finally blown dry with air.

4.1.3.E CIEF conditions and parameters

An Agilent 7100 CE system equipped with a UV absorbance detector (Agilent Technologies, Waldbronn, Germany) was used for performing CIEF experiments. The temperature settings were 25°C for the capillary cartridge. A 1.0 % w/v HEC stock solution was prepared by dissolving 0.4 g HEC in 40 mL doubly-deionized water at 70°C. Isoosmotic sodium chloride 0.9 % w/v was used to remove proteins from the capillary wall [Graf, 2005; Suratman, 2008]. The carrier ampholyte blank solution and the sample contained 2.0 % v/v Pharmalyte 3-10 carrier ampholytes and 0.1 % v/v HEC as a dynamic EOF modifier to minimize the EOF [Verzola, 2000]. 20 mmol/l phosphoric acid, 2.3 mol/l acetic acid or 1.0 mol/l formic acid were used as anolytes and 20 mmol/l sodium hydroxide (NaOH) 250 mmol/l trimethylamine (TEA) as catholyte each containing 0.1 % w/v HEC, respectively. The analytes were dissolved in Milli-Q water and mixed with the carrier ampholyte stock solution to a final concentration of 0.5 mg/ml for myoglobin, 1.0 mg/ml for β-lactoglobulin, 2.0 mg/ml for ribonuclease A and 0.02 mg/ml for 4-aminobenzoic acid. Each marker of the fluorescent IEF marker mix was added to the sample at a concentration of 0.01 mg/ml. The anolyte, catholyte, and the cleaning solution solutions were stored at room temperature, and the 1.0 % w/v HEC and the ampholyte stock solutions were stored at 4 to 8 °C. In general, the CIEF separations were carried out in the reversed mode (see Section 4.1.2.A), with detection at the anodic end. During the focusing process an initial voltage of -13 kV was applied over the capillary which was linearly ramped up to -11 kV within the focusing time of 4 min (0.3 kV×min^{-1}). Mobilization was achieved by applying a pressure of 30 mbar to the inlet vial while maintaining the final voltage of -11 kV as indicated in Figure 4-3. Detection wavelength for the analytes was λ = 260 nm and for monitoring the ampholyte gradient

λ = 214 nm, respectively. The current profile started at an initial value of about 5.0 μA and exponentially declined during focusing to a final value of ~0.8 μA.
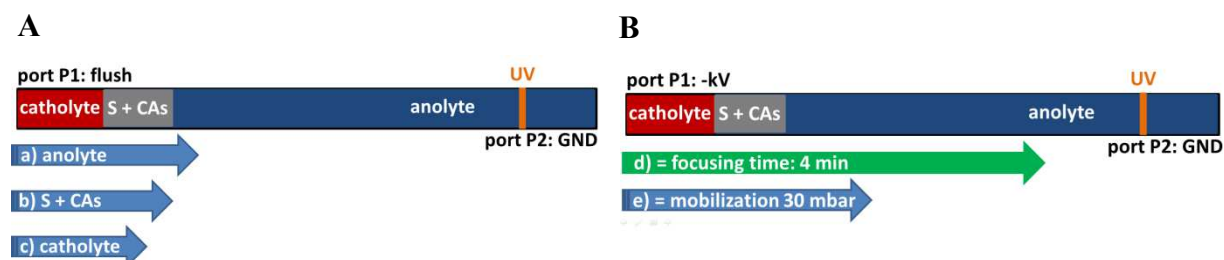
Figure 4-3: Operational scheme for CIEF separation in a single capillary setup: A) Flushing and injection protocol for different solutions into the separation capillary and B) focusing and mobilization scheme for the CIEF separations. During the focusing process an initial voltage of -13 kV linearly ramped to -11 kV within the focusing time. S = sample, GND = ground potential and CAs = carrier ampholytes

4.1.3.F pH gradient positioning experiments

Positioning of the CIEF pH gradient was accomplished filling the capillary with plugs of anolyte and catholyte varying their length. Prior to the sample loading, the capillary was rinsed with anolyte for 3 min at 1 bar. Afterwards, the sample solution (ampholyte-containing protein solution) was injected applying a pressure of 100 mbar for 25 sec. Finally, a plug of catholyte was injected by applying a pressure of 100 mbar for 0, 3, 6, 9, 12 or 15 sec pushing a certain anolyte volume out of the capillary as indicated exemplarily in Figure 4-4.
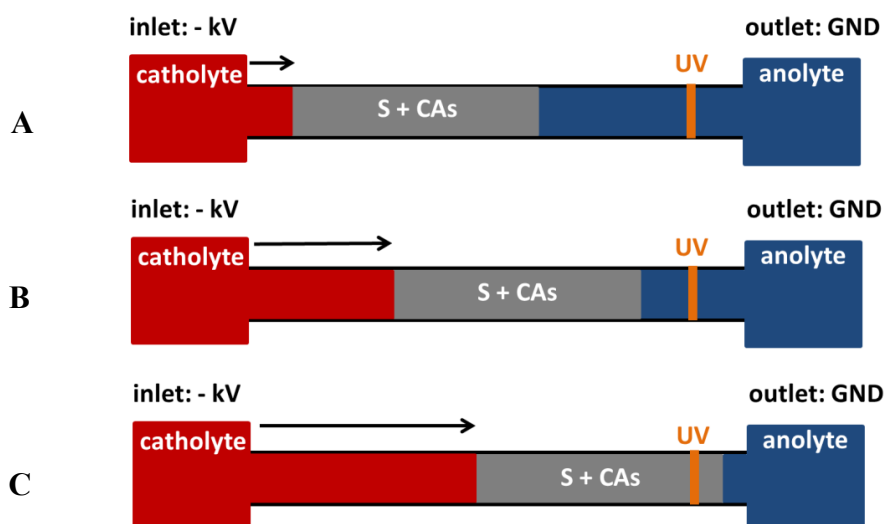
Figure 4-4: Positioning of the pH gradient in the separation capillary via different catholyte plug lengths, exemplarily for 10 (A), 25 (B) and 50% (C) of the total capillary volume.

Therefore, a defined sample solution plug was embedded by an anolyte and a catholyte plug with different lengths depending on the mentioned injection time of the catholyte plug. After each run the capillary was rinsed with aqueous sodium chloride solution 0.9 % w/v and doubly-deionized water for 5 min at 1 bar pressure.

4.1.3.G CIEF simulations parameters

Numerical simulations were performed using a finite element method code using the program PETSc-FEM as platform through a Python interface [Kler, 2013B; Kler, 2011]. The simulations were performed with two systems: a) On a beowulf cluster at CIMEC using five compute nodes with two quad-core Intel Xeon E5420 2.5 GHz processors, 8 GB DDR3–1333 MHz memory, interconnected via a switched Gigabit Ethernet network [Dalcin, 2011]. b) Simulations performed in the working group at the University of Tübingen were performed using an Intel Core i7-4770 3.4 GHz × 8 processor and 31.3 GB memory. Data post-processing was performed with Paraview [Ayachit, 2015], NumPy, SciPy and Matplotlib [van der Walt, 2011]. CIEF simulations were conducted as a whole column detection mode and therefore a mobilization was not included. The focusing process was directly viable inside the separation capillary (x-axis = capillary position of the visualization plots).

4.1.3.H Conditions and parameters for CE-MS separations

All electrophoretic separations were performed using an Agilent 7100 CE system with an integrated UV/Vis detector (Agilent Technologies, Waldbronn, Germany) providing pressure and voltage regimes, injection control, and vial handling. MS detection was achieved using an Agilent 6100 Series Single Quadrupole system (Agilent Technologies, Palo Alto, USA). The CE was coupled to the MS via a coaxial sheath liquid interface from Agilent using an Agilent isocratic pump 1260 (Agilent Technologies, Waldbronn, Germany) for delivering sheath liquid (50:50 (v/v) mixture of water and isopropanol, containing 0.1 % formic acid) at a constant volume rate of 4 µl/min. Nebulizer pressure was set to 0.28 bar and the drying gas was delivered at rate of 4 l/min at a temperature of 300°C. The single quadrupole was used in single ion mode (SIM) or scanning mode (scan). The respective conditions and related m/z values are given in Table 4-1. Separations were conducted in a single capillary with 70 cm length using a sample (injection was performed at 100 mbar for 2 sec) containing model protein and a certain concentration of the broad or a narrow range cut of the ampholyte stock

solution to evaluate the results from the simulations described in Section 4.1.3.G. To suppress protein adsorption a GPTMS coated capillary was used for the experiments. Separations were carried out in acetic (c = 2.3 mol/l) or formic acid (c = 1 mol/l) as the background electrolytes at pH 2.3 and 1.9 respectively.

Table 4-1: Sample conditions and MS detection parameters for the CE-MS separation of the model proteins and the respective ampholytes.

protein parameters			ampholyte parameters		
protein / pI	conc. [mg/ml]	SIM [m/z]	pI range	conc. v/v [%]*	scan [m/z]
RNase A (9.6)	1	978.1	8 - 10.5	2	
myoglobin (7.4)	1	679.0	5 - 8	2	550 to 1350
ß-lactoglobulin (5.1)	1	1080.9	2.5 - 5 and 5 - 8	1 for both pI ranges	

* = volume of the respective ampholyte stock solution in relation to the total volume

4.1.4 Results and discussion – 1D CIEF method development

4.1.4.A Control of EOF - coatings and separation modes

To achieve reproducible and stable CIEF separation conditions it is necessary to use capillary coatings in order to control or eliminate EOF velocity. Despite the usage of neutral coatings a slight residual-EOF is often present (< 1% of initial value) due to residual unshielded silanol groups on the inner surface of the separation capillary. For this reason a dynamic coating is often added to the separation solutions to further reduce the residual-EOF in CIEF assays (Section 4.1.2.B). For the first CIEF measurements a PVA and a GPTMS coated capillary were tested for their applicability regarding the performance of CIEF separations. Here, HEC was added at a concentration of 0.1 % v/v to the sample as well as to the anolyte and catholyte solutions as an additional EOF modifier. The HEC acts as a dynamic coating shielding residual silanol groups, increases the viscosity of the solution and thus, additionally reduces the EOF.

To further evaluate the the influence of the residual-EOF on the analyte detection times, the CIEF setup was performed in the normal and reversed mode by switching the anolyte and catholyte position while applying positive separation potential to the anode for the normal

mode or a negative separation potential to the cathode for the reversed mode. The EOF is always in the direction of the cathode and thus, acts as co-flow to the mobilization pressure in the normal mode and as a counter-flow to the mobilization pressure in the reversed mode.

Higher detection times are due to the discussed cathodic residual-EOF, which is now compensated due to the cathodic mobilization. The separations of the fluorescent marker mix in a single 1D capillary were performed in both separation modes with the inlet side at the anode (normal mode, Figure 4-5) and at the cathode (reversed mode, Figure 4-6). After the focusing time of 4 min the mobilization pressure (30 mbar) was applied at the inlet end of the CIEF pH gradient and the analytes were pushed towards the UV-detector placed at the cathodic or anodic end of the setup, respectively. Both separations were conducted using the same experimental parameters as described in Section 4.1.3.E. Using the normal separation arrangement the basic analytes are detected first, followed by the neutral and the acidic pI markers (Figure 4-5). In the following, both coatings were evaluated in more detail regarding their separation performance in terms of inter-day precision of detection time and peak area, linearity of the pH gradient in the normal and reversed separation mode, as well as overall detection time and peak shapes. With both coatings electropherograms with very similar peak patterns as well as overall separation performances for the respective separation modes were obtained (compare Figure 4-5 and Figure 4-6). For both coatings, baseline separation was achieved for all five pI markers within 15 to 16 min in the normal mode (Figure 4-5) and 18 to 20 min for the reversed mode (Figure 4-6). Symmetric peak shapes were recorded indicating no interaction between the anlytes and the capillary surface. Only the most basic marker (pI = 9.0) showed a slight tailing using the PVA coating in both separation modes, most probably due to adsorption phenomena, leading to a broader non-symmetric peak and therefore a lower peak height. For both coatings in both separation modes four repetitive separations (n = 4) were performed to evaluate repeatability of the separations, compare Table 4-2 and Table 4-3. The PVA and the GPTMS coating showed RSD values for the detection time below 1.6 % and for the peak area below 4.5 %, performed each at one day, indicating the stable performance of both separation systems in the normal mode (Table 4-2). For the reversed separation mode both coatings showed inter-day precisions with RSD values (n=4) for the detection time of below 1.2 % and for the peak area below 2.5 % except the most basic marker for the PVA coating (7.3 %) showing the stable performance of both separation systems (Table 4-3). In the normal mode the detection times are slightly higher (about 30 sec, compare Table 4-2 and Table 4-3) for the PVA coating compared to the

GPTMS coating and vice versa for the reversed mode, due to a lower residual-EOF in the same direction as the pressure-driven flow from the mobilization. The pH gradient length given by the detection time of the first to the last detected analyte ranges from about 9.0 to 15.2 min for the normal mode (length of detection time window 6.2 min) and for the reversed mode from 12.7 to 19.5 min (6.8 min).
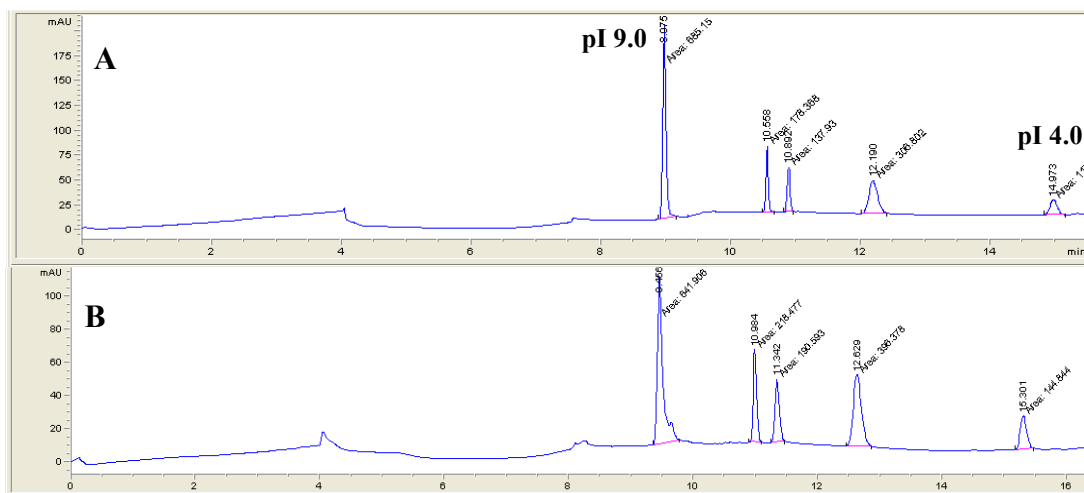
*Figure 4-5: CIEF separation in the normal mode of the pI marker mix with a focusing time of 4 min using **(A)** a GPTMS and **(B)** a PVA coated separation capillary with an ID of 50 μm and a length of 35 cm.*
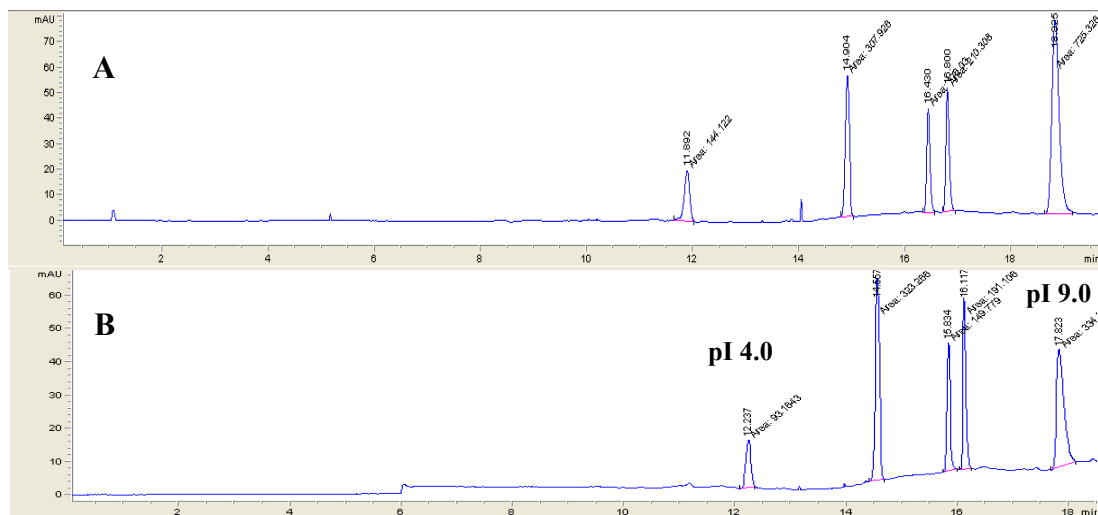
Figure 4-6: CIEF separation in the reversed mode of the pI marker mix with a focusing time of 4 min using (A) a GPTMS and (B) a PVA coated separation capillary with an ID of 50 μm and a length of 35 cm.

Higher detection times for the GPTMS coating are due to higher residual EOF as counter flow to the applied mobilization pressure-driven flow. As a result the whole pH gradient length is increased by about 30 sec from 6.2 to 6.8 min. The increased detection times (of 3 to 4 min) for both coatings comparing the separation carried out in the reversed vs. the

normal mode are due to the residual-EOF, now acting as a counter flow to the mobilization pressure and therefore reducing analyte velocity in the direction of the detector.

Table 4-2: Inter-day precision for CIEF separations (n = 4) of the pI marker mix in the normal mode using the GPTMS and the PVA coating.

GPTMS										
n = 4	pI 4.0		pI 5.5		pI 7.2		pI 7.6		pI 9.0	
	time	area	time	area	time	area	time	area	time	area
mean	15.08	116.63	12.30	307.85	11.01	138.48	10.67	177.65	9.09	697.0
SD	0.10	5.23	0.07	5.62	0.08	1.13	0.08	1.77	0.09	12.66
RSD%	0.66	4.49	0.61	1.82	0.73	0.82	0.76	1.0	0.97	1.82
PVA										
n = 4	pI 4.0		pI 5.5		pI 7.2		pI 7.6		pI 9.0	
	time	area	time	area	time	area	time	area	time	area
mean	15.49	150.38	12.75	403.08	11.43	196.95	11.06	226.00	9.49	671.38
SD	0.24	6.69	0.15	14.53	0.12	7.96	0.11	8.42	0.08	28.51
RSD%	1.57	4.45	1.19	3.60	1.02	4.04	0.99	3.73	0.84	4.25

Table 4-3: Inter-day precision for CIEF separations (n = 4) of the pI marker mix in the reversed mode using the GPTMS and the PVA coating.

GPTMS										
n = 4	pI 4.0		pI 5.5		pI 7.2		pI 7.6		pI 9.0	
	time	area	time	area	time	area	time	area	time	area
mean	12.70	152.50	15.61	375.03	17.17	205.35	17.53	248.05	19.62	801.83
SD	0.15	2.98	0.12	8.92	0.13	3.32	0.13	4.55	0.15	6.84
RSD%	1.21	1.95	0.74	2.38	0.73	1.62	0.73	1.84	0.74	0.85
PVA										
n = 4	pI 4.0		pI 5.5		pI 7.2		pI 7.6		pI 9.0	
	time	area	time	area	time	area	time	area	time	area
mean	12.28	94.38	14.61	325.30	15.86	150.25	16.14	190.80	17.85	343.25
SD	0.06	2.01	0.11	7.00	0.13	4.18	0.14	4.42	0.15	24.84
RSD%	0.52	2.13	0.73	2.15	0.85	2.79	0.88	2.32	0.84	7.24

Another parameter for the quality of CIEF separations is the linearity of the CIEF pH gradient, evaluated by plotting the detection time vs. the respective pI value of each marker. For the pI calibration curves R^2 values of 0.9688 (GPTMS) and 0.9704 (PVA) were achieved in the normal mode and values of 0.9808 (GPTMS) and 0.9803 (PVA) were achieved using the reversed mode as shown in Figure 4-7 and Figure 4-8. Both coatings showed comparable performance regarding the pH gradient linearity in the respective separation mode. In the reversed separation mode using the GPTMS coating the highest R^2 value for the detection time vs. pI value calibration curve was achieved most probably due to the residual-EOF acting as a counter flow to the mobilization pressure, and thus slight EOF differences are

compensated. These values are comparable to data found in the literature [Suratman, 2008; Graf 2005].
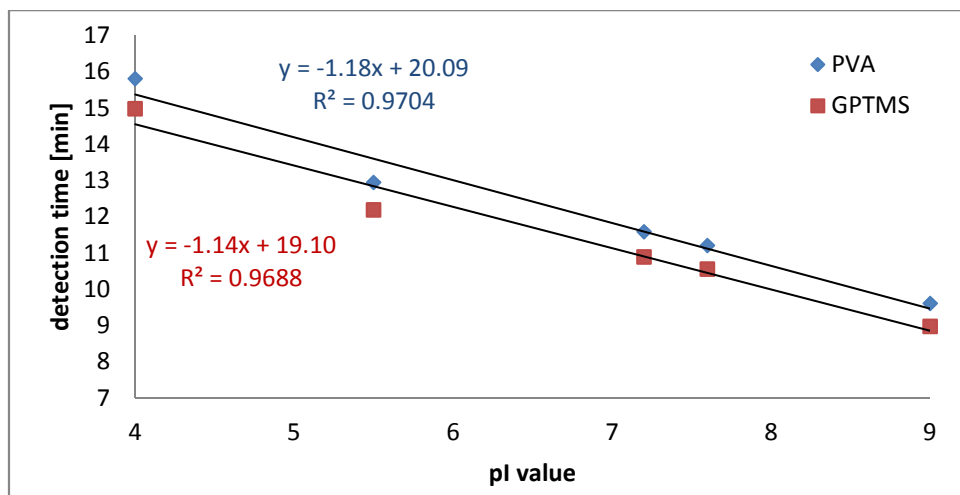
Figure 4-7: Calibration curve for the detection time vs. the respective pI value for the pI markers measured in the normal CIEF separation mode using a GPTMS and a PVA coated capillary.
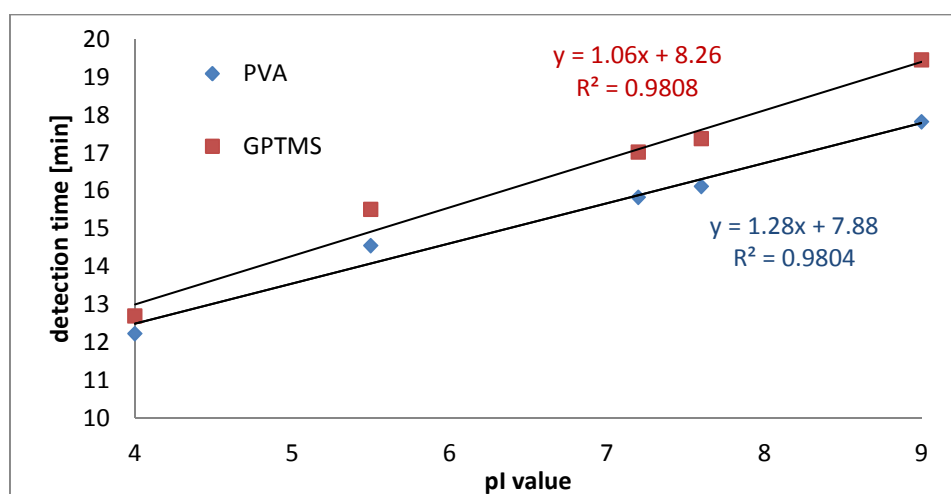
Figure 4-8: Calibration curve for the CIEF detection time vs. the respective pI value for the pI markers measured in the reversed separation mode using a GPTMS and a PVA coated capillary.

Therefore, the systems can be used for the determination of unknown pI values using the parameters of the calibration curve. R^2 values between 0.8 and 0.9 are typical for CIEF separations and due to a non-uniform distribution of the number of different ampholytes as well as their concentration for a window of respective pI values. The exact composition of the commercial ampholyte mixture is proprietary. Besides using the mentioned coating strategy (covalent neutral plus dynamic coating) and the chosen separation mode, the pH gradient linearity can be optimized adjusting the residual-EOF velocities during the separation: A

potential ramp from e.g. 13 to 11 kV can be applied during the focusing time to continuously reduce residual EOF velocity during the focusing step [Shimura, 2002; Chen, 2003]. The mobilization step includes a constant potential e.g. 11 kV to stabilize residual-EOF velocities. Despite the neutral coatings, the EOF is often not eliminated completely as mentioned before. The resulting residual-EOF depends on the local pH and therefore it is different throughout the separation capillary because of the formation of the CIEF pH gradient. In a gradient ranging from pH 2 to pH 11 the resulting local EOF for an uncoated capillary would gradually rise from the acidic to the most basic part of the pH gradient inside the capillary. Therefore, analyte velocity is first increased but then gradually decreases with mobilization time because the basic part of the pH gradient is pushed out of the capillary first in the normal mode. The neutral coatings (e.g. PVA or GPTMS) most often used for CIEF shield the silanol groups leaving the capillary with a neutral surface facing the separation solution inside the capillary. For neutrally coated capillaries the residual-EOF velocity increases with increasing pH. If the capillary is not uniformly coated or the silanol-groups are not shielded effectively, there pH-dependent local EOF differences will occur, disturbing the pH gradient linearity and related analyte detection times and peak widths. Using the reversed arrangement, a counter-EOF is present, where the fluid flow due to the mobilization pressure is much higher compared to that induced by the residual-EOF. Therefore, small changes in pH gradient velocity can be eliminated and a more uniform overall mobilization velocity and thus a higher linearity of the pH gradient and therefore elimination of analyte mobilization velocity changes due to pH dependent differences in local residual-EOF velocities.

4.1.4.B Analysis of model proteins

To further evaluate the performance of both coatings for the CIEF separations, the model proteins ß-lactoglobulin (ß-lact), myoglobin (myo) and ribonuclease A (RNase A) were added to the sample containing the fluorescent marker mix. The pI values are given in Table 4-4. The p-aminobenzoic acid - a small compound not interacting with the capillary surface - was chosen as a reference to monitor the injection parameters and control precision of the CIEF assay. In Figure 4-9, the separation of the model sample mix including the model proteins is shown for both coatings in the reversed separation mode under the same experimental conditions.

Table 4-4: Model analytes including the five pI markers as well as p-aminobenzoic acid and the model proteins ß-lactoglobulin, myoglobin and ribonuclease A.

analyte	pI value	pI [lit]
p-aminobenzoic acid	3.9	[Peakmaster 5.3]
Marker1	4.0	[***]
ß-lactoglobulin	5.1* (4.83 - 5.4)	4.83 - 5.4 [Redweik, 2013]
Marker2	5.5	[***]
Marker3	7.2	[***]
myoglobin	6.8 and 7.4**	[Righetti, 1976]
Marker4	7.6	[***]
Marker5	9.0	[***]
ribonuclease A	9.6	[Liu, 2011]

* = mean of two protein isoforms, * = two protein isoforms, *** = www.sigmaaldrich.com

Comparable to the separations performed with the pI marker mix alone, the resulting peak pattern for both coatings are comparable with slightly lower detection times for the PVA coating due to the lower residual-EOF and thus, lower induced counter flow.
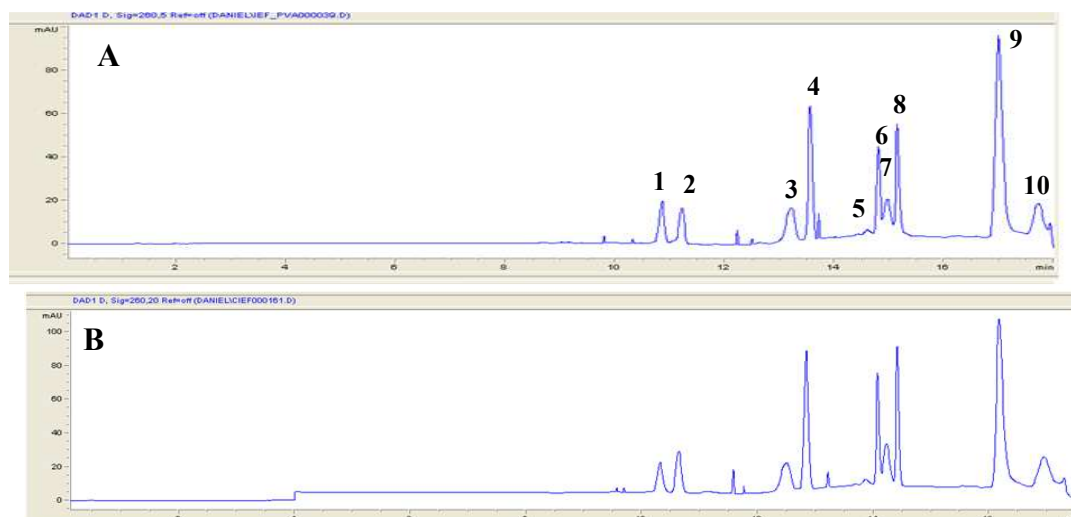
Figure 4-9: CIEF separation in the reversed mode of the pI marker mix and the model proteins with a focusing time of 4 min using (A) a GPTMS and (B) a PVA coated separation capillary with an ID of 50 μm and a length of 35 cm. 1 = p-aminobenzoic acid, 2 = Marker1, 3 = ß-lactoglobulin, 4 = Marker2, 5 = myoglobin (pI 6.8), 6 = Marker3, 7 = myoglobin (pI 7.4), 8 = Marker4, 9 = Marker5, 10 = ribonuclease A

It is noticeable here that the peaks for the proteins appear broader compared to the signals of the markers and the internal standard PABA. This is due to the intact proteins interacting with the capillary surface and therefore broadened signals are detected compared to the small

marker mix compounds as well as different diffusion coefficients of the proteins. Here, for both coatings the isoforms of myoglobin (signals 5 and 7) were baseline separated under the chosen separation conditions, even with the Marker3 (pI 7.0) being focused between them. The isoforms of the ß-lactoglobuin were not separable, but detected in one signal with an average pI value of 5.1.

4.1.4.C Conclusions for the CIEF method development

Both the PVA and the GPTMS coating showed acceptable and comparable separation performance regarding the pI marker mix and the model proteins, therefore, both coatings are applicable for CIEF separations using 0.1 % HEC as an additional modifier. The HEC acts as a dynamic coating shielding residual silanol groups and increases the viscosity of the solution and thus, additionally reduces the residual-EOF in comparison to the plain neutral capillary coating (GPTMS or PVA). The GPTMS coating is cheaper and the coating procedure is less laborious than the covalent PVA coating. The PVA coating on the other hand provides a lower residual EOF velocity due to a better shielding of the silanol groups of the fused silica surface and a shorter coating time of ca. 5 hours compared to ~10 hours for the GPTMS coating. Nevertheless, due to the easy and straight-forward coating protocol, the GPTMS coating can be performed overnight. The main drawback of the PVA coating is the high potential of capillary clogging during the coating procedure due to the used potassium t-butoxide and the high viscosity of the 5 % w/w aqueous PVA flushing solution which was especially critical for the application of the coating in the capillary-chip setup for the 2D separations. Therefore, the GPTMS was chosen as the coating for all following experiments. The reversed CIEF separation mode was preferred due to the increased linearity of the pH gradient. The higher detection times can be optimized using an adapted ratio of the injected anolyte and catholyte plug to position the pH gradient right in front of the detector as discussed in the introduction (Section 4.1.4.D). Thus, the GPTMS coating in combination with 0.1 % HEC as an additional EOF modifier was used for the positioning experiments as described in detail in the following Section.

4.1.4.D Positioning the pH gradient with anolyte and catholyte plugs

Regarding the 2D heart-cutting CIEF/CE-MS setup it is very important to be able to position a specific analyte with a known pI directly within the common intersection of the chip interface, to optimize the transfer from the first to the second separation dimension with

respect to analysis time and precision of the analyte plug transfer. Positioning of the pH gradient inside the separation capillary was accomplished by the injection of catholyte plugs with different lengths applying a pressure of 100 mbar for 0, 3, 6, 9, 12 and 15 sec after anolyte and sample injection. In Figure 4-10 the respective CIEF experiments using 0, 6 and 12 sec of catholyte plug injection are shown exemplarily. Focusing was accomplished after 4 min (see blue star in Figure 4-10).
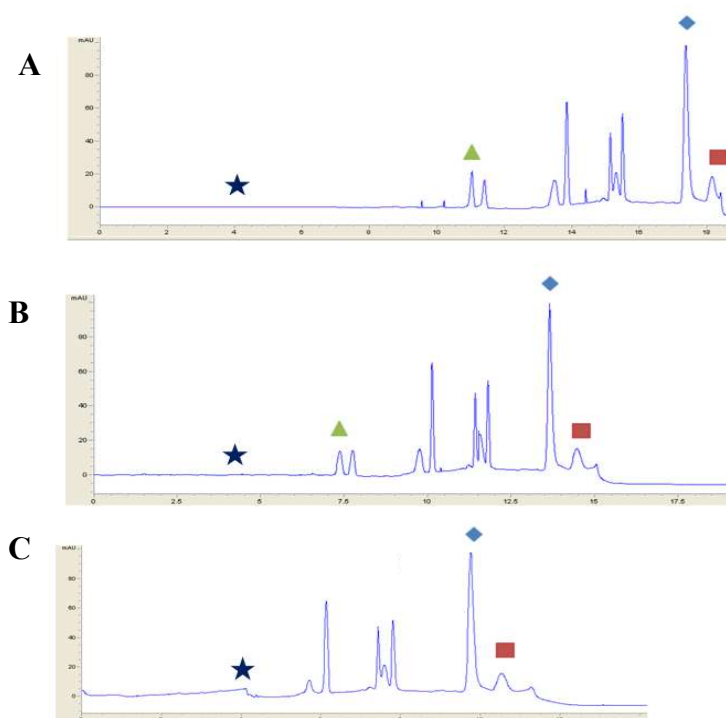
Figure 4-10: Positioning of the pH gradient inside the separation capillary was accomplished by the injection of different catholyte plug lengths applying a pressure of 100 mbar: A) for 0, (B) for 6 and (C) for 12 seconds after anolyte and sample injection. ■ = RNase A ◆ = Marker9, ▲ = PABA and ★ = mobilization time

Figure 4-10 shows that with increased catholyte plug injection time the whole pH gradient is pushed towards the detector prior to voltage application and therefore detection times of the analytes decreased. For a catholyte plug of 12 sec the two most acidic analytes are pushed beyond the detection window into the blind segment of the capillary, and thus, are no longer detected (Figure 4-10C), except when applying the mobilization pressure to the anode (outlet vial of the CE system) for the reversed CIEF separation setup. A linear relationship between the detection time and the injected catholyte plug was detected for all studied analytes as shown exemplarily for the most acidic (p-aminobenzoic acid) and the two most basic analytes, Marker5 and Ribonuclease A as shown in Figure 4-11. Therefore, analyte

positioning can easily be controlled via the length of the injected catholyte plug. If the detection time of an analyte is known it can directly be correlated to a certain position within the separation capillary using a defined catholyte plug length. If only the pI of an analyte is known it can be correlated to the detection time via the pH gradient calibration curve as shown in the previous Section.
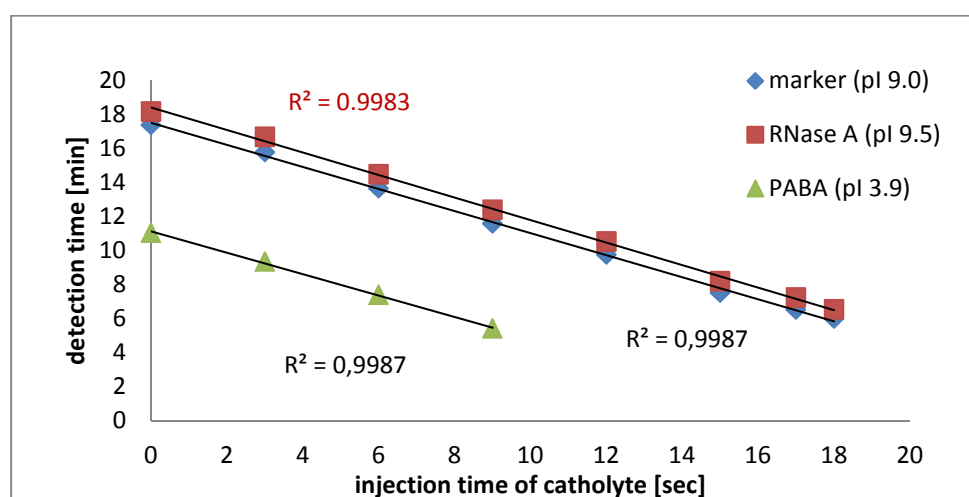
Figure 4-11: Calibration curve for CIEF analyte positioning. Exemplarily, detection time vs. the injection time of the catholyte at 100 mbar is shown for p-aminobenzoic acid (PABA), Marker5 and Ribonuclease A (RNase A)

The position of the analyte in the capillary depends on several CIEF experimental parameters: pI value of the analyte, ampholyte concentration and anolyte/catholyte plug as well as capillary length, thus experimental optimization or characterization can be laborious. In this work numerical modeling was more easily determining the catholyte/anolyte plug lengths necessary to position the analyte in the cutting window.

4.1.4.E Simulations for positioning the CIEF pH gradient

Regarding the 2D heart-cutting CIEF/CE-MS setup it is very important to be able to position a specific analyte with a known pI within the common intersection of the chip interface, as well as to optimize the transfer from the first to the second separation dimension with respect to analysis time and precision of the analyte plug transfer. Dynamic computer simulation software is a very promising tool to further understand and optimize fundamental electrophoretic separation mechanisms and to validate, explain and support the design and optimization of experiments and methodology [Thormann, 1987; Mosher, 1990;

Schwer 1993; Mosher, 2002; Thormann, 2004; Kim, 2006; Thormann, 2006; Thormann, 2007; Thormann, 2009]. Studies from Mosher [Mosher, 1990; Mosher, 2002] and Thormann et al. [Thormann, 2009] showed that all basic electrophoretic separation methods, including zone electrophoresis CZE, isotachophoresis ITP, moving boundary electrophoresis MBE, electrokinetic chromatography EKC, and isoelectric focusing IEF, can be simulated very close to experimental data. For IEF [Thormann, 1987; Mosher, 1990; Mosher, 2002; Thormann, 2004; Thormann, 2006; Thormann, 2007; Thormann, 2009], many examples of a good qualitative agreement between computational predictions and experimental results have confirmed the utility of simulations for predicting separation dynamics, focusing behavior of amphoteric sample components and pH gradient formation and stability. In this work, numerical simulations were performed using a finite element method code published by Kler et al. [Kler, 2013B; Kler, 2011] using the program PETSc-FEM as platform through a Python interface as described in Section 4.1.3.G. CIEF simulations of the positioning of the five pI markers in the separation capillary were successfully performed using 3 different plug lengths of catholyte as the cathodic spacer filling 5, 25 and 55 % of capillary volume with catholyte (Figure 4-12). As for the experimental results (Section 4.1.4.D), a linear relationship was observed between the injected catholyte plug length and the position of the analytes within the capillary. In Figure 4-13 the position of the analyte is shown in dependence of the catholyte plug length exemplarily for the pI Markers 4, 7.2 and 9. After the successful simulation of the CIEF pH gradient positioning the studied model proteins ß-lactoglobulin, myoglobulin and ribonuclease A as well as PABA were integrated into the simulations as described in the following section.
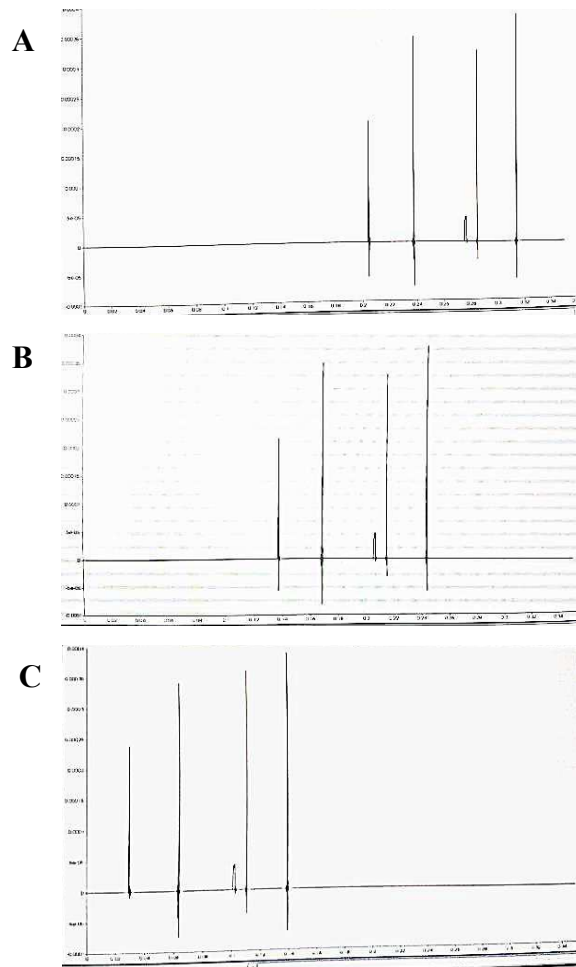
*Figure 4-12: IEF simulation of the positioning of the 5 pI markers. **A**: anolyte = 55%, ampholyte = 40% and catholyte = 5% of capillary volume **B**: anolyte = 35%, ampholyte = 40% and catholyte = 25% of capillary volume and **C**: anolyte = 5%, ampholyte = 40% and catholyte = 55% of capillary volume.*
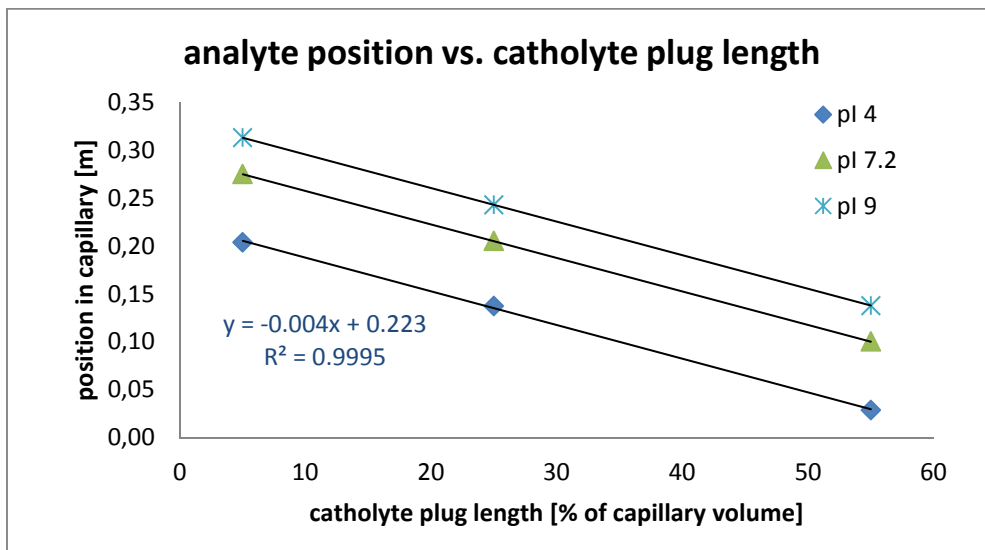
Figure 4-13: Detection time for the model analytes in blue pI Marker4, in green pI marker 7.2 and in light blue marker with pI 4.0 vs. the catholyte plug length 0, 6 and 12 sec. Total capillary length is 35 cm.

4.1.4.F Implementation of model proteins into the CIEF simulations

To support the pH gradient positioning inside the separation capillary as well as to allow a subsequent heart-cutting of a specific CIEF focused analyte followed by a second dimension CE separation, simulations were conducted in cooperation with Pablo A. Kler, CIMEC in the framework of a 3-month DAAD PhD research stay. Figure 4-14 shows the starting point for the simulations. Here, the five pI markers were simulated using the previously developed finite element method code (Section 4.1.3.G).
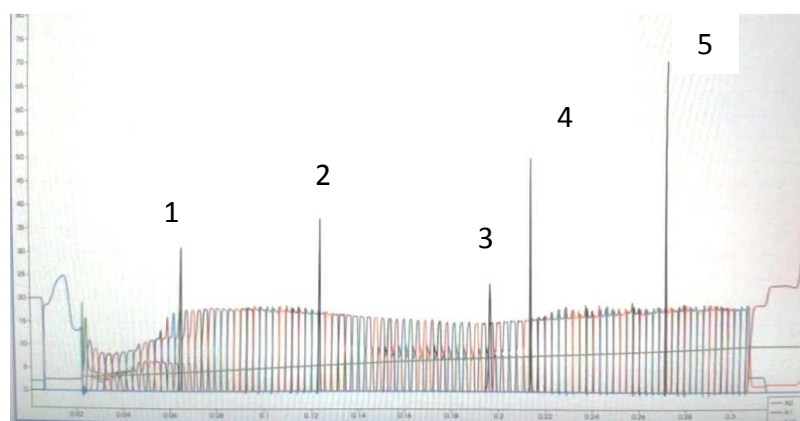
Figure 4-14: *Simulated CIEF electropherogram of five model peptides. For visualization of the analytes the respective detection response was increased in relation to the ampholytes. Black color: five pI markers: pI values of the markers are 1 = 4.0, 2 = 5.5, 3 = 7.2, 4 = 7.6 and 5 = 9.0. The ampholytes are colored.*

Model proteins were included to evaluate the method regarding real protein samples using literature data of the effective electrophoretic mobilities for each protein. Also, the different pK_a values of the proteins were required as input variables for the simulations to perform the calculation of the diffusion coefficients via their actual electromigrative behavior under CIEF separation conditions. For myo the electrophoretic mobility was estimated from the size to mobility ratios of ß-lact [Cannan, 1942] and RNase A [Tanford, 1956], because no literature value was found. Values for p-aminobenzoic acid were taken from Peakmaster 5.3 [Peakmaster 5.3]. In Table 4-5 all parameters are summarized. The simulation program needs 6 pK_a values for the prediction of different pH-dependent charge states of a specific molecule. For example p-aminobenzoic acid with one pK_a value of 4.83, the 5 residual pK_a values are set to generic values smaller than 1 (e.g. -1) and higher than 14 (e.g. 16) and thus, set outside of the pH range for CIEF. Regarding a protein, its respective pI value was used as the starting point and the residual 5 pK_a values were estimated at the beginning using increment steps of ± 1.25, starting from the initial pI value given in Table 4-5.

Table 4-5: *Values for electrophoretic mobility and pK$_a$ for the analytes p-aminobenzoic acid, ß-lactoglobulin, myoglobin and Ribonuclease A.*

analyte	effective electrophoretic mobility ($\times 10^{-8}$ V/m$^2\times$s)	literature	pK$_a$ values	analyte mass in kDa
p-aminobenzoic acid	3.16	[Peakmaster 5.3]	4.85	0.137
ß-lactoglobulin	1.74	[Cannan, 1942]	5.1[#] +/- 1.25	18.4
myoglobin	2.0*	n.a.	7.4[#] +/- 1.25	17.1
ribonuclease A	3.0	[Tanford, 1956]	9.5[#] +/- 1.25	13.7

* estimated from size to mobility ratio of known protein masses in kDa and mobilities for ß-lactoglobulin and ribonuclease A. [#]= pI values were used for pK$_a$ calculation, n.a. = not available

Figure 4-15A shows the first CIEF simulation of the chosen analytes to be compared to the experimental results given in Figure 4-9. In the simulation the proteins were not focused in the chosen time window of 300 sec in contrast to the experimental results. The double-peaks observed in the simulation results for the proteins ß-lact and RNase A are due to the fact that they are not yet fully focused under the chosen simulation parameters. Therefore, the features of the proteins were adapted to fit the experimental focusing time of 300 sec, which was obtained from the CIEF experimental separations by adjusting the pK$_a$ value differences from 2 to 1.25. The pK$_a$ differences proved to be one of the major parameters influencing the focusing efficiency of the analytes regarding the simulations. As a result, the electropherogram shown in Figure 4-15B was obtained. Here, the signal-to-noise-ratio (SNR) of the analytes, especially the two markers (4 and 5), were too low and the overall data points for describing the peaks were too few for the simulation of 2D heart-cutting (see Figure 4-15). A minimum of 20 data points is required to describe a simulated peak to reduce noise for the simulation of the second CE separation. Therefore, the data points were increased from 2000 to 4000 and the simulated ampholytes from 100 to 150, resulting in a 4 times longer simulation time. The simulation time/cost thereby increased from 9 to 36 hours. As a result, a proper CIEF simulation with a very high SNR and sufficient data points was achieved and is given in Figure 4-15C. This file was used for all following CIEF, heart-cutting and CE separation simulations as discussed in Section 4.2.1.
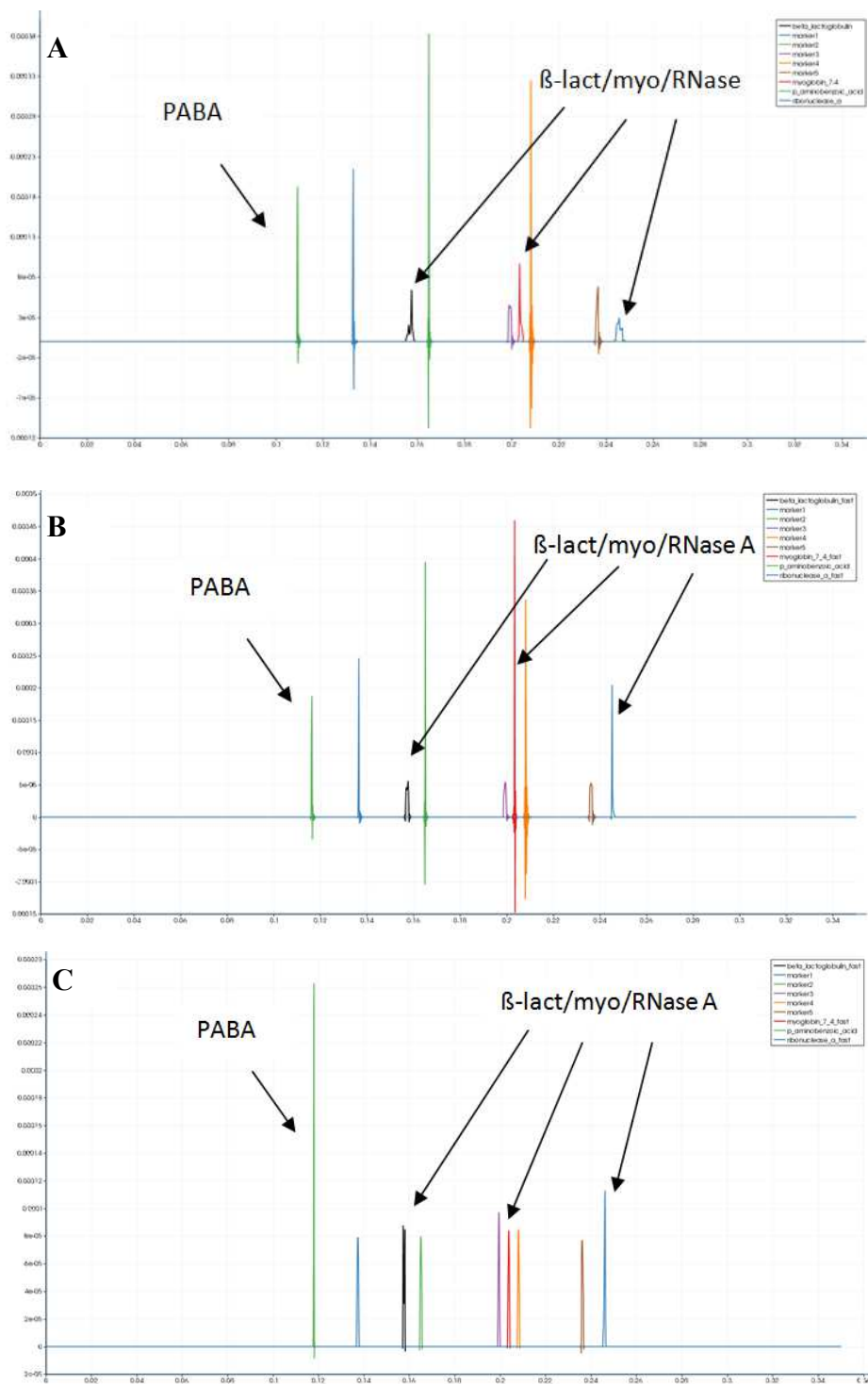
Figure 4-15: Simulation of 9 model analytes left to right: p-aminobenzoic acid (p-aminobenzacid, pI = 3.9), Marker1 (pI = 4.0), ß-lactoglobulin (ß-Lact, pI = 5.1), Marker2 (pI = 5.5), Marker3 (pI = 7.2), Myoglobin (Myo, pI = 7.4), Marker4 (pI = 7.6), Marker5 (pI = 9.0) and Ribonuclease A (RNase, pI = 9.5). A) The pKₐ value differences of the analytes were set initially to ±2 with 2000 data points and 100 ampholytes. B) The pKₐ value differences were set to 1.25 with 2000 data points and 100 ampholytes. C) The pKₐ value differences were set to ±1.25 with 4000 data points and 150 ampholytes.

4.1.4.G CIEF positioning tool "Focus"

To support the cutting process for the 2D CIEF/CE separation assay a CIEF positioning tool called "Focus" was realized in cooperation with Pablo A. Kler and Gabriel Gerlero from the CIMEC, Santa Fe, Argentina as shown in Figure 4-16. The linear relationship of the peak position inside the capillary on the injected catholyte plug length was used in both experiments and simulations as the basis for a software-based positioning tool including the model proteins. It takes into account the capillary length and inner diameter, concentrations of anolyte, catholyte as well as anodic and cathodic spacers (if used), pH range of the ampholyte stock solution and the injection parameters (pressure and time) for the injected sample, anolyte and catholyte plug. Using a linear calculation approach, and excluding the carrier ampholytes from the simulations, simulation time was reduced from 36 hours to several seconds. The peak pattern of the model sample was simulated successfully. Further evaluation of the tool will include the comparison of experimental and simulated positioning experiments, to evaluate its usability to simulate real life CIEF analyte positioning.
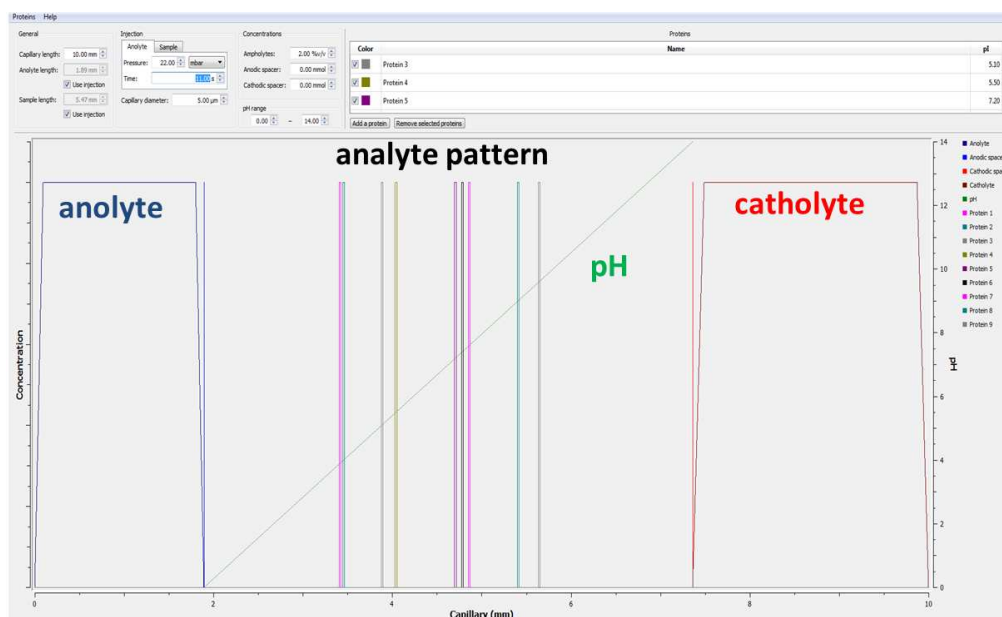
Figure 4-16: Simulation of CIEF analyte positioning of the pI markers and the model proteins within the capillary using the CIEF positioning tool "Focus".

4.1.4.H Optimized choice of the acids and bases for anolyte and catholyte

First CIEF separations were performed using 20 mmol/l phosphoric acid as anolyte and 20 mmol/l sodium hydroxide as catholyte. Using the CIEF assay in the reversed setup the mobilization is done by introducing catholyte at the cathodic end of the capillary to push the pH gradient towards the detector. Therefore, an increasing portion of the capillary volume

and thus the respective coating gets into contact with the catholyte with progressing mobilization time. In order to avoid impairment of the coating by strongly basic solutions (here, especially strong bases like sodium hydroxide) the catholyte was switched from 20 mmol/l NaOH to 250 mmol/l triethylamine (TEA) to match the resulting pH, however using a cation of lower pK_b value as shown in Table 4-6. For the anolyte, which was used as BGE in the second dimension CE separation, volatile acidic and formic acid at low pH (see Table 4-6) were preferred over H_3PO_4 for a higher MS compatibility. As no differences in the focusing efficiency were detected (data not shown) for the different catholytes and anolytes, 250 mmol/l triethylamine was used as catholyte and 2.3 mol/l acidic or 1.0 mol/l formic acid as anolyte for CIEF separations coupled to MS detection.

Table 4-6: Overview of the catholyte and anolyte solutions used for the CIEF separations.

catholyte	pK_a/pK_b values	concentration [mmol/l]	pH
triethylamine	10.86	250	12.12
sodium hydroxyde	13.70	20	12.23
anolyte			
phosphoric acid	12.67; 7.21; 2.16	20	2.07
acetic acid	4.76	2300	2.20
formic acid	3.75	1000	1.88

4.1.5 Summary and conclusions

The PVA and the GPTMS coating in combination with 0.1 % HEC proved to be suitable coatings for CIEF separation assays. RSD values (n = 4) below 1.6 % for the detection time and below 4.5 % for the peak area in the normal separation mode; but below 1.2 % and 2.5 % (except the most basic marker for the PVA coating with 7.3 %) for the reversed separation mode. The PVA coating resulted in a slightly lower overall EOF and thus an enhanced (normal mode) or decreased (reversed mode) width of the pH gradient compared to the GPTMS coating. The increased detection times (3 to 4 min) for both coatings in the reversed vs. the normal mode are due to the residual-EOF, evoking a counter flow to the mobilization pressure retarding analytes. Using the EOF as counter flow to the presuure-driven flow, a

better linearity of the pH gradient (detection time vs. pI) was achieved due to the elimination of pH induced EOF velocity differences and literature values could be reached with R^2 values of 0.9808 (GPTMS) and 0.9803 (PVA). Model proteins ß-lactoglobulin, myoglobin and ribonuclease A were successfully separated using the presented CIEF method using GPTMS and PVA as coating. Due to the well-known increased tendency of the proteins to interact with the separation capillary (and applied coating), increased peak widths (20 to 30 sec) compared to the separated pI peptide markers mix (10 to 15 sec peak widths) were observed. GPTMS proved advantageous for two dimensional CIEF assays due to its higher stability, ease of the coating protocol and lower risk for capillary clogging compared to the PVA coating.

Positioning a selected CIEF focused analyte in the heart-cutting section of the setup is possible injecting different catholyte plug lengths prior to separation voltage application. The experimental results demonstrated a linear relationship between the injected catholyte plug length and the detected analyte position inside the capillary; they were confirmed using numerical simulations. Model proteins and PABA were successfully implemented into the simulation model using respective electrophoretic mobilities, pK_a and pI values and deduced pK_a value differences representing different protein charge states. Regarding focusing efficiency of the proteins during the simulations the differences between the pK_a values of each charge state were found to be the most important parameter regarding focusing speed. The focusing behavior was successfully adapted to experimental data by choosing a pK_a value step of 1.25 for the proteins.

Combining experimental and simulated CIEF separation data a first version of a positioning tool called "Focus" was realized in cooperation with the working group of Pablo A. Kler during a study stay in Argentina to support CIEF analyte positioning and thus the cutting process for the 2D CIEF/CE separation assay. Here, different separation parameters like pI values, ampholyte and sample concentrations and capillary lengths were implemented into the tool as user-set parameters. Due to using a linear calculation approach, as well as not directly simulating the focusing of carrier ampholytes the calculation time was strongly reduced. First applications showed its ability to simulate protein positioning within the capillary.

Using a 250 mmol/l concentration of TEA instead of a 20 mmol/l concentrated NaOH solution as the catholyte, nearly the same pH and ionic strength were obtained with the benefit of a better compatibility of the basic solution with the neutral GPTMS coating.

Switching the anolyte from non-volatile phosphoric to volatile acidic and formic acid was successful and ensured compatibility of the anolyte with MS detection, enabeling its use as the 2nd dimension background electrolyte.

4.2 1D capillary electrophoresis method development

Following the successful simulations regarding CIEF separations and related pH gradient positioning, simulations were used to optimize the second CE separation dimension regarding type of background electrolyte and its pH to achieve the separation of the protein from the surrounding ampholytes. The second CE separation dimension was simulated in a one dimensional separation capillary using the appropriate section of the CIEF focused pH gradient including the protein of interest with its surrounding ampholytes as the sample. This was realized by defining a cutting window in the simulation representing the common intersection of the microfluidic glass chip interface. In the following simulations and respective experimental data are discussed in more detail.

4.2.1 Optimization of CE-MS separations using simulations

A cutting window comparable to the common intersection on the chip interface was selected inside the CIEF simulation data. It defined the sample volume for the second CE separation step with specific dimensions given for each cutting example A, B and C in detail, as shown in Figure 4-17. As background electrolyte for the CE simulations 1 mol/l acetic acid (pH 2.3) was used with an adaptation to 10000 points for the spatial resolution of the separation capillary in the simulation model. Separation voltage was +13 kV, if not stated otherwise.
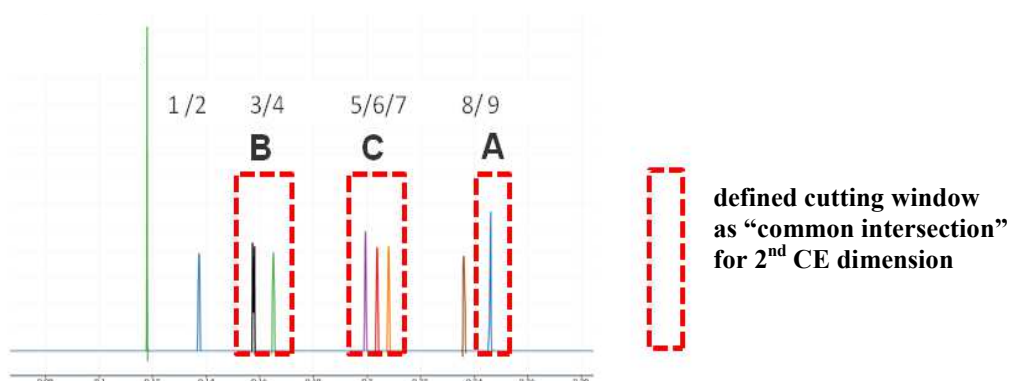
*Figure 4-17: Different cutting windows A, B and C of the simulated IEF pH gradient with proteins/markers as sample volume for the second separation dimension. **A:** RNase A, **B:** ß-lact and Marker2 and **C:** myo, Marker3 and Marker4 with the respective surrounding ampholytes.*

4.2.1.A Cutting window A: RNase A and ampholytes

The heart-cutting of the RNase A was done with 11 surrounding ampholytes from the CIEF simulation file (ampholytes not shown) via the simulated common intersection of the chip interface as shown in Figure 4-17, cutting window A. The time step t = 0 in Figure 4-18A shows the initial conditions of the second CE separation. The heart-cutting window including RNase A and some ampholytes is used as sample plug for the second CE dimension. At time step t = 30 sec after voltage application, the protein already moved to the boundary of the ampholyte stack and at t = 90 sec RNase A is separated from the ampholytes in the simulated CE separation. Here, only 6 of the 11 ampholytes are still visable due to the noise limit set in the simulation algorithm. Accordingly, in the following simulations the filter algorithm was adapted (data not shown). The simulation clearly shows that the basic protein RNase A (pI 9.5) can be separated from the surrounding ampholytes at pH 2.3 rather quickly due to high differences in electrophoretic mobilities based on the higher chargeability of the basic protein in the acidic environment compared to the ampholytes.

Figure 4-18: CIEF parameters are given in Figure 4-15C. An ampholyte stack as heart-cut from CIEF separation forms the sample plug of the 2nd dimension CE separation. CE separation of RNaseA from 11 surrounding ampholytes in 1 mol/l acetic acid as background electrolyte (pH = 2.3). A) Initial conditions of the CE simulation t=0 with cutting window A (Figure 4-17), B) Time step 1 represents 30 sec of simulated CE separation time C) 90 sec of simulated CE separation.

4.2.1.B Cutting window B: ß-lactoglobulin and ampholytes

A) Separation under acidic conditions

The heart-cutting of ß-lact and Marker2 in the cutting window B was conducted with 19 surrounding ampholytes from the CIEF simulation file in Figure 4-17 via the simulated common intersection of the chip interface. The time steps t = 0 and t = 300 sec are shown in Figure 4-19.

Figure 4-19: CIEF parameters are given in Figure 4-15C. An ampholyte stack as heart-cut from CIEF separation forms the sample plug of the 2nd dimension CE separation. CE separation of ß-lact and Marker2 with 19 surrounding ampholytes in 1mol/l acetic acid as background electrolyte (pH = 2.3). A) Initial conditions of the CE simulation t=0, B) Final condition after t = 300 sec of simulated CE separation time.

In addition to ß-lact, Marker2 was included in the cut to demonstrate its ampholyte-like migration behavior. Figure 4-19B shows the end of the simulation after 300 sec. Here, protein and Marker2 are still co-migrating with the ampholyte stack. The simulation indicates, that acidic conditions are not suitable to separate the acidic protein (pI 5.1) and Marker2 (pI 5.5) indicating a further need for optimization. Compared to the results in Section 4.2.1.A it can be assumed that at pH 2.3 the charge excess and therefore the effective electrophoretic

mobility of the protein and Marker2 are not sufficiently different to the smaller ampholytes. As a result the simulation was changed to a basic BGE for the CE separation system was changed to a basic background electrolyte.

B) Separation under basic conditions

For a better resolution the CE buffer system was switched from acidic (1 mol/l acetic acid, pH 2.3) to basic (1 mol/l ammonium hydroxide, pH 11.6) conditions keeping all other simulation parameters. With a basic buffer system for the second CE separation dimension ß-lact was now successfully separated from Marker2 and the surrounding ampholytes as shown in Figure 4-20A-C. Due to the basic pH value, ß-lact obtains an excess negative charge compared to the ampholytes and, thus, a high effective electrophoretic mobility and migrates faster than the ampholyte stack. After exiting the ampholyte stack the protein peak shows a slight shoulder (see Figure 4-20B), which diminishes upon simulated separation time due to refocusing but with a slight overall band broadening (see Figure 4-20C). With an increase of simulated capillary length the peak shape could be further optimized.
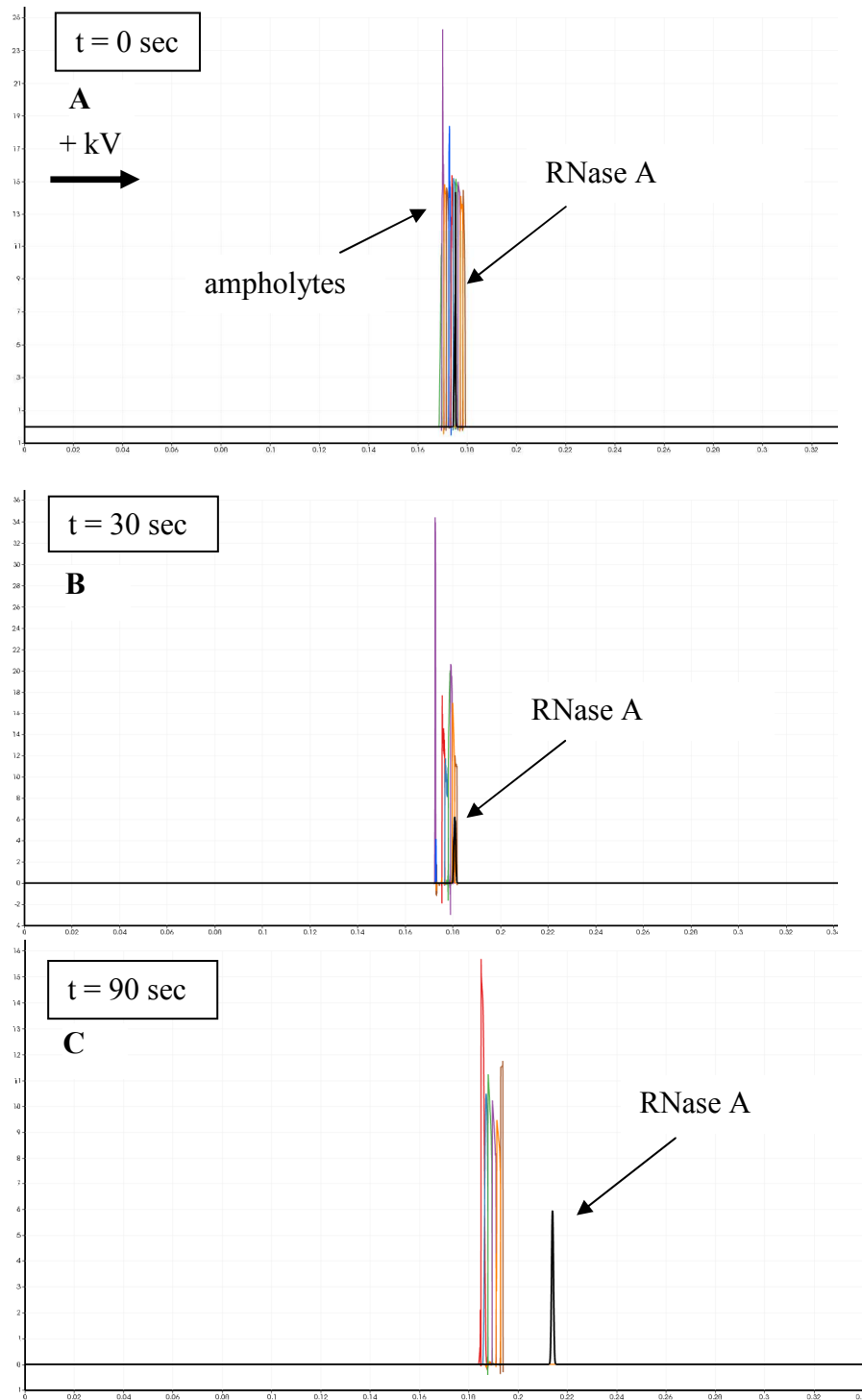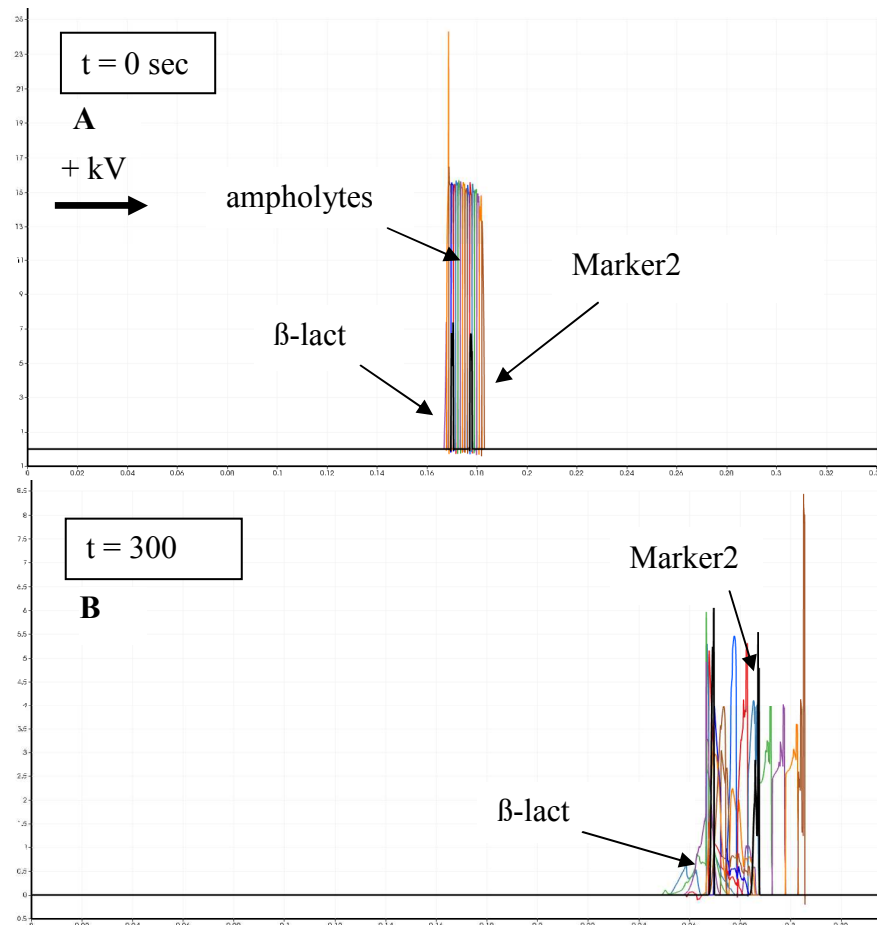
Figure 4-20: CIEF parameters are given in Figure 4-15C. An ampholyte stack as heart-cut from CIEF separation forms the sample plug of the 2ⁿᵈ dimension CE separation. CE separation of ß-lact with 19 surrounding ampholytes in 1 mol/l ammonium hydroxide as background electrolyte (pH = 11.6). A) Initial conditions of the CE simulation t=0, B) Time step t =100 sec of simulated CE separation C) t = 300 sec of simulated CE separation.

4.2.1.C Cutting window C: myoglobin and ampholytes

In the third cutting experiment (cutting window C in Figure 4-17) myo (pI 7.4) was heart-cut together with the Markers3 and Marker4 with 14 surrounding ampholytes from the CIEF simulation file via the simulated common intersection of the chip interface. Upon application of the separation voltage (see Figure 4-21A) myo overtakes the Marker4 due to its higher effective electrophoretic mobility (high positive charge) at pH 2.3 compared to ampholytes and markers. After the short co-migration of myo and Marker4 (Figure 4-21B) during the separation process, both peaks show a slightly impared peak shape: tailing of Marker4 and fronting of myoglobin (see Figure 4-21C). After ca. 200 sec of the simulated CE separation the myoglobin peak appears symmetrical and well separated from the markers as well as the ampholyte stack as shown in Figure 4-21D.

4.2.1.D Conclusions on simulations of CE separation

Simulated CE separations showed that the CIEF focused ampholytes migrate as a bulk zone most probably due to similar charge to mass ratios of the respective ampholytes. The basic protein ribonuclease A and the protein myoglobin being neutral at intermediate pH were separable from their surrounding ampholytes using 1 mol/l acidic acid as background electrolyte. In contrast, the acidic protein ß-lactoglobin was only separable under basic conditions with 1 mol/l ammonium hydroxide as BGE. The results indicate that the pH value of the background electrolyte of the second CE separation dimension should be as different as possible from the pI of the analyzed protein, to create a highly charged analyte protein with a clearly higher effective electrophoretic mobility compared to the markers and ampholytes and therefore achieve the separation and undisturbed MS detection of the protein.
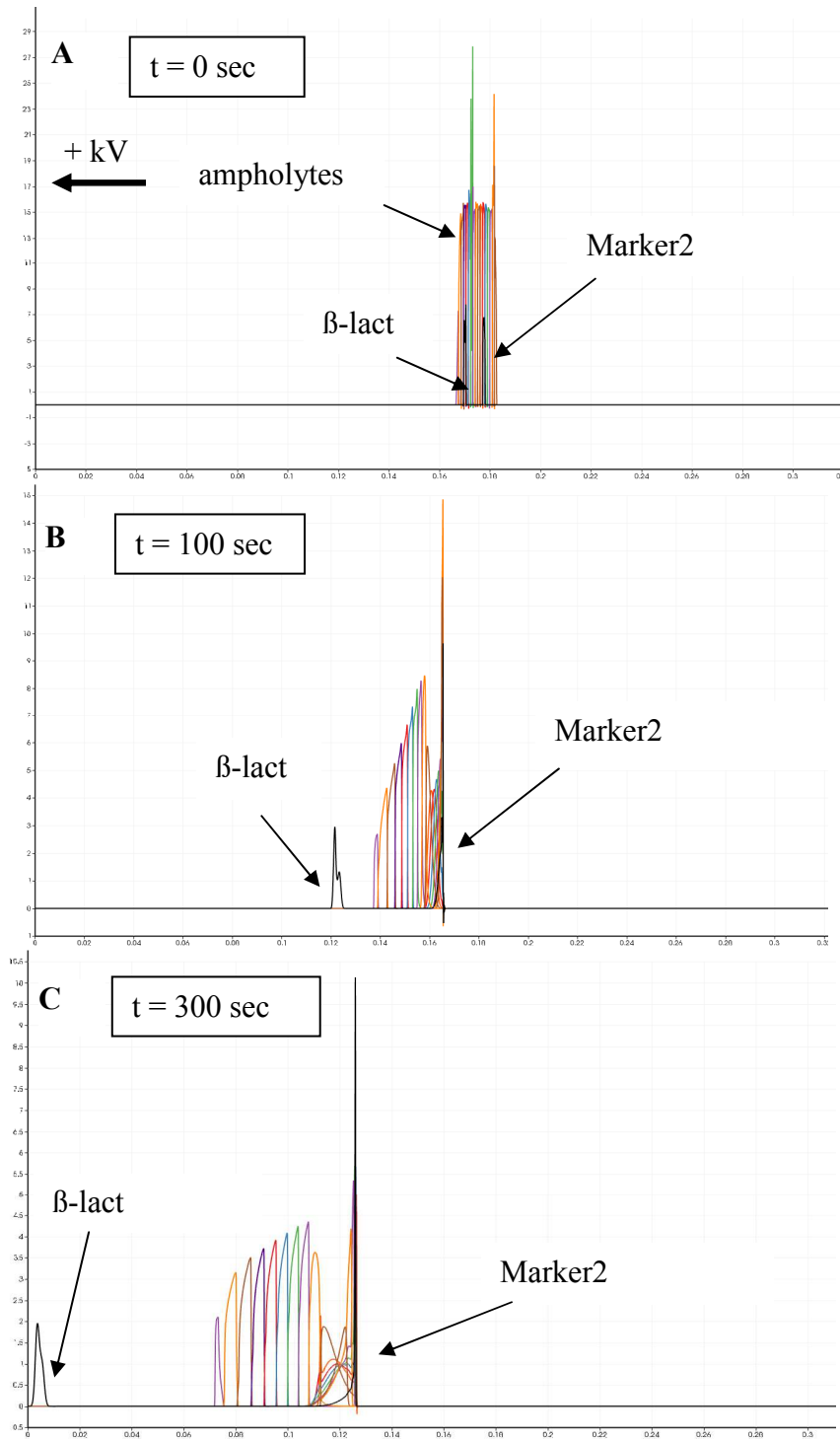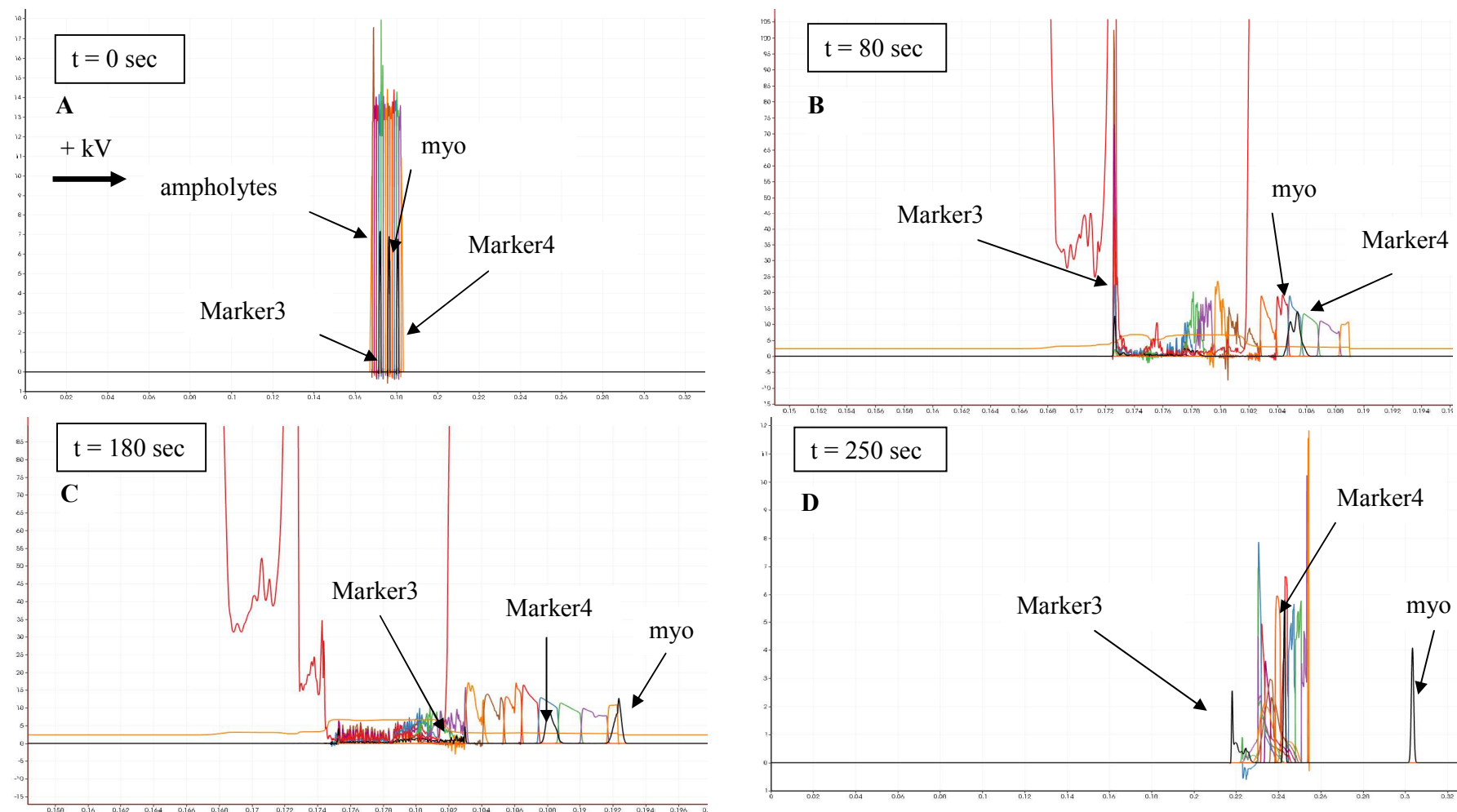
Figure 4-21: CIEF parameters are given in Figure 4-15C. An ampholyte stack as heart-cut from CIEF separation forms the sample plug of the 2nd dimension CE separation. CE separation of the myo, Marker3 and Marker4 with 14 surrounding ampholytes in 1 mol/l acetic acid as background electrolyte (pH = 2.3). A) Initial conditions of the CE simulation t=0, B) Time step 1 at t = 80 sec (zoomed), C) Situation after 180 sec of simulated CE separation (zoomed) and D) 250 sec of the simulated CE separation.

4.2.2 Optimization of experimental CE-MS conditions

The simulations of the second CE separation dimension were compared to experimental CE-MS separations of the respective model proteins RNase A, myoglobin and ß-lactoglobulin and the surrounding ampholytes. Simulations indicated that a lower pK_a value, and thus pH, of the acid used as the background electrolyte for the CE separation increased the positive charge of the protein to a larger extent than the ampholytes resulting in a higher resolution. To study this effect the separations were carried out in acetic and formic acid as the background electrolytes at pH 2.3 and 1.9, respectively. To evaluate the precision of the CE-MS separations three repetitive runs were conducted exemplarily for a sample containing 2.0 % of the broad range ampholyte cut with a pI value range from 3 to 10 and myoglobin as the model protein using 1 mol/l acetic acid (pH 2.3) as the separation buffer. There is no possibility to study the separation of a narrow pH gradient cut and a model protein as present for the simulations when using a 2D heart-cutting setup, therefore, this workaround was chosen. Results are shown in Figure 4-22. Comparable to the simulations the ampholytes (mass range from to 550 to 1350 m/z) migrated as a broad bulk zone with a peak broadness of ca. 4 min, which is expected due to the high compound diversity of using the full pI-range ampholyte mixture. The peak of myoglobin was ca. 40 sec broad and showed a slight tailing under the chosen separation conditions. For the respective runs (n = 3) RSD values for the detection time and the peak area for the ampholyte stack and the myoglobin peak were below 2.0 % and below 4.0 %, respectively. In contrast to the simulations, myoglobin was not separated from the ampholytes under the chosen experimental conditions.
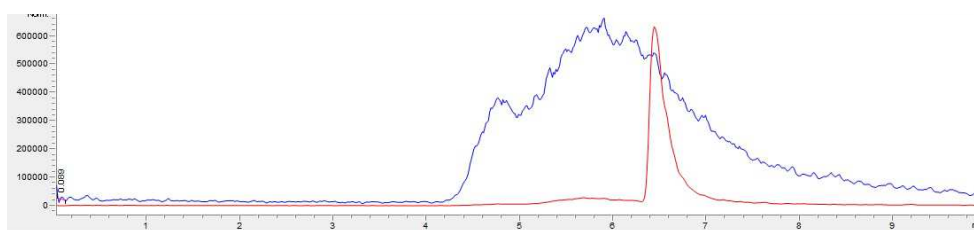
Figure 4-22: Exemplary measurement for the separation of myglobin and 2 % ampholyte stock solution pI 3 - 10 by CE-MS in 1 mol/l acetic acid. The ampholytes signal is given in blue (scan 550 to 1350 m/z) and the myglobin signal in red (SIM 679 m/z).

For a further evaluation, samples of the model proteins ribonuclease A and ß-lactoglobulin were spiked with ampholyte stock solutions matching the pI range as shown in Table 4-1 more closely representing the respective surrounding ampholytes which would be heart-cut in a 2D experiment and were analyzed via CE-MS. In Figure 4-23 the CE-MS separations are

shown for the two different background electrolytes (acetic and formic acid). With formic acid as low pH-BGE a better separation of the protein from the ampholyte stack was achieved for all protein/ampholyte samples. In addition, the ampholyte stack appeared narrower, most probably due to a more uniform charge to mass ratio of the ampholyte components. Both the stack as well as the protein peaks were shifted to shorter detection times due to a higher overall charge and therefore increased effective electrophoretic mobility. Using formic acid, near-baseline separation of the neutral and basic protein RNase A and myo (Figure 4-23B and C) from the respective ampholytes was achieved comparable to the results from simulations. ß-Lactoglobulin was not separable from the ampholytes using an acidic background electrolyte (Figure 4-23C).
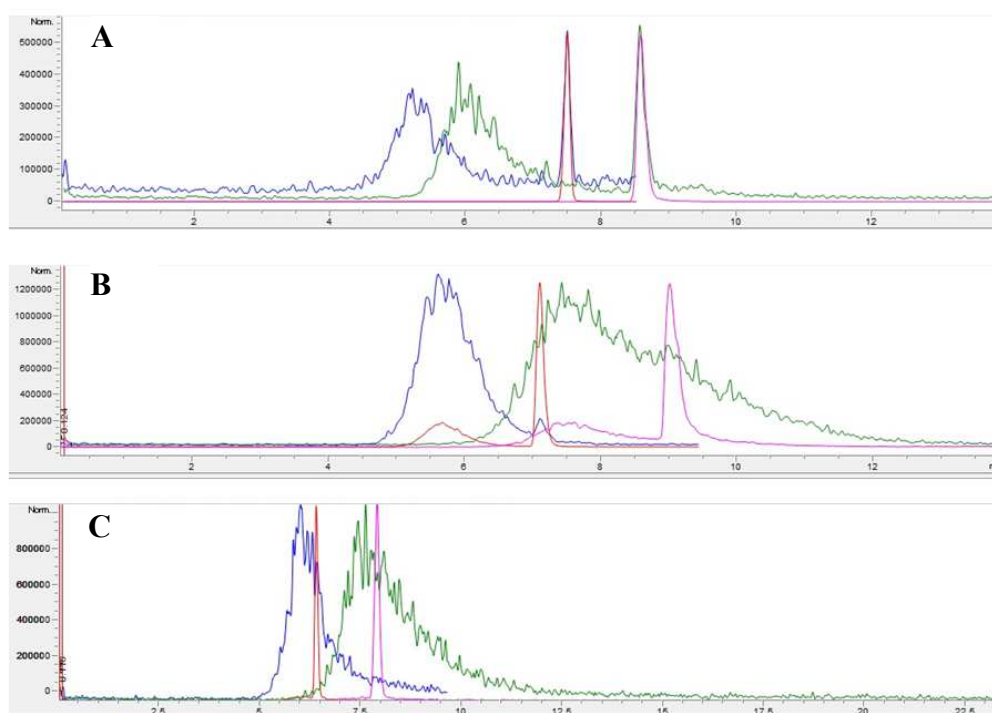
Figure 4-23: CE-MS separation in formic (FA) and acetic acid (HAc) of proteins (red = FA and pink = HAc) and ampholytes (blue = FA and green = HAc recorded in the MS scan mode from 550 to 1350 m/z): A) RNase A (SIM 978.1 m/z) in 2% ampholyte stock solution pI 8 – 10.5, B) myoglobin (SIM 679 m/z) and 2% ampholyte stock solution pI 5 – 8 and C) ß-lactoglobulin (SIM 1080.9 m/z) and 1% ampholyte stock solution pI 5 – 8 and 1 % ampholyte stock solution pI 2.5 – 5. The scan and SIM mode were applied in parallel with 50:50 recording time.

The results from the simulation and experimental data clearly show that the separation of the protein and the respective ampholyte stack is maximized for pH values opposite to the pI of the protein. Thus, acidic conditions are most suitable for basic proteins and basic conditions for acidic proteins. For the neutral protein myoglobin a separation was achieved using formic acid at pH 1.2. However, simulations and experiments showed a change in migration order of

the protein and ampholytes. Comparing the experimental and the simulated mobilities of both the proteins and the ampholytes (data not shown) it was clear to see that the protein mobilites are simulated according to their experimental migration behavior. That was not true for the ampholyte stack, where the experimental data showed higher mobilities compared to the simulations. This is most probably due to the fact, that the ampholyte mobility is simulated with only one amphoteric charge state via one cationic and on anionic functional group not as polyamines/polycarboxylic acids, resulting in singly charged compounds having a lower mobility than the proteins. Here, the simulation model has to be optimized for the ampholytes to adequately reflect their experimental behavior. Basic CE-MS separation conditions remain to be compared to the simulations.

4.2.3 Conclusions

Simulated and experimental CE separations showed that the ampholytes migrate as a bulk zone under CE separation conditions, most probably due to similar charge to mass ratios of the respective compounds. Stable CE experimental conditions (n = 3) with RSD values for the detection times below 2 % and for the peak area below 4 % were achieved using a GPTMS coated capillary. In contrast to the simulations, myoglobin was not separated from the ampholytes under the chosen experimental conditions using acetic acid. Here, simulations indicate a better separation by choosing an acidic background electrolyte with a lower pK_a and thus pH value. Using formic acid instead of acetic acid as the background electrolyte the ampholyte stack appeared narrower, most probably due to a more uniform charge to mass ratio of the ampholyte components and both the stack as well as the protein are shifted to shorter detection times with a higher charge and therefore increased mobility due to decreased pH value. Myoglobin and ribonuclease A were well separated from the respective ampholytes using formic acid BGE. However, the acidic protein ß-lactoglobulin was not separated from the ampholytes using an acidic background electrolyte. As a conclusion, for a good separation of the pH value of the background electrolyte of the second CE separation dimension should be as different as possible from the pI of the analyzed protein to create a highly charged protein compared to the respective markers and ampholytes. Overall, suitable conditions for 2nd dimension CE-MS were obtained.

5   Coupling of CIEF-LED-IF/CE-MS

5.1   Abstract

Direct coupling of capillary isoelectric focusing (CIEF) to mass spectrometry (MS) is not feasible for protein analysis due to the suppression of the analyte signal by the carrier ampholytes. With respect to the coupling of CIEF to MS several solutions have been presented to suppress, eliminate or separate proteins from ampholytes prior to MS detection: Two dimensional electrophoretic and/or chromatographic separation setups are increasingly used. Monitoring the analyte during the transfer step from the first to the second dimension in multidimensional electrophoretic separations is crucial to determine and control the proper time point for sample band transfer and thus to avoid band broadening or unwanted splitting of the sample band and sample loss. In this study, a spatially-resolved intermediate on-chip fluorescence detection system was successfully implemented for a 2D hybrid capillary-chip separation setup. The setup includes a high power 455 nm LED prototype as the excitation light source and a linear light fiber array consisting of 23 active 100 µm light fibers in combination with a push broom imager for hyperspectral imaging. The CIEF focused labeled protein was detected in a common intersection of changes in the chip interface via the fluorescence detection system. The whole 2D heart-cutting assay was performed in ca. 30 min. The CE separation step in the second separation dimension was able to separate the protein from the ampholytes at acidic separation conditions and therefore allows the undisturbed MS detection of CIEF separated proteins. Using the on-chip LED-IF detection system the analyte can directly be monitored during the cutting and transfer step and thus, a very precise control of the heart-cut and transfer process is possible. Using the on-chip intermediate optical detection band broadening and peak splitting can be eliminated as shown in this study.

5.2   Introduction

In capillary isoelectric focusing (CIEF) amphoteric analytes are separated by their isoelectric point (pI) in a pH gradient generated by different amphoteric polyamino-polycarboxylic acids, the so called carrier ampholytes (CAs) (Section 4.1.2.A). The hyphenation of capillary isoelectric focusing (CIEF) with mass spectrometry (MS) is a very promising tool for the characterization of proteins and peptides especially for R&D and quality control of monoclonal antibodies. However, the CIEF-MS coupling is still challenging due to the high

number of MS-incompatible carrier ampholytes [Liu, 1996; Tang, 1996; Wei, 1998; Dou, 2008; Sosic, 2008; Páger, 2011; Cao, 2014]: Their masses are in the same m/z-range as the proteins studied but they are much higher concentrated and therefore they suppress the analyte signal. In addition, ampholytes evoke MS source fouling. Therefore, strategies have been developed to reduce or separate ampholytes from the analytes prior to the MS detection:

1. In the direct one-dimensional coupling of CIEF to MS the reduction of the ampholyte concentration can be reduced from conventional used 2.0 % v/v to a minimum of 0.5 % v/v as described by several authors [Tang, 1997; Jensen, 1998; Wei, 1998; Wei 1999]. A further reduction, advantageous for MS detection, however, disturbs the pH-gradient so that resolution decreases or even the overall focusing is impaired.

2. Another strategy is to integrate interfaces between the CIEF separation and the MS detection to extract or remove the ampholytes prior to the MS detection. Here, microdialysis interfaces were proposed by different groups [Mohan, 2002; Mohan, 2003; Yang, 2003A; Yang, 2003B; Liu, 2005].

3. Also, immobilized pH gradients were discussed in the literature for a possible coupling to MS detection by Wang et al. [Wang, 2011], though - to our knowledge - not yet applied to MS detection.

4. Non-ampholyte pH-gradients using temperature or concentration gradients of buffers were described and showed potential for a direct coupling to MS detection [Pawliszyn, 1993; Macounová, 2000; Cabrera, 2011].

5. 2D separation assays combining CIEF in the first separation dimension with on- or off-line combinations of CE- [Hühner, 2016] or LC-MS [Chen, 2003; Zhou, 2004; Stroink, 2005; Zhang, 2006B; Kulka, 2006; Kang, 2006; Wei, 2011] in the second separation dimension to extract or separate the relatively small ampholytes from the larger proteins prior to MS detection. In general, different commercial or custom-made valves have been used for coupling the different electrophoretic or liquid chromatographic separation dimensions.

An easier coupling uses only electromigrative separation techniques, where mostly only voltage switching is required. Column-based two-dimensional electrophoretic separations using commercially available fused silica capillaries [Lemmo, 1993; Michels, 2004; Sahlin, 2007; Schoenherr, 2007; Flaherty, 2013] well as microfluidic chips [Figeys, 1998; Zhang, 1999; Zhang, 2000; Chiou, 2002; Samskog, 2003; Lu, 2012] were described in literature. Both, pre-concentration of sample constituents and matrix elimination for sample clean-up is described using different online combinations of ITP, CZE, MEKC as

well as CIEF (see introduction). Kler et al. [Kler, 2013A; Kler, 2014] presented a modular approach for online coupling of ITP–C^{4}D/CE–MS using a microfluidic glass chip interface for coupling commercially available capillaries and instrumentation. Following this approach, a heart-cut interface for coupling CIEF with intermediate on-chip fluorescence detection (LED-IF) to CE-MS using the glass chip interface is presented in this work. After the CIEF separation a specific part of the pH-gradient which includes the analyte of interest is injected into the 2nd separation dimension for CE separation and therefore to separate ampholytes and analyte prior to MS detection.

5.3 Experimental

5.3.1 Chemicals and solutions

The chemicals and solutions used are described in Section 4.1.3.A.

5.3.2 General instrumentation

All electrophoretic separations were performed using an Agilent 7100 CE system equipped with a UV absorbance detector (Agilent Technologies, Waldbronn, Germany) providing pressure and voltage regimes, injection control, and vial handling. MS detection was achieved using an Agilent 6100 Series Single Quadrupole system as well as an MSD Trap XCT Ultra (Agilent Technologies, Palo Alto, USA). The CE was coupled to the MS via a coaxial sheath liquid interface from Agilent using the Agilent isocratic pump 1260 (Agilent Technologies, Waldbronn, Germany) for delivering sheath liquid (50:50 (v/v) mixture of water and isopropanol, containing 0.1% acetic or formic acid depending on the used background electrolyte used) at a constant volume rate of 4 µl/min. Nebulizer pressure was set to 0.28 bar and the drying gas was delivered at a rate of 4 l/min at a temperature of 300 °C. The fragmentor was set to +150 V, the capillary voltage was +4 kV and the nozzle voltage +2 kV. The single quadrupole was operated in single ion mode (SIM) or scanning mode (scan). The respective mode and related m/z values or ranges are given in the respective Figure legend for each experiment.

5.3.3 Instrumentation for intermediate on-chip LED-IF detection

Intermediate LED-IF on-chip detection was realized as discussed in Section 3.4. The LED prototype as well as the software were developed and fabricated in cooperation with FutureLED (Berlin, Germany). For cooling the LED a Peltier element from head electronic GmbH (Prien am Chiemsee, Germany) was used. The collection of the fluorescence light was achieved via the custom-made linear fiber array from art photonics GmbH (Berlin, Germany), described in Section 3.4.4. The push broom imager used for hyperspectral detection of the fluorescence light and the push broom software for signal data recording version 1.0 (V.1.0) were custom-made by J&M Analytik AG (Essingen, Germany) as discussed in Section 3.4.4.D. The respective conditions and parameters of the push broom imager are listed in each section.

5.3.4 Capillary-chip interface - 2nd generation interface design

For capillary coupling a 2nd generation chip interface with a double-T channel design with etched channels of 60 µm in width and 25 µm in depth (2nd generation chip design, Section 3.1) was used. The preparation of the capillary-chip setup was performed as described in Section 3.2. The fused silica capillaries (ID 50 µm) were cut to a length of 40 cm for each of the four chip ports. After gluing the capillary to the chip the modular capillary-chip setup was coated with GPTMS.

5.3.5 Procedure for (3-glycidoxypropyl)trimethoxysilane (GPTMS) coating

The coating protocol described in Section 3.4.3.E was followed. Briefly, the GPTMS coating solution (c = 10 % w/w, pH ≈ 5) was introduced into the 2D setup at 2 bar for 120 minutes. Then, the setup was gently purged with compressed air overnight (minimum 10 hours at 1 bar). This process was repeated in order to achieve a homogeneous coating on the capillary surface. For conditioning, the respective 2D setup was flushed with water and anolyte for 30 min at 2 bar each using the Agilent 7100 CE system. To verify the quality of the coated 2D setup before first separation, the capillary was flushed with anolyte and +25 kV were applied to monitor if a stable current can be reached. The system was left in doubly-deionized water when not in use. For long-term storage the capillary-chip setups were flushed with air and left at room temperature.

5.3.6 *Protein labeling*

Myoglobin labeling was done as described in Section 3.4.3.G. A stock solution of 10 mg/ml concentration of the protein dissolved in doubly-deionized water was used. For injection a protein concentration of 2.0 mg/ml was chosen.

5.3.7 *Conditions and parameters for 2D CIEF-LED-IF/CE-MS experiments*

The sample contained 2.0 % v/v Pharmalyte 3-10 carrier ampholytes and 0.1 % v/v HEC as a dynamic EOF modifier to minimize EOF velocity and reduce protein adsorption. A 1.0 % w/v HEC stock solution was prepared by dissolving 0.4 g HEC in 40 ml doubly-deionized water at 70°C. 1 mol/l aqueous acetic acid was used as anolyte and 250 mM aqueous triethylamine (TEA) as catholyte both containing 0.1 % w/v HEC. The solution with the labeled protein was mixed with the carrier ampholyte stock solution to the final concentration of the model analytes (2.0 mg/ml myoglobin or 10 µg/ml of the pI markers). A custom-made multiport HV source (CalvaSens GmbH, Aalen, Germany) enabled the independent operation of 12 high voltage source channels, 6 positive (from 0 to 15 kV) and 6 negative (from -15 to 0 kV) [Kler, 2014]. Together with a home-made multi-vial unit this enabled the simultaneous and independent control of pressure and high voltage regimes for up to four vials. Pressure application of 1 bar for injection and flushing was achieved via the pneumatic unit of an Agilent 7100 CE system (Agilent Technologies, Waldbronn, Germany) by-passing the pneumatic connection of the inlet port via pneumatic valves Festo MFH-3-M5 (FESTO AG, Neuss, Germany) [Kler, 2014] controlled manually with an ad-hoc switch module. The CIEF separations were carried out with detection at the anodic end. Sample (ampholyte containing protein solution) injection was done for 13 sec at 2 bar for the experiments.

5.4   **Results and discussion**

5.4.1 *Repeatability of 1ˢᵗ CIEF dimension of the 2D CIEF/CE-MS setup*

The setup used for the first separations including the hybrid capillary-microchip setup for multidimensional separations is shown in Figure 5-1. The Agilent 7100 CE system equipped with a UV absorbance detector was used for pressure, voltage application and analyte detection using the integrated UV/VIS detector. The 2D capillary-chip setup was used in the one dimensional separation mode. Blocking of the side channels was realized via commercial CE vials filled with cured silicone comparable to works from Zhang et al. [Zhang, 2006A].
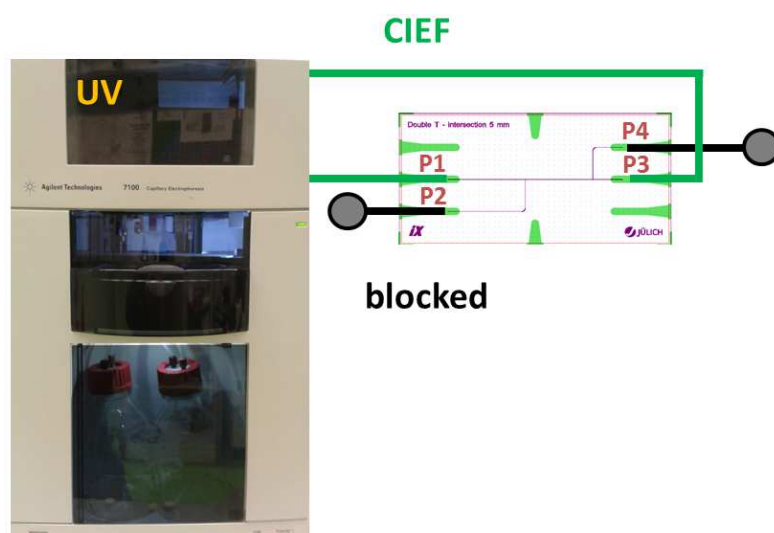
Figure 5-1: Instrumental setup for 1D CIEF-UV separation performed within the 2D hybrid capillary-microchip setup for multidimensional separations: Commercial CE instrument (Agilent 7100 CE system) – for controlling the pressure regime via a fast pneumatic connection. Analyte detection was achieved via the integrated UV/VIS wavelength detector at 280 nm. Capillary blocking was realized via commercial CE vials filled with cured silicone.

The injection and separation protocol for the experiment is illustrated in Figure 5-2. First, the whole setup was flushed with the anolyte solution (acetic acid, c = 1 mol/l) for 600 sec at 1 bar followed by the injection of the sample solution containing the carrier ampholytes (CA) and the labeled protein (S). After that, a catholyte plug (2 sec at 1 bar of TEA, c = 250 mmol/l) was injected as a sacrifice zone due to cathodic drift during voltage application (see Section 4.1.2.C). Finally, with the catholyte vial loaded to port P1 and the anolyte vial loaded to port P3 a separation potential of -17 kV was applied at the inlet (with the outlet vial of the CE instrument on ground potential (GND)) over the 2D setup. The focusing time was 7 min with ports P2 and P4 being blocked with silicone filled CE vials. The pH-gradient was mobilized by applying a pressure of 100 mbar to the inlet vial P1 while maintaining the focusing voltage of -17 kV. The current profile started at an initial value of about 12.0 µA exponentially declined during the focusing process to a final value of 3.0 µA. Detection of the analytes was done via the internal UV/VIS wavelength detector of the CE system.
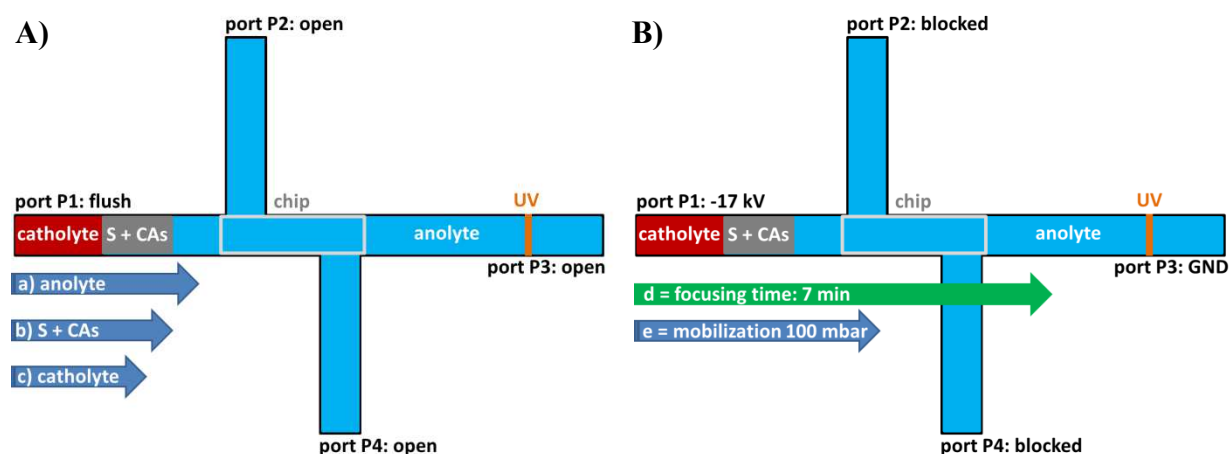
*Figure 5-2: Operational scheme for the two steps involved in 1D CIEF-UV separation performed along the 2D hybrid capillary-microchip setup: **A)** Prior to the sample injection the 2D setup was flushed with anolyte. After the sample injection a catholyte plug was injected as a sacrifice zone to avoid a cathodic drift during potential application. **B)** After completition of the focusing step at -17 kV, the CIEF pH-gradient was mobilized by pressure application from port P1 to port P3 with the detector, while ports P2 and P4 were blocked via commercial CE vials filled with cured silicone.*

To demonstrate the applicability of the first CIEF separation dimension within the 2D CIEF/CE-MS setup, the precision of migration time and peak area repeatability were determined to evaluate the robustness of the setup. Here, the complete capillary-chip setup was coated with the neutral GPTMS coating following the protocol given in Section 3.4.3.E. The model analytes p-aminobenzoic acid (PABA; pI = 3.9), β-lactoglobulin (β-lact; pI = 5.1), myoglobin (myo; pI = 7.0) and ribonuclease A (RNase A; pI = 9.5) were analyzed using CIEF-UV in the first dimension of the 2D setup, performing the detection after the chip interface to evaluate its influence on peak parameters. In Figure 5-3 a CIEF experiment is shown exemplarily. Symmetrical peak shapes were achieved for the separations performed through the chip interface for all four analytes. Regarding peak appearance, shape and broadness the separations within the 2D setup were comparable to one dimensional CIEF separations as shown in Section 4.1.4.B. Thus, the chip interface itself does not introduce band broadening. The observed linear relationship with $R^2 = 0.9905$ between the detection time and the pI values of the analytes underlines the principal applicability of interface and method. Long term repeatability was evaluated by performing fifteen repeated measurements (n = 15, Table 5-1) within three working days, using freshly prepared solutions daily. RSD values for the peak area lower than 8 % and for the detection time lower than 2 % were achieved, except for ribonuclease A (13 % RSD for the peak area) comparable to literature values [Graf, 2005; Suratman, 2008]
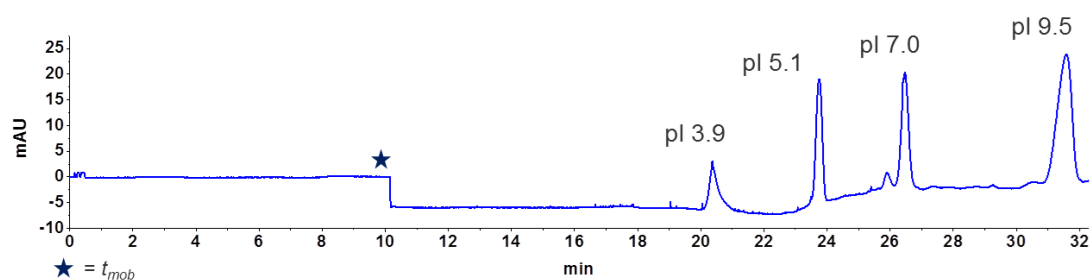
Figure 5-3: CIEF-UV separation over the chip interface. GPTMS was used as the coating in combination with 0.1 % HEC. Analytes: p-aminobenzoic acid (PABA; pI = 3.9; c = 0.25 µg/ml), β-lactoglobulin (β-lact; pI = 5.1; c = 0.5 mg/ml), myoglobin (myo; pI = 7.0; c = 0.7 mg/ml) and ribonuclease A RNase A; pI = 9.5; c = 1.0 mg/ml). The analytes were detected at 280 nm. Focusing time was 10 min (★ = mobilization time point) and for analyte mobilization a pressure of 100 mbar was used.

Thus, the CIEF method using covalently bound GPTMS coating in combination with 0.1 % HEC as a dynamic EOF modifier is suitable to coat and effectively shield the inner surface of the separation capillary as well as the chip interface of the 2D separation system. CIEF assays can be performed with a comparable quality to the intact capillary regarding peak parameters.

Table 5-1: Evaluation of long-term (intra- and inter-day) repeatability performing 15 CIEF-UV measurements in 3 days in the first dimension of the 2D setup for the analytes p-aminobenzoic acid (pI = 3.9), β-lactoglobulin (pI = 5.1), myoglobin (pI = 7.0) and ribonuclease A (pI = 9.5).

n = 15	pI 3.9	pI 5.1	pI 7.0	pI 9.5
RSD% (area)	3.80	5.86	7.55	12.99
RSD% (detection time)	1.48	1.34	1.48	2.47

In general, RSD% values for the peak area increase with longer detection times of proteins, here, higher pI. This is due to the fact that the CIEF focusing occurs at zero net charge of the proteins. During the focusing step, the protein concentration is increased at pH = pI within the pH-gradient and thus, the tendency of protein-protein interaction increases the chance for precipitation. The neutral protein will precipitate and/or absorb to the coated capillary wall. As a result, sample loss occurs, which increases with increasing time of the protein inside the separation capillary [Graf, 2005; Suratman, 2008]. Therefore, especially for CIEF assays the type of coating is of crucial importance in order to eliminate or reduce protein absorption to the capillary (see also Section 4.1.2.B).

5.4.2 CIEF analyte positioning in the interface with intermediate LED-IF detection

The setup used for the separations including the hybrid capillary-microchip setup for multidimensional separations is shown in Figure 5-4. The 2D capillary-chip setup was used in the one dimensional separation mode with on-chip intermediate LED-IF detection of P503-labeled myoglobin. Capillary blocking was realized via commercial CE vials filled with cured silicone [Zhang, 2006A].
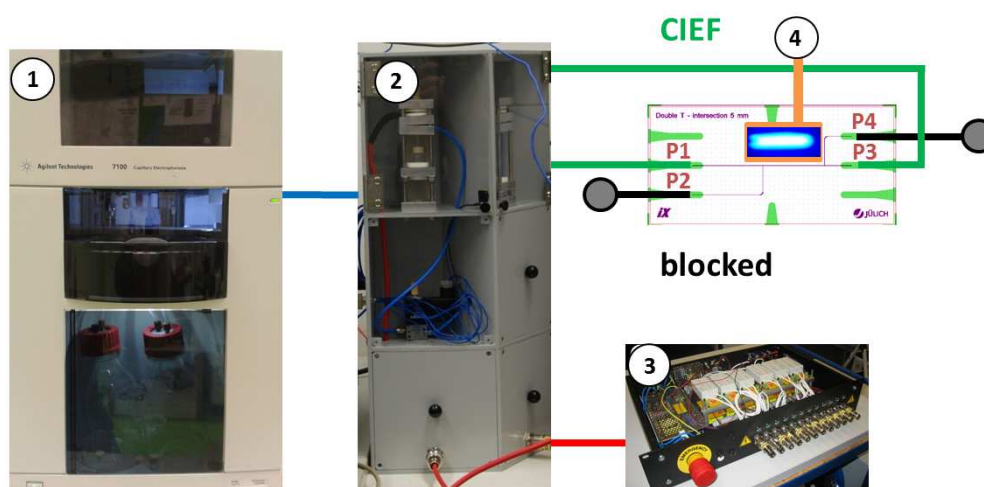
Figure 5-4: Instrumental setup for 1D CIEF-LED-IF separation performed within the 2D hybrid capillary-microchip setup for multidimensional separations: (1) CE Agilent 7100 – for controlling the pressure regime via a fast pneumatic connection, (2) home-made multi-vial unit, (3) custom-made multiport HV source and (4) custom-made on-chip LED-IF detection system. Capillary blocking was realized via commercial CE vials filled with cured silicone.

The injection and separation protocol for the experiment is described by Figure 5-2 but here, intermediate analyte detection using the on-chip LED-IF detection system was used. First, the whole setup was flushed with the anolyte solution (acetic acid, c = 1 mol/l) for 600 sec at 1 bar followed by the injection of the sample solution containing the carrier ampholytes (CA) and the labeled protein (S). After that, different catholyte (TEA, c = 250 mmol/l) plug lengths were injected to position the CIEF pH gradient within the separation capillary (Section 4.1.3.F). Finally, the catholyte vial was loaded to port P1 and the anolyte vial loaded to port P3 and separation potential was applied. During the experiment a separation voltage of -17 kV (-10 kV at port P1 and +7 kV at port P3, see Figure 5-2) was applied over the 2D setup. The focusing time was 7 min with ports P2 and P4 being blocked with silicone filled CE vials. Voltage application was realized via the custom-made multiport HV source together with a home-made multi-vial unit. Pressure application was achieved via the pneumatic unit of an Agilent 7100 CE system by-passing the pneumatic connection of the inlet port via

pneumatic valves (Section 3.3.3.B). Mobilization of the pH gradient was reached by applying a pressure of 100 mbar to the inlet vial P1 while maintaining the focusing voltage of -17 kV. The current profile started at an initial value of about 12.0 µA and exponentially declined with the progress of the focusing process to a final value of 3.0 µA. The model analyte myoglobin (labeled with P503) was detected via the on-chip LED-IF detection system, described in Section 3.4.5.H.

To further optimize the 2D CIEF-LED-IF/CE-MS separation platform regarding analysis time the idea was to position the pH gradient within the 2D separation setup so that the analyte is directly focused inside the common intersection of the glass chip interface and thus, mobilization can be omitted as far as the pI of the analyte is known. As indicated by Figure 5-5 the catholyte and anolyte plug lengths can be adjusted in a way that a specific analyte is directly focused inside the detection window of the intermediate detection system (here: LED-IF). To estimate the respective injection times for the catholyte plug (Section 4.1.4.D) the presented tool "Focus" could be used.
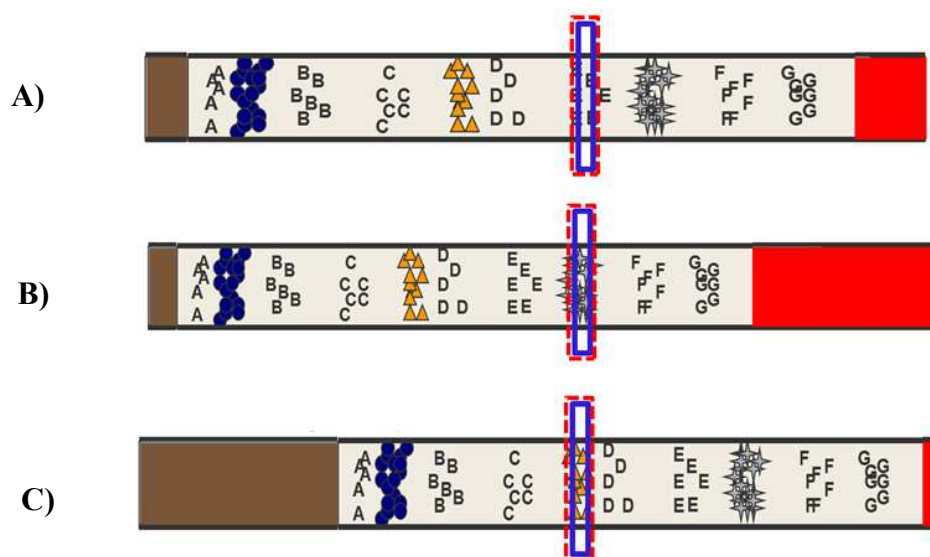
Figure 5-5: Direct focusing of the analyte of interest inside the common intersection as the cutting window (red dashed line) of the chip interface by using the on-chip LEF-IF detection system (blue line): A to detect the analytes (orange, blue or grey symbols) pH gradient mobilization towards the detector is necessary. B and C) Direct analyte focusing inside the common intersection via a proper usage of catholyte (brown) and anolyte (red) plug lengths inside the separation capillary. A - E = ampholytes

Comparable to the CIEF positioning experiment described for the one dimensional capillary setup as discussed in Section 4.1.4.G, the positioning was performed in the first separation dimension of the 2D capillary-chip setup to estimate if the linear relationship and therefore the positioning tool is also applicable for the 2D setup. Analyte detection was performed using the intermediate on-chip LED-IF detection using the setup as described in Section 3.4.

P503-labeled myoglobin was used as the model analyte and focusing time was 7 min for each experiment as described in Section 3.4.5.H. Here, the positioning was accomplished by injecting different catholyte plug lengths using a pressure of 1 bar for different time intervals of 5, 15 and 25 sec after anolyte and sample injection as shown in Figure 5-6. For the injection time of (A) 5 sec the detection time was 7.1 min, of (B) 15 sec the detection time was 4.5 min and for (C) of 25 sec it was 2.1 min. By plotting the recorded detection time of the labeled myoglobin against the injection time of the catholyte plug, a linear relationship was observed with an R^2 value of 0.9995, see Figure 5-7, comparable to the one dimensional positioning experiments discussed in Section 4.1.4.D.
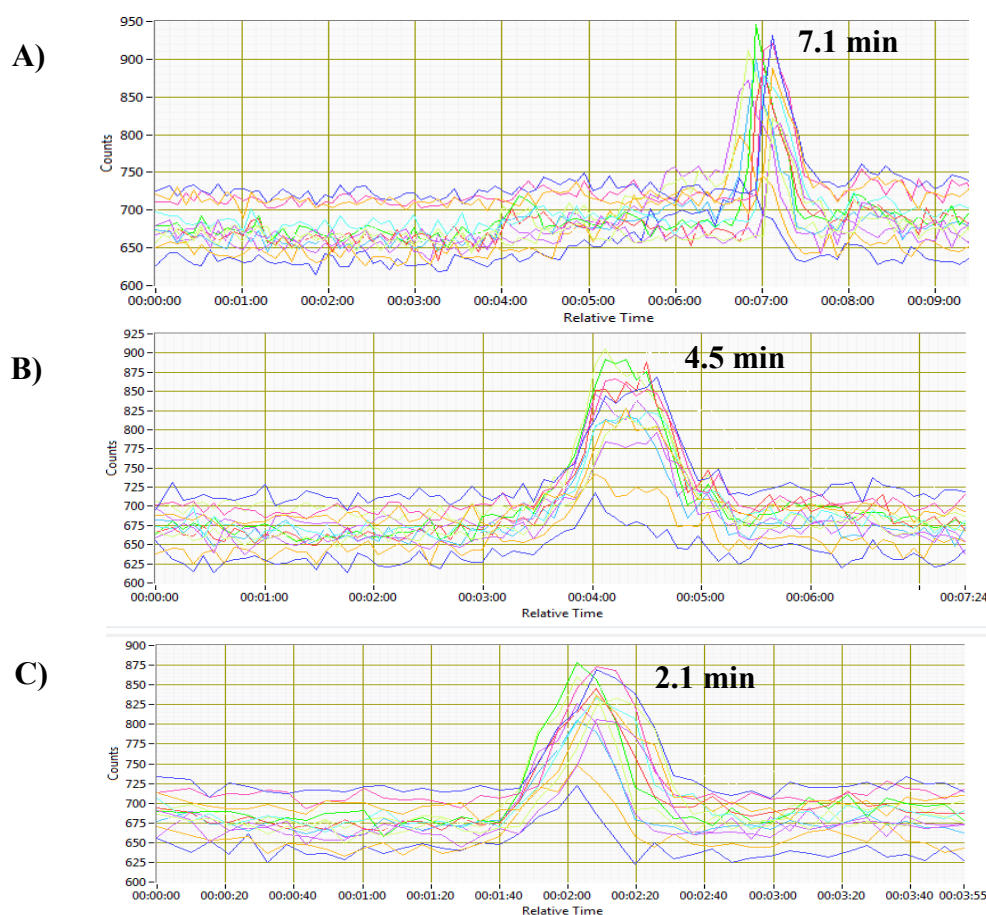
Figure 5-6: Positioning of the CIEF pH gradient inside the first separation dimension of the 2D setup accomplished by injecting catholyte plugs of different lengths applying a pressure of 1bar: A) for 5 sec, B) for 15 sec and C) for 25 sec after anolyte and sample injection. The model analyte was P503-labeled myoglobin. Intermediate on-chip detection was done by the LED-IF setup described in Section 3.4.

As the pH gradient positioning follows a linear relationship using different catholyte plug lengths, the positioning tool "Focus" described in Section 4.1.4.G can be used to estimate the catholyte plug length necessary for related experimental parameters of the CIEF separation to

predict or estimate the analyte positioning in the first separation dimension of the 2D modular capillary-chip setup.
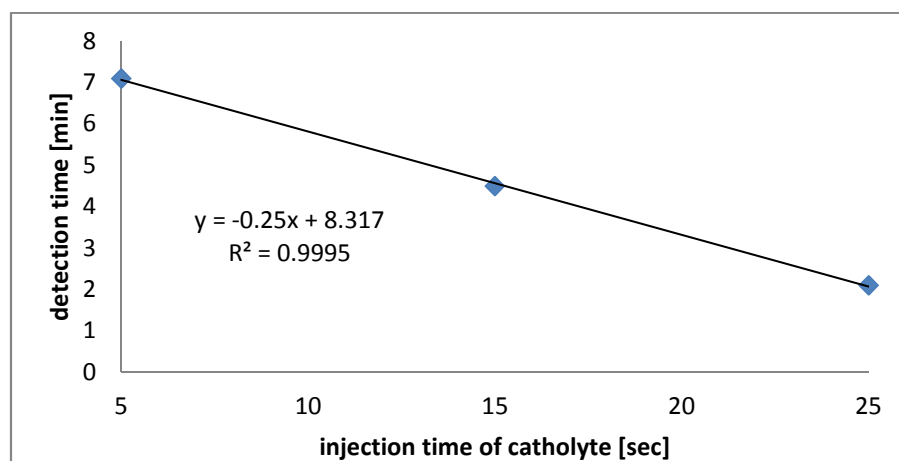

Figure 5-7: Calibration curve for CIEF analyte positioning inside the first separation dimension of the 2D setup accomplished by injecting different catholyte plug lengths applying a pressure of 1 bar for 5, 15 and 25 sec after anolyte and sample injection. Used model analyte was P503-labeled myoglobin. Intermediate on-chip detection was done by the LED-IF setup described in Section 3.4.

5.4.3 2D CIEF/CE-MS with on-capillary C⁴D detection

The setup used for the separations including the hybrid capillary-microchip setup for multidimensional separations is shown in Figure 5-8. The 2D capillary-chip setup was used in the two dimensional separation mode first with on-capillary C⁴D detection insead of on-chip LED-IF detection system (4) in Figure 5-4. Capillary blocking was realized via commercial CE vials filled with cured silicone [Zhang, 2006A]. The injection and separation protocol for the experiment is described by Figure 5-9. First, the whole setup was flushed with the anolyte solution for 600 sec at 1 bar followed by the injection of the sample solution containing the carrier ampholytes (CA) and the labeled protein (S). After that, a catholyte plug (2 sec at 1 bar of TEA, c = 250 mmol/l) was injected as a sacrifice zone due to cathodic drift during potential application (see Section 4.1.2.C). Finally, the catholyte vial was loaded to port P1 and the anolyte vial loaded to port P3 and separation potential was applied. During the experiment a separation voltage of -17 kV (-10 kV at port P1 and +7 kV at port P3) was applied over the 2D setup and the focusing time was 7 min with ports P2 and P4 being blocked with silicone filled vials. The voltage application for the first CIEF separation dimension was realized via the custom-made multiport HV source together with a home-made multi-vial unit. Pressure application was achieved via the pneumatic unit of an Agilent 7100 CE system by-passing the pneumatic connection of the inlet port via pneumatic valves. Mobilization of the pH gradient

was obtained by applying a pressure of 100 mbar to the inlet vial P1 while maintaining the focusing voltage of -17 kV.

Figure 5-8: Instrumental setup for 2D CIEF/CE-MS separations using the hybrid capillary-microchip setup for multidimensional separations and on-capillary C^4D detection: (1) CE Agilent 7100 – for controlling the pressure regime via a fast pneumatic connection, (2) home-made multi-vial unit, (3) custom-made multiport HV source, (4) C^4D conductivity detector and (5) Agilent 6100 Series Single Quadrupole system. Capillary blocking was realized via commercial CE vials filled with cured silicone.

The current profile started at an initial value of about 12.0 µA and exponentially declined with the progress of the focusing process to a final value of 3.0 µA. For the comprehensive heart-cutting of the pH gradient without on-chip LED-IF detection, a conductivity detector (C^4D) was placed in front of the chip interface at channel port P1 to detect the anolyte/ampholyte boundary passing the interface to trigger sampling for the second dimension CE-MS using 100 mbar. The pH gradient was sampled comprehensively in five fractions with injection times of 30 s each, followed by a CE-MS run of 10 min (I. to V., see Figure 5-10). The IEF gradient was stabilized during this time via voltage application of -17 kV. CE-MS separation was done at +17 kV from port P2 to port P3 and the CE-MS runs were performed for 10 min for each fraction.

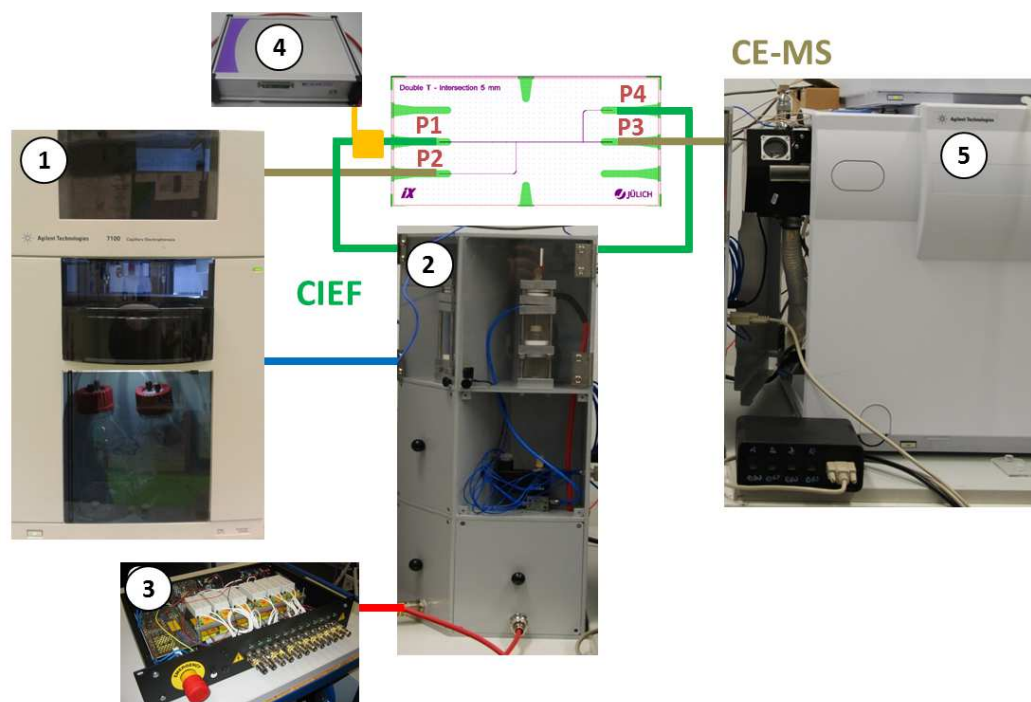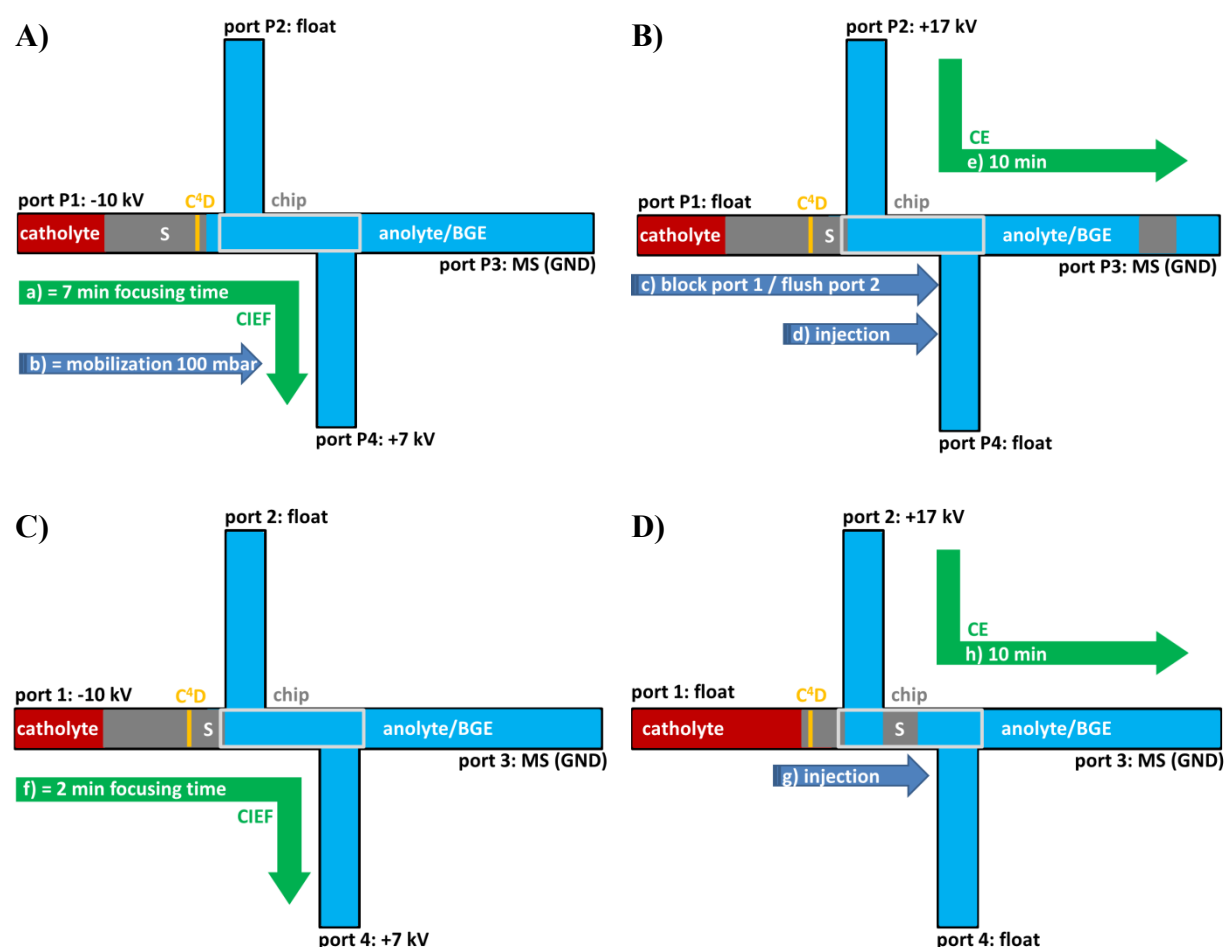*Figure 5-9: Operational scheme for the steps involved in 2D CIEF/CE-MS separations using the hybrid capillary-microchip setup for multidimensional separations and at-capillary C⁴D detection: Prior to the sample injection the 2D setup was flushed with anolyte. After the sample injection step a catholyte plug was injected as a sacrifice zone due to cathodic drift during potential application. A) After application of the focusing step the CIEF pH gradient was mobilized by pressure application from port P1 to the C⁴D conductivity detector placed 5 cm away from the chip interface on the separation capillary connected to port P1, while ports P2 and P3 were left at floating potential. B) When the anolyte/ampholyte boundary was detected in the C⁴D detector, port P1 was blocked and the 2D system was flushed from port P2 with CE-MS background electrolyte, a portion of the ampholyte gradient is injected (20 sec at 100 mbar) to the second dimension. CE separation was performed applying voltage between P2 and P3. C) When the ampholyte fraction was detected in the MS the potential was switched to port P1 and P4 to refocus the pH gradient for 2 min. D) After that another portion of the ampholyte gradient was injected (20 sec at 100 mbar and CE separation was performed. For each following heart-cut step the operational schemes (C) and (D) were repeated.*

In order to judge the impact of the 2D setup, prior to the first cutting experiment CIEF and CE methods were separately coupled to MS detection using myoglobin as the model analyte as shown in Figure 5-10A and B. Myoglobin (c = 0.5 mg/ml) was analysed via one dimensional CE-MS in an acidic background electrolyte to record the charge envelope of the myoglobin mass spectrum as shown in Figure 5-10A. Myoglobin was detected in the mass spectrometer after ca. 12 min using a background electrolyte consisting of 3:1 acetic/formic acid at c = 1 mol/l. The direct coupling of CIEF-MS injecting myoglobin at 0.5 mg/ml for 20 sec at

100 mbar did not allow detecting the protein as shown in Figure 5-10B as expected (see Section 5.2). The protein signal is not detectable in the mass spectrometer due to the ampholyte-induced protein signal suppression. For first proof of principle 2D CIEF/CE-MS experiments, the focused CIEF pH gradient was sequentially cut via defined heart-cutting steps with myoglobin as the model analyte as shown in Figure 5-10C.
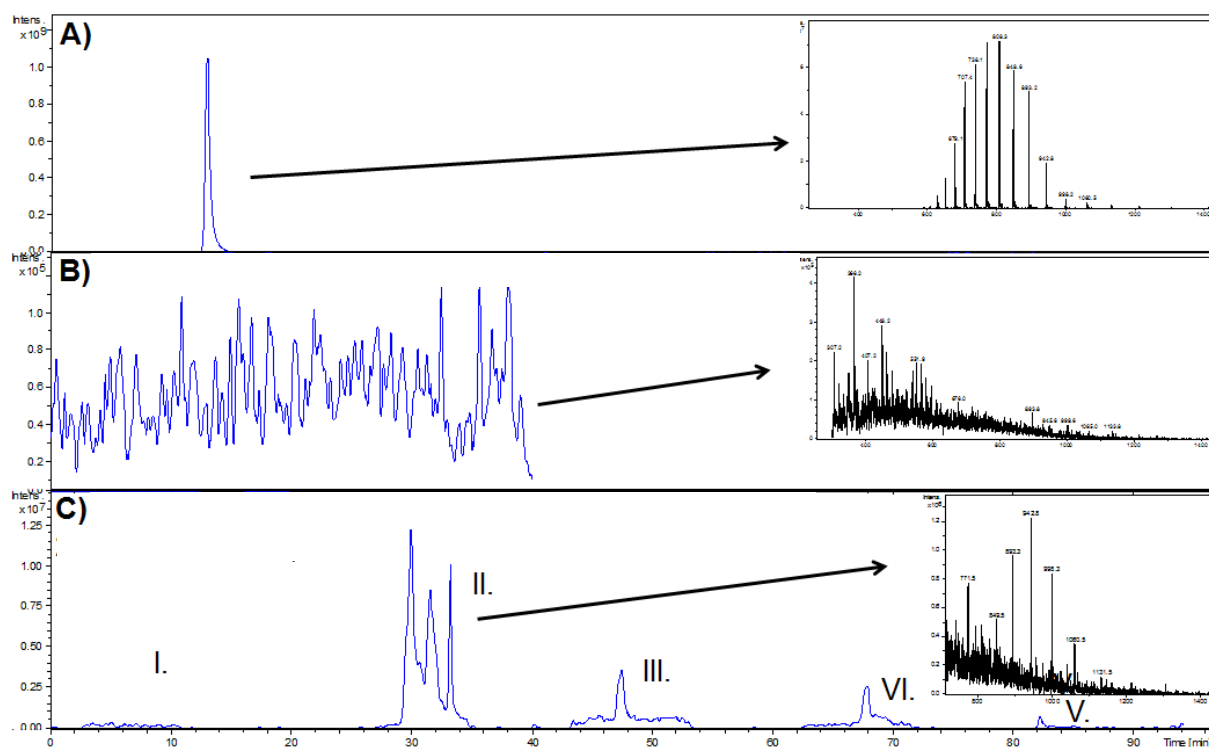
Figure 5-10: A) CE-MS of myoglobin at 0.5 mg/ml in a background electrolyte consisting of 3:1 acetic/formic acid at c = 1 mol/l, B) direct coupling of CIEF-MS injecting myoglobin at 0.5 mg/ml with a background electrolyte consisting of 3:1 acetic/formic acid at c = 1 mol/l as the anolyte and 250 mmol/l TEA in the reversed mode (Section 4.1.4) and C) comprehensive heart-cut sampling of the CIEF pH gradient followed by CE-MS analysis with myoglobin at a 0.5 mg/ml concentration background electrolyte consisting of 3:1 acetic/formic acid at c = 1 mol/l.

A conductivity detector (C^4D) was used to detect the anolyte/ampholyte boundary passing the interface to trigger sampling for the second dimension CE-MS using 100 mbar. The pH gradient was sampled comprehensively with injection times of 20 s each, followed by a CE-MS run of 10 min for each fraction I. to V. as shown in Figure 5-10C. The IEF pH gradient was stabilized during this time via voltage application. As shown in the electropherogram in Figure 5-10C, myoglobin was detected first in Fraction II. with the myoglobin band appearing as a triple-peak. The peak splitting is most probably due to sucking and/or back pressure effects induced by the cutting procedure or an unprecise cutting process [Fan, 1994]: The pH gradient was cut consecutively without knowing the exact position of the analyte as well as pressure variances due to the exchange of blocking and buffer vials. If the

analyte band is cut e.g. in the middle it can happen that some of the analyte is pushed into the non-active separation channels. Thus it becomes separated from its main zone. During the following

CE-MS separation the separated bands migrate separately to the MS due to identical effective electrophoretic mobilities and thus are not united before detection. Comparing the MS signal intensity of the direct CE-MS analysis (signal intensity of 1.0×10^9) and the CE-MS after heart-cutting a fraction of the CIEF pH gradient (signal intensity of 1.0×10^7) it is clear that for the 2D setup still ampholytes are co-migrating with the analyte and thus suppression of the protein signal leads to reduced signal intensity of over two orders of magnitude detected in the MS (despite the pre-concentration effect of CIEF). The following Fractions III. to V. also contained the protein at decreasing concentrations, due to analyte carryover between cutting steps. In total, the first experiments showed that identification of myoglobin is possible using the 2D setup with the partial removal of ampholytes in the second CE-MS dimension, though further optimization of the 2D setup is necessary with regard to the intermediate monitoring of the cutting process, the composition and pH of the CE-MS background electrolyte and thus being identical with the anolyte for the CIEF assay and the reduction of carryover from one fraction to another. To gain further insight into the sample transfer performed within the chip interface during the cutting process, on-chip LED-IF detection was implemented as described in Section 3.4. In Figure 5-11 a simplified assembly of the optical on-chip detection setup is shown without the aluminum blocks used for the fixation of the optical parts.
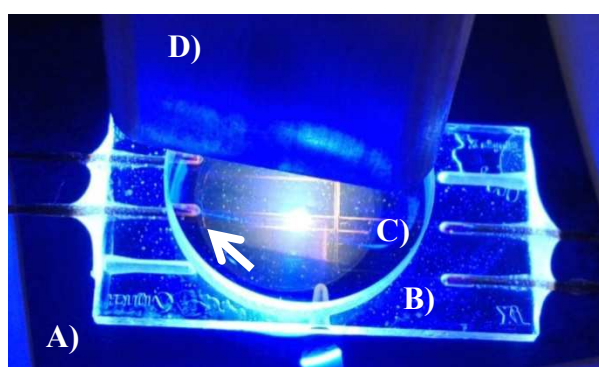
*Figure 5-11: **A)** 455 nm LED prototype, **B)** glass chip interface, **C)** direct coupling of CIEF-MS injecting labeled myoglobin at 0.5 mg/ml and **C)** 500 nm long pass filter and **D)** linear fiber array connected to the push broom imager*

Here, the chip interface (B) was directly placed on the LED chip (A) of the LED prototype for analyte excitation (P503-labeled myoglobin). Fluorescence light was collected via the linear fiber array (D) and detected via the push broom imager as described in Section 3.4.4 with the

500 nm long pass filter (C) between the glass chip and the fiber array to reduce the intensity of the excitation stray light. The chip was flushed with a solution of P503-labeled myoglobin (c = 2 mg/ml). Upon excitation with the blue LED light fluorescence light is emitted with a maximum at ca. 600 nm (orange). It is clear to see that the protein is accumulated in the dead volume of the chip cups at the entrance of the separation capillaries (white arrow). This residual dead volume (~20 pl) is filled with labeled protein and with every new cutting step it is partly flushed out of the chip cup. By applying additional rinsing steps with background electrolyte (e.g. 120 sec at 1 bar) between each heart-cutting fractionation the analyte carryover was reduced (data not shown). Further reduction of the carryover effect can be realized by reducing the dead volume of the interface. For this, the 3rd generation chip interface (see Section 3.1.5) is most promising due to the nearly dead-volume free capillary to chip coupling using the screw-tight fitting but it remains to be implemented.

5.4.4 2D CIEF/CE-MS with on-chip intermediate LED-IF detection

The setup used for the separations including the hybrid capillary-microchip setup for multidimensional separations is shown in Figure 5-8. The 2D capillary-chip setup was used in the two dimensional separation mode with on-chip intermediate LED-IF detection as shown in Figure 5-4 (4). Capillary blocking was realized via commercial CE vials filled with cured silicone [Zhang, 2006A]. The injection and separation protocol for the experiment is described by Figure 5-9. First, the whole setup was flushed with the anolyte solution for 600 sec at 1 bar followed by the injection of the sample solution containing the carrier ampholytes (CA) and the labeled protein (S). After that, a catholyte plug (2 sec at 1 bar of TEA, c = 250 mmol/l) was injected as a sacrifice zone due to cathodic drift during potential application (see Section 4.1.3.F). Finally, the catholyte vial was loaded to port P1 and the anolyte vial loaded to port P4 and separation potential was applied. During the experiment a separation voltage of -17 kV (-10 kV at port P1 and +7 kV at port P4, see Figure 5-9) was applied over the 2D setup and the focusing time was 7 min with port P2 being blocked with silicone filled vials. The voltage application for the first CIEF separation dimension was realized via the custom-made multiport HV source together with a home-made multi-vial unit. Pressure application was achieved via the pneumatic unit of an Agilent 7100 CE system by-passing the pneumatic connection of the inlet port via pneumatic valves (Section 3.3.3.B). Mobilization of the pH gradient was obtained by applying a pressure of 100 mbar to the inlet vial P1 while maintaining the focusing voltage of -17 kV. The current profile started at an initial value of about 12.0 µA and exponentially declined with the progress of the focusing

process to a final value of 3.0 µA. Detection of the model analyte myoglobin (labeled with P503) was done via the on-chip LED-IF detection system, described in Section 3.4. When the protein signal was initially detected inside the chip interface the mobilization pressure was switched off and port P1 was blocked with a silicone vial. After that the whole system was flushed with anolyte solution at 1 bar for 120 sec from port P2 to ports P3 and P4 to flush out remaining ampholyte solution and fill the system with anolyte. After that the protein - now being positioned right in front of the chip interface - was injected into the common intersection of the glass chip by applying a pressure pulse of 100 mbar for 30 sec to port P1 loaded with the catholyte vial and ports P2 and P4 being blocked with silicone vials. The injection process was monitored via the LED-IF detection system. Finally, a separation potential of +25 kV was applied as shown in Figure 5-9B from port P2 loaded with an anolyte vial to P3 to perform CE-MS analysis. CE-MS separation was done using an Agilent 7100 CE system at port P2 and an Agilent 6100 Series Single Quadrupole system at port P3. The runs were performed for ca. 20 min and afterwards the system was flushed with doubly-deionized water and anolyte for 300 sec at 1 bar for each solution for rinsing and conditioning of the setup.

First 2D CIEF-LED-IF/CE-MS separations were performed using P503-labeled myoglobin. The CIEF focused protein was detected inside the common intersection of the chip interface via the LED-IF system. In Figure 5-12A the time dependent signal from the CIEF electropherogram recorded by the push broom imager is shown. Each colored trace represents the signal collected via one optical fiber of the fiber array. The CIEF separation was performed inside the capillary connected to port P1 in front of the chip interface. After the 7 min of focusing time the pH gradient was mobilized by applying pressure to P1 and therefore pushing the pH gradient towards the LED-IF detection system. The first 4 signals between 1.0 and 2.0 min as well as 5 and 6 min are due to the gradient appearing at the detection window and pushing it back into the separation capillary connected to port P1 to show the ability to monitor the peak transport, and thus to control it via a mobilization pressure applied to the respective port P1 or P3. In a second separation run (Figure 5-12B) the analyte peak was transferred to the second separation dimension via a single heart-cutting process by cutting the detection window marked via the dashed lines. From 6 min onwards the protein was detected inside the LED-IF system and the mobilization pressure and the focusing voltage were stopped, indicated by the signal decrease. Now, the blocking vial was set to port P1 followed by the anolyte flushing for 30 sec of 2.0 bar from port P2 to port P3 to flush away the remaining ampholyte. After that the injection of the sample plug to the second

separation dimension from port P1 into port P3 was done while blocking port P2. The injection process is visible by a slight step in the detected signal at 10.5 min.
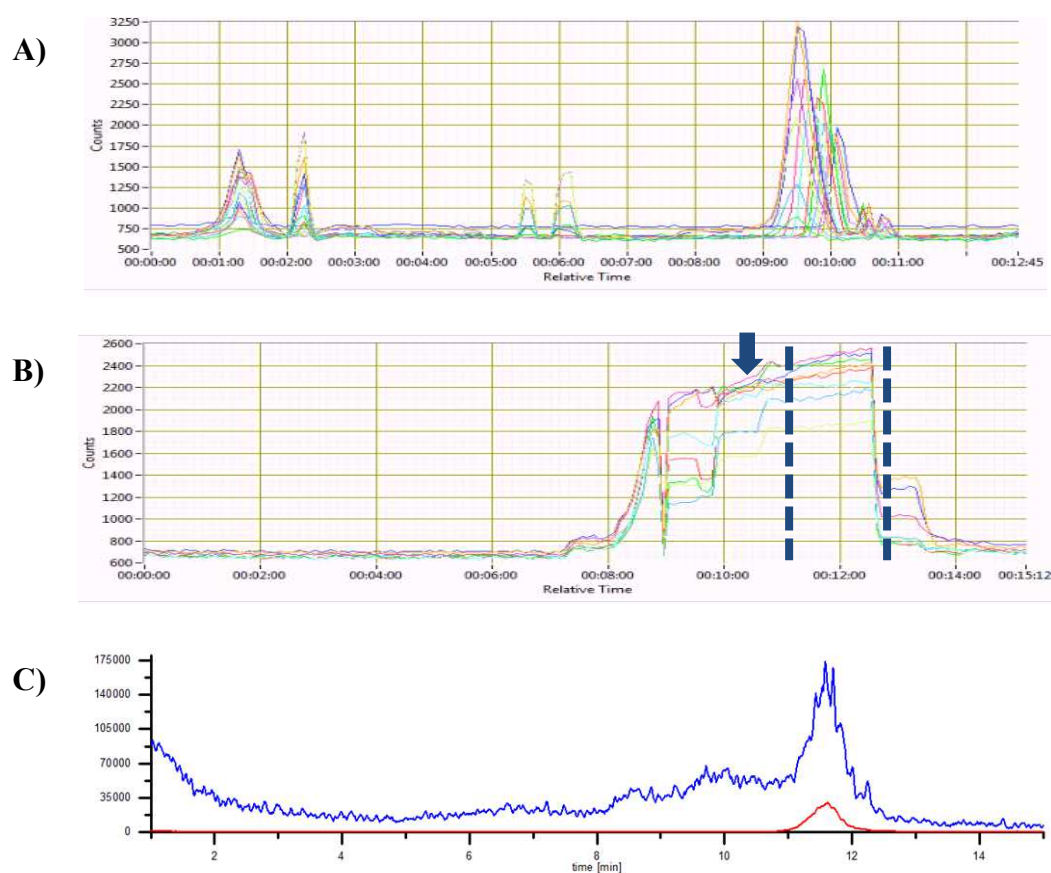

*Figure 5-12: **A)** First separation dimension of the modular 2D setup: CIEF-LED-IF of P503-labeled myoglobin without heart-cutting step. After completing the focusing time of 7 min the LED-IF system was switched on and mobilization pressure of 100 mbar was applied. Fluorescence light (at 603 nm) was collected with the linear fiber array and detection was done with the time dependent recording option of the push broom imager (Section 3.4.4.D). **B)** Separation as in **A)** but with heart-cutting procedure beginning at 9 min after application of mobilization pressure. Arrow = injection time point (100 mbar for 30 sec) and the dashed lines = cutting window resulting in 45 sec of voltage application in combination with pressure application of 100 mbar to the second CE-MS separation dimension. **C)** Second separation dimension: CE-MS in 1 mol/l acetic acid of myoglobin in blue, 679 m/z. ampholytes in blue in scan mode from 550 to 1350 m/z. The scan and SIM mode were applied in parallel with 50:50 recording time.*

Now, the separation voltage for the second CE-MS separation dimension was applied with ports P1 and P4 being blocked. After ca. 45 sec of voltage application in combination with pressure application of 100 mbar to the second separation dimension the protein signal in the interface decreased rapidly, indicating the complete injection into the CE-MS dimension. Here, a slight delay (ca. 30 sec) most probably due to an intermediate defocusing process where the protein needs to become charged by the acid used in the background electrolyte in order to be able to electrophoretically migrate in the second separation dimension to the MS. The slight signal increases signal plateau at ca. 13 min is most probably due to protein being

flushed out of the dead volume as discussed in the previous Section. After the signal decrease for the CIEF-LED-IF dimension the mobilization pressure of 100 mbar was switched off and the CE-MS separation voltage was applied. The ampholyte signal detected by the MS at the beginning of the CE-MS separation (Figure 5-12C) is due to the flushing process (30 sec at 2.0 bar) prior to the analyte injection process. After ca. 8 min of separation time the broad ampholyte band is detected and after ca. 12 min myoglobin is detected as a single peak (see Figure 5-12C) due to a proper cutting process using the LED-IF system for intermediate analyte detection (compare to Figure 5-10C). With a BGE of 1 mol/l acetic acid comigration of the protein and ampholyte band is observed (see Section 4.2.1). Total analysis time for one cutting experiment was 7 min focusing time including additional 12 min for the mobilization and cutting process and 12 min for the CE-MS analysis. Therefore, the whole 2D heart-cutting assay can be performed in ca. 30 min for myoglobin as the model analyte. The assay can be performed even faster by optimizing the analyte positioning up to a total reduction of the mobilization time by directly focusing the analyte within the common interception of the chip interface (see Figure 3-6). For a further optimization the whole switching process could be optimized by automation by using valves integrated into the separation channels instead of the manually moved blocking vials. By using valves the switching process between both separation dimensions would be performed faster, be less laborious and show a higher reproducibility. A valve-based approach for 2D CIEF/CE-MS separation assays is already published by Hühner et al. [Hühner, 2016] but without the possibility of intermediate analyte detection. Here, a combination of both 2D approaches could be most feasible for a robust multidimensional electrophoretic separation platform, advantageously by using valves for blocking the side channels of the 2D setup. This enables voltage switching and an easy filling. Besides that band broadening is reduced.

5.5 Conclusion and outlook

Intermediate precision of CIEF separations in the first dimension of the 2D capillary-chip setup was evaluated by performing repeated measurements (n = 15) at three working days. RSD values for the peak area lower than 8 % and for the detection time of lower than 2 % were achieved (except for RNase A with 13 % RSD). Similar RSD % values are reported in literature and are typical for CIEF separation assays [Graf, 2005; Suratman, 2008]. A high linearity of the pH-gradient was achieved with R² values > 0.99. Thus, the CIEF method presented here using the covalently bound neutral GPTMS coating in combination with 0.1 % HEC as a dynamic modifier is suitable to coat and effectively shield the inner surface of the separation capillary as well as the chip interface of the 2D separation system.

First poof of principle experiments have been conducted for coupling of CIEF to MS via a 2D CIEF/CE-MS approach using the modular capillary-chip setup introduced by the working group in earlier studies [Kler, 2013A; Kler, 2014]. With the 2D CIEF/CE-MS setup presented here, the CIEF focused pH-gradient can be sampled by single or sequential heart-cutting followed by the sample plug transfer to the second CE-MS separation dimension. By applying on-chip LED-IF as an intermediate detection method for labeled protein (myoglobin as a model analyte) the analyte can be monitored directly on-chip and thus, the cutting transfer can be controlled. Analyte positioning using different catholyte plug lengths was performed successfully in the first separation dimension of the 2D capillary-chip setup with a linear relationship (R² = 0.9995) between the detection time and the applied catholyte plug and therefore the positioning tool "Focus" is also applicable for CIEF experiments in the 2D setup. Further optimization of the setup will include direct CIEF analyte positioning inside the interface using the tool "Focus" as well as the use of valves at the side channels to minimize analysis time and increase the robustness and automation of the 2D CIEF-LED-IF/CE-MS setup.

6 Summary: Discussion and conclusions

In this thesis a previously presented modular two dimensional electrophoretic setup using a capillary-chip based approach [Tiggelaar, 2007] was further developed regarding interface stability, intermediate on-chip analyte detection and application to CIEF. In this regard, the interface was developed towards a 3rd generating interface with glue-free screw-tight capillary connections and evolution towards a dead volume-free interface coupling. The 2D setup was further used for coupling capillary isoelectric focusing (CIEF) to capillary electrophoresis (CE) with mass spectrometric (MS) detection for the analysis of proteins. By implementing an intermediate optical detection, the dynamics of the anayte transfer can be monitored in detail using spatially-resolved fluorescence detection for the first time. Prior to the hyphenation, both separation dimensions were first optimized independantly in a one-dimensional setup using model proteins. Here, one aspect was to achieve reproducible CIEF separation parameters for the first separation dimension as well as a good resolution of protein sample band and ampholyte stack in the CE separation dimension. For the successful optimization strategy, simulation and experimental data were successfully combined. In this context the reduction of preparation time and costs for the 2D setup, e.g. regarding used coatings used and chip prototype design, as well as better usability of the setup e.g. by the software tool "Focus" for the analyte positioning in the first CIEF separation dimension for heart-cutting 2D CIEF/CE-MS assays was achieved.

One important aspect was the optimization of the glass chip interface regarding stability and intermediate on-interface analyte detection sensitivity. Therefore, the chip interface was fabricated with a minimal cover plate thickness of 200 μm in the region of the common intersection to achieve maximum analyte detection sensitivity. To increase the stability of the chip, additional 500 μm glass blocks were bonded to the cover plate in the region of the capillary cups. Both adjustments define the 2nd generation interface. To overcome limiting performance parameters like dead volume and a glued capillary connection, a new (3rd generation) chip interface was successfully introduced and compared to the previously used 2nd generation design (**Section 3.1**). For this prototype a new and promising production process, the Selective Laser Etching (SLE), was evaluated and compared to the commonly used wet etching bonding process (PWEAB). Comparing both interfaces, the 3rd generation chip design showed up to 4 times better peak performance regarding resolution and peak width of the model analytes during the transfer step from capillary to capillary. The separation performed throughout the new chip prototype showed nearly the same peak performance as an

intact capillary with and without additional EOF-induced bulk flow. The outstanding performance of the interface is due to the used SLE process which allows a nearly dead volume free capillary-chip connection by using screw-tight fittings, and nearly circular chip channels, butted end connections of capillaries and chips and fully circular channel cross sections. Therefore, the 3rd generation chip is a promising interface solution for future applications. Similar high performanc capillary-chip interfaces have not been reported in literature.

Combining capillaries for multidimensional electrophoretic separations a general challenge is the control of the leakage of sample constituents and band broadening at the channel intersections in microchips or capillary-chip interfaces, which can be achieved using fixed bias or pullback potentials (**Section 3.3**). However, this is not possible for electrophoretic separations performed in a non-uniform background electrolyte like isotachophoresis and isoelectric focusing. To monitor and thus control potential variations at the cross section of the interface during electrophoretic separations, on-chip potential measurements were conducted via a passivated electrode inside the chip interface. On-chip intersection potential measurements were successfully conducted without disturbing CE and ITP analysis regarding separation and peak shape efficiency using a low current measuring prototype in combination with a SiN passivated Ti/Pt electrode inside a glass microchip interface. The repeatable results obtained for the potential measurements underline the excellent stability of the prototype and the suitability of the passivation of the electrode for avoiding disturbances of the electric field lines as well as electrolysis during potential measurements conducted during electrophoretic separations. Successful simulation of the ITP intersection potential allowed a deeper understanding of the potential development during the separation. The gradual exit of the leading electrolyte and the entrance of the adapted terminating electrolyte were monitored by potential changes with a high correlation with the experimental results. In order to accomplish a feedback system for potential adjustment by using bias voltages, a future development will be a software-controlled electrical feedback regulation of the applied potential via different HV power supplies to be implemented in the presented setup. With this combination it will be possible to electrokinetically close side channels and enable the hyphenation to systems at fixed potentials, e.g. mass spectrometry. One crucial parameter to guarantee high peak capacities and orthogonality and a sufficient sample transfer (minimal sample band broadening) from the first to the second separation dimension is the correct timing of the cutting process followed by the transfer step. By directly observing the analyte of interest during the transfer procedure its migration or transport can easily be controlled and optimized

regarding co-migration of analytes, matrix removal and even leakage phenomena occurring at the interface. Selectivity and sensitivity of the second separation step and final detection method and thus be incresed. For this reason an optical on-chip imaging system using LED induced fluorescence detection (LED-IF) was implemented (**Section 3.4**). To be able to detect analyte bands passing the common intersection channel segment of the 2nd generation chip interface with a high spatial, spectral and temporal resolution, a detector combining a linear fiber array consisting of 23 active light guides for fluorescence light collection and a push broom imager for signal detection was realized. Using this optical on-chip detection setup the LOD for a basic FITC solution was determined to be 0.04 fmol for an S/N ratio of 4 for in channel measurements (or even lower for TLC plates or solid dosage forms, e.g. tablets) being comparable with data from the literature but at the same time enabeling spatial resolution. Due to the fiber array developed here in combination with a push broom imager, the analyte can be monitored within the interface and thus, the setup allows a precise transfer from the first to the second separation dimension.

As an application the 2D setup was used to couple capillary isoelectric focusing (CIEF) to mass spectrometry (MS). This coupling arrangement is a very promising tool for the characterization of proteins and peptides especially for R&D and quality control of monoclonal antibodies. However, the direct CIEF-MS coupling is still challenging due to the high number of MS-incompatible carrier ampholytes (CAs). In literature several attempts have been presented to realize the coupling by reducing the ampholyte concentration from conventionally used 2.0% v/v to a minimum of 0.5% v/v as described by several authors [Tang, 1997; Jensen, 1998; Wei, 1998; Wei 1999] but with partly decrease in separation performance. Another strategy is to integrate interfaces between the CIEF separation and the MS detection to extract or remove the ampholytes prior to the MS detection. Here, microdialysis interfaces [Mohan, 2002; Mohan, 2003; Yang, 2003A; Yang, 2003B; Liu, 2005] as well as immobilized pH gradients [Wang, 2011] were discussed in the literature for a possible coupling to MS detection, but have not yet been realized. Despite that non-ampholyte pH-gradients using temperature or concentration gradients of buffers were described [Pawliszyn, 1993; Macounová, 2000; Cabrera, 2011]. The most common approach is using 2D separation approaches using capilary electrophoresis (CE) [Hühner, 2016] or liquid chromatography (LC) [Chen, 2003; Zhou, 2004; Stroink, 2005; Zhang, 2006B; Kulka, 2006; Kang, 2006; Wei, 2011] in the second separation dimension so separate the protein and ampholyte band before MS detection. Both strategies use commercially available or custom-made port valves for connecting the CE or LC dimension. Using the valve, the first

and second separation dimension are hydrodynamically separated form each other, but intermediate on-interface detection is not possible and thus, control of analyte position requires laborious calculation approaches. Using the interface valve with CE as the second separation dimension [Hühner, 2016] the maximum applicable separation potential was 20 kV. With separation potenials over 20 kV the movable plastic parts of the valve are affected leading to breakage and liquid leakage.

In this work, instead of a valve the microfluidic glass chip interface was used to couple CIEF to CE-MS. Using a glass chip interface, intermediate LED-IF was successfully applied to the 2D interface to monitor analyte position inside the glass chip for a precise sample transfer. Using an interface with similar surface properties compared to the fused silica separation capillaries similar separation properties, EOF bulk flows and coating strategies can be applied throughout the whole separation setup, impossible with all other 2D approaches presented so far. The optimization of the CIEF (**Section 4.1**) analyte positioning as well as the separation of the protein and the ampholyte fraction within the second CE (**Section 4.2**) dimension was achieved with the combination of computer simulations and experimental data. Finally, the optimized single separation dimensions were combined to a two dimensional CIEF/CE-MS detection setup (**Section 5**). First proof of principle experiments were presented with sequential and single heart-cutting experiments using myoglobin as a model analyte. The optimization of the sample transfer regarding carryover and peak broadening was achieved by monitoring and therefore controlling the IEF focused protein plug via intermediate on-chip LED-IF detection within the common intersection of the interface. This intermediate detection with its linear array and push broom imager for the first time allows time-, spatial- and wavelength- resolved monitoring of the movement of the analyte band, which is ideal for controlling the analyte transfer. Analyte positioning using diffenet catholyte plug lengths was successfully performed in the first separation dimension of the 2D capillary-chip setup with a highly linear relationship between the detection time and the applied catholyte plug. By combining experimental and simulation data, the positioning tool "Focus" was created in cooperation to forcast CIEF analyte positioning inside the first separation dimension and thus, decrease experimental effort. Further optimization of the setup could include direct CIEF analyte positioning inside the interface using the software tool "Focus" to minimize analysis time by reducing the mobilization time. Besides that, the integration of valves (comparable to the work from Hühner et al. [Hühner, 2016]) at the siede channels of the 2D setup would increase robustness by allowing to hydrodynamically close each single separation dimension of the 2D CIEF-LED-IF/CE-MS setup.

7 Literature

Adahchour M, Beens J, Vreuls R. J. J, Brinkman U. A. Th (2006) Trends Anal. Chem. 25: 438–454.

Alarie J. P, Jacobson S. C, Culbertson C. T and Ramsey J. M (2000) Electrophoresis 21: 100–106.

Anderson J. L and Prieve D. C (1984) Separ. Purif. Method. 13: 67–103.

Ayachit U, The ParaView Guide: A Parallel Visualization Application; Kitware Inc., 2015.

Beck W, van Hoek R and Engelhardt H (1993) Electrophoresis 14: 540-546.

Becker H, Lowack K and Manz A (1998) J. Micromech. Microeng. 8: 24–28.

Beckers J. L, Everaerts F. M, Ackermans M. T (1991) J. Chromatogr. 537: 429–442.

Belder D and Ludwig M (2003) Electrophoresis 24: 2422–2430.

Bergström S. K, Dahlin A. P, Ramström M, Andersson M, Markides K. E and Bergquist J (2006) Analyst 131(7): 791–798.

Bergstrom S. K, Samskog J and Markides K. E (2003) Anal. Chem. 75: 5461–5467.

Berli C.L.A (2008) Microfluid. Nanofluid. 4: 391–399.

Bianchi F, Ferrigno R and Girault H. H (2000) Anal. Chem. 72: 1987–1993.

Bings N. H, Wang C, Skinner C. D, Colyer C. L, Thibault P and Harrison D. J (1999) Anal. Chem. 71: 3292–3296.

Bodor R, Kaniansky D, Masár M, Silleová K and Stanislawski B (2002) Electrophoresis 23: 3630–3637.

Bowerbank C. R and Lee M. L (2001) J. Microcolumn Sep. 13: 361–370.

Bruin G. J. M (2000) Electrophoresis 20: 3931–3951.

Bushey M. M and Jorgenson J. W (1990) Anal. Chem. 62: 978–984.

Cabrera C. R, Finlayson B and Yager P (2001) Anal. Chem. 73: 658-666.

Cannan R. K, Palmer A. H and Kibrick A. C (1942) J. Biol. Chem. 142: 803-822.

Cao J, Sun W, Gong F and Liu W (2014) Electrophoresis 35: 1461-1468.

Chabinyc M. L, Chiu D. T, McDonald J. C, Stroock A. D, Christian J. F, Karger A. M and Whitesides G. M (2001) Anal. Chem. 73: 4491-4498.

Chan B. M. C and Brash J. L (1981) J. Colloid Interface Sci. 84: 263–265.

Chen J, Balgley B. M, DeVoe D. L and Lee C. S (2003) Anal. Chem. 75: 3145-3152.

Chen S and Lee M. L (1998) Anal. Chem. 70: 3777–3780.

Chen X, Wu H, Mao C and Whitesides G. M (2002) Anal. Chem. 74: 1772–1778.

Chiang M. T, Chang S. Y and Whang C. W (2000) J. Chromatogr. A. 877: 233-237.

Chiou C.-H, Lee G.-B, Hsu H.-T, Chen P.-W and Liao P.-C (2002) Sensors Actuat. B-Chem. 86: 280–286.

Chrambach A and Boček P (1985) TrAC-Trend Anal. Chem. 4: 224–229.

Chrambach A, Doerr P, Finlayson G. F, Miles L. E. M, Sherins R and Rodbard D (1973) Ann. N. Y. Acad. Sci. 209: 44–64.

Cong Y, Zhang L, Tao D, Liang Y, Zhang W, Zhang Y. (2008) J. Sep. Sci. 31: 588–594.

Cooper J. W, Wang Y and Lee C. S (2004) Electrophoresis 25: 3913–3926.

Coufal P, Zuska J, van de Goor T, Smith V and Gaš B (2003) Electrophoresis 24: 671–677.

Crabtree H. J, Cheong E. C. S, Tilroe D. A and Backhouse C. J (2001) Anal. Chem. 73: 4079–4086.

Craig D. B, Wetzl B. K, Duerkop A, Wolfbeis O. S (2005) Electrophoresis 26: 2208–2213.

Dada O. O, Ramsay L. M, Dickerson J. A, Cermak N, Jiang R, Zhu C and Dovichi N. J (2010) Anal. Bioanal. Chem. 397: 3305–3310.

Dalcin L. D, Paz R. R, Kler P. A and Cosimo A (2011) Adv. Water Resour. 34: 1124–1139.

Dale L. M, Thewis A, Boudry C, Rotar I, Dardenne P, Baeten V and Fernández Pierna J. A (2013) Appl. Spectrosc. Rev. 48: 142-159.

Deans D. R (1981) J. Chromatogr. 203: 19-28.

Dickerson J. A, Ramsay L. M, Dada O. O, Cermak N, Dovichi N. J (2010) Electrophoresis 31: 2650–2654.

Doherty E. A. S, Meagher R. J, Albarghouthi M. N and Barron A. E (2003) Electrophoresis 24: 34–54.

Dose E.V and Guiochon G (1992) Anal. Chem. 64: 123–128.

Dou P, Liu Z, He J, Xu J. J and Chen H. Y (2008) J. Chromatogr. A 1190(1-2): 372-376.

Egodage K. L, de Silva B. S and Wilson G. S (1997) J. Am. Chem. Soc. 119: 5295–5301.

Emrich C. A, Medintz I. L, Chu W. K and Mathies R. A (2007) Anal. Chem. 79: 7360–7366.

Evangelista R. A, Liu M-S and Chen F-T. A (1995) Anal. Chem. 67: 2239-2245.

Evans C. R and Jorgenson J. W (2004) Anal. Bioanal. Chem. 378 : 1952–1961.

Everaerts F. M, Verheggen T. P and Mikkers F. E (1979) J. Chromatogr. A 169: 21–38.

Fan Z. H and Harrison D. J (1994) Anal. Chem. 66: 177–184.

Fang X, Tragas C, Wu J, Mao Q and Pawliszyn J (1998) Electrophoresis 19: 2290-2295.

Felhofer J. L, Blanes L and Garcia C. D (2010) Electrophoresis 31: 2469–2486.

Figeys D, Gygi S. P, McKinnon G and Aebersold R (1998) Anal. Chem. 70: 3728–3734.

Flaherty R. J, Huge B. J, Bruce S. M, Dada O. O and Dovichi N. J (2013) Analyst 138: 3621–3625.

Fonslow B. R, Kang S. A, Gestaut D. R, Graczyk B, Davis T. N, Sabatini D. M and Yates J. R the 3rd (2010) Anal. Chem. 82: 6643-6651.

Foret F, Müller O, Thorne J, Götzinger W and Karger B. L (1995) J. Chromatogr. A 716: 157-166.

Foret F, Szoko E and Karger B. L (1992) J. Chromatogr. 608: 3–12.

François I, Sandra K, Sandra P (2009) Anal. Chim. Acta 641: 14–31.

Fu J.-L, Fang Q, Zhang T, Jin X-H and Fang Z-L (2006) Anal. Chem. 78: 3827-3834.

Fu L. M and Lin C. H (2003) Anal. Chem. 75: 5790–5796.

Fu L. M, Leong J. C, Lin C. F, Tai C. H and Tsai C. H (2007) Biomed. Microdevices 9: 405–412.

Airy G. B (1833) Philos. Mag. 3: 20-30.

Gao D, Liu H, Jiang Y and Lin J.-M (2013) Lab Chip 13: 3309–3322.

Gao L and Liu S (2004) Anal. Chem. 76: 7179-7186.

Gebauer P, Malá Z and Bŏcek P (2011) Electrophoresis 32: 83–89.

Geiger M, Hogerton A. L and Bowser M. T (2011) Anal. Chem. 84: 577–596.

Giddings J (1987) J. High Res. Chromatogr. 10: 319–323.

Gilar M, Olivova P, Daly A. E and Gebler J. C (2005) Anal. Chem. 77: 6426–6434.

Goetz A. F. H, Vane G, Solomon J. E, Rock B. N (1985) Science 228: 1147-1153.

Gottmann J, Hermans M and Ortmann J (2013) J. Laser Micro Nanoeng. 8: 115–123.

Götz S and Karst U (2007) Anal. Bioanal. Chem. 387: 183-192.

Graf M, R. G García and Wätzig H (2005) Electrophoresis 26: 2409–2417.

Guihen E (2014) Electrophoresis 35: 138–146.

Harrison D. J, Fluri K, Seiler K, Fan Z. H, Effenhauser C. S and Manz A (1993) Science 261: 895–897.

Hempe, J. M, McGehee A. M and Stoyanov A. V (2009) J. Chromatogr. B 877: 3462-3466.

Hermans M, Gottmann J and Riedel F (2014) J. Laser Micro Nanoeng. 9: 126–131.

Herr A. E, Molho J. I, Drouvalakis K. A, Mikkelsen J. C, Utz P. J, Santiago J. G and Kenny T. W (2003) Anal. Chem. 75: 1180–1187.

Hjertén S (1985) J. Chromatogr. 347: 191-198.

Hooker T. F and Jorgenson J. W (1997) Anal. Chem. 69: 4134–4142.

Horka M, Kubicek O, Ruzicka F, Hola V, Malinovska I and Slais K (2007) J. Chromatogr. A 1155: 164-171.

Horká M, Willimann T, Blum M, Nording P, Friedl Z and Šlais K (2001) J. Chromatogr. A 916: 65-71.

Hörstmann-Jungemann M, Gottmann J and Wortmann D (2009) J. Laser Micro Nanoeng. 4: 135–140.

Horvath J and Dolník V (2001) Electrophoresis 22: 644-655.

Huhn C and Pyell U (2010) J. Chromatogr. A 1217: 4476–4486.

Huhn C, Pütz M and Pyell U (2008) Electrophoresis 29: 783–795.

Hühner J and Neusüß C (2016) Anal. Bioanal. Chem. 408: 4055–4061

Hühner J, Lämmerhofer M and Neusüß C (2015) Electrophoresis 36: 2670–2686.

Hutterer K and Dolník V (2003) Electrophoresis 24: 3998-4012.

Issaq H. J, Chan K. C, Janini G. M, Conrads T. P and Veenstra T. D (2005) J. Chromatogr. B 817: 35–47.

Jacobson S. C, Ermakov S. V and Ramsey J. M (1999) Anal. Chem. 71: 3273–3276.

Jaros M, Stedry M, Hruska V, Zuskova I and Gas B (2013) software "Peakmaster version 5.3 Complex". http://web.natur.cuni.cz/gas/. 2013

Jensen P. K, Harrata A. K and Lee C. S (1998) Anal. Chem. 70: 2044-2049.

Jiang L, Jiang X, Lu Y, Dai Z, Xie M, Qin J and Lin B (2007) Electrophoresis 28: 1259–1264.

Jooß K, Sommer J, Bunz S.-C and Neusüß C (2013) Electrophoresis 35: 1236–1243.

Jung B, Zhu Yand Santiago J. G (2007) Anal. Chem. 79: 345-349.

Kang D and Moon M. H (2006) Anal. Chem. 78: 5789–5798.

Kaniansky D and Marák J (1990) J. Chromatogr. 498: 191–204.

Kaniansky D, Madajová V, Marák J, Šimuničová E, Zelenský I and Zelenská V (1987) J. Chromatogr. A 390: 51–60.

Kaniansky D, Masár M and Bielčíková J (1997) J. Chromatogr. A 792: 483–494.

Kaniansky D, Masár M, Bielčíková J, Iványi F, Eisenbeiss F, Stanislawski B, Grass B, Neyer A and Jöhnck M (2000) Anal. Chem. 72: 3596–3604.

Kaniansky D, Masár M, Bodor R, Žúborová M, Ölvecká E, Jöhnck M and Stanislawski B (2003) Electrophoresis 24: 2208–2227.

Kăsička V (2014) Electrophoresis 35: 69–95.

Keynton R. S, Roussel T. J Jr, Crain M. M, Jackson D. J, Franco D. B, Naber J. F, Walsh K. M and Baldwin R. P (2004) Anal. Chim. Acta 507: 95–105.

Kilár F, Végvári Á and Mód A (1998) J. Chromatogr. A 813: 349–360.

Kim K, Nakayama Y and Yamamoto R (2006) Phys. Rev. Lett. 96: 1-4.

Kitagawa F, Inoue K, Hasegawa T, Kamiya M, Okamoto Y, Kawase M and Otsuka K (2006) J. Chromatogr. A 1130: 219–226.

Kler P. A and Huhn C (2014) Anal. Bioanal. Chem. 406: 7163–7174.

Kler P. A, Berli C. L. A and Guarnieri F. A (2011) Microfluid. Nanofluid. 10: 187–198.

Kler P. A, Dalcin L. D, Paz R. R, Tezduyar T. E (2013B) Comput. Mech. 51: 171–185.

Kler P. A, Posch T. N, Pattky M, Tiggelaar R. M and Huhn C (2013A) J. Chromatogr. A 1297: 204–212.

Kler P. A, Sydes D and Huhn C (2015) Anal. Bioanal. Chem. 407: 119–138.

Kohl F. J, Sánchez-Hernández L and Neusüß C (2015) Electrophoresis 36: 144–158.

Kostal V. and Arriaga E. A (2008) Electrophoresis 29: 2578-2586.

Kubačák P, Mikuš P, Valášková I and Havránek E (2006) Arch. Pharm. Chem. Life Sci. 339: 96–99.

Kubáň P and Hauser P. C (2004) Electroanal. 16: 2009–2021.

Kulka S, Quintás G and Lendl B (2006) Analyst 131: 739–744.

Kutter J. P, Jacobson S. C, Matsubara N and Ramsey J. M (1998) Anal. Chem. 70: 3291–3297.

Lada M. W, Schaller G, Carriger M. H, Vickroy T. W and Kennedy R. T (1995) Anal. Chim. Acta 307: 217–225.

Lalwani S 2006 Opening the IEF Blackbox, Part 1, 8th Symposium on the Practical Applications of CE in Biotechnology and Pharmaceutical Industries, Jersey City, N.J., October 4.

Lalwani S, Tutu E and Vigh G (2005) Electrophoresis 26: 2503–2510.

Lamoree M. H, Tjaden U. R and van der Greef J (1997) J. Chromatogr. A 777: 31-39.

Lee W.-H and Her G.-R (2009) Electrophoresis 30: 1675–1683.

Lee W.-H, Wang C.-W and Her G.-R (2011) Rapid Commun. Mass Sp. 25: 2124–2130.

Lemmo A. V and Jorgenson J. W (1993) Anal. Chem. 65: 1576–1581.

Lewis K. C, Opiteck G. J and Jorgenson J. W (1997) J. Am. Soc. Mass Spectrom. 8: 495–500.

Li J, Thibault P, Bings N. H, Skinner C. D, Wang C, Colyer C and Harrison J (1999) Anal. Chem. 71: 3036–3045.

Li Q, Zhang H, Wang Y, Tang B, Liu X and Gong X (2009) Sens. Actuators, B 136: 265–274.

Li Y, Wojcik R and Dovichi N. J (2011) J. Chromatogr. A 1218: 2007–2011.

Lin C. H, Yang R. J, Tai C. H, Lee C. Y and Fu L. M (2004) J. Micromech. Microeng. 14: 639–646.

Lin Y. W, Chiu T. C and Chang H. T (2003) J. Chromatogr. B 793: 37–48.

Liu C, Mo Y-Y, Chen Z-G, Li X, Li O-l, Zhou X (2008) Anal. Chim. Acta 621: 171–177. Schwarz M. A and Hauser P. C (2001) Lab Chip 1: 1–6.

Liu H, Yang C, Yang Q, Zhang W and Zhang Y (2005) J. Chromatogr. B 817: 119–126.

Liu H, Zhang L, Zhu G, Zhang W and Zhang Y (2004) Anal. Chem. 76: 6506–6512.

Liu Q, Shi J, Sun J, Wang T, Zeng L and Jiang G (2011) Angew. Chem. Int. Ed. 50: 5913 – 5917.

Liu X, Sosic Z and Krull I. S (1996) J. Chromatogr. A 735: 165-190.

Liu Z and Pawliszyn J (2003) Anal. Chem. 75: 4887-4894.

Liu Z, Lemma T and Pawliszyn J (2006) J. Proteome Res. 5: 1246-1251

Liu Z, Ou J, Samy R, Glawdel T, Huang T, Ren C. L and Pawliszyn J (2008) Lab Chip 8: 1738-1741.

Lopes F. S, Coelho L. H. G and Gutz I. G. R (2011) Electrophoresis 32: 939–946.

Lopes F. S, Junior O. A and Gutz I. G (2010) Electrochem. Commun. 12: 1387–1390.

Lu J. J, Wang S, Li G, Wang W, Pu Q and Liu S (2012) Anal. Chem. 84: 7001–7007.

Macounová K, Cabrera C. R, Holl M. R and Yager P (2000) Anal. Chem. 72: 3745-3751.

Madou M. J (2002) Fundamentals of microfabrication: the science of miniaturization, CRC Press, Boca Raton.

Malá Z, Gebauer P and Boček P (2013) Electrophoresis 34: 19–28.

Manabe T, Miyamoto H, Oota H and Toyota Y (1998) Electrophoresis 19: 1319-1324

Manz A, Graber N and Widmer H (1990) Sensors Actuat. B 1: 244–248.

Mao Q and Pawliszyn J (1999) J. Biochem. Biophys. Methods 39: 93-110.

Mao Y and Zhang X (2003) Electrophoresis 24: 3289–3295.

Mao Y, Li Y and Zhang X (2006) Proteomics 6: 420–426.

Martin R. S (2006) Methods Mol. Biol. 339: 85–112.

Mazereeuw M, Spikmans V, Tjaden U and van der Greef J (2000) J. Chromatogr. A 879: 219–233.

Mazereeuw M, Tjaden U and van der Greef J (1994) J. Chromatogr. A 67: 151–157.

Mellors J. S, Black W. A, Chambers A. G, Starkey J. A, Lacher N. A and Ramsey J. M (2013) Anal. Chem. 85: 4100–4106.

Michels D. A, Hu S, Dambrowitz K. A, Eggertson M. J, Lauterbach K and Dovichi N. J (2004) Electrophoresis 25: 3098–3105.

Michels D. A, Hu S, Schoenherr R. M, Eggertson M. J, and Dovichi N. J (2002) Mol. Cell. Proteomics 1: 69–74.

Literature

Mikuš P and Marákova K (2011) Column coupling electrophoresis in biomedical analysis. In R Fazel-Rezai, (ed.), Biomedical engineering - From theory to applications, Intech, Rijeka.

Mohan D and Lee C. S (2002) Electrophoresis 23: 3160–3167.

Mohan D, Paša-Tolić L, Masselon C. D, Tolić N, Bogdanov B, Hixson K. K, Smith R. D and Lee C. S (2003) Anal. Chem. 75: 4432–4440.

Mohan, D and Lee, C. S (2002) J. Chromatogr. A 979: 271-276.

Molho J. I, Herr A. E, Mosier B. P, Santiago J. G and Kenny T. W, Brennen R. A and Gordin G. B, Mohammadi B (2001) Anal. Chem. 73: 1350–1360.

Moore A. W and Jorgenson J. W (1995) Anal. Chem. 67: 3448–3455.

Mosher R. A and Thormann W (1990) Electrophoresis 11: 717-723.

Mosher R. A and Thormann W (2002) Electrophoresis 23: 1803-1814.

Mou S, Sun L and Dovichi N. J (2013) Anal. Chem. 85: 10692–10696.

Norde W, Macritchie F, Nowicka G and Lyklema J (1986) J. Colloid Interface Sci. 112: 447–456.

North R. Y and Vigh G (2008) Electrophoresis 29: 1077–1081.

Novak L, Neuzil P, Pipper J, Zhang Y and Lee S (2007) Lab Chip 7: 27–29.

O'Farrell P. H (1975) J. Biol. Chem. 250: 4007–4021.

Oh Y. J, Bottenus D, Ivory C. F and Han S. M (2009) Lab Chip 9: 1609–1617.

Ostuni E, Chapman R. G, Liang M. N, Meluleni G, Pier G, Ingber D. E and Whitesides G. M (2001) Langmuir 17: 6336–6343.

Ouidir T, Jarnier F, Cosette P, Jouenne T and Hardouin J (2014) Anal. Bioanal. Chem. 406: 6297-6309.

Paegel B. M, Hutt L. D, Simpson P. C and Mathies R. A (2000) Anal. Chem. 72: 3030–3037.

Páger C, Dörnyei Á and Kilár F (2011) Electrophoresis 32: 1875-1884.

Páger C, Vargova A, Takacsi-Nagy A, Dörnyei Á and Kilár F (2012) Electrophoresis 33: 3269-3275.

Panic S, Boskovic D, and Loebbecke S, (2011) Book of abstracts 15th International Conference on Miniaturized Systems for Chemistry and Life Sciences October 2-6, Seattle, Washington, USA

Pattky M and Huhn C (2013) Anal. Bioanal. Chem. 405: 225-237.

Pawliszyn J and Wu J (1993) J. Microcol. Sep. 5: 397-401.

Peterson Z. D, Bowerbank C. R, Collins D. C, Graves S. W and Lee M. L (2003) J. Chromatogr. A 992: 169–179.

Poitevin M, Morin A, Busnel J. M, Descroix S, Hennion M. C and Peltre G (2007) J. Chromatogr. A 1155(2): 230-236.

Posner J. D and Santiago J. G (2006) J. Fluid Mech. 555: 1–42.

Puig P, Tempels F, Borrull F, Calull M, Aguilar C, Somsen G. W and de Jong G. J (2007) J. Chromatogr. B 856: 365–370.

Qu J, Feng S, Dong J, Dong X, Kong L, Ye M and Zou H (2007) Anal. Chem. 79: 639-646.

Ramsay L. M, Dickerson J. A, Dada O, Dovichi N. J (2009) Anal. Chem. 81: 1741–1746.

Redweik S, Cianciulli C, Hara M, Xu Y and Wätzig H (2013) Electrophoresis 34: 1812–1819.

Righetti P. G and Candiano G (2011) J. Chromatogr. A 1218: 8727-8737.

Righetti P. G and Caravaggio T (1976) J. Chromatogr. A 1976 1: 1–28.

Righetti P. G, Gelfi C and Conti M (1997) J. Chromatogr. B. 699: 91-104.

Righetti P. G, Sebastiano R and Citterio A (2013) Proteomics. 13: 325-340.

Righetti, P. G (1983) Isoelectric Focusing: Theory, Methodology and Applications, Elsevier Biomedical, Amsterdam, pp. 299-303.

Rocklin R. D, Ramsey R. S and Ramsey J. M (2000) Anal. Chem. 72: 5244–5249.

Rodriguez I and Li, S. F. Y (1999) Anal. Chim. Acta. 383: 1-26.

Rodriguez-Diaz R, Wehr T and Zhu M (1997) Electrophoresis 18: 2134-2144.

Ryvolova M, Preisler J, Brabazon D and Macka M (2010) Trends Anal. Chem. 29: 339-353.

Sahlin E (2007) J. Chromatogr. A 1154: 454–459.

Salplachta J, Kubesova A and Horka M (2012) Proteomics. 12: 2927-2936.

Samskog J, Bergström S. K, Jönsson M, Klett O, Wetterhall M and Markides K. E (2003) Electrophoresis 24: 1723–1729.

Schäferling M (2012) Angew. Chem. Int. Ed. 51: 3532–3554.

Schoenherr R. M, Ye M, Vannatta M and Dovichi N. J (2007) Anal. Chem. 79: 2230-2238.

Schwer C, Gas B, Lottspeich F and Kenndler E (1993) Anal. Chem. 65: 2108–2115.

Seiler K, Fan Z. H, Fluri K and Harrison D. J (1994) Anal. Chem. 66: 3485–3491.

Shadpour H and Soper S. A (2006) Anal. Chem. 78: 3519–3527.

Shao X, Shen Y, O´Neill K and Lee M. L (1999) J. Chromatogr. A 830: 415-422.

Shen Y and Smith R. D (2000B) J. Microcolumn Sep. 12: 135-141.

Shen Y, Berger, S. J, Anderson G. A and Smith R. D (2000A) Anal. Chem. 72: 2154-2159.

Shim J, Dutta P and Ivory C. F (2008) Electrophoresis 29: 1026-1035.

Shimura K (2002) Electrophoresis 23: 3847–3857.

Shimura K (2009) Electrophoresis 30: 11-28.

Shin S, Kim B. S, Song J, Lee H and Cho H. H (2012) Lab Chip 12: 2568–2574.

Shultz-Lockyear L. L, Christa L, Colyer C. L, Fan Z. H, Roy K. I and Harrison D. J (1999) Electrophoresis 20: 529–538.

Silvertand L. H. H, Toraño J. S, van Bennekom W. P and de Jong G. J (2008) J. Chromatogr. A 1204: 157-170.

Simpson D. C and Smith R. D (2005) Electrophoresis 26: 1291-1305.

Sjöback R, Hygren J and Kubista M (1995) Spectrochim Acta A 51: 7-21.

Skinner C. D (2010) Analyst 135: 358–367.

Sluszny C, He Y and Yeung E. S (2005) Electrophoresis 26: 4197–4203.

Smejkal P, Bottenus D, Breadmore M. C, Guijt R. M, Ivory C. F, Foret F and Macka M (2013) Electrophoresis 34: 1493–1509.

Smithies O and Poulik M (1956) Nature 177: 1033-1033.

Soderquist M. E and Walton A. G (1980) J. Colloid Interface Sci. 75: 386–397.

Sosic Z, Houde D, Blum A, Carlage T and Lyubarskaya Y (2008) Electrophoresis 29: 4368-4376.

Sosic Z, Houde D, Blum A, Carlage T and Lyubarskaya Y (2008) Electrophoresis 29: 4368-4376.

Stegehuis D. S, Irth H, Tjaden U. R and van der Greef J (1991) J. Chromatogr. 538: 393–402.

Storms H. F, van der Heijden R, Tjaden U. R and van der Greef J (2004) Electrophoresis 25: 3461-3467.

Stroink T, Ortiz M. C, Bult A, Lingeman H, de Jong G. J and Underberg W. J (2005) J. Chromatogr. B 817: 49–66.

Suratman A and Wätzig H (2008) J. Sep. Sci. 31: 1834–1840.

Tanford C. and Hauenstein J.D (1956) I. Am. Chem. Sot. 78: 5287- 5291.

Tang Q, Harrata A. K and Lee C. S (1996) Anal. Chem. 68: 2482-2487.

Tang Q, Harrata A. K and Lee C. S (1997) Anal. Chem. 69: 3177-3182.

Tempels F, Wiese G, Underberg W. J, Somsen G. W and de Jong G. J (2006) J. Chromatogr. B 839: 30–35.

Thormann W, Caslavska J and Mosher R. A (2007) J. Chromatogr. A 1155: 154-163.

Thormann W, Caslavska J, Michael C. Breadmore M. C, Mosher R. A (2009) Electrophoresis 30: S16–S26.

Thormann W, Huang T, Pawliszyn J and Mosher R. A (2004) Electrophoresis 25: 324-337.

Thormann W, Mosher R. A (2006) Electrophoresis 27: 968-983.

Thormann W, Tsai A, Michaud J.-P, Mosher R. A and Bier M (1987) J. Chromatogr. A 389: 75-86.

Tia S and Herr A (2009) Lab. Chip 9: 2524–2536.

Tiggelaar R, Benito-Lopez F, Hermes D, Rathgen H, Egberink R, Mugele F, Reinhoudt D, van den Berg A, Verboom W and Gardeniers H (2007) Chem. Eng. J. 131: 163–170.

Tiggelaar R, Benito-Lopez F, Hermes D, Rathgen H, Egberink R, Mugele F, Reinhoudt D, Tomáš R, Klepárník K and Foret F (2008) J. Sep. Sci. 31: 1964–1979.

Tong W and Yeung E. S (1995) J. Chromatogr. A 718: 177-185.

Tranchida P. Q, Sciarrone D, Dugo P and Mondello L (2012) Anal. Chim. Acta 716: 66–75.

Tsai C. H, Wang Y. N, Lin C. F, Yang R. J and Fu L. M (2006) Electrophoresis 27: 4991–4998.

Tsai C. H, Yang R. J, Tai C. H and Fu L. M (2005) Electrophoresis 26: 674–686.

Valcárcel M, Arce L and Ríos A (2001) J. Chromatogr. A 924: 3–30.

van den Berg A, Verboom W and Gardeniers H (2007) Chem. Eng. J. 131: 163–170.

van der Vlis E, Mazereeuw M, Tjaden U, Irth H and van der Greef J (1995) J. Chromatogr. A 712: 227–234.

van der Walt S, Colbert S. C and Varoquaux G (2011) Comput. Sci. Eng. 13: 22–30.

Végvári Á and Hjertén S (2002) Electrophoresis 23: 3479–3486.

Verzola B, Gelfi C and Righetti P. G (2000A) J. Chromatogr. A 868: 85-99.

Verzola B, Gelfi C and Righetti P. G (2000B) J. Chromatogr. A. 874: 293-303.

Vlckova M, Kalman F and Schwarz M. A (2008) J. Chromatogr. A 1181: 145-152.

Wang T and Hartwick R. A (1992) Anal. Chem. 64: 1745-1747.

Wang T, Ma J, Wu S, Sun L, Yuan H, Zhang L, Liang Z and Zhang Y (2011) J. Chromatogr. B 879: 804–810.

Wang Y.-C, Choi M. H and Han J (2004) Anal. Chem. 76: 4426–4431.

Wei J, Gu X, Wang Y, Wu Y and Yan C (2011) Electrophoresis 32: 230–237.

Wei J, Lee C. S, Lazar I. M and Lee M. L (1999) J. Microcolumn Separations 11: 193-197.

Wei J, Yang L, Harrata A. K and Lee C. S (1998) Electrophoresis 19: 2356-2360.

Wenclawiak B. W and Püschl R. J (2006) Anal. Lett. 39: 3–16.

Wetzl B. K, Yarmoluk S. M, Craig D. B and Wolfbeis O. S (2004) Angew. Chem. Int. Ed. 40: 5400–5402.

Wojcik R, Swearingen K. E, Dickerson J. A, Turner E. H, Ramsay L. M and Dovichi N. J (2008) J. Chromatogr. A, 1194: 243–248.

Wojcik R, Vannatta M and Dovichi N. J (2010) Anal. Chem. 82: 1564–1567.

Woltmann E, Meyer H, Weigel D, Pritzke H, Posch T. N, Kler P. A, Schürmann K, Roscher J and Huhn C (2014) Anal. Bioanal. Chem. 406: 6347-6362.

Wu J and Pawliszyn J (1992) Anal. Chem. 64: 2934-2941.

Wu J and Pawliszyn J (1995) Analyst 120: 1567-1571.

Wu Z.-Y, Fang F, He Y.-Q, Li T.-T, Li J.-J and Tian L (2012) Anal. Chem. 84: 7085–7091.

www. sigmaaldrich.com_Technical data sheet fluorescent IEF-Marker, 2013

www.activemotiv.com_Technical data sheet ChromeoTM P503, 2014

www.weicon.de_ Technical data sheet epoxy glue, 2015

www.wiko-klebetechnik.de_Technical data sheet 2-K Epoxy-Klebstoff, 2015

Xiao D, Yan L, Yuan H, Zhao S, Yang X and Choi M. M. F (2009) Electrophoresis 30: 189–202.

Xiao D, Zhao S, Yuan H and Yang X (2007) Electrophoresis 28: 233–242.

Xu L, Dong X.-Y and Sun Y (2009) J. Chromatogr. A 1216: 6071–6076.

Xu L, Dong, X.-Y and Sun, Y (2010) Biochem. Eng. J. 53: 137-142.

Xu X, Liu K and Fan Z. H (2012) Expert Rev. Proteomics. 9: 135-147.

Yang C, Liu H, Yang Q, Zhang L, Zhang W and Zhang Y (2003) Anal. Chem. 2003: 215–218.

Yang C, Zhang L, Liu H, Zhang W and Zhang Y (2003) J. Chromatogr. A 1018: 97–103.

Yang C, Zhang W, Zhang J, Duan J and Zhang Y (2005) J. Sep. Sci. 28: 78-86.

Yang X, Zhang X, Li A, Zhu S and Huang Y (2003) Electrophoresis 24: 1451–1457.

Zelenský I, Zelenská V, Kaniansky D, Havaši P and Lednárová V (1984) J. Chromatogr. A 294: 317–327.

Zhang B, Foret F and Karger B. L (2000) Anal. Chem. 72: 1015–1022.

Zhang B, Liu H, Karger B and Foret F (1999) Anal. Chem. 71: 3258–3264.

Zhang F, Daghighi Y and Li D (2011) J. Colloid Interf. Sci. 364: 588–593.

Zhang J, Hu H, Gao M, Yang P and Zhang X (2004) Electrophoresis 25: 2374–2383.

Zhang L. H, Zhang C. J and Wu X. Z (2006A) Anal. Sci. 22: 1039-1041.

Zhang M and El Rassi Z (2006B) J. Proteome Res. 5: 2001–2008.

Zhang Z, Zhang F and Liu Y (2013) J. Chromatogr. Sci. 51: 666–683.

Zhang Z.-X, Zhang X.-W and Zhang S.-S (2009) Anal. Biochem. 387: 171–177.

Zhou F and Johnston M. V (2004) Anal. Chem. 76: 2734–2740.

Zhu C, He X, Kraly J. R, Jones M. R, Whitmore C. D, Gomez D. G, Eggertson M, Quigley W, Boardman A and Dovichi N. J (2007) Anal. Chem. 79: 765–768.

8   Appendix

Figure A1: CAD drawing of the overview of the intermediate LED-IF detection setup by J J&M Analytik AG (Essingen, Germany) modified
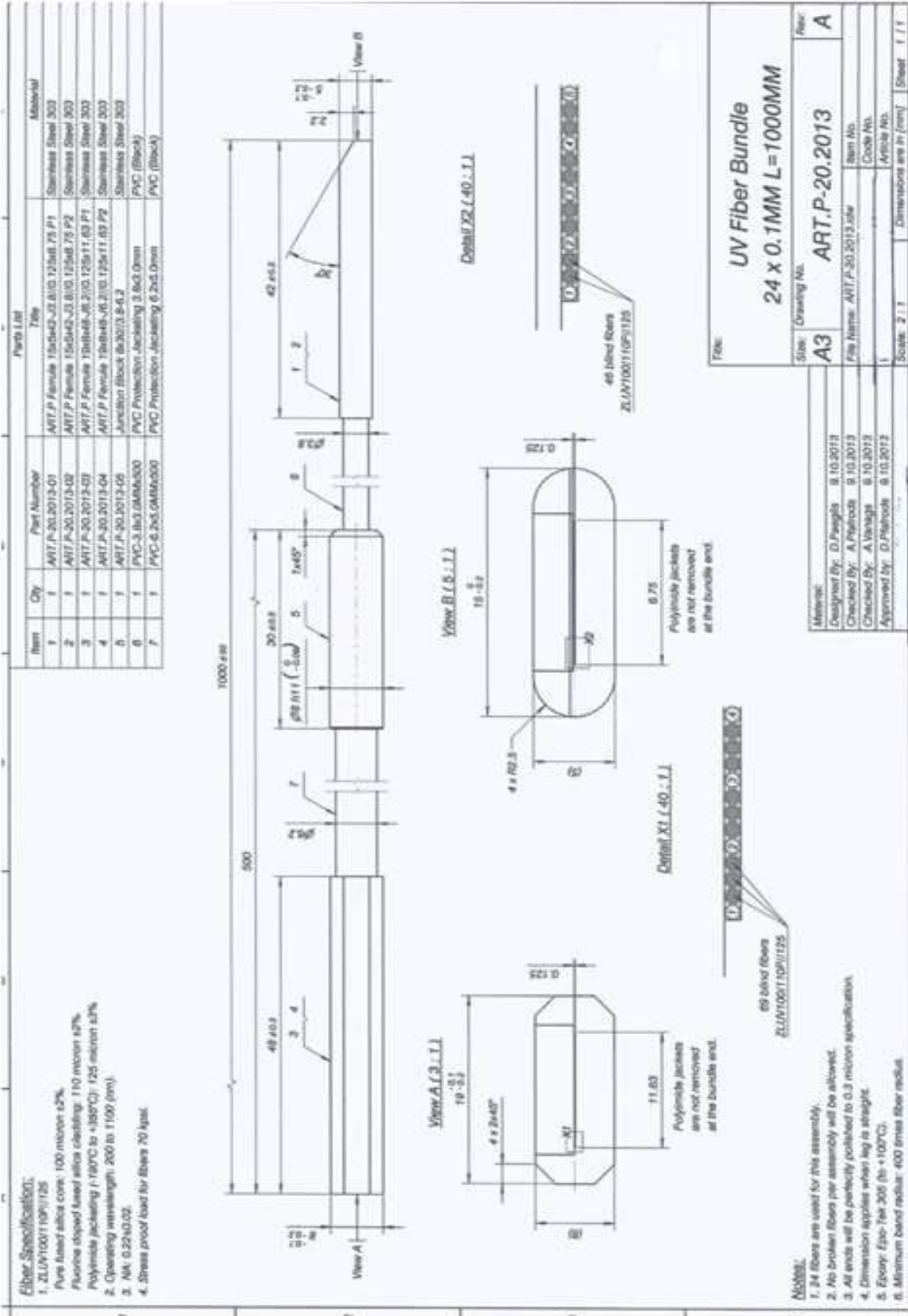
Figure A2: CAD drawing of the linear fiber array 24 × 100 µm active fibers of the intermediate LED-IF detection setup by art photonics GmbH (Berlin, Germany)
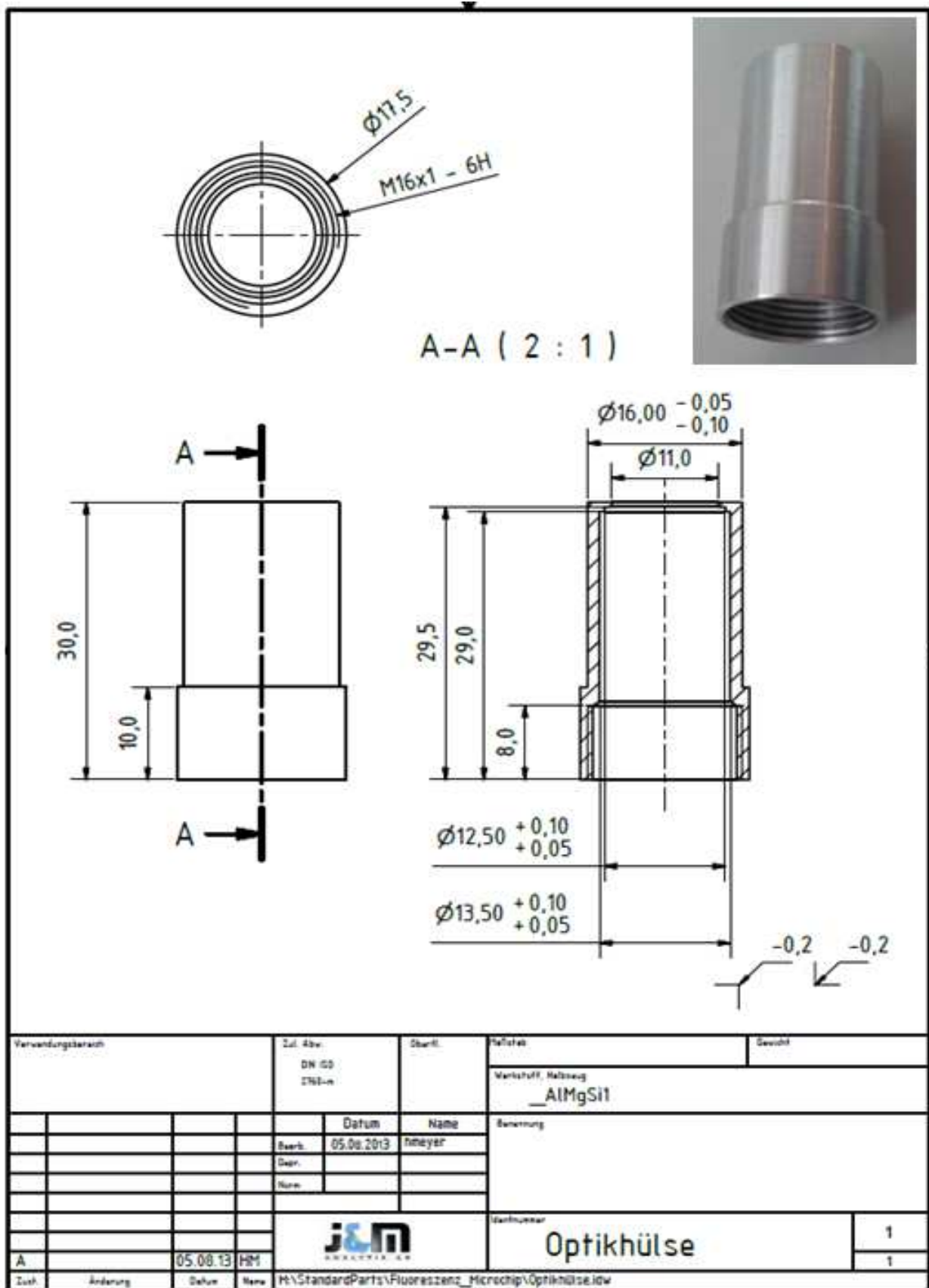
Figure A3: CAD drawing of the fixed optical Shell 1 of the intermediate LED-IF detection setup by J&M Analytik AG (Essingen, Germany) modified
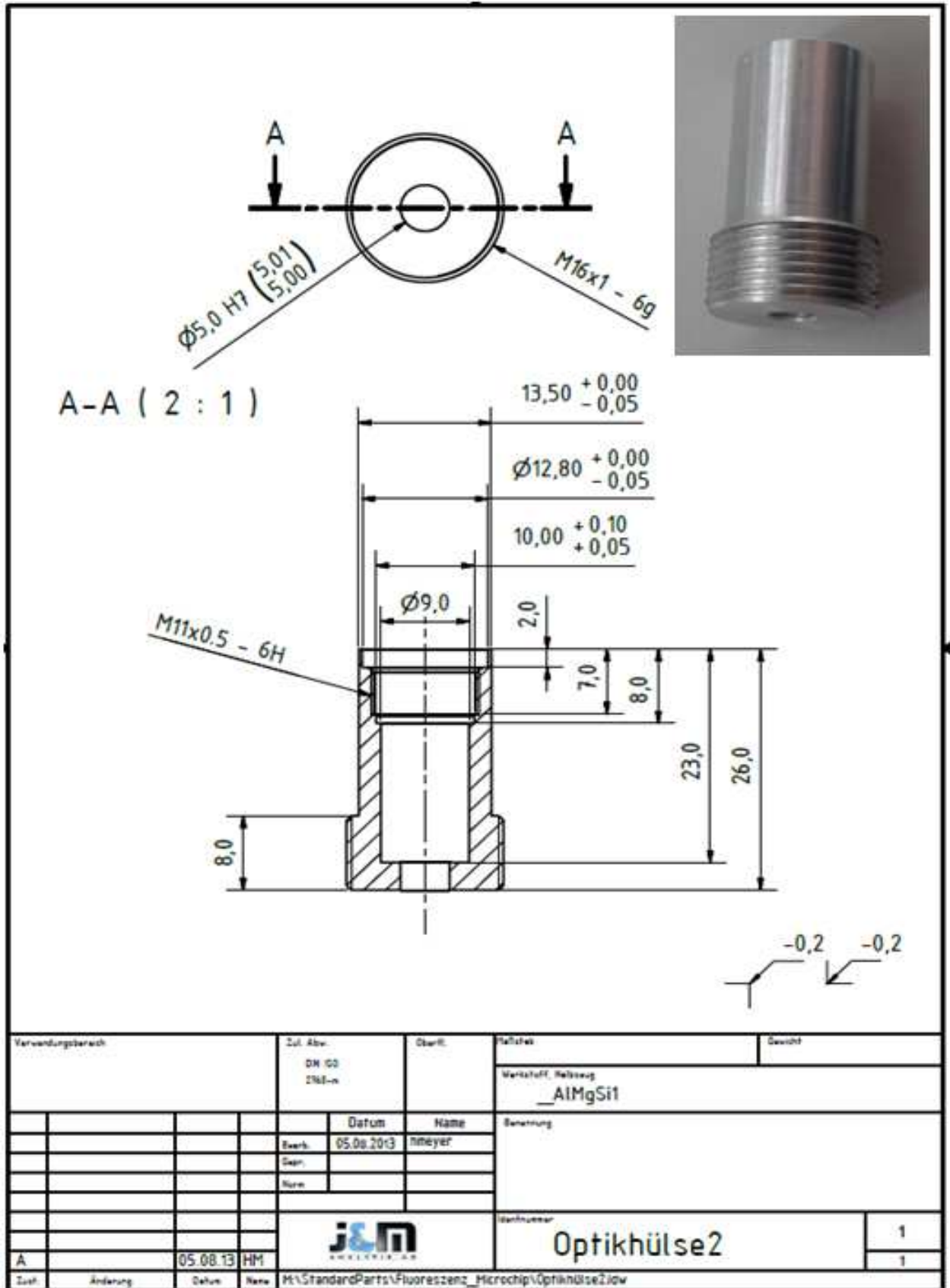
Figure A4: CAD drawing of the fixed optical Shell 2 of the intermediate LED-IF on-chip detection setup by J&M Analytik AG (Essingen, Germany) modified
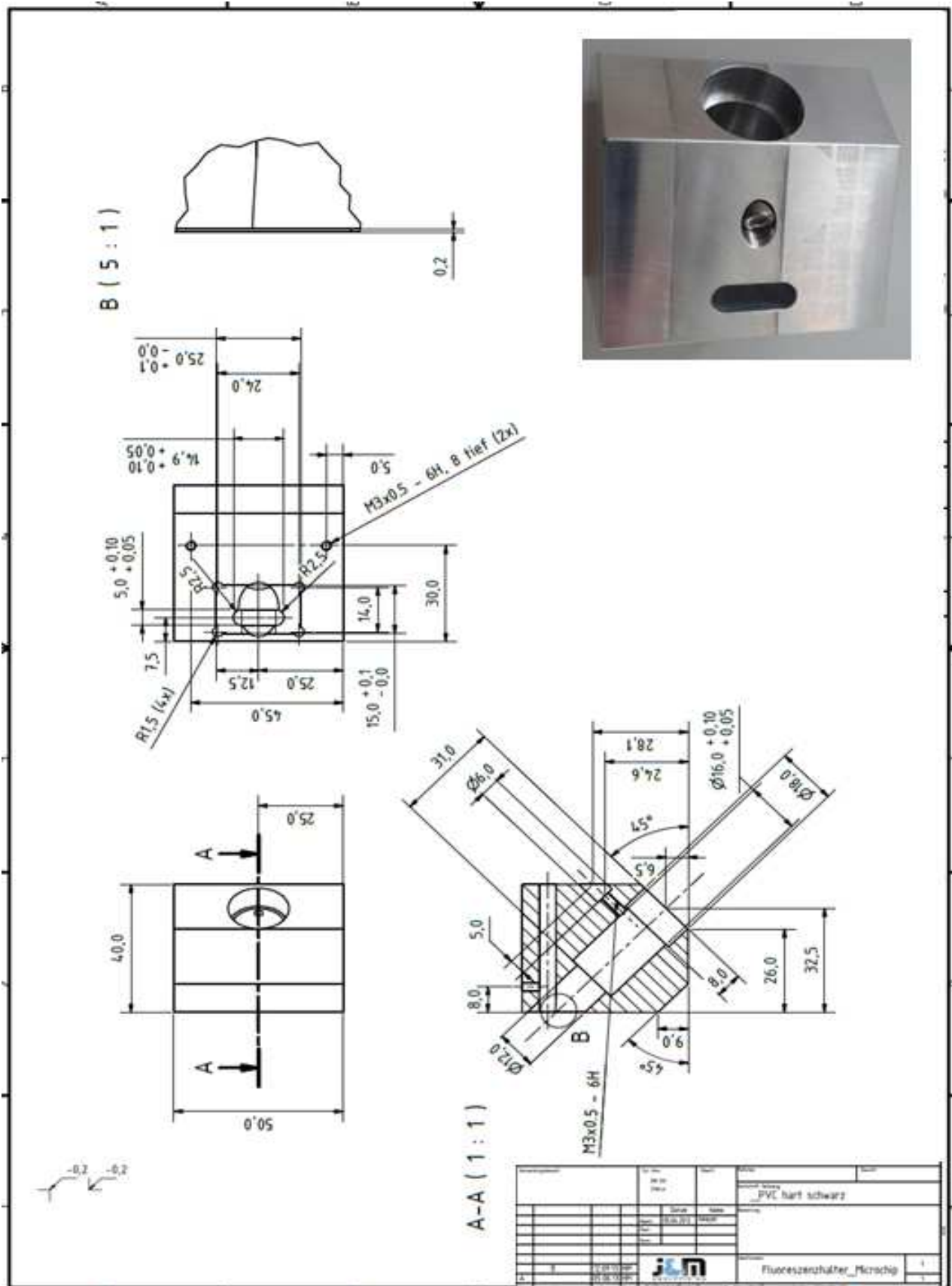
Figure A5: CAD drawing of the aluminum housing of the intermediate LED-IF on-chip detection setup by J&M Analytik AG (Essingen, Germany) modified
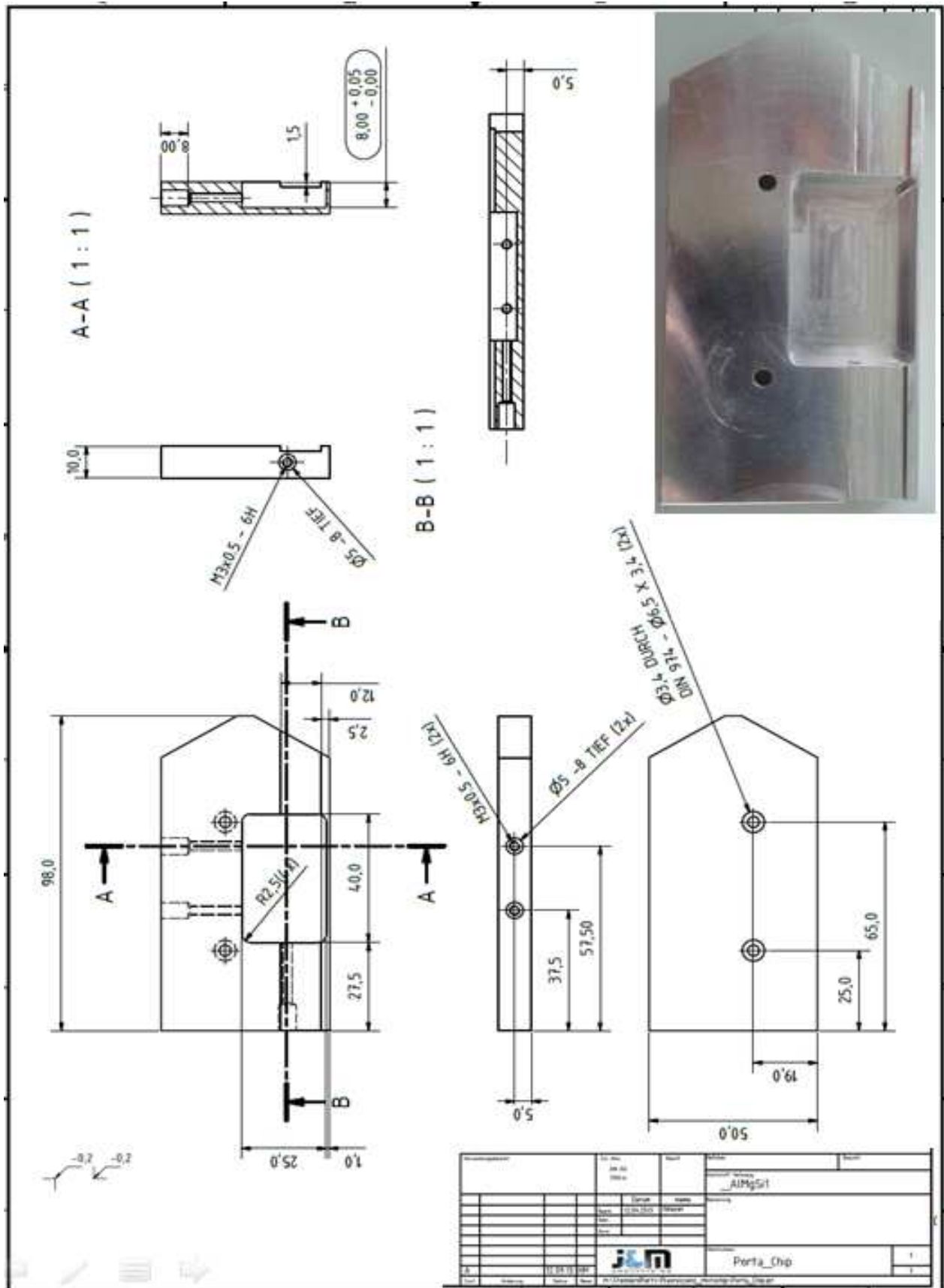
Figure A6: CAD drawing of the aluminum bottom plate of the intermediate LED-IF on-chip detection setup by J&M Analytik AG (Essingen, Germany) modified
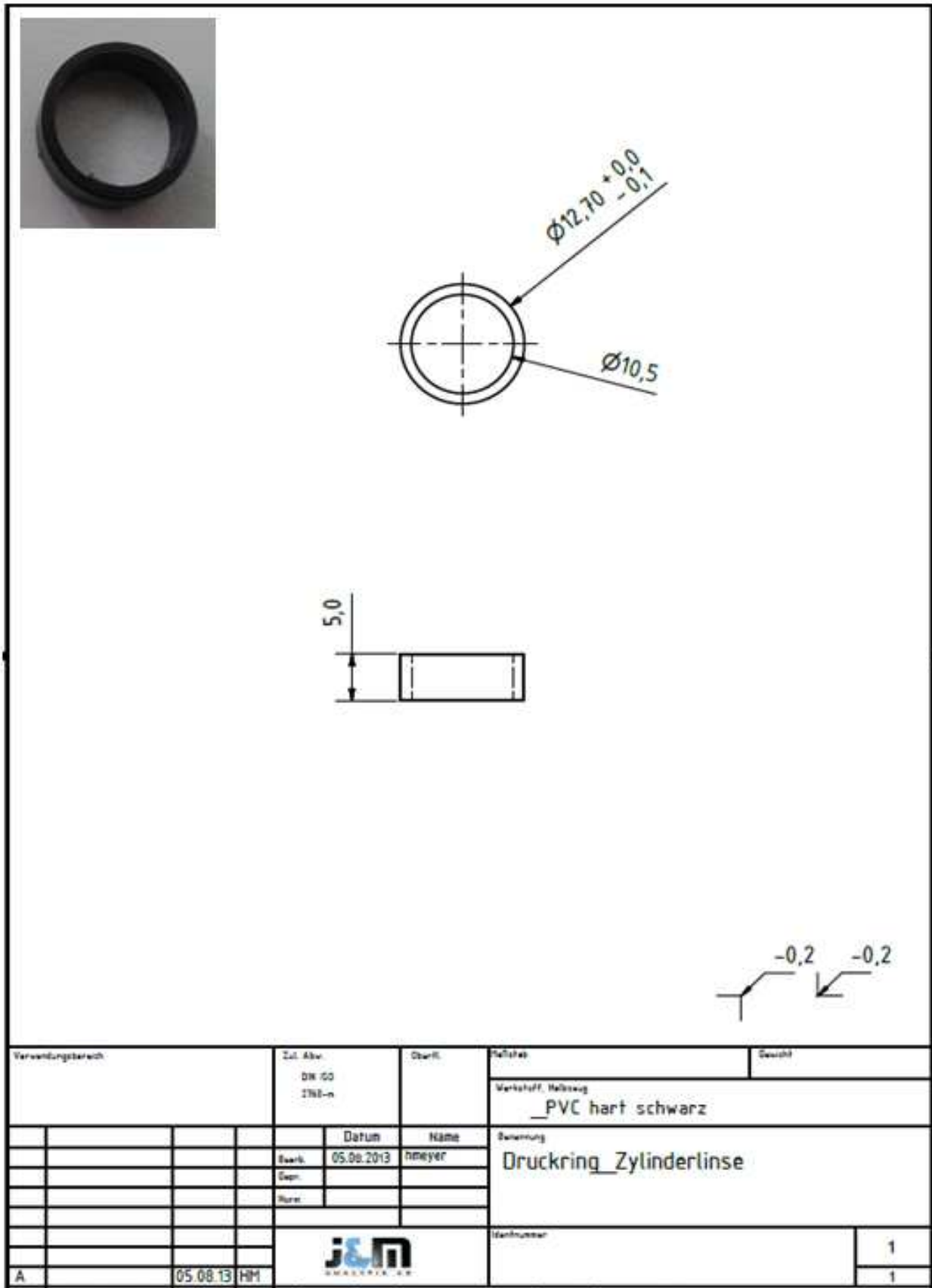
Figure A7:CAD draing stabilizaton ring fo the cylindrical lens for slit focusing of the intermediate LED-IF on-chip detection setup by J&M Analytik AG (Essingen, Germany) modified

9 List of publications and scientific contributions

Peer-Reviewed publications

2016   Sydes, D., Kler, P. A., Meyer, H., Zipfl, P., Lutz, D., Huhn, C., On-chip intermediate LED-IF-based detection for the control of electromigration in multichannel networks, Anal. Bioanal. Chem. (2016) Doi:10.1007/s00216-016-0033-8

2016   Sydes, D., Kler, P. A., Hermans, M., Huhn, C., Zero-dead-volume interfaces fort two-dimensional electrophoretic separations, Electrophoresis (2016) Doi:10.1002/elps.201600262

2016   Sydes, D., Kler, P. A., Zipfl, P., Lutz, D., Bouwes H., Huhn, C., On-chip intermediate potential measurement for the control of electromigration in multi-channel networks in case of time-dependent potential changes, Sens. Actuators B Chem. (2017) 240, 330-337 (available online 2016)

2015   Pattky, M., Nicolardi, S., Santiago-Schübel, B., Sydes, D., van der Burgt, Y. E. M., Klein, A. N., Jiang, N., Mohrlüder, J., Hänel, K., Kutzsche, J., Funke S. A., Willbold, D., Willbold S., Huhn, C., Structure characterization of unexpected covalent O-sulfonation and ion-pairing on an extremely hydrophilic peptide with CE-MS and FT-ICR-MS, Anal. Bioanal. Chem. (2015), 407, 6637-6655

2015   Sydes, D., Weber, P., Krieg, K., Widmaier, J., ANAKON 2015-Graz: a warm welcome for analytical chemists in the heart of Styria, Anal. Bioanal. Chem. (2015), 407, 6591-6592

2014   Kler, P. A., Sydes, D.,·Huhn, C., Column–coupling strategies for multidimensional electrophoretic separation techniques, Anal. Bioanal. Chem. (2014), 407, 119-138

2011   Lehnert, N., Krings, U., Sydes, D., Wittig, M., Berger, R. G., Bioconversion of car-3-ene by a dioxygenase of Pleurotus sapidus, J.Jbiotec. (2011), 159, 329-35

2009   Masár, M., Sydes, D., Luc, M., Kaniansky, D., Kuss, H. M., Determination of ammonium, calcium, magnesium, potassium and sodium in drinking waters by capillary zone electrophoresis on a column-coupling chip, J. Chromatogr. A (2009), 1216, 6252–6255

Non Peer-Reviewed publications

2015	Sydes D., conference report, 17th Symposium on the Practical Applications for the Analysis of Proteins, Nucleotides and Small Molecules – CE Pharm 2015, Brooklyn (USA), Mitteilungsblatt der Fachgruppe Analytische Chemie Gesellschaft Deutscher Chemiker (GDCh), Ausgabe 4/2015
2014	Sydes D., conference report, Fifteenth Symposium on the Practical Applications for the Analysis of Proteins, Nucleotides and Small Molecules – CE Pharm 2013, Arlington (USA), Mitteilungsblatt der Fachgruppe Analytische Chemie Gesellschaft Deutscher Chemiker (GDCh), Ausgabe 2/2014
2013	Sydes D., report Junganalytikertreffen, Alles fließt - Ein Besuch beim Kooperationslabor Ruhrverband, Emschergenossenschaft und Lippeverband in Essen, Mitteilungsblatt der Fachgruppe Analytische Chemie Gesellschaft Deutscher Chemiker (GDCh), Ausgabe 2/2013

Talks

2015	7th CE Forum - Eberhard Karls University Tübingen; 2D heart cutting CIEF-IF/CE-MS: Instrumental and method development
2015	Centro de Investigación de Métodos Computacionales (CIMEC), Santa Fe, Argentina; Multidimensional electrophoretic separations for bioanalytical applications: Instrumental and method development using computer simulations
2014	Comenius-University Bratislava, Slovakia; Multidimensional electrophoretic separations
2014	24th Doktorandenseminar Hohenroda; Coupling of capillary isoelectric focusing to mass spectrometry: Towards CIEF/CE-MS
2013	5th CE Forum - Friedrich-Schiller-University Jena; Developments on coatings and spacers for isoelectric focusing: Towards CIEF/CE-MS

Posters

2015	7th CE Forum - Eberhard Karls University Tübingen; On-chip intermediate fluorescence, conductivity and potential detection for 2D electrophoretic separations
2015	CE in the Biotechnology & Pharmaceutical Industries: 17th Symposium on the Practical Applications for the Analysis of Proteins, Nucleotides and Small Molecules - CE Pharm, Brooklyn, USA; Hyphenation of 2D heart cutting CIEF/CE-MS
2015	ANAKON 2015, Graz, Austria; On-chip intermediate fluorescence, conductivity and potential detection for 2D electrophoretic separations
2014	6th CE Forum - Philipps-University Marburg; On-chip intermediate optical and conductivity detection for 2D electrophoretic separations
2013	CE in the Biotechnology & Pharmaceutical Industries: 15th Symposium on the Practical Applications for the Analysis of Proteins, Nucleotides and Small Molecules - CE Pharm, Arlington, USA; Coatings and spacers for isoelectric focusing: Towards CIEF/CE-MS
2013	Wissenschaftsforum Chemie 2013, Darmstadt; Coatings and spacers for isoelectric focusing: Towards CIEF/CE-MS
2013	ANAKON 2013, Essen; Capillary isoelectric focusing for the characterization of glycoproteins

10 Resume

Name	Daniel Sydes
Date of birth	2/9/1983
Place of birth	Kassel
Marital status	single
Nationality	German

Work experience

since 12/2013	Eberhard Karls University Tübingen, Research Assistant; Instrumental development 2D Capillary Electrophoresis
10/2012 – 12/2013	Jülich Research Center, Research Assistant; Instrumental development 2D Capillary Electrophoresis
04/2010 – 10/2012	Sysmex Europe GmbH in Norderstedt, Product Manager Quality Control and Reagents
10/2008	„BioTech 4U" in Hannover; Project Assistant
07/2008 – 10/2008	Leibniz University Hannover; Technical Assistant at the Institute for Inorganic Chemistry
08/2003 – 05/2004	Therapy Institute Böddiger Berg, Falkenberg; Social Service

Education

10/2007 – 11/2009	Leibniz University Hanover; Master's Degree Course in Analytical Chemistry; focus: Instrumental Analytics - Master Thesis: Institute of Food Chemistry
10/2004 – 09/2007	University Duisburg-Essen; Bachelor's Degree Course in Water Science; focus: Analytics, Chemistry, and Microbiology - 3-month Bachelor Thesis: Comenius University Bratislava, Slovakia
08/1994 – 06/2003	Theodor - Heuss Grammar School Homberg (Efze); high school diploma; - special subjects: Chemistry and Biology

Advanced training

11/2012 – 12/2013	Forschungszentrum Jülich; Impulsplus – Interdisciplinary qualification: Project Management, Team Communication, and Presentation
10/2008 – 01/2009	Hanover Medical School (MHH); Laboratory work und lectures: Pharmacology and Toxicology
12/2007	Leibniz University Hanover; Lecture: Introduction to mathematical statistics

Internships

08/2008 – 09/2008	DIK – "German Institute for Rubber Technology"; Laboratory
07/2002	B. Braun in Bethlehem Pennsylvania, USA; OEM Division

Awards

03/2015	Best Poster Award, conference: ANAKON 2015, Graz, Austria
12/2008	"1st Prize in Bachelor's Degree Course Water Science" for an outstanding Bachelor's Thesis at the Department of Chemistry at the University of Duisburg-Essen
10/2007	"Henkel Award" - 1st prize - from Henkel KGaA for an outstanding Bachelor's Thesis at the Department of Chemistry at the University of Duisburg-Essen

Scholarships

03/2015 – 06/2015	German Academic Exchange Service (DAAD - Deutscher Akademischer Austauschdienst), Research Stay at the CIMEC, Santa Fe, Argentina
09/2015	California Separation Science Society (CASSS) "student travel grant" - Conference: CE Pharm 2015; Brooklyn, USA

Memberships

since 10/2012	GDCh - German Chemical Society (Gesellschaft Deutscher Chemiker) - Analytical Chemistry and Separation Science division